Durham E-Theses

The surface chemistry of polymeric bioseparation materials

Tasker, Simon

How to cite:

Use policy

A Thesis Entitled

THE SURFACE CHEMISTRY OF POLYMERIC

BIOSEPARATION MATERIALS

Submitted for the Degree of

Doctor of Philosophy

by

Simon Tasker, BSc. (Dunelm)

November 1996

University of Durham

ACKNOWLEDGEMENTS

ABSTRACT

The aim of this thesis was to test existing theories concerning biocompatibility of polymeric materials, and in the process to try and identify the major factors which pertain to their use as bioseparation matrices. The surface chemistry of cellulose and poly(tetrafluoroethylene) based bioseparation materials have been examined. We have been able to demonstrate a direct link in the case of the cellulose materials between the crystallinity and the accessibility of the hydroxyl groups which are the primary sites of functionalization. In addition, the effect of processing conditions on the pore structure of an amorphous cellulose matrix was demonstrated and this has been shown to have a direct consequence for the protein binding characteristics of the material.

The functionalisation of PTFE has been achieved by reaction with sodium naphthalenide, which lead to the defluorination of the PTFE surface and the formation of a unsaturated carbonised layer containing oxygenated functionalities. The reaction has also been shown to alter the morphology of PTFE membranes as evidenced by AFM analysis. In the case of powdered PTFE we observed the formation of a microporous layer, however this was found to revert back to a fluorinated layer with gentle heating.

A novel insight in to the defluorination reaction was obtained using the bombardment of PTFE and PVDF with a Na atom beam under ultra-high vacuum conditions. This demonstrated the single valence electron mechanism of the reaction and also showed the formation of NaF at the surface of the polymer. The formation of CF_3 groups was attributed to the nucleophilic attack of fluoride ions from molecular NaF species formed at the initial stages of the reaction.

DECLARATION

The work described in this thesis was undertaken in the Department of Chemistry at the University of Durham between October 1991 and September 1994. It is the original work of the author except where indicated or where specific reference is made to the source material.

No part of this thesis has been previously submitted for a degree, however the following articles which are based on work contained in this thesis have been published as indicated:

'Hydroxyl Accessibility in Celluloses'

S. Tasker, J. P. S. Badyal, *Polymer*, **35**, 4717 (1994).

'Influence of Crosslinking upon the Pore Structure of Cellulose'

S. Tasker, J. P. S. Badyal, *J. Phys. Chem.*, **98**, 7599 (1994).

'Surface Defluorination of PTFE by Sodium Atoms'

S. Tasker, J. P. S. Badyal *J. Phys. Chem.*, **98**, 12442 (1994).

CONTENTS

1. INTRODUCTION

The present level of understanding of the chemistry involved at the interface between polymers and biological media represents the culmination of over fifty years of intensive research which has lead to the widespread use of polymers for *in-vivo* and *in-vitro* biomedical applications. The impetus for this research has arisen due to the growing demands placed upon medical science by the increasing size and longevity of the global population[1], and the attractive rewards to be gained from the commercialisation of this technology. More specifically, the work involved in the development of novel polymeric bioseparation media has addressed many questions central to the physicochemical nature of polymer surfaces and requires an appreciation of the complex intermolecular forces between a solute, the stationary phase and the mobile phase.

This chapter serves as a general introduction to the work presented in this thesis and includes an appraisal of the biomaterials field, outlines current theories concerning the interaction of biomolecules and polymer surfaces and examines the effectiveness of the latest generation of bioseparation materials. In the light of the world-wide expansion in the biotechnology industry over recent years, some of the more pressing challenges involved in the design of polymeric bioseparation media with predictable physical and flexible chemical properties will be discussed.

1.1. BIOMATERIALS

A biomaterial[2-4] is defined as a *non-living* material designed to interact favourably with

biological systems[4]. Specifically this involves the interaction of a biomolecule; for example a protein, enzyme, immunogenic or cellular species with the surface of a material, which could typically be inorganic, metallic, or one of a range of naturally and synthetically derived polymers[5]. It is this last category of materials that we are primarily interested in for the subject of this thesis and some examples are discussed below.

1.1.1. Polymeric Biomaterials

Since the first attempt to implant a poly(methyl methacrylate) hip prosthesis[6] in 1947, and the use of plastics in middle ear surgery[7] in the early 1950's, the biomedical exploitation of synthetic and natural polymers has been primarily targeted toward implant applications. This is still a dominant area of research today, accounting for the majority of medical applications using polymers[8]. Materials which exhibit biocompatibility *invivo* have been used as prosthetics, artificial organs[2, 9 - 13] and blood plasma substitutes[14]. PVC is the most widely used polymer for short term blood contacting devices such as catheters and blood bags[5, 15]. Polyethylene, polyamides and polyesters have been used as biodegradeable/resorbable suture materials and drug tablet formulations, whereas fluoropolymers[16] have become important in cardiovascular surgery and hydrogels[17] are widely used in opthalmic applications.

Advances in synthetic polymer chemistry have enabled the development of many new classes of biocompatible polymers. The poly(hydroxy-alkyl-methacrylates)[18], poly(alkyl-siloxanes) and poly(ether)[19] systems are but a few examples. Novel bulk polymers incorporating naturally derived biocompatible segments form a range of natural/synthetic hybrid protein resistant materials, for example poly(ether-urethane) ionomer[20] derivatives based upon crosslinked collagen have demonstrated favourable

2

chemical and physical properties. Polymers incorporating lactic and glycolic acid have high hydrolytic susceptibilities and form a range of biodegradable materials[21-23].

The value of these types of materials is based upon their tolerance within a living environment, i.e. the ability of the material to overcome the natural response of the biological system which is to reject the foreign material. The nature of the cellular reaction has been found to be dependent upon both the microscopic and macroscopic properties of the polymer, for example the size, shape and surface chemistry of the biomaterial has been shown to influence this behaviour[24].

1.2. INTERFACIAL BIOCOMPATIBLITY OF POLYMERS

All polymers can be considered to be biocompatible[25] to some degree, and the range of materials which have potential as biomedical products is extensive on first consideration. However the use of many polymers has been prevented due to strict biocompatibility, toxicity and mechanical property standards[26]. In order to meet these requirements and be considered as an acceptable biomaterial the polymer in question must meet many criteria even before its interfacial biocompatibility is considered. Firstly, it must be non-toxic, the presence of unreacted monomer, initiators, plasticizing and stabilizing agents in most commercial grade polymers has hindered their use, though the introduction of ultra pure medical grade polymers[27,28] has eased the problem to a degree. The mechanical or as it is often termed bulk biocompatibility is also an important consideration. Polymers with good mechanical strength and permeability often produce poorly tolerated surfaces in biological media.

The mechanical compliance of polymers differs significantly from that of a typical blood vessel wall[29] for example and subtle effects such as turbulence produced in the blood stream have been shown to cause hemolysis, platelet activation and aggregation[30,31]. Consequently rough surfaces are more likely to cause blood clotting or thrombogenesis[29] and considerations involved in the design of biocompatible surfaces include mechanical as well as chemical factors.

1.2.1. Protein/Polymer Interactions

The behaviour of blood at the interface with a biomaterial is a crucial problem in the biomedical application of polymers. The extent of blood/polymer interaction is often used as a general indicator of the biocompatibility of a polymer. The adsorption of plasma proteins on to the polymer surface is thought to be the first step in the breakdown of biocompatibility, leading to cell adhesion, and ultimately a series of enzymatically catalysed biochemical reactions occur which may result in tissue growth and blood clot formation[32]. Consequently a large amount of effort has been devoted to improving the understanding of blood and protein/polymer interactions[30-34].

The chemically heterogeneous and mobile nature of polymer surfaces combined with the fact that proteins in solution are complex polyamides from 40000 to several million Daltons in weight and possess a range of amphiphilic domains and dynamic conformational characteristics, have made an understanding of their interaction an extremely challenging area of research. Protein adsorption at surfaces can be driven by a combination of hydrophobic, polar and electrostatic interactions. This has lead to the *multi domain interaction hypothesis*, which describes the system in terms of a protein with differing chemical domains interacting with a heterogeneous polymer surface.

Providing that the chemical domains are of comparable size a matching complementarity between the domains on the polymer and the protein will cause the protein to orient itself on the surface in such a way as to maximize the force of interaction. If the domain matching is not ideal, see Figure 1.1a the protein may conformationally adapt (denature) to the more rigid polymer surface. The illustration in Figure 1.1b shows the restructuring of both the protein and the water equilibrated polymer surface in response to the new microenvironment.

1.2.2. The Polymeric Biosurface

The interfacial biocompatibility of polymers is ultimately defined by the nature of the biosurface and these can be divided in to two main types, the bioadhesive and molecularly non-stimulative surface. The former type of surface achieves enhanced biocompatiblity by provoking a strong interaction between the surface and proteins contained in the biological medium, causing a microscopic bonding. These bound fragments are then thought to camouflage the surface preventing a thromboembolic or immune response. The best examples of these types of materials are composite resins for dentistry and bioactive polymers for bone bonding and joint replacement.

The non-stimulative type of surface is as its name suggests is aimed at provoking a minimal response from the biological system. These materials have been widely studied, incorporated in to a wide range of biopolymer devices, show considerable promise for the development of matrices capable of bioseparation and consequently form the basis of the following section.

POLYMER   WATER   PROTEIN

Polar Groups

Hydrophobic Domain

(A)

POLYMER   WATER

PROTEIN

(B)
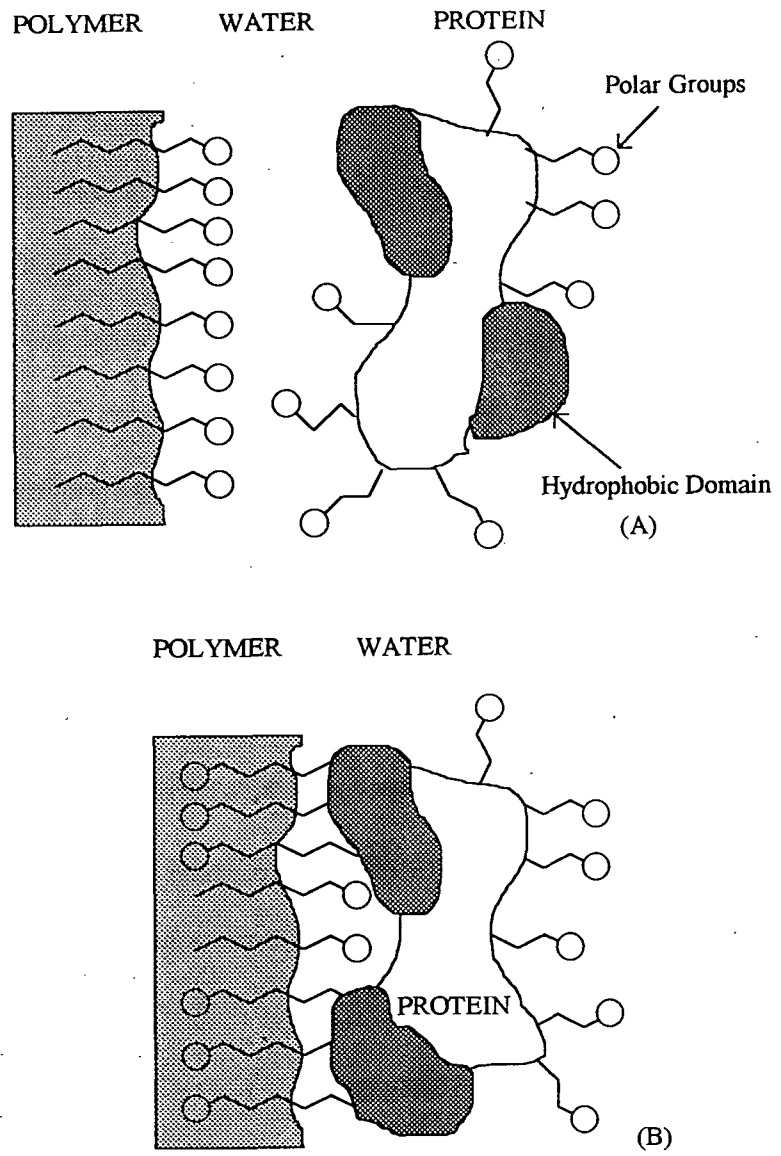
Figure 1.1   **Schematic representation protein adsorption at a polymer/water interface.**

1.2.2.1. *Surface Dynamics*

Biomaterial surfaces as well as biomolecules show significant restructuring of their surfaces in response to the imbalance of forces associated with adsorption at the surface. Surface distortions are sometimes found as deep as the fifth atomic layer in metallic or inorganic crystal systems, whereas in polymeric materials[35] this can extend to many hundreds of atomic layers due to the increased mobility and lower intermolecular forces between the polymer chains.

Polymer surfaces are unique in that they are characterised by high chain mobility, compositional gradients, heterogeneous chain lengths and unique water structuring. Even high molecular weight polymer surfaces are rarely at equilibrium, and mechanical and relaxation studies have demonstrated the time/temperature[36] dependency of polymer dynamics. Surface reorganisation of polymers is a low energy process, poly(hydroxy-methacrylate) (p-HEMA) contact lenses[37] have been shown to behave as hydrophobic surfaces in air and hydrophilic surfaces under water. High chain mobility allows surface reorganisation and rapid minimisation of interfacial energies.

1.2.2.2. *Electrical Properties*

The net electrical charge of surfaces has for some time been linked with the adsorption of proteinaceous material. Sawyer[38,39] showed that both the inner walls of veins and the surfaces of bodies formed in blood bear a net negative charge under physiological conditions. It was also noted that damage to a blood vessel wall led to a thrombogenic response which was associated with an increasingly positive net charge at the damage site. In-vitro studies[40], using polymeric biomaterials have also shown the

importance of negatively charged surfaces. Lower platelet adhesion was measured for

surfaces containing higher proportions of anionic groups, whereas cationic surfaces

promoted adsorption. In general, the interaction between the components of blood

serum (a strong electrolyte) and a charged surface has been shown to determine whether

thromboembolic responses or biocompatible behaviour are observed at a biomaterial

surface.

1.2.2.3. *Interfacial Energetics*

Interfacial processes such as biomacromolecular adsorption were initially thought

to be driven by the interfacial free energy of the surface[41]. Baier stated[42] that blood

compatibility could be achieved by the minimisation of the adhesion between blood

components and foreign surfaces, which could then lead to the control of

thromboembolic phenomena. A zone of minimum bioadhesion found by Baier[43] was

quoted as 20-30 mJ/m^2 of critical surface tension and this was suggested to be the

optimum zone of biocompatibility as shown in Figure 1.2.

Even so, Andrade[44] pointed out that the working environment of biomaterials

was aqueous and therefore Baier's relationship between critical surface tension of a

polymeric materials measured in air and the degree of bioadhesion was somewhat flawed.

Polymer surfaces are unusual in that in aqueous systems the high surface tension of water

combined with the low surface free energy of most polymers leads to the development of

a high interfacial free energy or surface tension[45] whereas in air the reverse is observed.

Based on these observations the surfaces of hydrophilic water swollen polymers were

identified as attractive candidates for minimising bioadhesion. Andrade subsequently

demonstrated that in the case of hydrogel-like polymers with high water content the

surface free energy was very similar to the surface tension of water, hence interfacial energies were minimised and this led to a reduced affinity for protein adsorption[46].

In contrast to the large amount of work supporting the importance of minimising interfacial free energy as route to increasing biocompatibility, Ratner et al[47] suggested that an optimum ratio of polar/apolar sites on the biomaterial surface could be shown to be an important factor. This has since been vindicated in the work of Sharma[48] where surfaces with the correct balance of polar and dispersion forces were able to preferentially bind albumin at the surface, a plasma protein which subsequently exhibited greatly increased thromboresistance.

Groups such as Ikada[49] have tried to specify biocompatibility in terms of the non-interaction of proteins whereas others have favoured the adsorption of specific proteins which in turn confer biocompatibility[48]. This is a testament to the complexity of the system in question and lead Andrade[34] to advocate the use of a multi-parameter approach to protein-surface interactions in which we consider the components of a blood mixture, the nature of the polymer surface and as many interfacial events which arise from their interaction as possible.

Most common polymers

Strong

Relative biological interaction

Good bioadhesion

Weak

10   20   30   40   50   60

Surface tension (mJ/m²)

Zone of minimum bioadhesion
(hypothetical zone of biocompatibility)
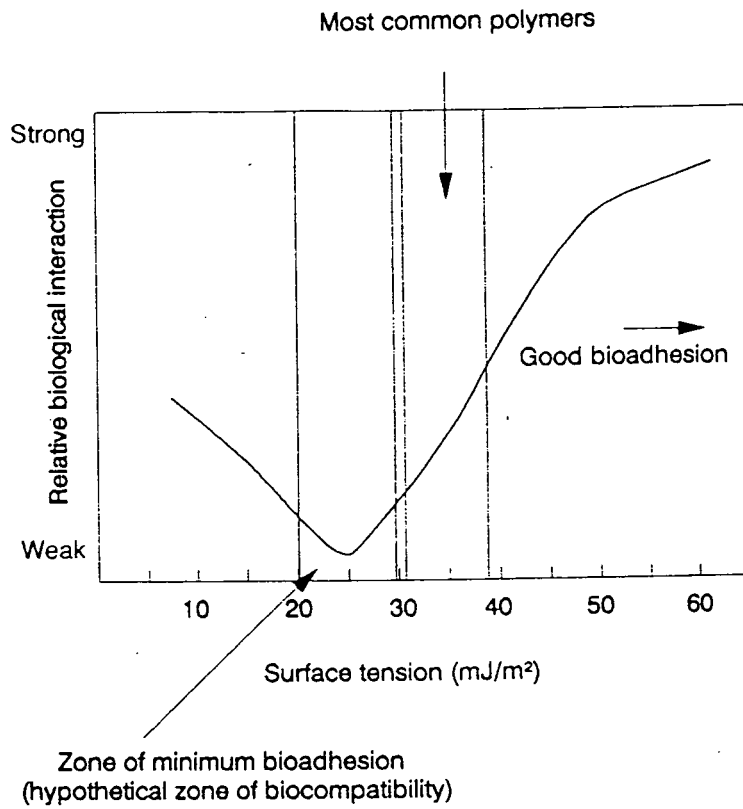
Figure 1.2   **Correlation between surface tension of materials and their biological interaction. After Baier et al[43].**

1.3. SURFACE MODIFICATION OF POLYMERS FOR ENHANCED BIOCOMPATIBILITY

We have already discussed some of the polymers used for biomedical applications in section 1.1.1, and in the majority of cases the biocompatible response at the surface of the polymer was determined by its bulk chemical structure. This section outlines some of the methods which can be employed to 'engineer' the biological response of the polymer surface. The commonest approaches which facilitate some control of the surface properties of the polymer are via the modification of its bulk chemical structure. This involves the incorporation of a polymer with desirable chemical and physical properties in to the structure of the polymer which we intend to use in the biological environment. This can be achieved by two methods, block co-polymerization of each polymer or by the blending of one polymer in another. These approaches have found application in the fabrication of replacement joints, where the material of choice often possesses the necessary mechanical properties of strength and durability but exhibits poor interfacial biocompatibility. Alternatively this could be of value in a controlled drug release matrix where the blended or co-polymerized polymer can be designed to degrade at a specific rate suitable for the particular *in-vivo* application and therefore exhibit desirable drug release kinetics[50].

1.3.1. Polymer Blends

Blended polymer systems constitute one polymer phase dispersed within another as shown in Figure 1.3a, the free energy of mixing (ΔG_{MIX}) (1.1) depends upon enthalpic (ΔH_{MIX}) and entropic (ΔS_{MIX}) terms which can be related to the molecular characteristics of the components in the system, such as molecular weight for example using the Flory-

Huggins theory[51].

$$\Delta G_{MIX} = \Delta H_{MIX} - T\Delta S_{MIX} \qquad (1.1)$$

The study of the surfaces of polymer blends differs markedly from the study of bulk mixtures of polymers and requires an appreciation of the effect of introducing a surface on the rules applied to understand the bulk phase structure. Generally we expect the component with a lower surface energy to dominate the surface of the polymer, and the surface composition is consequently enriched in that component. This seems fairly straightforward, however surface enrichment leads to de-mixing of the polymer phases and a reduction in the entropic contribution. A balance between the surface energetics which favours the enrichment of the lowest energy component at surface versus the free energy of mixing is observed in most cases.

A wide range of two component polymer blends have been studied to date, and these have included poly(methyl-methacrylate)/poly(vinyl-chloride) (PMMA/PVC)[52], poly(ε-caprolactone)/poly(vinyl-chloride) (PCL/PVC)[53] and poly(styrene)/poly(vinyl-methylether) (PS/PVME)[54]. However techniques such as X-ray photoelectron spectroscopy (XPS), static secondary ion mass spectrometry (SSIMS) and neutron reflectometry which are surface sensitive enough to characterise the segregation phenomena tend to operate under non-physiological conditions conditions. This has prevented the study of segregation at the surface/liquid interface and with the exception of a recent paper by Davies et al[55] concerning immiscible and miscible blends of poly(sebacic anhydride)/poly(lactic acid) (PSA/PLA) few blends have been examined with a view to their development as biomedical materials.

1.3.2. Co-polymerization

Block co-polymerized systems differ from polymer blends in their degree of connectivity, that is the respective components of the mixture are covalently bonded to each other as we can see in Figure 1.3b. Although many of the theoretical approaches that were used for blended systems can be applied to co-polymer surfaces, the theory must take in to account the limiting effect of the respective block lengths of each component on the domain sizes of each phase, in addition to molecular weight and the preparation conditions.

In common with blended multi-component systems, co-polymerized materials exhibit a degree of segregation of one component at the surface. By careful selection of each component based upon their chemical structure and by varying their relative amounts it has been possible to design surfaces with remarkably different surface properties compared to either of the component polymers. Segmented polyurethanes (SPU)[56] composed of alternating hard blocks containing aliphatic of aromatic di-isocyanates and soft blocks containing polyester or polyether materials have shown great promise as blood contacting materials. However their excellent biocompatibility is not thoroughly understood. There is general agreement that the SPU surface is highly mobile, and the soft segments tend to dominate the interfacial region. Some groups have suggested that the presence of the soft segment chains prevent protein adsorption by steric exclusion[57], whereas in another study Ratner[47] used this system to validate his suggestion that it is the balance of polar and apolar domains at the interface that confers biocompatibility. Other materials that have been developed for their surface segregation properties include poly(methyl-methacrylate)-co-poly(ethylene-glycol-methacrylate)[58]

and poly(ethylene-oxide)-co-poly(lactide-co-glycolide)[59] systems to name a few of the many.

1.3.3. Chemical Modification of Surfaces

Despite the large amount of work aimed at tailoring the bulk compositions of polymers to improve interfacial biocompatiblity, an alternative and increasingly common approach over recent years has involved the chemical and physical modification[60] of the polymer surface. The drive to exploit the complex interactions of polymer surfaces with surrounding environment has led to interest in methods able to control the nature, distribution and orientation of functional groups on the surface of the polymer.

Oxidation of poly(propylene) (PP) and poly(ethylene) (PE) by concentrated solutions of chromic acid was first devised as a method of improving metal-polymer adhesion, this was attributed to the roughening of the polymer surface which occurred due to the preferential etching of the more amorphous areas of the polymer[61]. Later work[62] demonstrated that the etching reaction led to chemical as well as mechanical modification and XPS analysis has shown the presence of hydroxyl, carbonyl, and carboxyl groups[63,64]. Hydrolysis of polymers using strong bases such as NaOH and KOH have been used to increase the hydrophilicity of polymers such as PET[65], poly(imide)[66] and poly(ester)[67]. Finally alkali metal based etchants have been successfully used to functionalise unreactive fluorocarbon containing polymers[68,69].
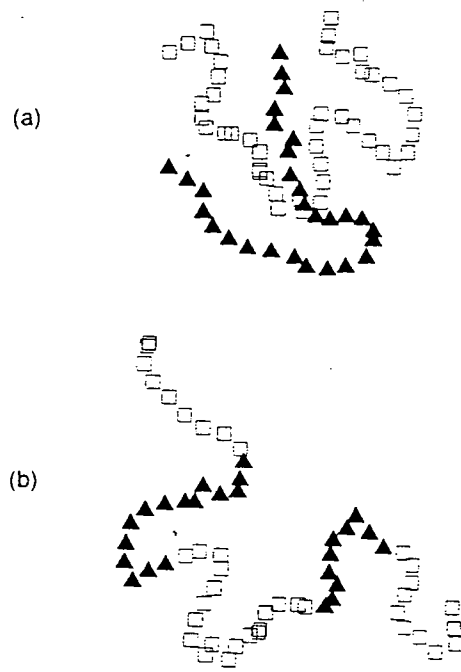
Figure 1.3   Schematic representation of a blended (a) and a co-polymerized polymer (b).

1.3.4. Chemical Grafting

The chemistry described in section 1.3.3 can be used to alter the physico-chemical properties of a range of polymer materials. This is important for a range of applications ranging from adhesion, wetting and the primary functionalisation of the surface. More interestingly, the hydroxyl, carbonyl and carboxyl functionalities can be further reacted to introduce larger moieties. This process is known as *chemical grafting* and it involves the covalent bonding of new macromolecules on the substrate surface rather than concentrating on the modification of existing polymer chains. The oxidative etching of the surface can be considered an initiation step which enables the further reaction of the surface. In practice however the activation of a polymer surface can be achieved using UV irradiation or glow discharge treatments (discussed in section 1.3.5) in preference to the wet chemical treatments, because they tend to produce a cleaner surface and require less harsh reagents.

The chemical grafting[17] of poly(ethyleneoxide) (PEO)[70,71] to surfaces has proven to be a common route to more bioresistant surfaces. These materials have been shown to provide a neutral, hydrophilic, steric barrier which is extremely efficient at preventing biomacromolecular adsorption[29]. Grafting of natural macromolecules to surfaces has been a major development. Collagen[72,73] and a range of polysaccharides[74,75] have been successfully grafted on to a range of surfaces using redox systems such as ceric (IV) ions or potassium persulphate to activate the hydroxyl functionalities on the surface. The immobilisation of species such as heparin[76,77], a well known anticoagulant and albumin[78], a major blood plasma protein to polymer surfaces has been shown to significantly reduce non-specific adsorption of proteins leading to thromboresistant surfaces.

1.3.5. Glow-discharge Modification

Plasma[60, 79, 80], ion beam and electrical discharge[81] treatments have had an increasing role to play in polymer surface modifications and have proven to be an extremely versatile method of altering surface functionality and morphology[82]. The deposition of plasma polymers and the direct modification of surfaces has been used to minimise interfacial energies[83]. This has been achieved for example, by the introduction of hydrophilic groups at polymer surfaces using water and oxygen plasma treatments[84]. Glow discharge treatments have been used to initiate the grafting of acrylic acid, methacrylic acid and acrylamide[85, 86], glycidyl acrylate and methacrylate monomers[87]. Finally, the bombardment of poly(propylene) membranes using an ammonia plasma has led to amino functionalised[79] membranes which can be used to selectively bind albumin.

1.3.6. Bioactive Polymer Systems

As the uses of polymeric biomaterials[8, 35, 88-90] in the medical industry have become more diverse and allied with a growth in molecular bioengineering, the possibility of constructing specific molecular architectures at the polymer/biophase interface and developing materials which promote highly selective surface interactions[91] has become an attractive goal for biomaterial researchers. This has generated much excitement and lead to a growing liaison between polymer scientists and molecular biologists.

The incorporation of biofunctional units such as cell receptors, antibodies or enzymes into macromolecular systems has great possibilities, and polymers able to exhibit true biomolecular recognition have potential application in areas such as

controlled drug delivery[92-94], controlled drug release[8,35,90] agents and as diagnostic assays or biosensors[3,95]. With reference to this thesis, these types of materials could enable highly efficient protein chromatography [96,97-99] and blood purification systems[9,96,100-102] to be developed.

It is possible to characterize the recognition sites of important proteins and peptides, synthesize the corresponding peptide fragment and immobilize[78,103,104] it on a support. However, initial indications[105] suggest that the immobilised biomolecules are extremely sensitive their microenvironment, their stability and bioactivity are often compromised by the nature of the polymer support. Therefore the successful exploitation these systems will require a remarkable advance in the understanding of molecular structure and dynamics at polymer interfaces.

1.4. BIOSEPARATION

1.4.1. Introduction

Bioseparation is based on chromatographical procedures pioneered in the years following its initial discovery[106,107] in 1903. The technique has since evolved into an experimentally simple, rapid, reproducible, high resolution technique with high recovery rates for the purification of biomolecules[96]. The development of rigorous approaches to biomolecular chromatography and a growth in high performance techniques in the early 1980s has enabled bioseparation systems to become essential research and development tools in virtually every area of life science. The application of instrumental methods that are capable of quantitatively determining changes in composition, topology and dynamics of biomacromolecules have made significant contribution to the understanding of

fundamental issues such as the biological process involved in integrated cellular responses, protein folding and domain assembly, protein and biopolymer aggregation and biomolecular recognition[91].

On a wider perspective, biopharmaceutical and biotechnological quality control, vaccine development, industrial food manufacture, blood dialysis, and the growth in gene technology have all benefited from growing research in to process bioseparation[108-110]. New challenges to the wider scientific community involve the scaling up and commercialisation of laboratory bioseparation processes.

1.4.2. Chromatographic Considerations

In 1968 a general definition for separation was proposed by Rony[111], *'Separation is the hypothetical condition where there is complete isolation, by m separate macroscopic regions, of each of the m chemical components which comprise a mixture. In other words, the goal of any separation process is to isolate the m chemical components, in their pure form, into m separate vessels.'*

Bioseparation is the process of separation or partition of biomacromolecular species from a biological liquid phase, this may be on the basis molecular size and/or shape, affinity for a particular chemical functional group, electrostatic attraction for ionic sites or as a result of hydrophobic interactions, examples of which are shown in Figure 1.4. Separation is achieved by virtue of the differing nature of interaction of the biosolutes with the mobile and stationary phase.
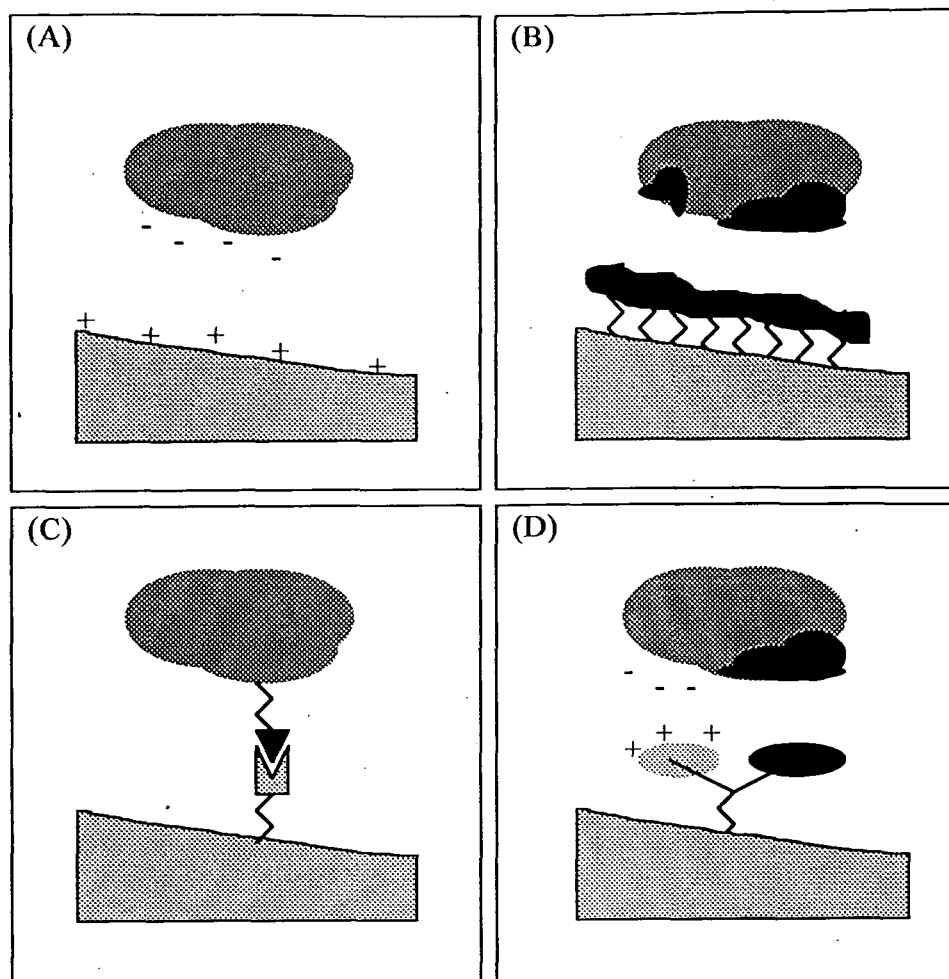
Figure 1.4   Schematic representation of the more common modes of biomolecule ligand interaction; **(A)** ion exchange : interaction between oppositely charged ionic groups; **(B)** reversed phase/hydrophobic interaction : interaction of mainly hydrophobic moities of biomolecule and stationary phase; **(C)** affinity interaction : ligand tailored to specific chemical functionality of biomolecule; **(D)** mixed mode system : combined ionic and hydrophobic interaction.

When the interaction of a specific biosolute with the stationary phase is strong then that solute is retained in the matrix to a greater extent than another component that interacts less strongly. Therefore, solute zones containing to each component migrate through the column at differing velocities, and are separated in the process.

The type of interaction between the stationary phase and the biosolute which is used to promote the separation of the component molecules must be based upon knowledge of the physicochemical properties of the biomolecules in the mobile phase, and must also reflect the required resolution, recovery and speed of separation. One or even a combination of the methods mentioned above can be applied to optimise performance. For example the separation of mixtures of proteins with a wide range of molecular weights can be achieved purely on the basis of molecular size using size exclusion chromatography[112] by passing the mixture through a stationary phase with a well defined pore structure. Amino acids can be separated on the basis of ion exchange[113] interactions, whereas other more complex dye affinity ligands have been designed to combine with ionic and hydrophobic moities of more complicated target molecules.

1.4.3. Factors Affecting the Performance of a Chromatography System

Several publications have discussed in a great amount of mathematical detail the theory and limitations of chromatographical separation[96, 114, 115], however only a general appreciation is required for the purposes of this thesis. In the majority of cases the poor performance of a chromatography system or loss of bioactivity of the biomacromolecules following separation can be linked to factors related to the mobile and stationary phases. The pH, temperature, ionic strength and buffer composition of the mobile phase are

parameters which require careful tuning in order to optimise performance[116]. The properties of the stationary phase however are much more difficult to adjust. Chemical and physical properties governing the efficiency of the matrix include ligand composition, ligand density, surface heterogeneity, surface area and pore structure. Inhomogenieties in the stationary phase, non linear flow characteristics, resistance to diffusion and inappropriate kinetics of solute distribution between the mobile and stationary phases cause differential retention effects and variable residency times. This can lead to non-linear adsorption processes[117,118], which appear as peak broadening, poor resolution, and may influence mass and bioactivity recovery.

Loss of bioactivity in protein purification has been associated with conformational reordering of proteins[34] on the stationary phase, and this has been shown to cause multizoning of the components in to active and inactive fractions. Another phenomena often observed in affinity chromatography separations is known as the *split breakthrough effect* which has been linked to poor surface area-ligand accessibility characteristics[119].

In summary, it is apparent that the separation process can be optimised by careful choice of the mobile phase. However it is the properties of the stationary phase that ultimately defines the limits of performance of the separation column. The aim is therefore to design a stationary phase that meets as many of the criteria discussed above. This will enable the most efficient partition of the components in a mixture, with maximum recovery and a retention of activity, this is a challenging target for the polymer scientist and must be considered the ultimate goal of the chromatographer.

1.5. STATIONARY PHASES FOR HIGH PERFORMANCE BIOSEPARATION

1.5.1. Introduction

The rapid developments in high performance liquid chromatography of low molecular weight materials at the beginning of the 1960's were due to the development of porous microparticulate silica materials[120]. By the early 1980's the manufacture and modification of silica based packing materials had been refined to such a high degree that an unparalleled speed, specificity and selectivity in chromatographic separation became possible. This has enabled high performance liquid chromatography to dominate over most other forms of analytical chemical separation techniques.

Despite the great advances in the high performance separation of mixtures of low molecular weight compounds, the development of silica based materials which exhibit similar performance characteristics for the separation of biomolecules has proven much more difficult for two main reasons. Firstly, the hydrolytic cleavage of siloxane bonds confers poor chemical stability and solubilization[121] of the silica matrix has been demonstrated at pH > 9. Secondly, the presence of weakly acidic silanol groups on the surface of silica promotes undesirable non-specific adsorption of biomacromolecules from aqueous solution[122, 123]. However, the use of ionic/alkylated surfactants, and the physical or chemical immobilisation of polymeric coatings[124] on the silica particles has enabled many of the major problems to be alleviated and consequently bioseparation systems based on silica packing materials have become the market leading products. Even so, these *bonded* silica phases[125] are far from ideal and are characterised by relatively poor chromatographic resolution and often cause a loss in bioactivity of the immobilised biomolecule. This is thought to be due to the energetic and geometric

heterogeneity[120] of the silica surface and the tortuosity and connectivity of the pore structure which tends to slow the mass transfer kinetics of the system.

As well as the continued drive to develop polymeric coatings which will improve the level of performance of existing silica based technology, there has been over the last few years an increasing amount of research focused on replacing the silica stationary phase altogether. Polymeric bioseparation matrices have proven attractive because they promise greater biocompatibility, and have greater chemical stability at basic pH than existing silica materials and also because of the wide range of functional reactive groups that can be incorporated in to the surface of the support.

1.5.2. Polymeric Bioseparation Materials

Historically, the classical packing materials for bioseparation applications were soft gels based upon polysaccharides[126,127] for example agarose, cellulose and dextrans, and hydrophilic synthetic polymers[128] such as polyamides and poly(acrylamides). These types of materials formed a wide range of extremely versatile liquid chromatography systems which could be easily modified depending on the required chromatographic mode. Until recently however, the poor mechanical stability of these polymeric packing materials prevented their use as high performance chromatography stationary phases.

Hence there is a strong case for the development of new polymer based bioseparation materials with suitable mechanical and chemical stability. Research in to polymeric stationary phases has grown to the point where several of the commercially available immobilised proteins and enzymes are obtained through the use of organic matrices[78]. Synthetic porous and non-porous polymer matrices based upon poly(methy-

methacrylate)[129], poly(styrene-divinylbenzene)[130] and polyolester copolymers[131] have been synthesised, and exhibit properties rivalling those of the traditional silica support materials. Crosslinking[132] of natural polymers such as polysaccharides with bis-epoxides, glycidylethers and divinylsulphones[133] coupled with the use of chromatography columns which give the matrix more support, have been shown to improve mechanical stability at the high flow rates required for high performance separation whilst maintaining the favourable chemical properties which made them effective as liquid chromatography systems.

1.6. OUTLINE OF THESIS

This section briefly outlines the structure of the following chapters which comprise this thesis. Chapter 2 contains a brief account of each of the analytical techniques used in the subsequent experimental chapters and provides a source of background information for the reader. Each of the experimental chapters 3-7 contain more detailed experimental information pertaining to the particular techniques which we have employed with reference to the aspect of the surface chemistry of the materials which we have examined.

We have concentrated on two contrasting types of polymeric material during the course of this project, cellulose and poly(tetrafluoroethylene) (PTFE), both were attractive candidates due to their mechanical and chemical stability, although they differed widely in their surface reactivity. The crystallinity of a range of celluloses was examined in chapter 3. In chapter 4 we took this further and investigated how the pore structure of an amorphous cellulose matrix was affected by chemical treatment and examined the link between pore structure and protein binding. Later studies focussed on

the surface modification of PTFE using sodium naphthalenide and its subsequent functionalisation; this is examined in chapter 5. Chapter 6 was concerned with the analysis of the chemical and structural properties of the etched layer. The nature of the defluorination reaction was examined in more detail in chapter 7. Chapter 8 contains the concluding remarks.

1.7. REFERENCES

1   Hench L L, Wilson J, *Mat. Res. Symp. Proc.*, **55**, 65 (1986).

2   Tighe B. J., *Macrmol. Chem.*, **17**, 375 (1982).

3   Ratner B. D., Castner D. G., Horbett T. A., Lenk T. J., Lewis K. B., Rapoza R. J., *J. Vac. Sci. Technol. A.*, **3**, 2306 (1990).

4   Dekker A., Beugeling T., Wind H., Poot A., Bantjes A., Feijen J., *J. Mater. Sci. : Mater. Med.*, **2**, 227 (1991).

5   Szycher M. (Ed.), *Biocompatible Polymers, Metals and Composites*, Technomic, Lancaster PA, 1983.

6   USP XVIII, *The Pharmacopeia of the USA* (18th Revision), US Pharmacopoeial Convention Inc., Rockville, Maryland, Sept. 1 1970.

7   Desilets C. P., Hollinger J. O., Marten L. M., Quigley N., *Polym. Mater. Eng.*, **62**, 719 (1990)

8   Dumitriu S., *Polymeric Biomaterials*, Dekker Inc., New York, 1994.

9   Uzhinova L. D., Plate N. A., Krasovkaja S. M., *J. Mater. Sci. : Mater. Med.*, **2**, 189 (1991).

10   Lee J. M., *Mat. Res. Symp. Proc.*, **55**, 39 (1986).

11   Woodward E. G., Interdisciplinary Sci. Rev., 7, 53 (1982).

12   Triolo P. M., Andrade J. D., *J. Biomed. Mater. Res.*, **17**, 149 (1983).

13   Tighe B J, *Chem. Ind.*, **21**, 796 (1981).

14   Groenwall A, Ingelman B., *Vox. Sang.*, **47**, 96 (1984).

15   Hastings G. W., Ducheyne P., *Macromolecular Biomaterials*, CRC Press, Boca Raton, 1984.

16   Shea J. J., Sanabria F., Smyth G. D., *Arch. Otolaryngol.*, **76**, 516 (1962).

17   Ratner B D, Weathersby P K, Hoffman A S, *J. App. Polym. Sci.*, **22**, 643 (1978).

18   Briggs D., Hearn M. J., Ratner B. D., *Surf. Inter. Anal.*, **6**, 184 (1984).

19   Hearn M. J., Ratner B. D., Briggs D., *Macromolecules*, **21**, 2950 (1988).

20   Planck H., Egbers G., Syré I., *Polyurethanes in Biomedical Engineering*, Elsevier, Amsterdam, 1984.

21   Stolnik S., Dunn S. E., Garnett M. C., Davies M. C., Coombes A. G. A., Taylor D. C., Irving M. P., Purkiss S. C., Tadros T. F., Davis S. S., Illum L. I., *Pharm. Res.*, **11**, 1800 (1994).

22   Allémann E., Gurny R., Doelker E., Skinner F. S., Schütz H., *Proc. Int. Symp. Control. Rel. Bioact. Mater.*, **20**, 129 (1993).

23   Gref R., Minamitake Y., Peracchia M. T., Trubetskoy V., Torchilin V., Langer R., *Science*, **263**, 1600 (1994).

24   Salthouse T. N., *J. Biomed. Mater. Res.*, **10**, 197 (1976).

25   Sevastjanova N. A., Mansurova L. A., Dombruska L. E., Slutskii L. L., *Biomaterials*, **8**, 242 (1987).

26   Hastings G. W., Ducheyne P. (Eds.), *Macromolecular Biomaterials*, CRC Press, Boca Raton, 1984.

27   Merritt K., *Biomaterials*, **5**, 47 (1984).

28   Anderson J. M., Miller K. M., *Biomaterials*, **5**, 5 (1984).

29   Harper G., Davies M. C., Davis S. S., Illum L. I., Taylor D., Irving M., Tadros T. F., *Biomaterials*, **12**, 695 (1991).

30   Annis D., Fisher A. C., How T. V., de Cossart L., *Polymers in Medecine*, Migliaresi C. Ed. Vol. 29, Plenum Press, New York 1986.

31   Vroman L., Leonard E. F., *Ann. N. Y. Acad. Sci.*, **283**, 1 (1977).

32   Sieg J. W., Robinson J. R., *J. Pharmaceut. Sci.*, **65**, 1816 (1976).

33   Anderson J. M., Kottke-Marchant K., *CRC Critical Reviews in Biocompatibility*, Vol. 1, Issue 2, pp. 111-204, CRC Press, Boca Raton, 1985.

34   Andrade J. D. (Ed.), Surface and Interfacial Aspects of Biomedical Polymers, Vol. 2, Plenum, New York, 1985.

35   Shalaby S. W., Ikada Y., Langer R., Williams J. Eds., *ACS Symp. Ser.*, **540** (1994).

36   Billmeyer F. W. Jr., *Textbook of Polymer Science*, 3rd Ed., Wiley, 1984.

37   Holly F. J., *Refojo M. F., Biomed. Mater. Res.*, **9**, 315 (1975).

38   Srinivasan S., Sawyer P. N., *J. Colloid Inter. Sci.*, **32**, 456 (1970).

39   Sawyer P. N., *Ann. N. Y. Acad. Sci.*, **416**, 561 (1984).

40   Boffa M. C., Farges J. P., Dreyer B., Conche B., Pusineri C., Vantard G., Biomaterials, Winter G. D., Gibbon D. F., Plencks H., (Eds.), pp. 399, Wiley, Chichester, 1980.

41   Lyman D. J., Muir W. M., Lee I. J., *Trans. Amer. Soc. Artif. Int. Organs*, **11**, 301 (1965).

42   Baier R. E., *Bull. N. Y. Acad. Med.*, **48**, 257 (1972).

43   Baier R. E., *Proceedings of the Third Internation Conference on Marine Corroison and Biofouling*, Acker R. F., Brown B. F., De Palma J. R., Iverson W. P.,(Eds.), pp 633,Northwestern University Press, Illinois 1973.

44   Andrade J. D., *J. Ass. Adv. Med. Inst.*, **7**, 110 (1973)

45   Andrade J. D., *J. Intel. Mater. Syst. Struct.*, **5**, 612 (1994).

46   Brash J. L., in *Biocompatible Polymers, Metals and Composites*, Szycher M. (Ed.), Technomic, Lancaster PA, pp. 35-52, 1983.

47   Ratner B. D., Hoffman A. S., Hanson S. R., Harker L. A., Whiffen J. D., *J. Polym. Sci. Polym. Symp.*, **66**, 363 (1979).

48   Sharma C. P., *Biomaterials*, **2**, 57 (1981).

49   Ikada Y., *Adv. Polym. Sci.*, **57**, 103 (1984).

50   Shakesheff K., Chen X. Y., Davies M. C., Domb A., Roberts C. J., Williams P. M., *Langmuir*, **11**, 10 (1995).

51   Flory P. J., *Principles of Polymer Chemistry*, Cornell University Press, Ithaca N. Y., 1953.

52   Schmidt J. J., Gardella J. A. (Jr.), Salvati L. (Jr.), *Macromolecules*, **22**, 4489 (1989).

53   Clark M. B. (Jr.), Burkhadt C. A., Gardella J. A. (Jr.), *Macromolecules*, **22**, 4495 (1989).

54   Bhatia Q. S., Pan D. H., Koberstein J. T., *Macromolecules*, 21, 2166 (1988).

55   Davies M. C., Shakesheff K. M., Shard A. G., Domb A., Roberts C. J., Tendler S. J. B., Williams P., *Macromolecules*, 29,2205 (1996).

56   Planck H., Egbers G., Syre R., (Eds.), *Polyurethanes in Biomedical Engineering*, Elsevier, Amsterdam, 1984.

57   Yoon S. C., Ratner B. D., *Polymer Surface Dynamics*, Andrade J. D., (Ed.), Plenum Press, New York, 1988.

58   Shard A. G., Davies M. C., Tendler S. J. B., Nicholas C. V., Purbrick M. D., Watts J. F., *Macromolecules*,28,7855 (1995).

59   Shard A. G., Davies M. C., Volland C., Kissel T., *Macromolecules*, 29, 748 (1996).

60   Poncin-Epaillard F., Legeay G., Brosse J., *J. App. Polym. Sci.*, 44, 1513 (1992).

61   Fitchmun D. R., Newman S., Wiggle R., *J. App. Polym. Sci.*, 14, 2441 (1970).

62   Briggs D., Brewis D. M., Konieczo M. B., *J. Mater. Sci.*, 11, 1270 (1976).

63   Lee K. W., McCarthy T. J., *Macromolecules*, 21, 309 (1988).

64   Lee K. W., McCarthy T. J., *Macromolecules*, 21, 2318 (1988).

65   Namboori C. G. G., Haith M. S., *J. App. Polym. Sci.*, 12, 1999 (1968).

66   Lee K. W., Kowalczyk S. P., Shaw J. M., *Polymer Preprints*, 31, 712 (1990).

67   Zeronian S. H., Wang H. Z., Alger K. W., *J. App. Polym. Sci.*, 41, 527 (1990).

68   Bee T. G., Dias A. J., Franchina N. L., Kolb B. U., Lee K. W., Patton P. A., Schoichet M. S., McCarthy T. J., *Polymer Surfaces and Interfaces II*, Feast W. J., Munro H. S., Richards R. W., (Eds.), pp 1-25, Wiley, Chichester, 1992.

69   Garbassi F., Morra M., Occhiello E., *Polymer Surfaces-From Phsics to Technology*, pp243, Wiley, Chichester, 1994.

70   Amiji M., Park K., *Biomaterials*, 13, 682 (1992).

71   Peracchia M. T., Gref R., Minamitake Y., Domb A., Langer R., *Proc. Int. Symp. Control. Rel. Bioact. Mater.*, 21, 513 (1994).

72   Rao K. P., Joseph K. T., Nayudamma Y., *J. Appl. Polym. Sci.*, 16, 975 (1971).

73   Patil D. R., Smith D. J., , *J. Appl. Polym. Sci.*, 40, 1541 (1990).

74   Hermans J. J., *Pure Appl. Chem.*, **5**, 147 (1962).

75   Garnett J. L., *Cellulose:Structure, Modification and Hydrolysis*, Young R. A., Rowell R. M., (Eds.), Wiley, New York, 1986.

76   Lyman D. J., *Rev. Makromol. Chem.*, **1**, 355 (1966).

77   Casu B., *in Polymeric Biomaterials*, Dimitriu S. (Ed.), Marcel Dekker Inc., New York, 1994.

78   Taylor R. F. (Ed.), *Protein Immobilization, Fundamentals and Applications*, Marcel Dekker Inc., New York, 1991.

79   Kusabiraki M., *Jap. J. App. Phys.*, 29, 2809 (1990).

80   Chawla A. S., *NATO ASI Series E.*, **106**, 231 (1986).

81   Greenwood O. D., Tasker S., Badyal J. P. S., *J. Polym. Sci.: A Polym Chem.*, **32**, 2479 (1994).

82   Hopkins J., Badyal J. P. S., *Macromolecules, J. Phys Chem.*, **99**, 4261 (1995).

83   Yasuda H., Gasicki M., *Biomaterials*, **3**, 69 (1982).

84   Klee D., Gribbin D., Kirch D., *Angew. Makromol. Chem.*, **131**, 145 (1985).

85   Allmer K., Hult A., Ranby B., *J. Polym. Sci., Polym. Chem.*, **26**, 2099 (1988).

86   Uchida E., Uyama Y., Iwata H., Ikada Y., *J. Polym. Sci., Polym. Chem.*, **28**, 2837 (1990).

87   Allmer K., Hult A., Ranby B., *J. Polym. Sci., Polym. Chem.*, **27**, 3405 (1989).

88   Braybrook J H, Hall L D, *Prog. Polym. Sci.*, **15**, 715 (1990).

89   Peppas N. A., Langer R., *Science*, **263**, 1715 (1994).

90   Donaruma L. G., Vogl O., Eds., *Polymeric Drugs*, Academic Press, New York, 1978.

91   Hoffman A. S., *Artif. Organs.*, **16**, 43 (1992).

92   Duncan R., Kopacek J., *Adv. Polym. Sci.*, **57**, 51 (1984).

93   Kim S. W., Petersen R. V., Feijen J., *Polymeric Drug Delivery Systems in Drug Design*, pp 193-245, Ariens E. J., Ed., Academic Press, New York, 1980.

94   Tomlinson E., Davis S. S. Eds., *Site* Specific *Drug Delivery*, Wiley, Chichester, 1986.

95   Hall E. A. H., *Biosensors*, Open University Press, Milton Keynes 1990.

96   Hearn M. T. W. (Ed.), in *HPLC of Proteins Peptides and Polynucleotides*, pp1-35, VCH, New York, 1991.

97   Griesser H. J., Chatelier R. C., Gengenbach T. R., Vasic Z. R., Johnson G., Steele J. G., *Polym. Int.*, **27**, 109 (1992).

98   Royston W. P, Ratner B. D., *Surf. Interf. Aspect. Biomed. Polym.*, **2**, 189 (1984).

99   Uvdal K., Bodo P., Liedberg B., *J. Coll. Int. Sci.*, **149**, 162 (1992).

100   Everhart D. S., Reilley C. N., *Anal. Chem.*, **52**, 655 (1981).

101   Jacobs H., Okano T., Kim S. W., *Artif. Organs.*, **12**, 506 (1988).

102   Ratner B. D., Johnston A. B., Lenk T. J., *J. Biomed. Mater. Res: App. Biomat.*, **21**, 59 (1987).

103   Meirovitvh H., Rackovsky S., Scheraga H. A., *Macromolecules*, **13**, 1398 (1980).

104   Hayward J. A., Durrani A. A., Shelton C. J., Lee D. C., Chapman D., *Biomaterials*, **7**, 126 (1986).

105   Pierschbacher M. D., Ruoslahti E., *Nature*, **309**, 30 (1984).

106   Tswett M., *Trav. Soc. Nat.*, **14**, 1903 (1903).

107   Tswett M., *Ber. Deut. Botan. Ges.*, **24**, 385 (1906).

108   Rousseau R. W., *Handbook of Separation Process Technology*, Wiley, New York, 1987.

109   Hamel J. F. P., Hunter J. B., Sikdar S. K., *Downstream Processing and Bioseparation*, American Chemical Society, Washington D. C., 1990.

110   Ladish M. R., Willson R. C., Painton C. C., Builder S. E. (Eds.), *Protein Purification from Molecular Mechanism to Large Scale Processes*, ACS Symp. Ser. 427, Washington D. C., 1990.

111   Rony P. R., *Separ. Sci.*, **3**, 239 (1968).

112   Cox J. M., *Blood Compatibility of Polymers for Biomedical Applications*, B.Sc. Dissertation, 1987.

113   Moore S., Stein W. H., *J. Biol. Chem. Soc.*, **75**, 1460 (1951).

114   Grushka E., *Preparative Scale Chromatography*, Dekker, New York, 1989.

115   Horvath Cs. (Ed.), *High Performance Liquid Chromatography: Advances and Perspectives*, Vol. 5, Academic Press, San Diego, 1988.

116   Hearn M. T. W., in *Chemical Separations*, Navratil J, King C. T. (Eds.), pp 71-88, Litvarian Press, 1986

117   Johnston A., Hearn M. T. W., *J. Chromatgr.*, **512**, 101 (1992).

118   Lin B., Ma Z., Golshan-Shirazi S., Guiochon G., *J. Chromatgr.*, **500**, 101 (1990).

119   Hage D. S., Walters R. R., Heathcote H. W., *Anal. Chem.*, **58**, 274 (1986).

120   Unger K., *Porous Silica*, J. Chrom. Library, Vol. 16, Elsevier, Amsterdam, 1979.

121   Iler R. (Ed.), *Chemistry of Silica*, Wiley, New York, 1979.

122   Unger K. K., *Porous Silica, Its Properties and Use as a Support in Liquid Chromatography*, Elsevier, Amsterdam, 1979.

123   Mizutani T., Mizutani A., *J. Chromatogr. Sci.*, **111**, 216 (1976).

124   Schomburg G., *LC/GC Int. Mag.*, **1**, 34 (1988).

125   Unger K. K., Lork K. D., Wirth H.-J., in *HPLC of Proteins, Peptides and Polynucleotides*, Hearn M. T. W. (Ed.), pp 59-117, VCH, New York, 1991.

126   Porath J., Flodin P., *Nature*, **183**, 1657 (1959).

127   Regnier F. E., Noel R., *J. Chromatogr. Sci.*, **14**, 316 (1976).

128   Majors R. E., *LC Mag.*, **3**, 774 (1985).

129   Burke D. J., Duncan J. K., Dunn L. C., Cumming L., Siebert C. J., Scott G., *J. Chromatogr.*, **353**, 435 (1986).

130   Rounds M. A., Rounds W. D., Regnier F. E., *J. Chromatogr.*, **397**, 25 (1987)

131   Kitagawa N., *J. Chromatogr.*, **443**, 133 (1988).

132   Arnott S., Fulmer A., Scott W. E., Dea I. C. M., Maorhouse R., Rees D. A., *J. Mol. Biol.*, **90**, 269 (1974).

133   Porath J., Låås T., Janson J.-C., *J. Chromatogr. Sci.*, **103**, 49 (1975).

2. EXPERIMENTAL TECHNIQUES

2.1. INTRODUCTION

In general it is the nature of the biosurface[1] that ultimately governs the biological response of the system[2-5], however a complete understanding of the molecular level interactions between synthetic materials and biological systems has yet to be achieved. The surface of a material can be defined as its topmost few atomic layers[6], a $1cm^2$ area of may contain as few as 10^{15} atoms or 10^{-9} mole. An *ideal* surface is generally considered to be that formed from the cleavage at a crystalline plane of a bulk material, resulting in a surface of well defined order. In reality surfaces tend to be much less well defined, atoms deviate from their bulk lattice positions, structural defects and irregularities are common. The geometric and electronic properties differ from the bulk[6] especially when dealing with polymeric systems.

Few definite correlations have been derived between the surfaces of biomaterials and their biological response, but the parameters such as surface compliance, functional group distribution, functional group orientation, surface domain distribution, molecular mobility, surface contamination, and molecular texture[7] have been identified in previous studies as being particularly significant[8]. To date a greater understanding of the processes involved has only been obtained through the use of a wide range of complementary techniques for surface analysis. This chapter is aimed at providing an insight in to the analytical tools used in the subsequent experimental chapters. The techniques covered include X-ray Photoelectron Spectroscopy (XPS), Attenuated Total

Reflectance Fourier Transform Infra-red Spectroscopy (ATR-FTIR), surface area and pore distribution using nitrogen sorption, Atomic Force Microscopy (AFM), Scanning Electron Microscopy (SEM) and X-ray Diffraction (XRD).

2.2. X-RAY PHOTOELECTRON SPECTROSCOPY (XPS)

X-ray photoelectron spectroscopy[9-12] has since the latter half of the 1960's, become a widely used tool for the analysis of solid surfaces and has found application in metallic[13,14], semiconductor[13,15] and polymer[16-19] material studies. The XPS technique involves the determination of the kinetic energies of electrons ejected from core level energy states of atoms using X-ray photons as an excitation source. The energy required to liberate electrons from the core energy states of the atom or molecule of interest is known as the 'binding energy' and is characteristic of the element from which the electron is derived and this enables elemental quantification of the surface layer to depths of approximately 50Å. More subtle variations in the binding energies of photoelectrons ejected from a particular element are termed 'chemical shifts', and these allow the nature of the bonding of the element in the material to be investigated. It is this wealth of detailed chemical structure and bonding information coupled with extreme surface sensitivity that has enabled XPS to become one of the most significant surface analytical techniques in recent times.

2.2.1. The Photoexcitation Process

The basis for the excitation process employed in XPS and first observed by Siegbahn[20] is the absorption of a photon of energy (hυ) by an electron in a core atomic

energy level, leading to its excitation to the vacuum energy level. This manifests itself as the ejection of a photoelectron from the atom with a characteristic kinetic energy E_{KE}, and leads to the formation a singly charged ionic species, Figure 2.1. The kinetic energy of the ejected photoelectron can be measured and related to the core level binding energy E_B using equation (2.1).

$$E_{KE} = h\upsilon - E_B - \phi_{sp} \qquad (2.1)$$

where E_{KE} is the kinetic energy of ejected photo-electron, $h\upsilon$ is the energy of incident photon, E_B is the binding energy of the core level electron and ϕ_{sp} is the spectrometer work function[10,13].

2.2.2. Spectral Features

The binding energies (E_B) of electrons ejected from core level energy states of elements in the periodic table excluding H and He, are sufficiently unique to enable elemental analysis[21] of the material under investigation. Relative peak intensity measurements allow the determination of elemental stoichiometries.

Non-bonding core level electrons are sensitive to valence electron distributions and this leads to small variations in the binding energies. These differences arise due to variations in oxidation state of the atom under examination, its molecular environment for example the effect of highly electronegative neighbouring groups shifts the binding energy of the carbon 1s electron to higher values, as shown in Figure 2.2.
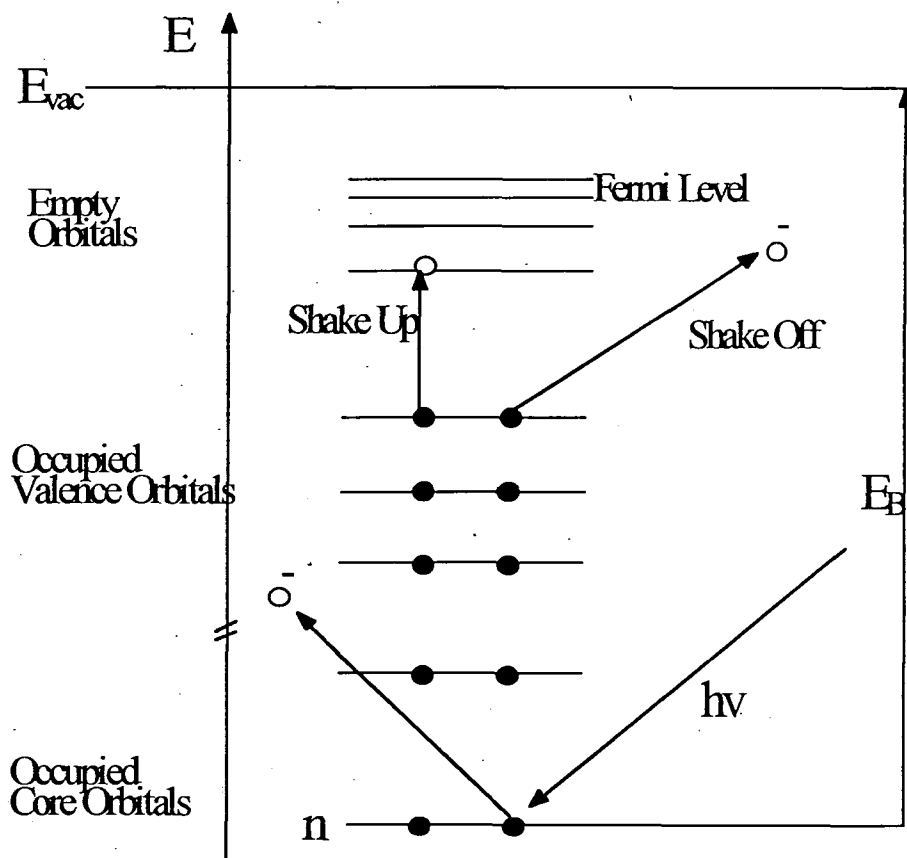
Figure 2.1   Photoexcitation, Shake Up and Shake Off Effects

Core electron removal during photoemission leads to an effective increase in nuclear charge[10,11,13] as far as a valence electron is concerned, this perturbation may lead to simultaneous excitation of a valence electron from an occupied to an unoccupied energy level, and a 'shake-up'[22,23] phenomena may be observed, Figure 2.1. This leads to a peak towards the higher binding energy side of the main photoelectron peak. Conjugated and aromatic organic systems exhibit this type of satellite structure and it has been attributed to $\pi \rightarrow \pi_*$ transitions, apart from these examples the satellite structure has only been significantly prominent in atomic systems e.g. neon gas; and also for certain transition metal and rare earth compounds with unpaired 3f or 4d electrons. Alternatively if this second electron is excited in to a continuum state a 'shake-off' phenomena is observed, see Figure 2.1.

X-ray satellites and ghosts, arise from the non-monochromatic nature of the X-ray emission from standard sources, for example magnesium and aluminium sources produce a series of lower intensity lines, K_β and $K_{\alpha3,4}$. X-ray ghosts are due to impurities within the source, the most common being the Al $K_{\alpha1,2}$ present in the Mg source.

2.2.3. Spectral Deconvolution

It is clearly apparent from Figure 2.2 that the peaks for each of the chemical environments within the molecule are not perfectly resolved. Peak broadening can be attributed to several factors. The X-ray line used to excite the electronic transition has an inherent line width see Table 2.1, lifetime broadening effects in either the initial or final state can lead to Lorentzian shaped broadening of the peaks and there is also a
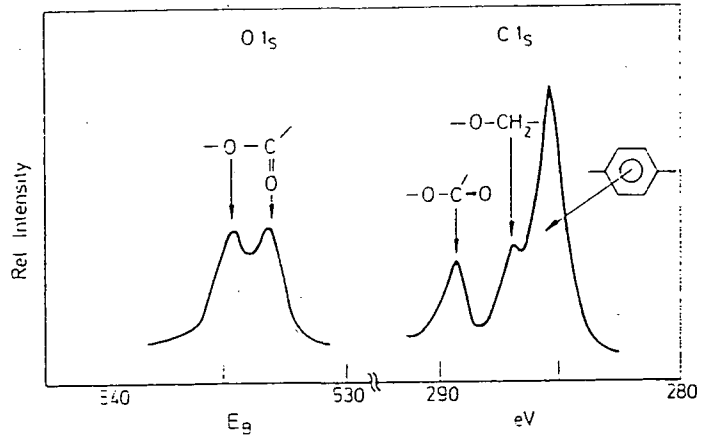
Figure 2.2 **Chemical Shift Information from XPS**
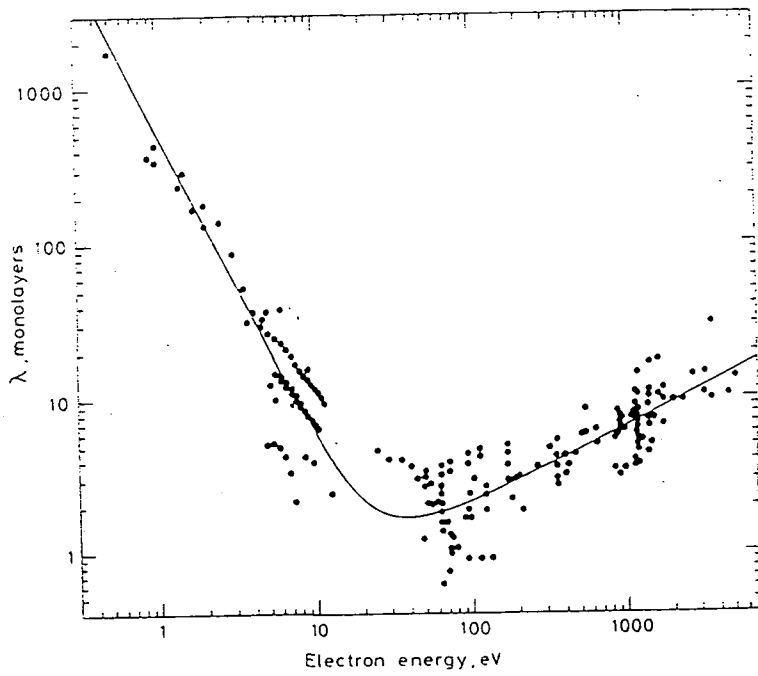
Figure 2.3 **Graph of Inelastic Mean Free Paths vs. Electron Kinetic Energies**

contribution due to the resolving power of the spectrometer itself. All of these factors combined with relatively small chemical shifts can lead to spectra consisting of a number of overlapping peaks. In order to cope with this, deconvolution techniques have been developed to maximise the yield of information from the XP spectra.

XPS peaks can been fitted with a combined Gaussian-Lorentzian peak shape. The Gaussian contribution is due to the finite resolution of the spectrometer and the Lorentzian contribution comes from the incident radiation[24] and a range of computer based fitting algorithms have been developed to enable more accurate fitting of the convoluted spectra.

Table 2.1   Energies and Line widths of the Main X-ray emission Lines for Mg and Al Sources.

X-ray Anode Material	Energy of X-rays/eV	Line width/eV
Mg Kα	1253.6	0.7
Al Kα	1486.6	0.85

2.2.4. Surface Sensitivity

The probability of an electron escaping the sample surface from a given depth following photoexcitation is determined by the magnitude of its kinetic energy. Referring to the graph of inelastic mean free paths (λ) versus electron energy[10], Figure 2.3 it can be seen that at kinetic energies between 1-80 eV there is a great variation in the electron

escape depth of around 1000 atomic layers, at energies between 100-1000 eV which are the energies probed during XPS the average escape depth varies between 5-50 atomic layers.

The inelastic mean free path (λ) of an electron varies as $\sqrt{E_{KE}}$ within energy range of electron spectroscopy[25] and the intensity of electrons (I) emitted from a depth (d) is given by the Beer-Lambert relationship (2.2).

$$I = I_0 \exp(-d/\lambda \sin\theta) \qquad (2.2)$$

where I_0 is the intensity from an infinitely thick clean substrate and θ is the electron take off angle relative to the sample surface. This relationship can be used to show that 95% of the electron intensity emanates within a depth of 3λ at 90° from the surface, and since inelastic mean free paths are in the order of tens of Angströms the extreme surface sensitivity of XPS can be appreciated.

2.2.5. X-Ray Monochromatization

The emission spectrum from an X-ray source is rather complex, having a continuous background signal called Bremsstrahlung, with a series of X-ray emission lines superimposed upon it. Monochromatization provides a much more coherent incident radiation beam, although only a fraction of the of the initial X-ray flux leaves the monochromator. For a particular power dissipation the photon flux is severely reduced compared to unmonochromatised sources.

2.2.6. Sample Charging Phenomena

Surface charging may arise as a consequence of photoionization, however for samples with good electrical conductivity in contact with the spectrometer the potential at the surface can be fixed at zero providing a reference energy level for the binding energy measurements. Insulating materials however, are in poor electrical contact with the spectrometer and the surface will be at a floating potential. An alternative approach to energy referencing is required. The simplest method involves measuring the build up of extraneous hydrocarbon contamination which tends to form a uniform coverage and acquires the same surface potential as the sample. The contamination is almost invariably made up of long chain hydrocarbon material and on an uncharged surface provides a reference binding energy peak at 285eV. On a charged sample the peak is shifted due to the potential build up and this provides a measure of the magnitude of the charging which can be allowed for when interpreting the spectra.

In most conventional XPS spectrometers the photon source is so close to the sample that the flux of electron secondaries emitted by the source serve to counteract the charging. Removal of the Bremmstrahlung background radiation due to monochromatization, removes the electron secondaries and this results in charge build up This necessitates the use of charge compensation which often takes the form of a low intensity electron flood gun[26].

2.2.7. Angular Dependent Studies

Enhanced XPS information[10] can be obtained by varying the 'take off' angle

between the sample and the analyser Figure 2.4, this provides a method for differentiating between the surface and subsurface in a solid sample. Advantage is made of the fact that at low angles of electron exit relative to the sample surface we get enhancement of sensitivity. The vertical sampled depth is given by d, see (2.3) and is related to λ, the attenuation length and angular dependence σ,

$$d = 3\lambda \sin\sigma \qquad (2.3)$$

The angular variation of intensities is given by (2.2), where I is the intensity of the emitted electrons at a given angle. The major assumption of this approach is that the surface is morphologically homogenous; roughness leads to the averaging of electron exit angles and shadowing effects, which reduces the angular resolution and ultimately leads to poorer quality data. At extreme grazing angles some surface sensitivity enhancement is also observed due to the reduction in the penetration depth of the X-ray photons in addition to the angularly resolved detection of the emitted photoelectrons.

2.2.8. Electron Spectroscopy of Polymers

X-ray irradiation of polymeric materials can lead to extensive polymer degradation[27], the sample often becoming discoloured due to radiation effects in the 'bulk' caused by high energy Bremstrahlung radiation. Thermal heating effects can cause higher degrees of degradation, since the sample is placed close to the X-ray source. Excited secondary electronic species passing through the sample can also initiate degradation[28].

e $^-$

X-rays

σ

d

3λ

SAMPLE
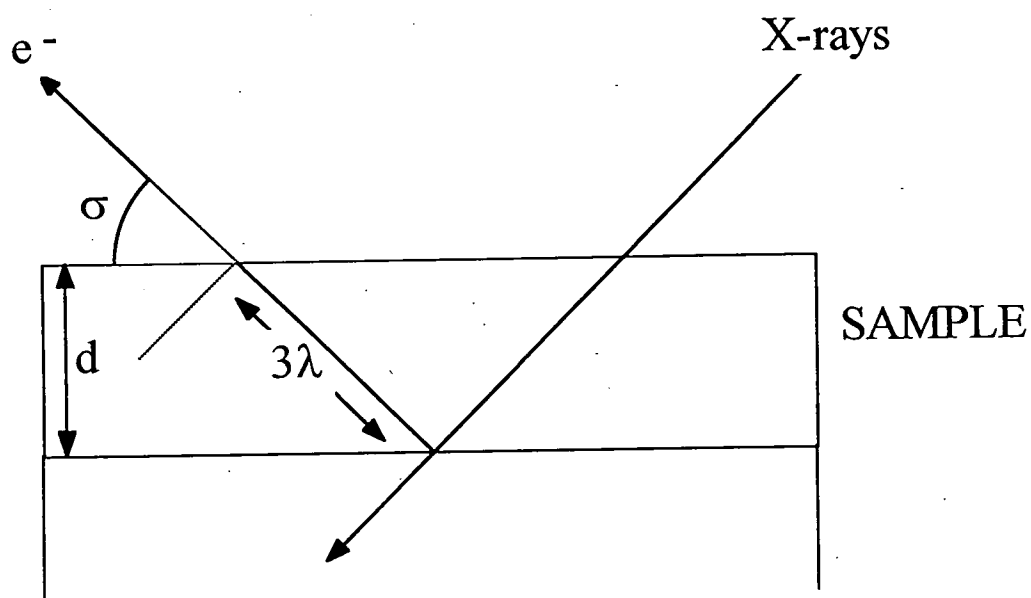
Figure 2.4   **Diagram of Angular Dependency of Depth in XPS Spectroscopy**

In order for the photoelectrons ejected from the surface of a material under analysis to be quantified they must be allowed to reach the detector part of the spectrometer. Consequently the spectrometer must be maintained at ultra high vacuum (UHV) conditions. Maintaining the integrity of a biomaterial within a surface science instrument is an area where problems have been experienced in the past[29], whereas the non-polymeric inorganic single crystal systems adapt well to a UHV environment. Fortunately the many of polymers are reasonably stable[10] under UHV conditions, although evidence of out-gassing of the sample within the spectrometer is often apparent, particularly if the material contains physisorbed gaseous molecules or water vapour. Surface morphologies can suffer extensively, biological molecules are normally hydrated [30,31] and in most cases they require this hydration to maintain their structure. Placing the sample in vacuo leads to excessive out-gassing of specimens with high water contents, this dehydration can cause relaxation of the conformation[31] of the macromolecular adsorbates and potentially alters the intrinsic interfacial interactions. We must also consider such factors as polar group orientation, polymer chain mobility and substrate permeability with respect to the limitations of any surface specific technique involving UHV apparatus. The preservation of the integrity of such samples has almost become a science in itself, and techniques such as rapid freezing, freeze drying[32-34], aerogel formation[35] and critical point drying are becoming widespread. Using pre-outgassed, or frozen samples, choosing particularly volatile solvents in preparation and by minimising the potential for surface beam damage[36] during examination are all methods that have been adopted to try and reduce these complications.

2.2.9. Instrumentation

The X-ray photoelectron spectrometer generally consists of the components shown in Figure 2.5. All analyses are performed in ultra high vacuum (UHV) conditions usually at pressures better than 1×10^{-9} Torr. Photoexcitation is achieved using a 'soft' X-ray source, providing photons at lower energies and flux densities than those used for example in X-ray diffraction. This reduces damage to the sample surface during analysis. Mg or Al K_α lines are used in the majority of instruments due to their convenient photon energies and narrow inherent linewidths, see Table 2.1. electron energy analyser, detector and counting electronics.

The electron energy selection was achieved using concentrically placed hemispherical plates. Energy selection is achieved by means of an applied potential voltage across the two plates. The concentric hemispherical analyser (CHA) was operated in the fixed analyser transmission (FAT) mode where the electrons are decelerated to a constant pass energy providing constant absolute energy resolution at the expense of signal to noise characteristics. Detection of photo-electrons was achieved using a channeltron electron multiplier and the output was fed via an appropriate computer interface to data accumulation software running on IBM PC compatible computer workstations.
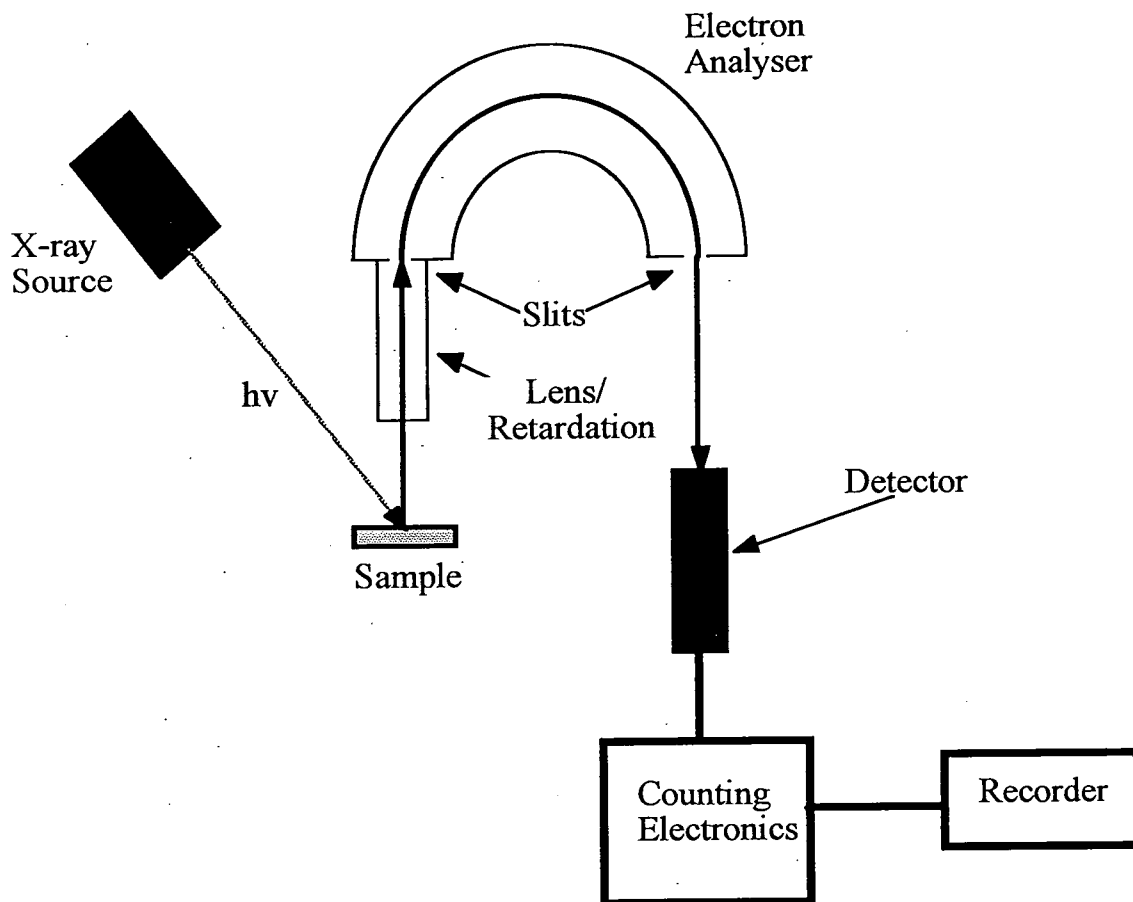
Figure 2.5   Schematic of the XPS Spectrometer

2.3. ATTENUATED TOTAL REFLECTANCE FOURIER TRANSFORM INFRA-RED SPECTROSCOPY (ATR-FTIR)

2.3.1. Background

Molecular vibrations of molecules arise due to the elastic nature of chemical bonds, which can be elongated or twisted, or the angles between bonds which can be changed periodically. The characteristic vibrational frequency of oscillation (v) of a chemical bond can be described by the classical expression for a simple harmonic oscillator see (2.4), where k is the force constant and μ is the reduced mass of the vibrating masses.

$$v = \frac{1}{2\pi}\sqrt{\frac{k}{\mu}} \qquad (2.4)$$

The solution of the Schrödinger equation for a simple harmonic oscillator results in a quantized set of energy eigenvalues which describe the energetic state of the vibrating molecule, see (2.5).

$$E = hv(v + 1/2); v = 0,1,2... \qquad (2.5)$$

Excitation of a molecule from a lower vibrational energy state can occur at infra-red (IR) frequencies and a transition is infra-red active provided that the vibration produces a permanent change in the electric dipole of the molecule. The frequency is related to the relative mass of the covalently bonded atoms, the force constant of the

bond and the geometry of the neighbouring atoms within the molecule. Excitation can be measured as a depletion in the transmitted IR intensity and this occurs at a frequency which is characteristic of the molecular group. Infra-red spectroscopy has therefore evolved as an efficient method for identifying specific chemical groups within a molecule.

2.3.2. Fourier Transform Infra-red Spectroscopy

In general the majority of modern infra-red spectrometers rely upon Fourier transform (FT) processing and multiple averaging of the absorption signal to improve the rate of spectral acquisition and the signal to noise characteristics of the instrument. The development of the Fourier Transform Infra-Red (FTIR) spectrometer has transformed infra-red spectroscopy in to an extremely powerful and sensitive technique for chemical characterisation. This has become possible through the use of the interferometry and the advent of cheaper and faster computing equipment.

FTIR spectrometers are made up of a source, interferometer arrangement and detector array linked to a data processing workstation. The incident radiation is generated by a filament composed of rare-earth oxides maintained at red or white heat by an electric current. The Michelson interferometer is the heart of an FTIR spectrometer, see Figure 2.6 and it consists of one concave and two plane mirrors and a beam splitter which reflects 50% of the radiation falling upon it and transmits the other 50%. The split beams continue and are reflected back from the mirrors M_1 and M_2. The interferometer works by measuring the constructive and destructive interference patterns of the reflected radiation from the plane mirrors M_1 and M_2 as it reaches the meeting point at B. Detecting the change in the interference patterns over time as mirror M_2 is moved

towards and away from the beam splitter and computing the Fourier Transform of this signal allows the frequencies of the incident radiation to be computed. If this interference signal is then passed through a sample prior to detection then the IR absorption spectra of the sample can be determined.

To summarise, the main advantages of this approach are its rapid rates of data acquisition, constant resolving power across the whole frequency range and improved signal/noise characteristics.

2.3.3. Attenuated Total Reflection Spectroscopy

Attenuated total reflection (ATR) infra-red spectroscopy is the most widely used infra-red technique for the surface analysis of biomaterials and polymers[8]. It is based upon the phenomena of total internal reflection of the IR radiation at the interface between a crystal and sample (e.g. a polymer film) of differing refractive indices. Absorption of the infra red radiation occurs in the thin surface layer which is penetrated by the IR beam. The penetration depth is dependent upon the refractive indices of the sample (n_2) and the crystal (n_1) and the angle of reflection[37] see Figure 2.7(a), and this is approximately one tenth of the wavelength of the radiation ($\lambda/10$) which equates to a maximum depth between 1 and 5 μm.

The relatively small amount of material in the surface region results in a small absorption signal and poor sensitivity of the technique has been a major problem. The sensitivity has been improved using multiple reflection of the IR beam within the surface region using a suitably shaped crystal with a high refractive index, shown in Figure

2.7(b). This increases the effective path length of the incident radiation and hereby improves the sensitivity of the technique.

2.3.4. Vibrational Spectroscopy of Polymers

The application of theoretical molecular physics to explain the vibrational spectra of polymers has been largely restricted to crystalline polymers where the symmetry of the system is well defined. The characterisation of amorphous polymers and those in solution has been limited to empirical approaches. The assignment of group frequencies are based upon monomer and oligomer reference spectra[38]. In common with the vibrational spectroscopy of small molecules, characteristic absorption frequencies in polymers arise due to inefficient coupling of the infra-red absorbing group with the rest of the molecule. Small deviations in the group frequencies may be observed for polymer systems and these can be used to explain more subtle bonding modes of the group, for example molecular ordering in crystalline phases[39] and hydrogen bonding interactions.

M$_1$

M$_2$

Source

B

To sample and detector
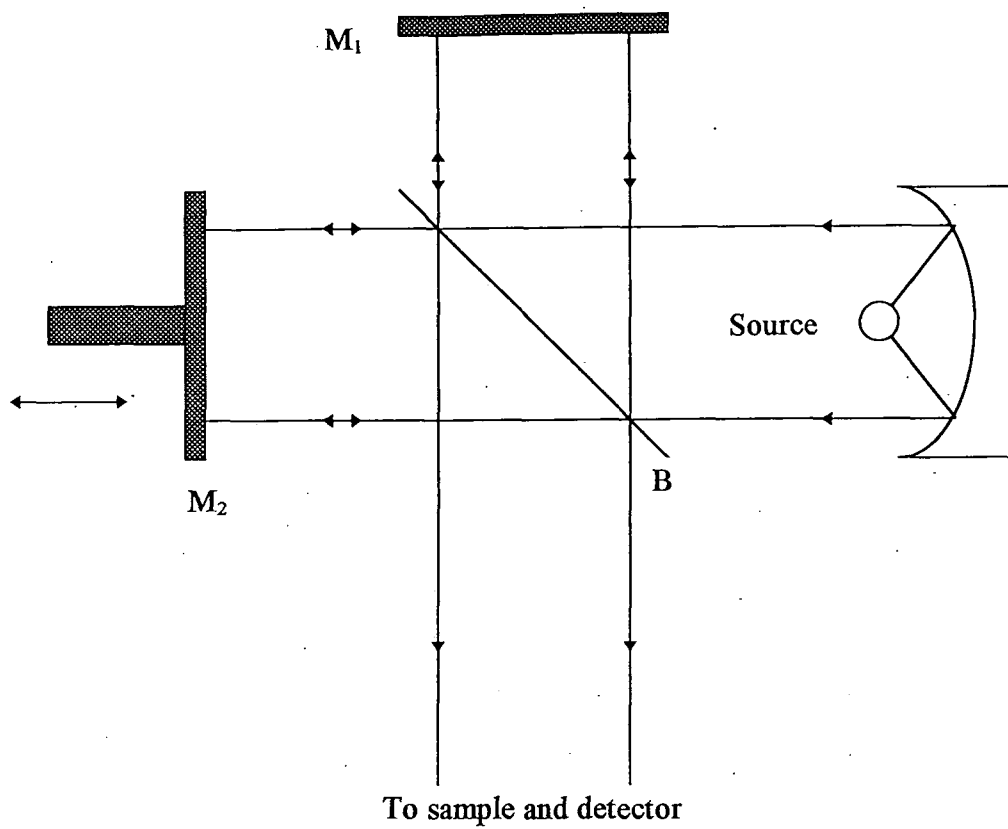
Figure 2.6   **The Michelson Interferometer**

(a)

Polymer (n_2)

To Detector

Crystal (n_1)

IR-Beam

Polymer (n_2)

(b)

Sample

n_2

~ $\lambda/10$

$n_1 > n_2$

n_1
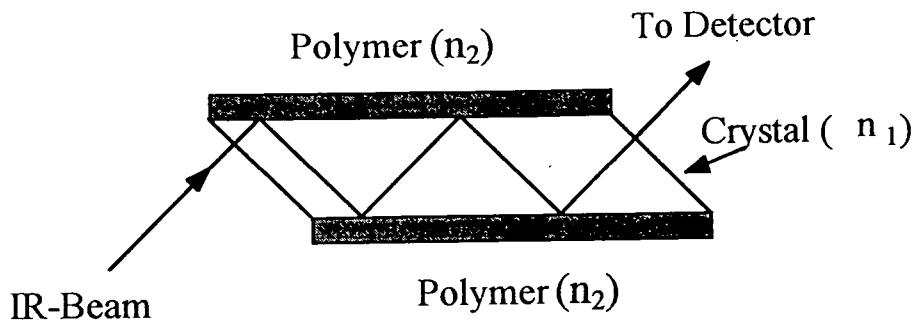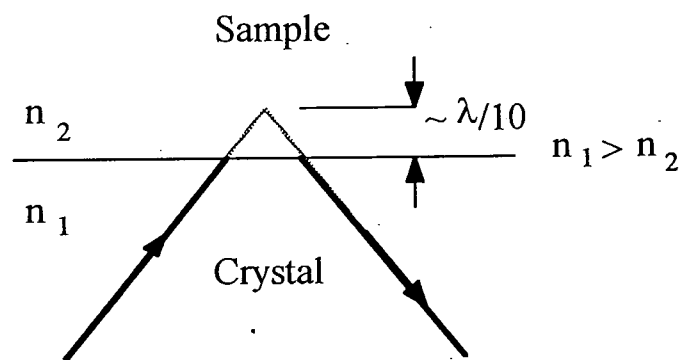
Crystal

Figure 2.7   Schematic diagram of an ATR-IR crystal (a), and the penetration depth of the infra-red radiation (b).

2.4. SURFACE AREA AND PORE SIZE DISTRIBUTION BY GAS SORPTION EXPERIMENTS

2.4.1. Introduction

The ability of a porous solid to take up large volumes of condensable gas was first observed by Fontana[40] in 1777 who noted that freshly calcined charcoal was able to take up several times its own volume of various gases. It was soon realised that the volume of gas taken up varied from one type charcoal to another, de Saussure[41] suggested that this was related to the area of exposed surface present on the solid whereas Mitscherlich[42] concentrated on the role of the pores within the charcoal. Both these factors are recognised today as playing significant parts in adsorption phenomena, not only in charcoal but a whole range of solid materials.

2.4.2. The Adsorption Isotherm

A gas or vapour brought into contact with the surface of a solid will adsorb onto it. The solid is generally referred to as the adsorbent and the gas or vapour as the adsorbate. All solids attract an adsorbed layer of gas molecules although to varying degrees, which for non-porous materials at equilibrium is dependent upon the temperature and pressure of the adsorbate and the effective surface area of the adsorbent material. The relationship at a given temperature between the equilibrium amount gas adsorbed and the pressure of the gas is known as the adsorption isotherm, see Figure 2.8. The adsorption isotherm is extremely important source of information, it can be used to determine the total surface area of the sample by measuring the point at which a

monolayer coverage of the adsorbate is detected and the shape of the isotherm may give some indication of the nature of the internal pore structure of the material.

2.4.3. Classification of adsorption isotherms

The amount of gas adsorbed on the material under investigation can be calculated by measuring the fall in pressure when a known quantity of gas is exposed to the sample. Plotting these values against the differential pressure (p/p_o) of the gas results in an adsorption isotherm. There is a vast amount of published literature detailing types of isotherms for a wide range of adsorbent materials however the majority of isotherms resulting from physical adsorption have been grouped into the five classes shown in Figure 2.8.

Type I isotherms are associated with microporous systems. The sharp uptake is due to micropore filling and the final amount adsorbed is related to the pore volume. Type II are characteristic of unrestricted monolayer/multilayer adsorption on macroporous and non porous solids. If the isotherm has a sharp knee then the uptake at point B, the beginning of the middle linear section, is a good indication of the monolayer capacity. Most solids give a type II adsorption isotherm with nitrogen. Type III occur when interaction between adsorbate and adsorbent are weak, e.g. water and carbon or any other non polar adsorbent. Nitrogen adsorbed on various polymers give a cross between type II and type III isotherms which give no obvious B point. Type IV can be obtained with mesoporous solids. If well defined, the B point provides an indication of the monolayer coverage. Often an hysteresis loop is obtained which is associated with capillary condensation. Type V are hard to interpret and also uncommon, they are

obtained with microporous systems which have weak adsorbent-adsorbate interactions. The secondary pore filling leads to limited uptake. Type VI are obtained when the multilayer adsorption is stepwise. Adsorption of each layer takes place on a uniform surface within a limited p/p_o range. Such a system is rare as it requires an homogeneous surface, also not normally of practical importance. An example of such a system is krypton on graphitised carbon.

2.4.4. Classification of Pore Sizes

The classification of pores has been arbitrarily set and should not be treated as strict boundary conditions. Pores with width less than 2.0 nm are termed micropores. Large pores with width greater than 50 nm are macropores and mesopores is the term for the intermediate sized pores.

A solid that contains micropores will be subject to preferential filling of the pores as an alternative to monolayer/multilayer adsorption. Micropore filling is therefore regarded as a primary process. Capillary condensation in mesopores only occurs after an adsorbed layer has formed on the pore walls and is therefore a secondary process. Capillary condensation does not occur until the vapour pressure is close to the saturation value. A macroporous solid exhibits very similar adsorption properties to a non-porous solid and the surface area determined via physisorption experiments will be the sum of the external and internal surface area.

Amount of Gas

Adsorbed

Relative Pressure (p/p$_o$)
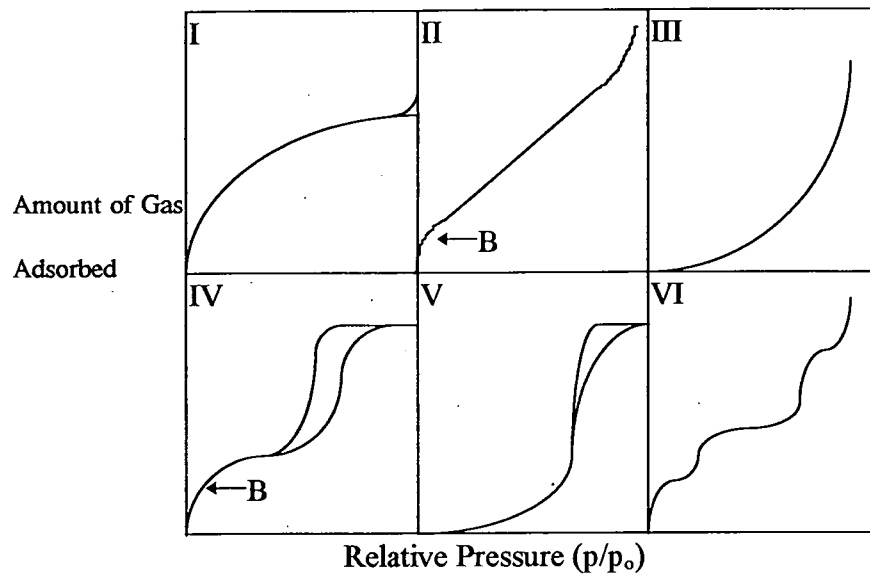
Figure 2.8   **The five types of adsorption isotherm, I to V, in the classification**

of Brunauer, Deming, Deming and Teller (BDDT), together with

Type VI, the stepped isotherm.

2.4.5. Adsorption Forces

The forces involved in the adsorption of gases and vapours by solids are divided in to two types. Firstly, non specific dispersion[43] forces and coloumbic (if either the solid or the adsorbate are polarised) forces are responsible for physisorption processes and secondly, stronger specific forces leading to the formation of chemical bonds result in chemisorption. The majority of studies have concentrated on the physisorption processes, since the attainment of equilibrium is rapid, no activation energy is required and the process is essentially reversible causing no damage to the sample surface.

2.4.6. Surface Area Measurement

The Brunauer, Emmett and Teller[44-47] (BET) method for specific surface area determination is the most popular approach and is an extension of the Langmuir model of monolayer adsorption to allow for multilayer adsorption. The BET equation (2.6) was derived by balancing the rates of evaporation and condensation of the adsorbed molecular layers, the first monolayer has a characteristic heat of adsorption ΔH_1, whereas the next layer and all subsequent layers heat of adsorption is the equal to the heat of liquefaction ΔH_L of the adsorbate. The assumptions made in the model are as follows; the surface is energetically uniform, adsorption of a monolayer creates sites of uniform energy for the next layer, evaporation condensation characteristics are the same for all layers except the first layer heats of adsorption for the second and higher layers are equal to the heat of condensation for the adsorbate and the number of layers of adsorbate tends to infinity as the pressure tends to the saturation value.

The BET equation (2.6) is,

$$\frac{p}{n(p_o - p)} = \frac{1}{n_m c} + \frac{(c-1)}{n_m}\left(\frac{p}{p_o}\right)$$
(2.6)

where p is the pressure of the adsorbate, p_o is the saturation pressure of the adsorbate at that temperature, n_m is the monolayer capacity (moles of adsorbate per gram of adsorbent), n is the amount of condensed adsorbate per gram of adsorbent and $c \approx \exp$ $[(\Delta H_L - \Delta H_l)/RT]$. Therefore the BET plot, $p/n(p_o-p)$ vs. p/p_o, gives a linear relationship with intercept of $1/n_m c$ and slope of $(c-1)/n_m$ and this is used to calculate the monolayer capacity. The specific surface area is easily determined using equation (2.7),

$$A_{BET} = n_m N_A A_m$$
(2.7)

where A_{BET} is the specific surface area, N_A is Avagadro's constant and A_m is the molecular cross-sectional area of the adsorbate molecule.

2.4.7. Determination of Micropore Size

As already stated the adsorption isotherm for a microporous adsorbent will usually be of type I. If the external surface of the adsorbent is small then the Gurvich rule can be applied, *viz* . the plateau corresponds to the pore volume, Vp. This gives a good agreement over a wide range of adsorbates, but obviously fails if the size of the adsorbates becomes too big. This very observation can give an indication of the pore distribution however.

Dubinin and his co-workers[46] use the 'characteristic curve' principle of the Polanyi potential theory (2.8)

$$\frac{n}{n_p} = \exp\left[\left(-\frac{A}{E}\right)^m\right] \qquad (2.8)$$

where n/n_p is the fractional filling of the micropores, E is the characteristic free energy of adsorption for the system, m is a small integer and A is the differential free energy of adsorption, given by (2.9)

$$A = -RT\ln\left(\frac{p}{p_o}\right) \qquad (2.9)$$

This will give the following equation

$$\log n = \log n_p - D\left(\log p_o / p\right)^m \qquad (2.10)$$

where D is a constant related to E . The normal case is for m = 2, equation (2.10) should give a linear plot.

2.4.8. Determination of Meso and Macropore size distribution

This uses the 'Kelvin Equation', (2.11) which relates the vapour pressure (*p*) of a condensed liquid in a cylindrical capillary to the radius of curvature of a hemispherical

meniscus (r).

$$\ln p / po = -2V\gamma / rRT \cos \phi \qquad (2.11)$$

Here p_o is the saturation pressure of the adsorbate, γ the surface tension, V the molar volume of the liquid, and ϕ is the angle of contact between the liquid and the pore walls ($\cos \phi = 1$)[47]. Since r increases as p/p_o increases, it follows that condensation occurs at lower relative pressures in smaller radii pores. However r is not the radius of the pore, and therefore the thickness of the adsorbed layer (t) on the walls of the pore must be taken into account using the 'Halsey Equation', (2.12).

$$t = \sigma\left[5 / (\ln po / p)\right]^{\frac{1}{3}} \qquad (2.12)$$

Where σ is the thickness of an adsorbed monolayer (in Angströms), this then allows calculation of the critical pore radius ($r_{p,c}$), (2.13).

$$r_{p,c} = r + t = -(2V\gamma \cos \phi / RT(\ln p / po)) + t \qquad (2.13)$$

Incremental gas adsorption on the surface of cellulose pores eventually leads to pore closure[48], and differences in the quantity (ΔN) of adsorbed gas at different relative pressures can be expressed as an equivalent volume of liquid ΔV_L, this can then be used to calculate the pore size distribution from the adsorption isotherm using (2.14). Cylindrical pore shapes are assumed:

$$\Delta V_L = (\Delta N)V_L \approx (\Delta V_P)\big[\bar{r}/r_{p,c}\big]^2 + 2(\Delta t) \sum_{rp,c}^{rp} (\Delta V_P)(\bar{r}_p - \bar{t})\big/r_p^2 \qquad (2.14)$$

here $\bar{r}$, $\bar{t}$, $r_{p,c}$ and Δt correspond to average values of the Kelvin radius, adsorbed film thickness, critical pore radius and the change in adsorbed film thickness for the increment in relative pressure respectively; ΔV_p, and $\bar{r}_p$ relate to pore volume and average pore radius within a specified pore size interval. By plotting $\Delta V_p/\Delta r_{p,c}$ versus $r_{p,c}$ one can obtain a pore radius distribution (or diameter).

2.4.9. Experimental

A schematic diagram of the gas sorption apparatus is shown in Figure 2.9, the sample to be investigated is placed in the sample tube and attached to the gas sorption apparatus. The tube is evacuated and the sample is initially outgassed at elevated temperature, typically 60°C which removes physisorbed material. The 'dead space' volume in the sample tube is determined using helium gas this is achieved by pressurising the volume enclosed within the gas sorption apparatus, labelled as V_i in Figure 2.9 to a known pressure, opening the sample tube to the helium containing chamber and then allowing the helium gas to equilibrate in the combined volume, V_c. By comparing the equilibrium pressure of helium for an empty sample chamber with the equilibrium pressure for a sample chamber containing sample material for the same initial pressure of helium, and assuming no physisorption of helium at room temperature, then the volume of the chamber occupied by the sample material can be determined.

Following this the sample is evacuated once again and the sample chamber is

immersed in a bath of liquid nitrogen as shown in Figure 2.9. In a similar manner that the dead space volume was determined the surface area of the sample material can be quantified by admitting a known quantity of nitrogen gas (although other gases such as krypton and carbon dioxide are commonly used) into the sample chamber. Unlike the helium measurement above, when a known quantity of nitrogen gas is exposed to a solid sample a proportion of the nitrogen will adsorb on to the sample surface. The equilibrium pressure therefore represents the amount of gas contained in the initial volumes space less the amount of gas molecules physisorbed. The adsorbed amount can be calculated from the difference between the pressure of gas at equilibrium and the pressure of gas prior to the opening of the sample chamber valves provided the free volume of the sample chamber and the volume of inside the gas sorption apparatus is known.

In a complete experiment we use incremental adsorption of nitrogen to determine the adsorption isotherm for a sample. From this we can calculate as described above the amount of nitrogen adsorbed on to the surface for each pressure of nitrogen up to the saturation vapour pressure, p_o. These isotherms can be treated mathematically as described in the previous sections to yield surface area and pore diameter information.
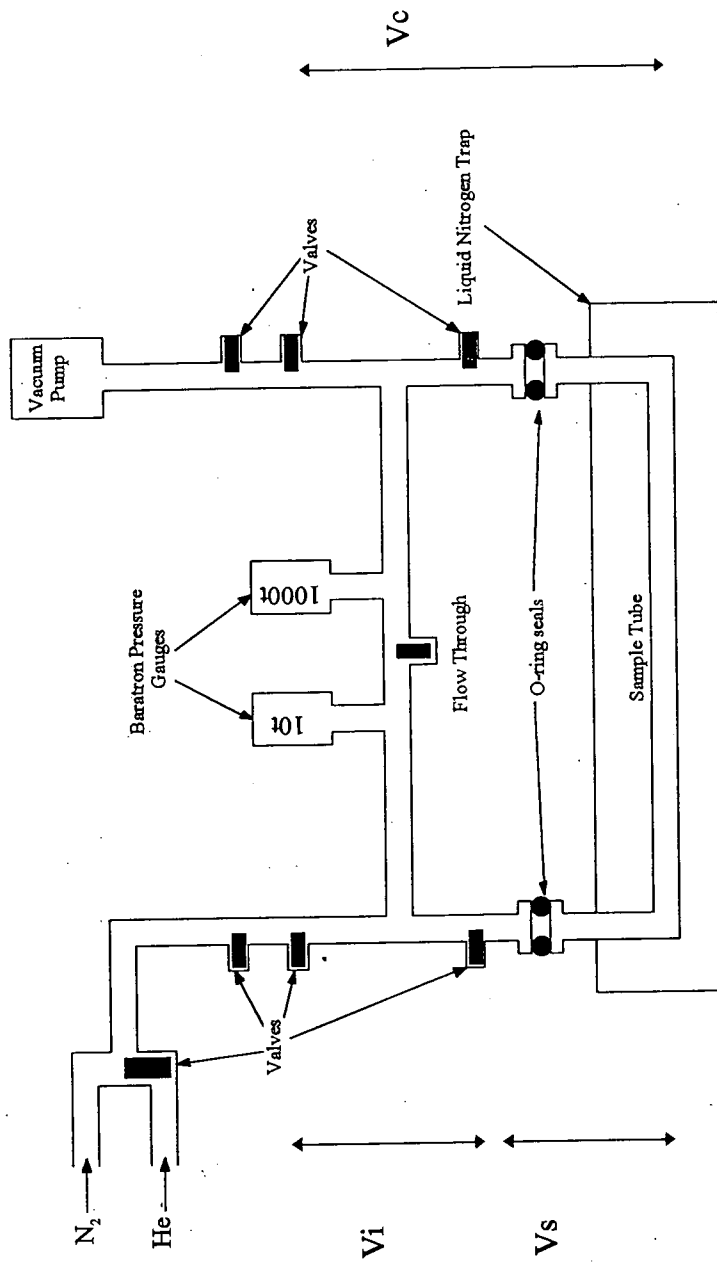
Figure 2.9   Schematic Diagram of the Gas Sorption Apparatus

2.5. ATOMIC FORCE MICROSCOPY

2.5.1. Introduction

Invented by G. Binnig, C. Quate and C. Gerber[49] in 1986, the Atomic Force Microscope (AFM) in conjunction with the Scanning Tunnelling Microscope (STM) has revolutionalized surface imaging capabilities of surface science. In the most favourable cases the imaging has been refined to the atomic scale, enabling the surface to be pictured with immense detail. Observations of phenomena such as atomic steps, random atomic vacancies and screw dislocations have been possible[50].

The AFM[50-52] operates upon the basis of measuring the forces between an atomically sharp stylus tip and the surface under investigation. Rastering or scanning the probe tip across the surface enables topographical mapping to take place giving an image of the surface. In contrast to the STM, AFM does not require that the sample be electrically conductive, and therefore it is especially applicable to non-conductors, for example polymers. The probing AFM tip is attached to a cantilever assembly Figure 2.10, and the tip/cantilever deflects in response to forces exerted by the sample, which are usually in the order of 10^{-13} - 10^{-6} N. A displacement sensor measures these deflections, a commonly used sensor is based upon the optical lever technique. Laser light is focussed upon the end of a 200 or 100 μm long microfabricated cantilever. The light reflected off the cantilever is picked up by a two segment photodiode and the difference in intensity between the segments is measured. Other types of sensor include ones that operate via optical interferometry, or detect electron tunnelling current and/or capacitance.

Laser Diode

Photodetector

Cantilever

Imaging Tip
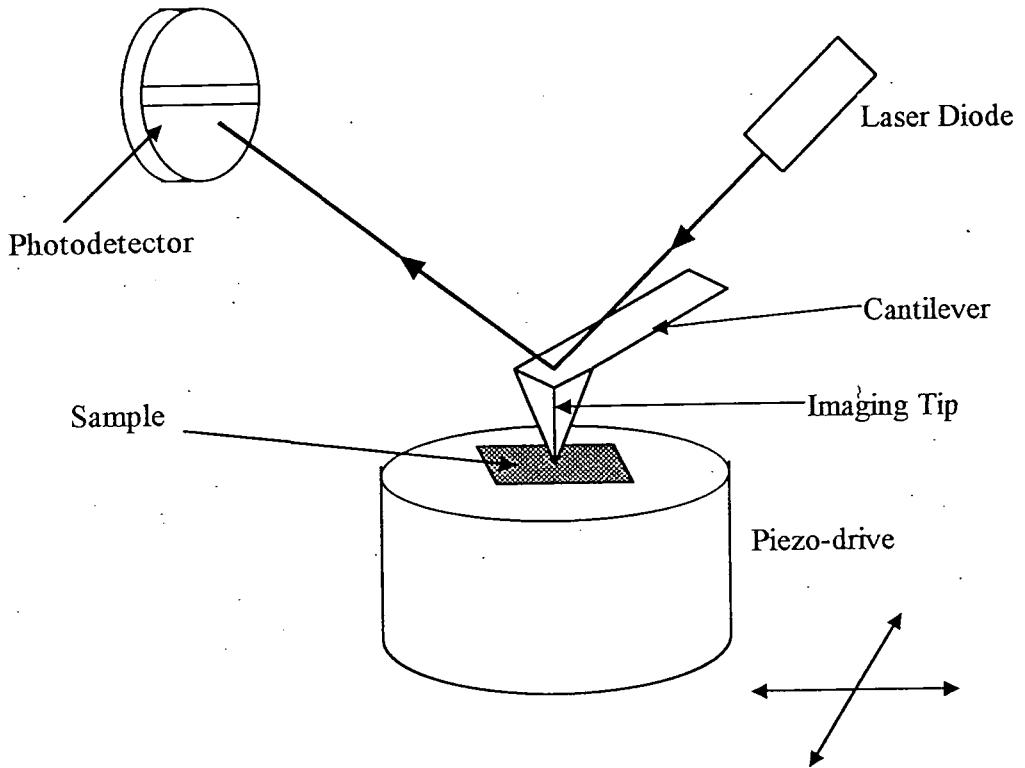
Sample

Piezo-drive

Figure 2.10   Schematic Diagram of AFM Apparatus

The AFM tip is commonly made from silicon nitride[50] and the sample, which is mounted upon a cylindrical piezodrive (x y z translator) can be guided by a feedback signal from the displacement sensor system, allowing the surface to be scanned with a constant force. The tip/surface displacement is held constant through the z displacement vector of the piezodrive and this is where the mapping capabilities are derived.

AFM is not confined to measuring solely force data, it can be adapted to study magnetic samples, having a stylus with a magnetic moment causes a response to any field of the magnetised sample giving us Magnetic Force Microscopy (MFM). Similarly we can have Electrostatic Force Microscopy (EFM) where the electrostatic interaction between the tip and the sample is monitored. AFM is flexible in that it can operate under UHV conditions, in controllable atmospheres, low temperatures and will even perform when the tip is submerged in a liquid.

2.5.2. AFM Analysis of Polymers

AFM is applicable in the surface imaging of polymeric materials, until recently studies were limited to conducting polymers[51] using the STM (Scanning Tunnelling Microscope), which measures the tunnelling current of electrons on the surface of a material. Under optimum conditions AFM has been able to resolve atoms, molecules, polymers and their low molecular weight analogues.

Imaging of extruded poly(ethylene) highlighted its microfibrillar structure[51], though the probe tip does have some problems faithfully duplicating the surface profile since the 45° angle on the stylus prevents the more steeply inclined and deepest grooves

from being exactly followed. Extended polymer chains were also registered, and the technique was able to detect the conformational structure of these features. Dendritic crystals of poly(ethylene) have been observed[53] using AFM, thickness of lamellae could be measured, showing the quantitative aspects of the technique.

Further work using PTFE[54] exhibited defect structures and characterized individual intermolecular spacings of the PTFE crystal. Information was extracted at an atomic level, not only concerning the surface geometry of the polymer but also atomic scale mechanical properties[55].

Dynamic processes at the surface of polymers have been studied using AFM, for example lamellar ordering in disordered block copolymers[56], and the kinetics of the formation of island and hole structures during the annealing of the disordered polymers have been measured.

Conversely AFM can be used to induce structural changes in polymer surfaces. Reducing the distance between the stylus and polymer results in greater tip/surface interactions, in the case of polystyrene[57] continued exposure to the stylus tip caused buckling of the polymer chains and aggregation to form lumps, these were in the order of nanometres in height. Taking in to account the small contact areas involved (10^{-15} m) the force/contact area is high (10^6 N/m^2). When this is coupled with scanning of the stylus at low speeds (~17 nm/s) larger scale surface modifications can be made. With repeated scanning, surface ordering has been achieved[57], the polymer molecules aggregating to form ridges, the uniformity of which suggested periodicity.

2.6. SCANNING ELECTRON MICROSCOPY

2.6.1. Introduction

SEM involves scanning a focussed beam of electrons across a small area of a sample surface (e.g. 100 μm x 100 μm), a proportion of the incident electrons are back scattered from the sample surface. The back scattering phenomenon arises when a primary electron (with energy around 20keV) passes close to a charged atomic nucleus and is deflected with minimal energy loss (<1eV), so-called elastic scattering. Many of the electrons are deflected through angles greater than 90° and these may re-emerge from the sample surface. This flux of back scattered electrons can be detected and converted in to an electrical signal. Changes in the signal intensity can be related to the topography of the sample and this can be used to form an image of the surface of the material.

2.6.2. Experimental

The action of the electron beam used in SEM technique often leads to the build up of negative charge on the surface of all but the most highly conducting samples. This leads to the repulsion of the incoming primary electron beam and results in poorer image quality. In order to obtain images of the highest resolution using non-conducting samples coating of the material with a metallic layer is performed. This has two advantages, as we have already pointed out it reduces charging and it also in the case of materials which are easily damaged by the electron beam such as polymers, the metallic layer provides a convenient method of conducting the beam induced heat away from the

sample. In this thesis the materials were coated with a thin gold film of approximately 15 nm thickness, this was found to provide the best imaging conditions with a minimal disruption of the true surface morphology.

2.7. X-RAY DIFFRACTION

Whilst it is not by any means a surface analytical technique X-ray powder diffraction was used during the course of this work and hence in the interests of completeness a brief outline of the technique has been included here.

2.7.1. Introduction

X-rays were discovered by Röntgen[58] in 1895, but it was a further 17 years before Max von Laue noticed that they could be diffracted by crystalline material. This simple discovery has evolved in to an extremely powerful technique for determining the structure of solid materials.

The wavelength of X-rays are of the order of the separation of lattice planes in a crystalline material and when an X-ray beam passes through a crystalline sample and diffraction occurs, constructive and destructive interference is observed depending on the path lengths of the interacting waves. When the path length difference is an integral number of wavelengths the reflected waves are in phase and interfere constructively. It has been found that the constructive interference occurs when the glancing angle satisfies the Bragg law[59] (2.15),

$$\lambda = 2d\sin\theta \qquad\qquad (2.15)$$

where λ is the wavelength of the X-rays, d is the lattice spacing of the crystal and θ is the diffraction angle of the constructively interfered X-ray line.

2.7.2. Experimental

The powder diffraction method of Debye-Scherrer[59] was used for the purposes of this study. This enables the analysis of powdered rather than wholly crystalline samples and it relies upon the fact that in a powdered sample containing crystallites, a proportion of these crystallites will be oriented in such a manner to produce the same diffraction pattern that we would expect from a pure crystal of the same material. The crystallites with a particular diffraction angle will lie at all possible angles around the incoming beam. So, the diffracted beams will form a cone around the incident beam of half angle 2θ.

The original Debye-Scherrer method required the sample to be contained in a capillary tube which underwent continuous rotation to ensure a random orientation of the crystallites in the sample. The diffracted cones of X-ray radiation were recorded on a photographic strip surrounding the sample. In the modern day powder diffraction apparatus the sample is spread on a flat plate and the diffraction intensity is measured electronically as shown in Figure 2.11.

X-ray beam

Detector

2θ

Sample
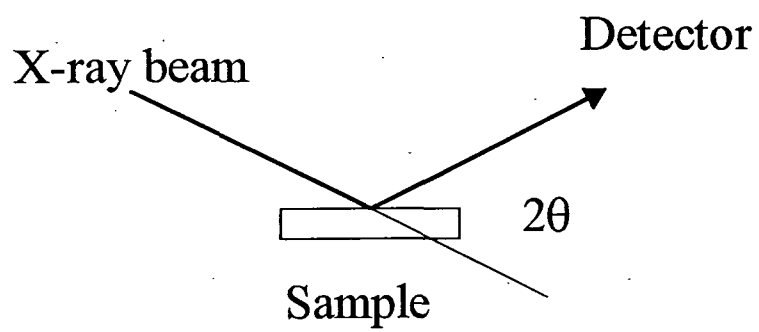
Figure 2.11   **Schematic Diagram of a modern powder X-ray diffractometer.**

2.8. REFERENCES

1   Braybrook J. H., Hall L. D., *Prog. Polym. Sci.*, **15**, 715 (1990).

2   Carter S. B., *Nature*, **5016**, 1183 (1965).

3   Yasuda H., Yamanashi B. S., Devito D. P., *J. Biomed. Mater. Res.*, **12**, 701 (1978).

4   Dexter S. C., Sullivan J. D., Williams J., Watson S. W., *Appl. Microbiol.*, **30**, 298 (1975).

5   Ratner B. D. in *Photon, Electron and Ion Probes of Polymer Structure and Properties*, Dwight D. W., Fabish T. J., Thomas H. R., Eds., ACS Symp. Ser., Amer. Chem. Soc., Washington D. C., 1981.

6   Cox P. A., *The Electronic Structure and Chemistry of Solids*, Oxford University Press, Oxford, 1987.

7   Ratner B. D., Schoen F. J., Hoffman A. S., Lemons J., (Eds.), *Biomaterials Science: An Introductory Text.*, San Diego, Academic Press, 1993.

8   Ratner B. D., Cardiovasc. Pathol., 2, 87 (1993).

9   Hollas M. J., *Modern Spectroscopy*, Wiley, Chichester, 1990.

10   Brigss D., Seah M. P., *Practical Surface Analysis-Auger and X-ray Photoelectron Spectroscopy*, 2nd Ed., Wiley, Chichester, 1990.

11   Brundle C. R., Baker A. D., *Electron Spectroscopy: Theory, Techniques and Applications*, Vol 2, Academic Press, 1978.

12   Wagner C. D., Riggs W. M., Davis L. E., Moulder J. F., Muilenberg G. E., *Handbook of X-ray Photoelectron Spectroscopy*, Perkin Elmer Corp., U.S.A., 1979.

13   Ertl G., Kuppers J., *Low Energy Electrons and Surface Chemistry*,

Verlagsgesellschaft, Germany, 1985.

14   Cox P. A., *The Electronic Structure and Chemistry of Solids*, Oxford University Press, Oxford, 1989.

15   Salaneck W. R., *Rep. Prog. Phys.*, **54**, 1215 (1991).

16   Pireaux J. J., Riga J., Boulanger P., Snauwert P., Novis Y., Chtaib M., Gregoire C., Fally F., Beelen E., Caudano R., Verbist J., *J. Elect. Spectr. Rel. Phenom.*, **52**, 423 (1990).

17   Dilks A., Ph.D. Thesis, University of Durham, Durham, 1977.

18   Beamson G., Briggs D.,in *High Resolution XPS of Organic Polymers-The Scienta ESCA 300 Database* p. 236. John Wiley, Chichester, 1992.

19   Spells S. J. (Ed.), *Characterization of Solid Polymers-New Techniques and Developments*, Chapman and Hall, London, 1994.

20   Siegbahn K., *ESCA:atomic, molecular and solid state structure studied by means of electron spectroscopy*, Almqvist and Wiksells, Uppsala, 1967.

21   Clark D. T., Thomas H. R., *J. Polym. Sci. Polym. Chem. Ed.*, **16**, 791 (1978).

22   Clark D. T., Dilks A., *J. Polym. Sci. Polym. Chem. Ed.*, **14**, 533 (1976).

23   Keane M. P., *Chem. Phys.*, **155**, 379 (1991).

24   Davis G. D., Viljoen P. E., Lagally M. G., *J. Electr. Spectrosc.*, **21**, 135 (1980).

25   Seah M. P., Dench W. A., *Surf. Int. Anal.*, **1**, 2 (1979).

26   Brundle C. R., *J. Vac. Sci. Technol.*, **11**, 212 (1974).

27   Pireaux J. J., Riga J., Boulanger P., Snauwert P., Novis Y., Chtaib M., Gregoire C., Fally F., Beelen E., Caudano R., Verbist J., *J. Electr. Spectr. Rel. Phenom.*, **52**, 423 (1990).

28   Davies M. C., *Polymer Surfaces and Interfaces 2*, Feast W. J., Munro H. S.,

Richards R. W. (Eds.), Wiley,Chichester,1993.

29   Ratner B. D., Castner D. G., Horbett T. A., Lenk T. J., Lewis K. B., Rapoza R.
      J., *J. Vac. Sci. Technol. A.*, **3**, 2306 (1990).

30   Meirovitch H., Rackovsky S., Scheraga H. A., *Macromolecules*, **13**, 1398
      (1980).

31   Ratner B. D., Weathersby P. K., Hoffman A. S., *J. App. Polym. Sci.*, **22**, 643
      (1978).

32   Weatherwax R. C., *J. Colloid. Int. Sci.*, **62**, 432 (1977).

33   Rowland S. P., *ACS Symp. Ser.*, **2**, 20 (1977).

34   Weatherwax R. C., *J. Colloid. Int. Sci.*, **49**, 40 (1974).

35   Weatherwax R. C., *Tappi.*, **54**, 985 (1971).

36   Brown N. M. D., Hewitt J. A., Meenan B. J., *Surf. Int. Anal.*, **18**, 199 (1992).

37   Mirabella F. M., *Applied Spectroscopy Reviews*, **21**, 45 (1985).

38   Bellamy L. J., *The Infra-red Spectra of Complex Molecules*, 2nd Ed., Methuen,
      London, 1974.

39   Wadsworth L. C., Cuculo J. A., in *Modified Cellulosics*, Rowell R. M., Young
      R. A., Eds.,p. 117. Academic Press, New York, 1978.

40   Fontana F., *Memorie Mat. Fis. Soc. Ital. Sci. I*, **1**, 679 (1777).

41   de Saussure N. T., *Gilbert's Ann.*, **47**, 113 (1814).

42   Mitscherlich E., *Pogg. Ann.*, **59**, 94 (1843).

43   London F., *Z. Physik*, **63**, 245 (1930).

44   Brunauer S., Emmet P.H.,Teller E., *J. Amer. Chem. Soc.*, **60**, 309 (1938).

45   Brunauer S., Deming L.S., Deming W.S., Teller E., *J. Amer. Chem. Soc.*, **62**,
      1723, (1940).

46   Sing K. S. W., *Characterisation of catalysts*, (Eds. Thomas J. M. and Lambert R. M.), Chap. 2, Wiley , Chichester, 1980

47   Greg S.J. and Sing K. S. W. , *Adsorption, surface area and porosity* , Academic Press , London and New York , 1967 .

48   Orr, C.; Dalla Valle, J.M. in *Fine Particle Measurement*; Macmillan, London 1959; p271.

49   Binning G., Quate C., Gerber C., *Phys. Rev. Lett.*, **56**, 930 (1986).

50   Frommer J., Meyer E., *Condens. Mater.*, **3**, 51 (1991).

51   Magonov S., Quarnstrom K., Elings V., Cantow H. J., *Polymer Bulletin*, **25**, 689 (1991).

52   Gould S. A. C., Drake B., Prater C. B., Weisenhorn A. L., Manne J., Klederman G. L., Butt H-J., Hansma H., Hansma P. K., Magonov S., Cantow H. J., *Ultramicroscopy*, **33**, 93 (1990).

53   Patil R., Kim S-J., Smith E., Reneker D. H., Weisenhorn A. L., *Polymer Communications*, **31**, 455 (1990).

54   Hansma H., Motamedi F., Smith P., Hansma P., Wittman J. C., *Polymer*, **33**, 647 (1992).

55   Annis B. K., Noid D. W., Sumpter B. G., Reffner J. R., Wunderlich B., *Makromol. Chem., Rapid Commun.*, **13**, 169 (1992).

56   Collin B., Chatenay D., Goulon G., Ausserre D., Gallot Y., *Macromolecules*, **25**, 1621 (1992).

57   Leung O. M., Goh M. C., *Science*, **255**, 64 (1992).

58   Rontgen W. C., *Nature*, **53**, 274 (1896).

59   Atkins P. W., *Physical Chemistry*, 5th Ed., pp726, Oxford University Press ,

London 1994.

3. HYDROXYL ACCESSIBILITY IN CELLULOSES

3.1. INTRODUCTION

This initial experimental chapter concerns the cellulose microstructure and its effect upon the hydroxyl accessibility. There are several excellent articles[1-6] and books[7-9] reviewing the vast amount of published literature concerning the chemical and physical properties of cellulose, the range of chemical modifications it is able to undergo, and its subsequent uses in industry. The introduction to this chapter summarises the physical and chemical properties pertaining to its application as a bioseparation matrix, the importance of hydroxyl accessibility, and outlines a novel approach to studying the phenomena.

3.1.1. The Chemical Modification of Cellulose

The physicochemical merits of cellulose may be attributed to its structural characteristics, and the variety of chemical modifications that it can undergo via its hydroxyl functionalities[1]. Derivatization is generally achieved via esterification or etherification[10] of the cellulosic hydroxyl groups and consequently the availability of these species is of vital importance when considering the application of cellulose as a bioseparation medium.

In kind with other semi-crystalline polymers, cellulose undergoes two phase crystalline/amorphous reactions and as such four different reaction patterns may be

observed:

(a)   Surface reaction.

(b)   Macroheterogenous reaction, begins as a surface reaction but proceeds through the fibre from layer to layer as the cellulose chains dissolve or swell in the reactant.

(c)   Microheterogenous reaction, cellulose is swollen by the reaction medium but the crystalline regions remain inaccessible.

(d)   Permutoid reaction, intrafibrillar or intercrystalline reactions extend in to the highly ordered and crystalline regions without dissolving them leading to a transformation of the lattice[11].

The chemical modification of cellulose may be undertaken for several reasons, for example the manufacture of fibres and films often requires a solubilised form of cellulose, thermoplasticization[12,13] is important for moulding, extrusion or coating applications. Bulk chemical modifications can lead to increased resilience and dimensional stability, imparting properties such as flame retardency or resistance to micro-organisms. Cellulose can be employed as a naturally occurring substitute for synthetic polymers, and has found use in hemodialysis, electrophoresis and protein separation[14-17] applications.

3.1.2. The Chemical and Physical Structure of Cellulose

Cellulose belongs to the class of materials which is commonly referred to as polysaccharides; it is built up of anhydro β-D-glucopyranose units, Figure 3.1, linked via 1-4 glycosidic bonds, this results in a basic dimeric repeat unit which has a length of 1.03

nm and a rotation of 180° from one glucose residue to the next. The monomer fragment

has an empirical formula of $C_6H_{10}O_5$, and has a molecular weight of 162 gmol^{-1}.

3.1.2.1. Hydroxyl Group Reactivity

Each β-D-glucopyranose unit within a polymer chain has a primary OH(6) group

and two secondary groups, OH(2) and OH(3), the numbers in brackets designate where

they are situated on the cellulose monomer fragment, see Figure 3.1. Taking

neighbouring group effects in to account the relative reactivity of the hydroxyls increases

OH(6) < OH(3) < OH(2). However OH(6), being a primary hydroxyl, is the least

sterically hindered of the three groups and is more likely to react with bulky substituents.

3.1.2.2. The Crystalline and Amorphous Microenvironment

The previous section outlined the reactivities of the hydroxyl functionalities in the

cellulose monomer unit, however an assessment of the reactivities on the basis of

electronic neighbouring group effects and steric considerations is somewhat incomplete.

It fails to take in to account intra and inter-molecular hydrogen bonding interactions

which are the primary source of cohesion between the polymer chains, giving rise to

crystalline (ordered) and amorphous (disordered) regions which have a profound effect

upon the reactivity of the hydroxyl functionalities.

Intramolecular hydrogen bonding has been suggested[9, 18] within the cellulose

chain between OH(3) groups and the neighbouring pyranose ring oxygen and also

between OH(6)....OH(2) of adjacent glucose residues, see Figure 3.2, this gives rise to a

surprisingly rigid polymer structure. Intermolecular hydrogen bonding between the OH(6) and the OH(3) of a nearby cellulose chain results in the polymer adopting a layered structure, Figure 3.3. These layers are then weakly bound together via van der Waals interactions to form a three dimensional lattice.

3.1.2.3. *The Cellulose Lattice.*

X-ray[19,20], electron[21,22] and neutron[23,24] diffraction, optical scattering and electron microscopy studies have managed to elucidate five different allomorphic structures based on the cellulose lattice. They have been designated cellulose I, II, III, IV and X, each one is defined by its unit cell characteristics which are based upon the origin or the history of it's preparation. Cellulose I is the most common diffraction pattern, exhibited by a wide range of naturally occurring cellulose materials. Cellulose II can be prepared from I by dissolving or precipitating it, or treating it with an alkaline swelling agent. Cellulose III can be prepared from I by swelling under anhydrous conditions and Cellulose IV results from thermal treatment of I.

The crystallites in cellulose tend to be small and imperfectly ordered, therefore there are a limited number of diffraction spots available with which to determine the allomorphic structure, hence unambiguous characterisation of the five forms of cellulose has proved difficult. However recent studies using improved computer methods for data analysis have allowed more detailed information to emerge[7].
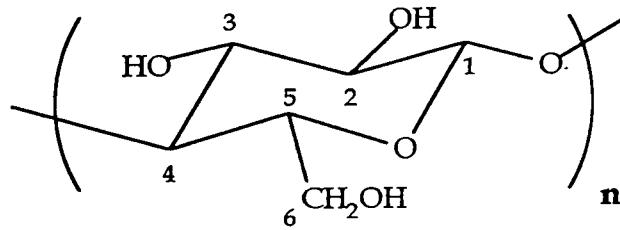
Figure 3.1   **The Cellulose Repeat Unit.**
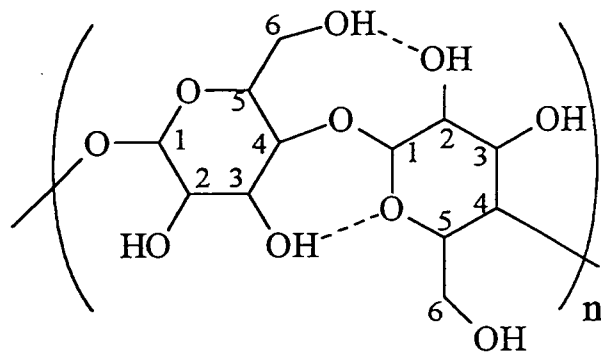
Figure 3.2   **Intramolecular Hydrogen Bonding in Cellulose**
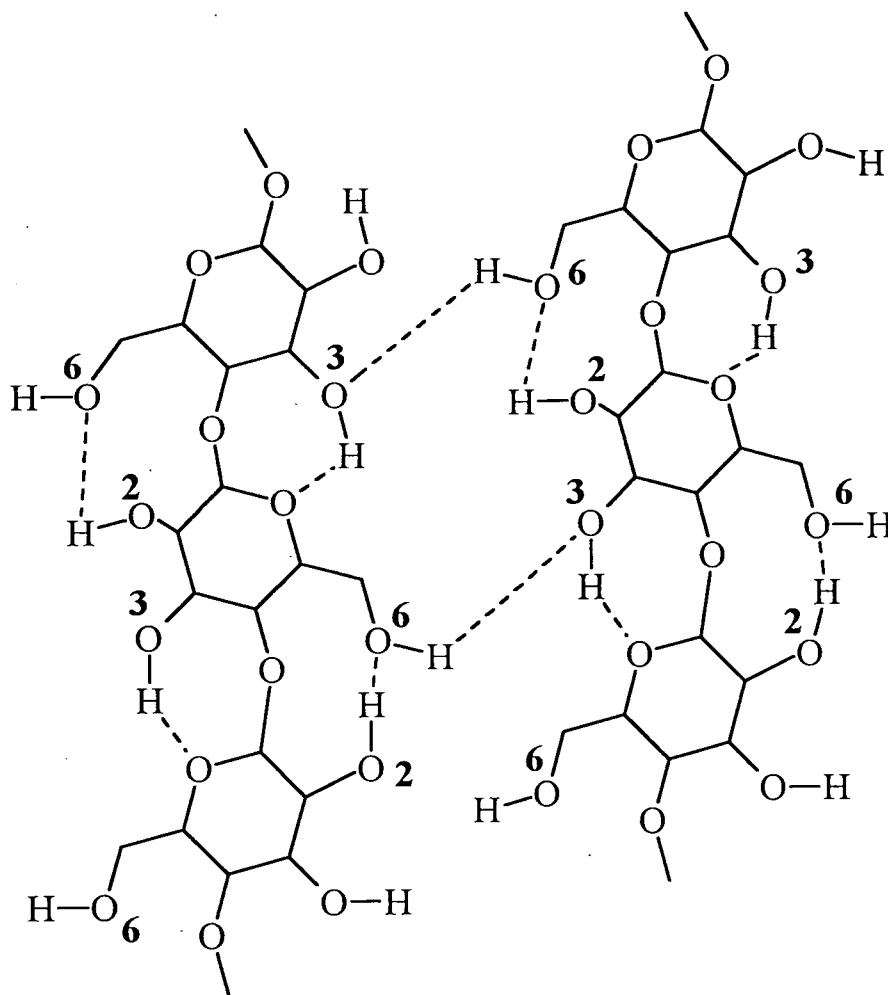
Figure 3.3   **Intermolecular Hydrogen Bonding in Cellulose.**

3.1.2.4. The Fibrillar Structure.

Intermolecularly bonded cellulose chains form fibrous strands called elementary fibrils. The elementary fibrils have been shown[3] to aggregate in to arrays called microfibrils, which are crystalline in nature. Derivatization reactions are believed to occur preferentially at the surfaces of cellulose fibrils, whereas the interior of such fibrils tend to be inaccessible to ordinary chemical attack due to the close packed (strongly hydrogen bonded) nature of the polymer matrix[2]. However, chain end dislocations, surface imperfections and chain order bonding irregularities lead to the formation of areas of disorder within the microfibrils known as amorphous regions. It is in these sites that significant reactant penetration and activity is observed, and a case linking hydroxyl group reactivity and the microstructural nature of cellulose has been suggested[6].

3.1.3. Accessibility and the Microstructural Nature of Cellulose

A number of attempts have been made in the past to establish whether any correlation exists between hydroxyl group reactivity and the microstructural nature of cellulose.

3.1.3.1. Methods to Determine Cellulose Microstructure

The determination of the degree of crystallinity in cellulose can be broken down in to two general methods, direct physical measurements and indirect chemical hydroxyl accessibility studies. The physical methods include X-ray diffraction[25-27], ^{13}C NMR[28], infra-red absorption[11, 29, 30] and density measurements. A variety of chemical methods

have been previously used and these can be described in terms of their swelling (chemical reaction based) or non-swelling (sorption based) character. Aqueous systems, which include moisture regain[31], deuteration[32], acid hydrolysis, alcoholysis[33], periodate oxidation, formylation[34] and iodine adsorption[35], tend to lend their extent of penetration to their swelling capacity of the matrix and as a result tend to give a semi-quantitative measure of the degree of disorder. Non aqueous systems, chromic acid oxidation and thallation[36] for example, do not tend to swell the polymer network. More recently, Verlac and Rowland[37] attempted to probe the absolute and relative reactivities of the primary and secondary hydroxyls within the monomer unit by chemical microstructural analysis (CMA)[38].

3.1.3.2. *Chemical Labelling and XPS Analysis as a Probe for Hydroxyl Accessibility.*

XPS suffers from lack of specificity in chemical environment analysis because of the similar core level electron binding energy shifts for many surface species[39]. Labelling has been of use in distinguishing between ethers, alcohols, hydroperoxides, aldehydes, ketones, acids and esters[40,41].

The reaction used must be quantitative, the group introduced must be easily detectable and perturbation of the surface must be minimised. Major problems involve reproducibility and this can often be attributed to the following problems:

a)   inhomogenous reaction within the sampling depth,

b)   reorganisation of the materials surface layers through swelling,

c)	adsorption of unreacted solvent.

In spite of the potential problems associated with this type of analysis, a range of publications have emerged in which chemical labelling has been demonstrated as a reliable method to quantify a wide range of functionalities. Batich[42] compiled a list of the most effective labelling agents and this is shown in Table 3.1.

Vapour phase reactions have found application in this area since they avoid the potential loss of surface material to the solution phase, and adsorption of unreacted solvent. TFAA (trifluoroacetic anhydride) is a reagent well suited to this task and has been used in the derivatization of surface hydroxyls. Alternative vapour phase labelling agents include TMSI (trimethylsilylimidazole) which has been used to label acidic functionalities[43].

The major limitation of the non-sorption based chemical methods described above for hydroxyl accessibility determination has been their wet nature, which in turn disturb the polymer structure via swelling, aqueous systems tending to disrupt the cellulosic hydrogen bonds and penetrate the structure through this mechanism. In this chapter, a gas phase labelling reagent is used: trifluoroacetic anhydride (TFAA) vapour, Scheme 1. This molecule reacts with hydroxyl groups and generates a volatile by-product[44]. Direct quantification of this reaction can be easily achieved using X-ray photoelectron spectroscopy (XPS)[45,46], since the -CF$_3$ exhibits a large C(1s) core level shift towards higher binding energy[47]. A range of cellulosic materials (with varying degrees of crystallinity) have been evaluated by this method for hydroxyl accessibility and this is then related to the cellulose microstructure.

Table 3.1.   A range of labelling agents used for XPS analysis of polymer surfaces[42].

Functional Group	Labelling species
C-OH	$(CF_3CO)_2O$ $(i\text{-}Pr\text{-}O)_2Ti(acac)_2$ CF_3COCl CBr_3CO_2H $(NO_2)_2C_6H_3COCl$ $CF_3(CH_2)_2Si(CH_3)_2NCOCH_3$ ClC_6H_4NCO $(NO_2)_2C_6H_3F$
-NH₂	C_6F_5CHO CS_2 HCl $CH_3CH_2SCOCF_3$
-SH	$AgNO_3$ $[C_6H_3(NO_2)_2(CO_2Na)S]_2$ $HgCl_2$
-OOH	SO_2
Si-OH	$CF_3(CH_2)_2Si(CH_3)_2NCOCH_3$
-COOH	$NaOH$ $BaCl_2$ $AgNO_3$ $TlOC_2H_5$ CF_3CH_2OH $C_6H_5CH_2Br$ $(CF_3CO)_2O$ $Ca(NO_3)_2$ H_2NR $Ba(OH)_2$ $^{45}CaCl_2$
C=C	Br_2 $Hg(CH_3CO_2)_2O$ $Hg(CF_3CO_2)_2O$ OsO_4
C-C	HCl

$$+ \ CF_3COOH(g)$$
(boiling point at 1atm   75°C)

SCHEME 1: Labelling of surface hydroxyls with trifluoroacetic anhydride (TFAA).

3.2. EXPERIMENTAL

Four types of cellulose with differing crystallinities were used in these studies: Avicell (Fluka Chemie AG), Sigmacell (Sigma Chemical Company Ltd), regenerated sponge cellulose (BPS Separations Ltd), and bacterial cellulose (BPS Separations Ltd). Polyvinylalcohol ($-CH_2CH(OH)-)_n$ (PVA, Aldrich Chemicals, 98% purity, 100% hydrolysed) served as a model polymer substrate for the surface derivatization experiments. Each material was washed in a Soxhlet solvent extraction apparatus for 12 hrs with isopropanol (Analar grade), and then for a further 12 hrs with dry hexane (Analar grade). Any remaining solvent was subsequently driven off under vacuum at 60 °C over several days. The cleaned samples were then cryomilled to ensure a similar particle size distribution (50 μm) prior to characterization. Trifluoroacetic anhydride (99% purity, Aldrich Chemicals) vapour was used as the labelling reagent.

A labelling apparatus was assembled[48], Figure 3.4. All joints were grease-free. The whole system routinely achieved a base pressure of better than 5×10^{-2} Torr and a

leak rate[49] of less than 1×10^{-3} Torr/min by using an Edwards single stage rotary pump

fitted with a liquid nitrogen cold trap. The trifluoroacetic anhydride (TFAA) was

subjected to repeated freeze-thaw cycles to ensure thorough degassing of the reagent

was achieved. Following evacuation of the sample cell, it was isolated from the vacuum

pump, and thenTFAA vapour was allowed to equilibrate into the empty volume at

ambient temperature ($\sim$ 25 °C). At this point, timing of the labelling reaction

commenced. Upon termination of exposure, the TFAA reservoir was isolated, and the

apparatus/sample pumped back down to its initial base pressure. For each material, a

reaction profile was compiled by varying the length of contact time with TFAA followed

by XPS quantification of the level of hydroxyl functionalization.

X-ray photoelectron spectroscopy (XPS) analysis was carried out on a AEI

ES200 X-ray photoelectron spectrometer operating in the fixed analyser transmission

(FAT) mode, at a pass energy of 65 eV, and an electron take-off-angle of 30° from the

substrate normal. Mg $K_{\alpha1,2}$ (1253.6 eV) ionising radiation was used as the

photoexcitation source. C(1s) photoelectron spectra were fitted with Gaussian

components having equal full widths at half maximum intensity (FWHM). All spectra

are referenced to the C(1s) core level shift for adventitious hydrocarbon at 285.0 eV[50].

Attenuated total reflection infrared (ATR-IR) measurements were taken on a Mattson

Polaris FTIR instrument, equipped with a Specac optical table and a KRS-5 ATR crystal.

Cryomilled samples were pressed into discs and then mounted into the cell. Infrared

spectra were accumulated at 4 cm^{-1} resolution in the range 400 cm^{-1} to 4000 cm^{-1} over

100 scans. X-ray diffraction measurements were taken at room temperature on a

Siemens D5000 diffractometer, using a Cu $K_{\alpha1,2}$ source operating at 40 kV and 40 mA,

over a $2\theta = 5°- 60°$ angular range.

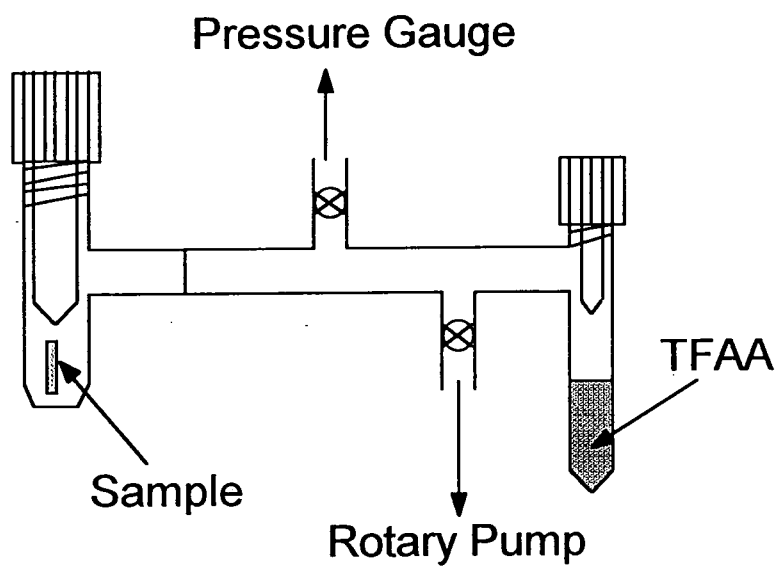Figure 3.4   TFAA labelling apparatus.

3.3. RESULTS

3.3.1. XPS and TFAA Labelling

C(1s) XPS spectra of unlabelled and labelled PVA are shown in Figures 3.5a and 3.5b. Chemical information about each modified polymer surface was obtained by fitting the C(1s) XPS spectrum to a range of carbon functionalities: hydrocarbon ($\underline{C}H_x$ ~285.0 eV), carbon singly bonded to one oxygen atom ($\underline{C}$-O ~286.6 eV), carbon singly bonded to two oxygen atoms (O-$\underline{C}$-O ~288.1 eV), carboxylate groups (O-$\underline{C}$=O ~289.1 eV), central carbon in a trifluoroacetate group (O=$\underline{C}$OCF$_3$ ~289.7 eV), and trifluoromethyl carbon ($\underline{C}F_3$ ~292.8 eV)[47]. Any contribution from Mg K$\alpha_{3,4}$ radiation was also taken into consideration, e.g. the CF$_3$ group introduces a satellite feature around 283.5 eV in the C(1s) spectra. The proportion of labelled hydroxyl groups was calculated from the CF$_3$(1s)/C(1s)$_{tot}$ peak area ratios normalised with respect to the maximum hydroxyl functionalization theoretically possible.

C(1s) XPS spectra of clean and labelled cellulose are shown in Figures 3.6a and 3.6b respectively. C(1s) binding energies for clean cellulose are in close agreement with those reported by Brown et al[51]. A minor carboxylate impurity at 289.1 eV, was also detected for all of the cleaned celluloses[51]. The extent of hydroxyl derivatization has been plotted out against time for each of the cellulose samples studied, Figure 3.7. It can be concluded that the relative rates of labelling decrease in the following order: Bacterial > Regenerated > Sigmacell > Avicell. The limiting level of hydroxyl functionalization in each case was around 80% of the maximum theoretical value. The times taken to reach this plateau value are summarised in Table 3.2.

3.3.2. ATR-FTIR of Cellulose Materials

Figure 3.8 shows an ATR-FTIR spectrum of Avicell, this can be assigned as follows: 670 cm^{-1} (OH wagging)[29], 893 cm^{-1}(C_1 group vibration)[52], 1000 cm^{-1} (C-C stretching modes)[53], 1060 cm^{-1} (C-C-O stretching mode)[53], 1120 cm^{-1} (C-O-C asymmetric stretch)[53], 1370 cm^{-1} (CH$_2$ bending mode)[29], 1429 cm^{-1} (in-plane OH bend)[22], 2893 cm^{-1} (C-H stretching mode)[53], 3300 cm^{-1} (intermolecularly bonded OH stretching mode)[53].

Infra-red crystallinity indices (C) were calculated from the absorbance peak area ratios[29, 52]:

$$C_a = \frac{A_{1370}}{A_{670}}$$

$$C_b = \frac{A_{1429}}{A_{2900}}$$

Table 3.2 lists the crystallinity indices C_a and C_b as determined by ATR-FTIR measurements. A linear correlation is found between the crystallinity indices and the limiting XPS labelling times, as illustrated in Figure 3.9. Laszkiewicz et al[11] have previously suggested that the 1429/893 cm^{-1} peak area ratio is representative of cellulose crystallinity, however no such linear relationship was found in this study.

Table 3.2.   **Summary of labelling, and crystallinity results.**

Sample	Plateau Time (Mins)	Crystallinity Ratio (XRD)	Crystallinity Indices (ATR-IR)	
			C_a (1370/670)	C_b (1429/2900)
PVA	3	-	-	-
Bacterial	20	0.69	2.31	0.043
Regenerated	200	0.49	2.45	0.068
Sigmacell	600	0.85	2.61	0.088
Avicell	1500	0.85	3.26	0.161
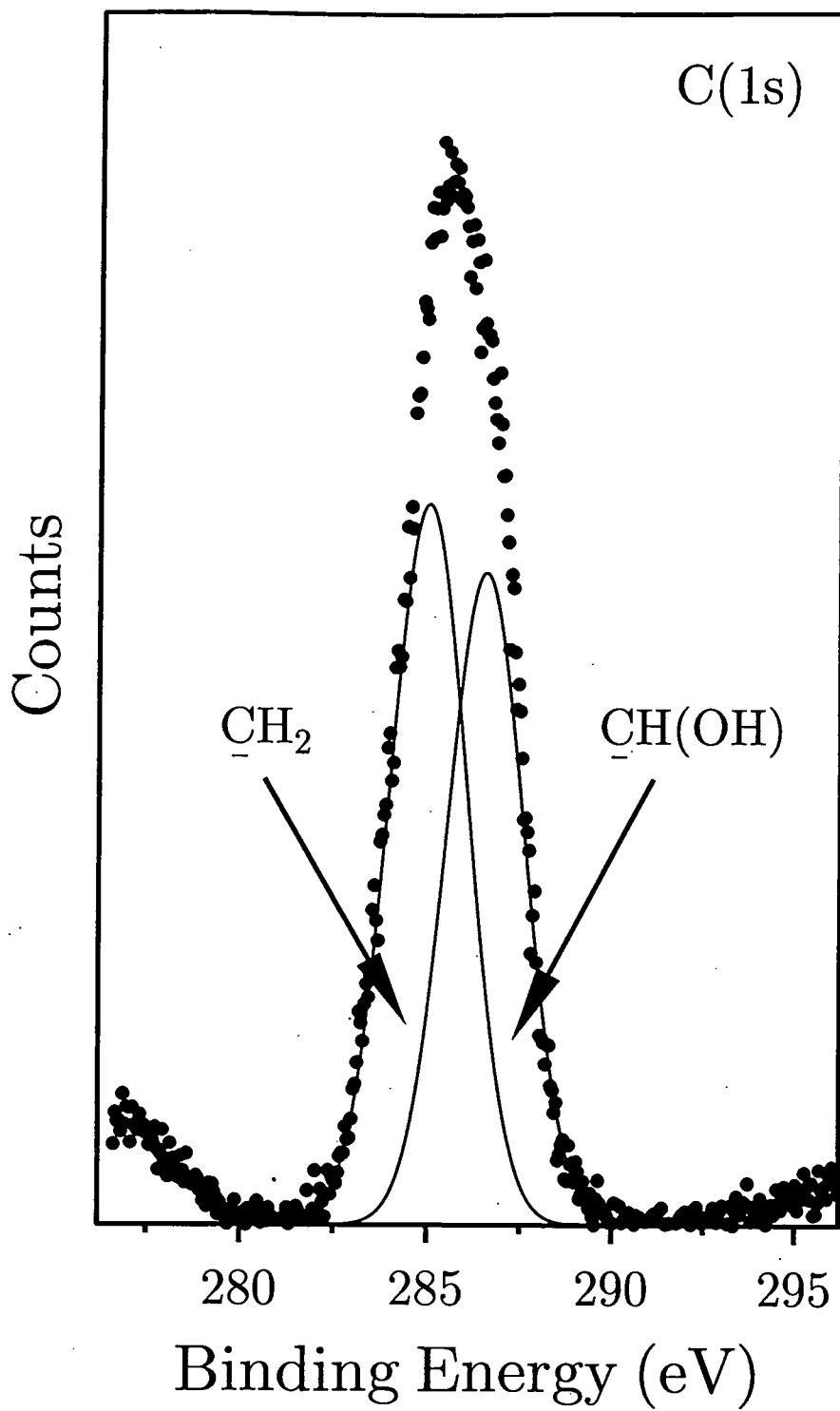
Figure 3.5(a)   C(1s) XPS spectra of clean PVA
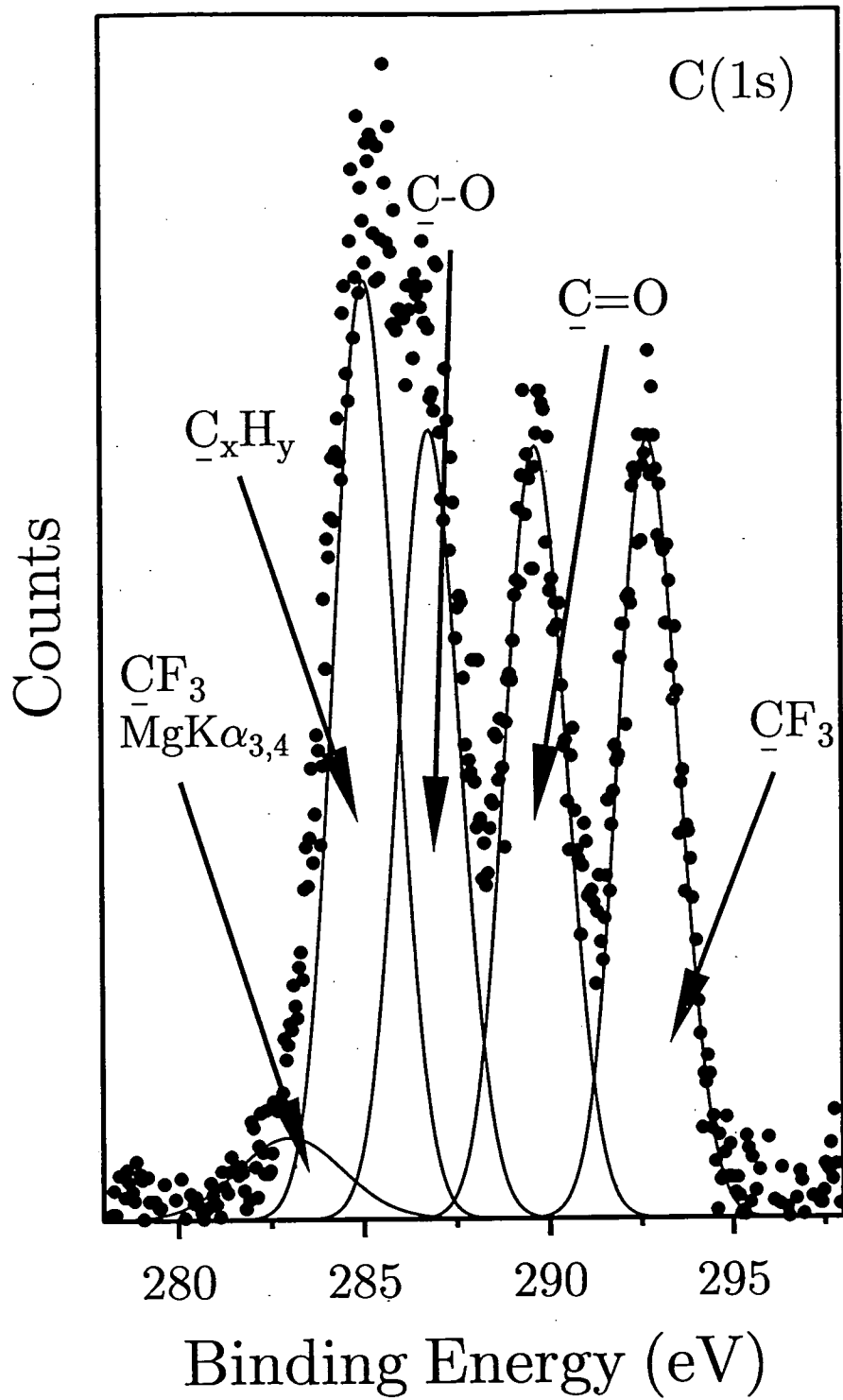
Figure 3.5(b) **C(1s) XPS spectra of clean TFAA labelled PVA.**
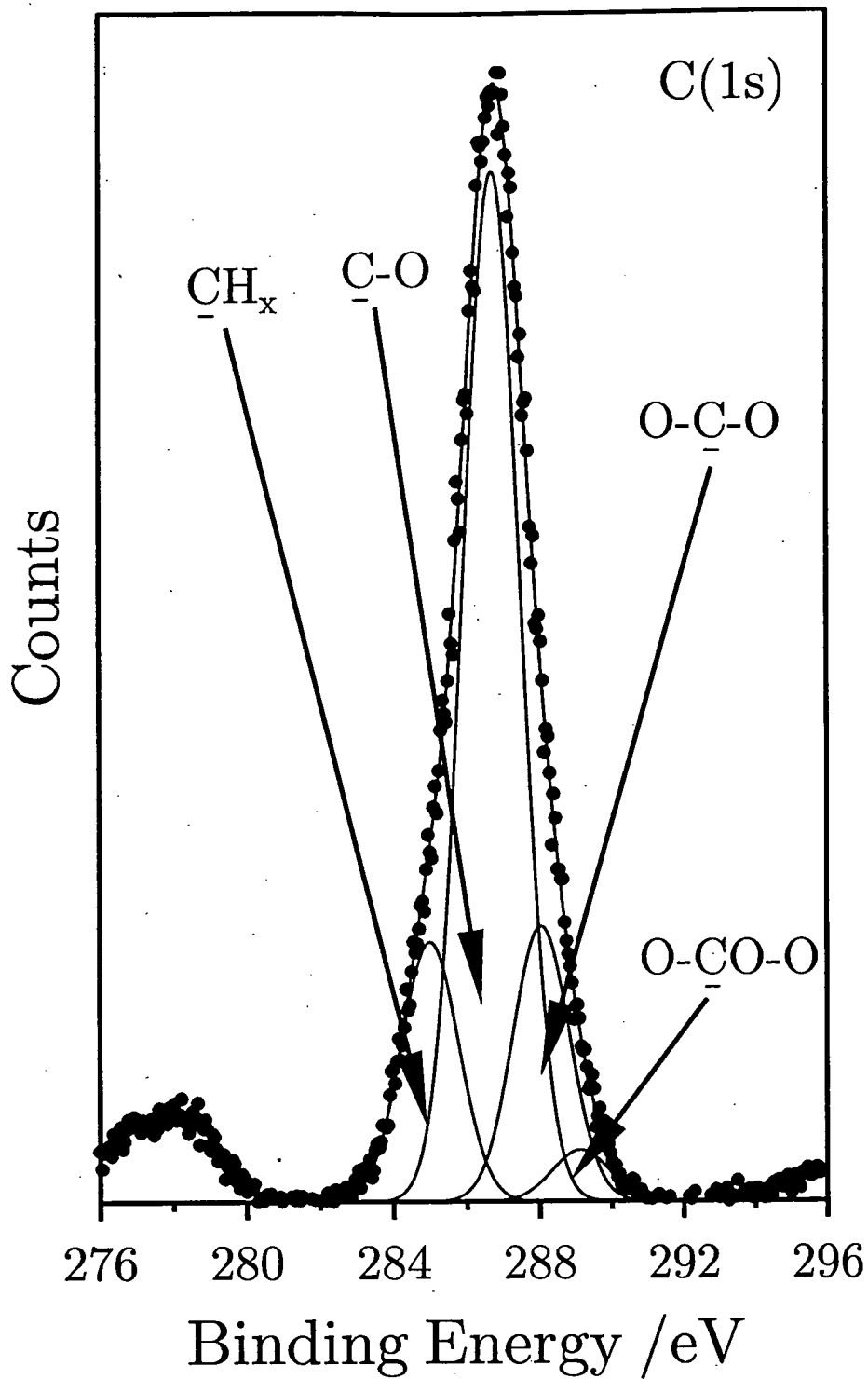
Figure 3.6(a) **C(1s) XPS spectra of: clean Avicell cellulose.**
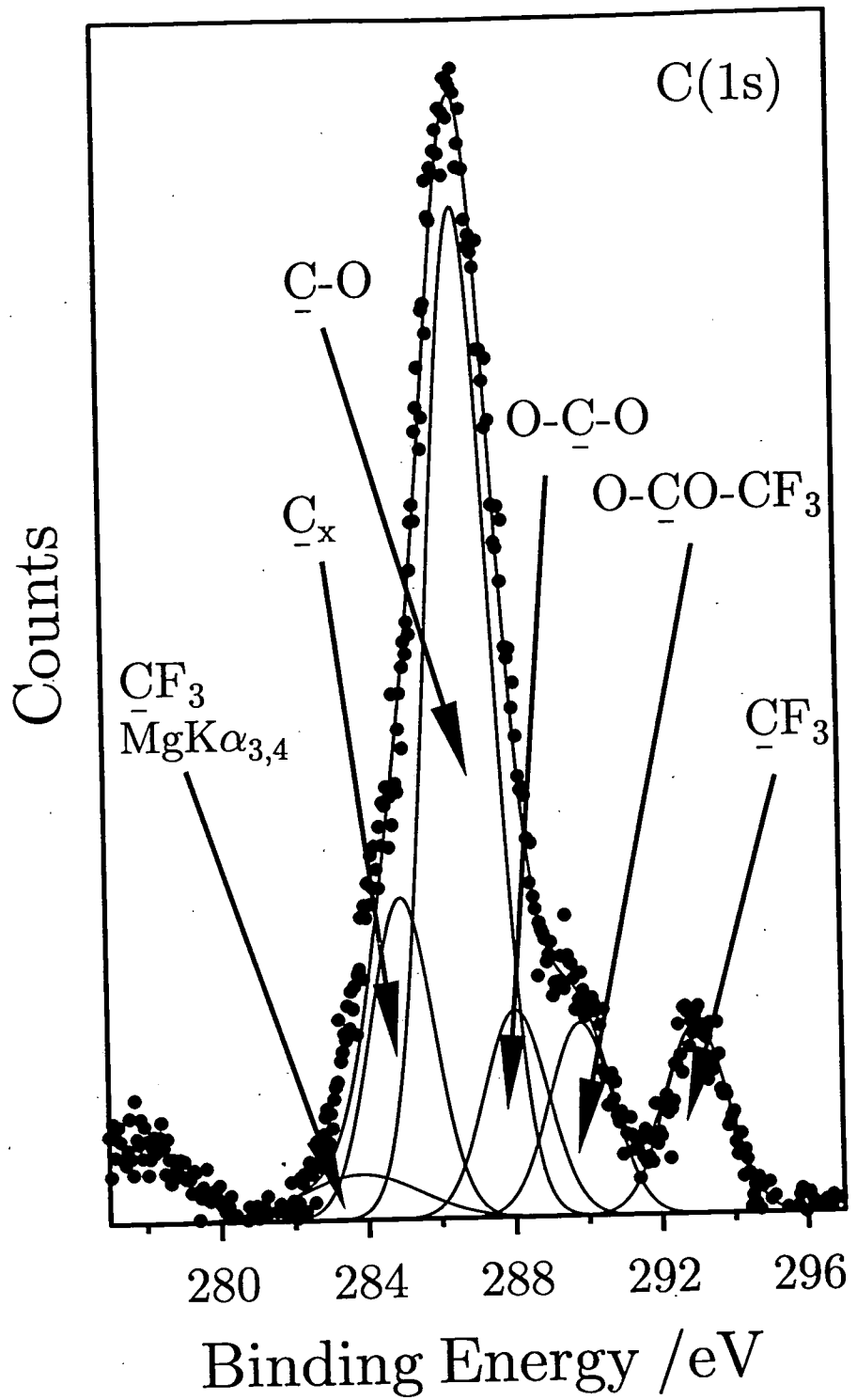
Figure 3.6(b)   **C(1s) XPS spectra of: TFAA labelled Avicell cellulose.**
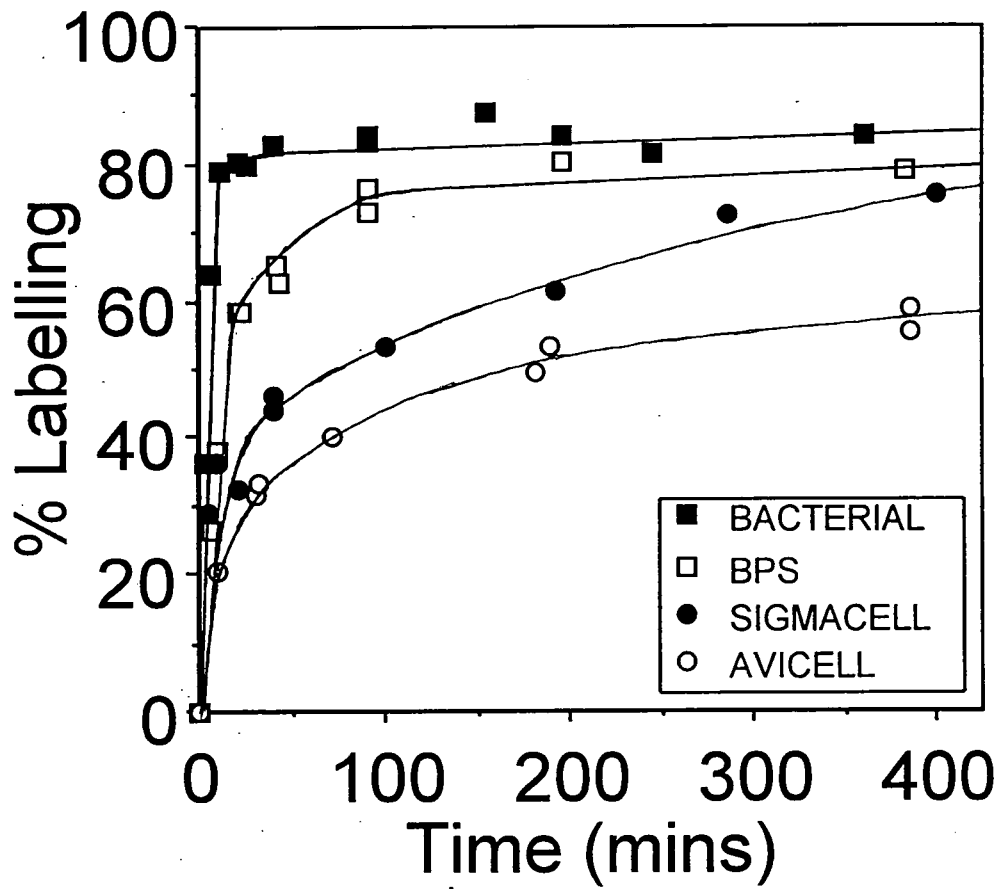
Figure 3.7   **Relative rates of hydroxyl functionalization by TFAA.**
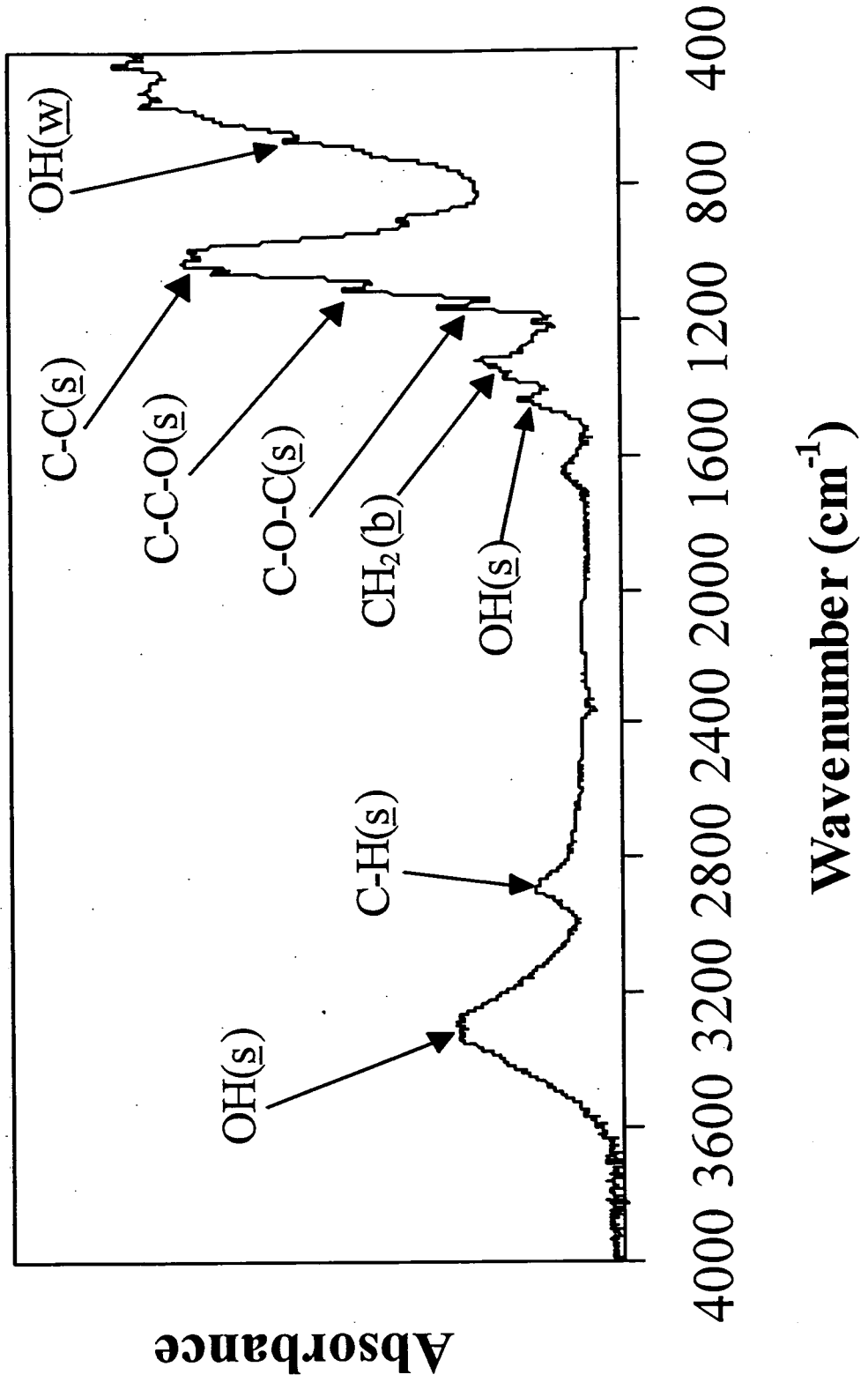
Figure 3.8   ATR-FTIR spectrum of Avicell cellulose. Stretching (s), bending (b) and wagging (w).
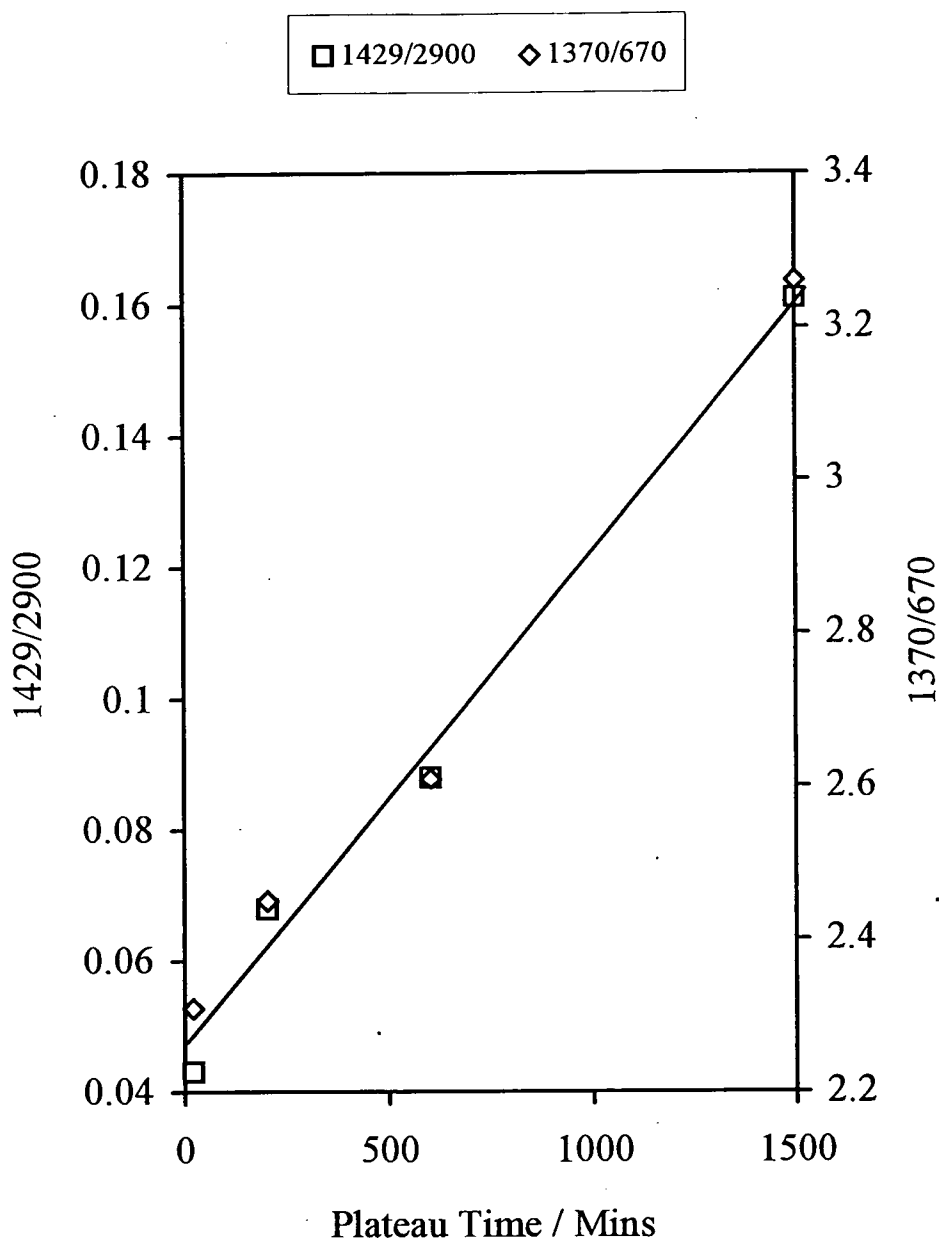
Figure 3.9   Crystallinity indices (as determined by ATR-FTIR) versus limiting TFAA labelling times.

3.4. X-RAY DIFFRACTION

The observed X-ray diffraction peaks for powdered cellulose can be attributed to crystalline scattering, and the diffuse background to disordered regions, Figure 3.10. Marked differences are evident between the four types of cellulose used in this study. Spectra corresponding to Sigmacell, Avicell and bacterial cellulose exhibit diffraction features at the following 2θ angles[52]: 23° (002), 21° (021), 17° (10$\bar{1}$) and 15° (101), these can be assigned to a Type I polymorphic phase of cellulose. The regenerated (BPS) cellulose is a Type II material, the 23° (002) and 20°(10$\bar{1}$) lattice planes having similar intensity, we would expect to see another diffraction feature around 2θ = 15° due to the (101) lattice plane[52] but this seems to be obscured by the amorphous background scatter. Crystallinity ratio (CR) values have been calculated by using a similar method to that described by Zeronian et al[54], Table 3.2. From these measurements it can be concluded that Sigmacell and Avicell have comparable crystallinities, the bacterial sample is more disordered, and the regenerated cellulose has the largest amorphous content. No obvious correlation is evident between the crystallinity ratio and the limiting TFAA labelling time, Table 3.2. For a polycrystalline specimen, the profile of each diffraction line is determined by crystallite size distribution, the nature and magnitude of lattice distortions, and the spectral distribution of energy in the incident radiation[55]. The cellulosic materials under investigation potentially have varying crystallite size distributions and therefore would be expected to exhibit different broadening effects.
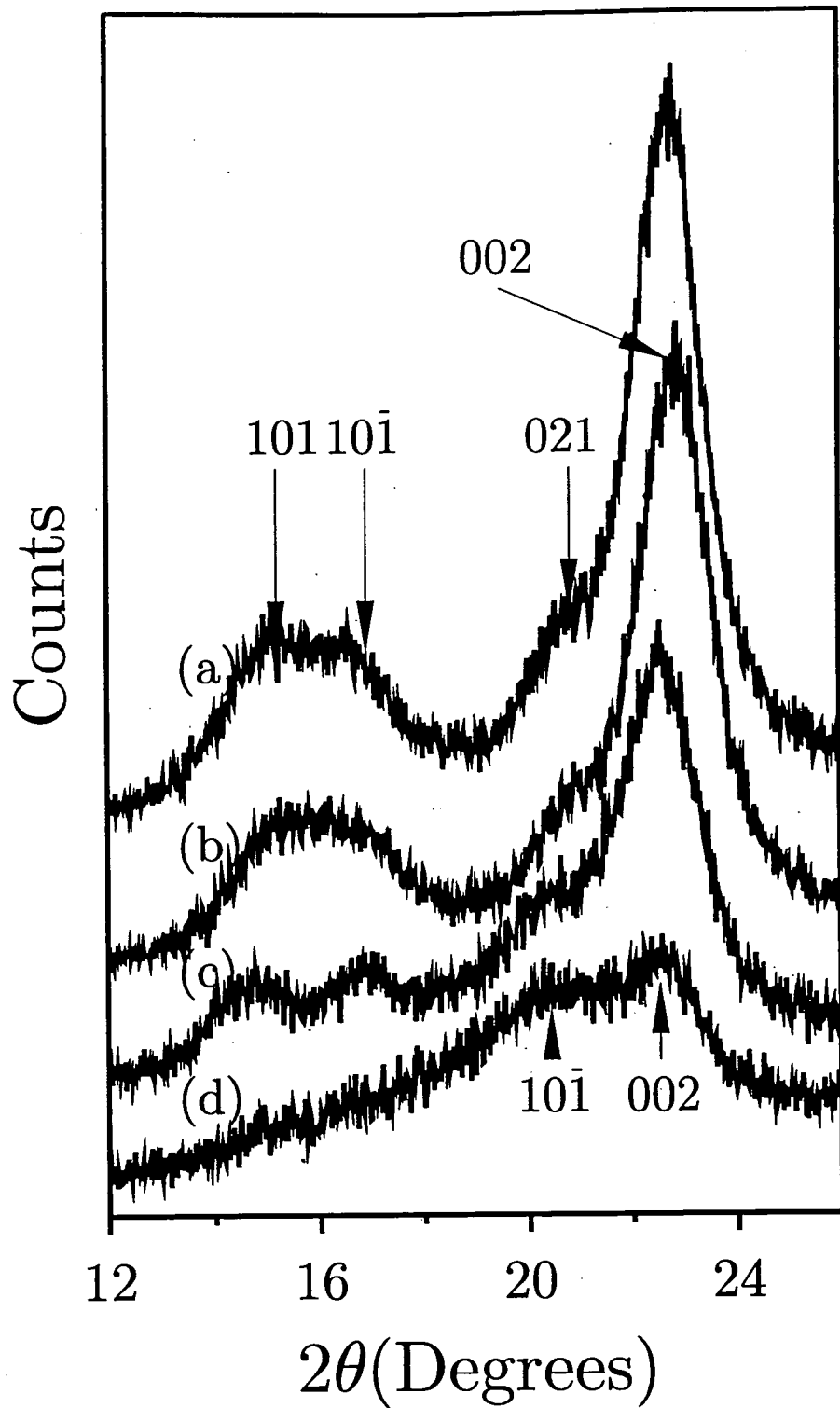
Figure 3.10   **Powder X-ray diffraction patterns for: (a) Sigmacell, (b) Avicell, (c) bacterial cellulose, and (d) regenerated cellulose.**

3.5. DISCUSSION

3.5.1. Chemical Accessibility and Crystallinity

In common with many other studies[45, 46, 55] PVA labelling occurs very rapidly, and to total completion. Whereas we have shown TFAA derivatization of the cellulosic materials to be sluggish in comparison, never reaching the predicted theoretical value. This can be attributed to the microcrystalline nature of the cellulose structure. Tightly packed cellulose chains experience strong hydrogen bonding leading to crystallite formation, whereas poorer packing leads to an open amorphous structure. Hence the efficiency of hydroxyl derivatization should be dependent upon the degree of cellulose crystallinity under consideration.

Our findings indicate that the rate of labelling by TFAA vapour is influenced by the degree of cellulose crystallinity. The form of the percentage labelling curves Figure 3.7, are consistent with those described for the methylation of hydroxyl groups in the review article of Jeffries[3]. The uptake of labelling reagent was observed to occur in two stages, an initial rapid phase was attributed to the derivatisation of the accessible hydroxyl groups followed by a much slower penetration of the labelling agent in to the more ordered regions. It is interesting to note however, the linear relationship between the accessibility defined by the maximum labelling times for each of the cellulose materials and the infra-red crystallinity indices, Figure 3.9, and the inconsistency present when we compare these values with those obtained from X-ray diffraction measurements, see Table 3.2.

3.5.2. XRD vs Infra-red Crystallinity Indices

XPS samples the topmost 20-50 Å whereas ATR-FTIR probes deeper down into the 100-1000 Å range, and XRD is a bulk characterization technique. Since there is a linear correlation between the XPS and infrared data, it can be concluded that the crystallinity measured at the surface resembles that present within the subsurface region. The non linear dependence of the XPS data upon crystallinity determined by X-ray diffraction can be explained in terms of X-ray diffraction being only sensitive to well-ordered regions above a minimum crystallite size[56, 57], infrared spectroscopy on the other hand measures crystallinity at the molecular level (i.e. interchain packing has a direct influence on the vibrational behaviour of the cellulose polymer)[52].

3.5.3. TFAA Labelling.

The derivatization of the hydroxyl groups with TFAA is irreversible, and prevents them from participating in hydrogen bonding, therefore a reduction in the strength of the hydrogen bonded network making the polymer more susceptible to swelling by solvent media would be expected. This was clearly evident during the labelling of PVA, where over long exposure times, a visible swelling of the polymer was observed, and is characteristic of a macroheterogenous reaction of a semi-crystalline polymer. In contrast to other techniques used for determining surface hydroxyl accessibility in celluloses, this method is non-solvent based and is therefore less likely to suffer from swelling effects. No comparable swelling was found for the cellulosic materials. This may be attributed to one or more of the following factors: (i) cellulose possesses a greater porosity[58], and this pore structure may accommodate any observable swelling; (ii) hydrogen bonding may be

more extensive within cellulose preventing a rapid disruption of the network; or (iii) since surface hydroxyl density is much lower in cellulose, this should result in a smaller number of trifluoroacetyl groups being incorporated into the material. The only major limitation of the TFAA labelling technique appears to be that it is unable to discriminate between the reactivities of the three different types of hydroxyl groups present within an individual cellulose monomer unit.

3.6. CONCLUSIONS

This study has demonstrated the application of a non-solvent based labelling technique followed by XPS quantification, the hydroxyl reactivity can be related to the crystallinity of the cellulose matrix determined by infra-red methods. Amorphous celluloses can be functionalized much more readily than their crystalline counterparts and this is an important factor to take in to consideration when selecting a cellulose material.

3.7. REFERENCES

1   Hon D. N. S., *ACS Symp. Ser.*, **476**, 176 (1992).

2   Kremer R. D., Tabb D., *International Laboratory*, **July/August**, 40 (1989).

3   Jeffries R., Jones D. M., Roberts J. G.,Selby K., Simmens S. C., Warwicker J. O., *Cellulose. Chem. Technol.*, **3**, 255 (1969).

4   Callstrom M. R., Bednarski M. D., *MRS Bulletin*, **Oct.**, 54 (1992).

5   Rowland S. P., *ACS Symp. Ser.*, **49**, 20 (1977).

6   Allen T. C., Cuculo J. A., *J. Polym. Sci: Macromol. Rev.*, **7**, 189 (1973).

7   Nevell T. P., Zeronian S. H., in *Cellulose Chemistry and its applications*, John

Wiley, New York, 1986.

8   Rowell R. M., Young R. A., Eds., *Modified Cellulosics*, Academic Press, New York, 1978.

9   Kennedy J. F., Phillips G. O., Wedlock D. J., Williams P. A., Eds. *Cellulose Chemistry and Its Applications*, Ellis Horwood, Chichester, 1985.

10   Durso D.F., in *Modified Cellulosics*, Rowell R. M., Young R. A., Eds.,p. 23. Academic Press, New York, 1978.

11   Laszkiewicz B., Wcislo P., *J. App. Polym. Sci..*, **39**, 415 (1990).

12   Hon D. N. S., Ou N-H., *J. Polym. Sci. : Part A : Polym. Chem.*, **27**, 2457 (1989).

13   Hon D. N. S., Sanlius J. M., *J. Polym. Sci. : Part A : Polym. Chem.*, **27**, 4143 (1989).

14   Peterson E. A., Sober H. A., in *Chromatography of Proteins : I Cellulose Ion Exchange Adsorbents*, *J. Am. Chem. Soc.*, **78**, 751 (1956).

15   Chen H-L., Hou K. C., *Reactive Polymers*, **5**, 5 (1987).

16   Paul D., Malsch G., Bossin E., Weise F., Thomaneck U., Brown G. S., Werner H, Falkenhagen D., *Artif. Organs.*, **14**, 2 (1990).

17   Woffindin C., Hoenich N. A., Matthews J. N. S., *Nephrol. Dial. Transplant.* **1992**, *7*, 340.

18   Liang C. Y., Marchessault R. H., *J. Polym. Sci.*, **37**, 385 (1959).

19   Sarko A., Muggli R., *Macromolecules*, **7**, 86 (1974).

20   Woodstock C., Sarko A., *Macromolecules*, **13**, 1183 (1980).

21   Moss B., Dorset D. L., Douglas L., *J. Polym. Sci., Polym. Phys. Ed.*, **20**, 1789 (1982).

22   Honjo G., Watanabe M., *Nature*, **161**, 326 (1958).

23   Beg M. M., Aslam J., Khan Q. H., Butt N. M., Rolandson S., Ahmed A. U., *J. Polym. Sci., Polym. Lett. Ed.*, **12**, 311 (1974).

24   Ahmed A. U. , Ahmed N., Aslam J., Butt N. M., Khan Q. H., Atta M. A., *J. Polym. Sci., Polym. Lett. Ed.*, **12**, 311 (1974).

25   Hemans P. H., Weidinger A., *J. Appl. Phys.*, **19**, 491 (1948).

26   Wakelin J. H., Virgin H. S., Crystal E., *J. Appl. Phys.*, **30**, 1654 (1959).

27   Hosemann R., *Polymer*, **3**, 349 (1992).

28   Newman R. H., Hemmingson J. A., *Holzforschung*, **44**, 351 (1990).

29   Nelson M. L., O'Connor R. T., *J. Appl. Polym. Sci.*, **8**, 1311 (1964).

30   Richte U., Krause T., Schempp W., Braun D., *Angew. Makromol. Chemie.*, **185/186**, 155 (1991).

31   Zeronian S. H., Cooke M. L., Alger K. W., Chandler J. M., *J. Appl. Polym. Sci. : Appl. Polym. Symp.*, **37**, 1053 (1983).

32   Mann J., Marrinan H. J., *Trans. Faraday. Soc.*, **52**, 492 (1956).

33   Heath J. E., Jeffries R., *J. Appl. Polym. Sci.*, **12**, 455 (1968).

34   Rowland S. P., Post A. W., *J. Appl. Polym. Sci.*, **10**, 1751 (1966).

35   Hessler L. E., Power R. E., *Textile Research J.*, **24**, 822 (1954).

36   Assaf A. G., Haas R. H., Purves C. B., *J. Amer. Chem.Soc.*, **66**, 59 (1944).

37   Verlhac C., Dedier J, Chanzy H., *J. Polym. Sci. : Part A : Polym. Chem.*, **28**, 1171 (1990).

38   Rowland S. P., Howley P. S., *J. Polym. Sci. : Part A : Polym. Chem.*, **26**, 1769 (1988).

39   Braybrook J. H., Hall L. D., *Prog. Polym. Sci.*, **15**, 715 (1990).

40   Everhart D. S.,Reilley C. N., *Anal. Chem.*, **52**, 655 (1981).

41   Bradley A., Czuha M., *Anal, Chem.*, **47**, 1838 (1975).

42   Batich C. D., *Appl. Surf. Sci.*, **32**, 57 (1988).

43   Davies C., Munro H. S., *Polym. Comm.*, **29**, 47 (1988).

44   Gerenser L. J., Elman J. F., Mason M. G., Pochan J. M., *Polymer* **26**, 1162 (1985).

45   Dickie R. A., Hammond J. S., DeVries J. E., Holubka J. W., *Anal. Chem*, **54**, 2045 (1982).

46   Chilkoti A., Castner D. G., Ratner B. D., Briggs D., *J. Vac. Sci. Technol.*, **A8**, 2274 (1990).

47   Beamson G., Briggs D., in *High Resolution XPS of Organic Polymers-The Scienta ESCA 300 Database* p. 236. John Wiley, Chichester, 1992.

48   Wilson R., PhD. Thesis, University of Durham , Durham, 1984.

49   Ehrlich C. D., Basford J. A., *J. Vac. Sci. Technol.*, **A10**, 1 (1992).

50   Johansson G., Hedman J., Berndtsson A., Klasson M., Nilsson R. J., *Electron Spectr.*, **2**, 295 (1973).

51   Brown N. M. D., Hewitt J. A., Mennan B. J., *Surf. Int. Anal.,* **18**, 199 (1992).

52   Wadsworth L. C., Cuculo J. A., in *Modified Cellulosics*, Rowell R. M., Young R. A., Eds.,p. 117. Academic Press, New York, 1978.

53   Silverstein R. M. , Bassler G. C., Morrill T. C., Spectrometric Identification of Organic Compounds, 4th Ed., John Wiley, New York, 1981.

54   Buschle-Diller G., H. Zeronian S., *J. App. Polym. Sci.*, **45**, 967 (1992).

55   Davies C., Munro H. S. , *Polym. Comm.,* **29**, 47 (1988).

56   Wilson A. J. C. , in *Mathematical Theory of X-ray Powder Diffractometry,*

Cleaver-Hume Press, London, 1963.

57   Klug H.P., Alexander L. E., in *X-ray Diffraction Procedures - For Polycrystalline and Amorphous Materials*, John Wiley, New York, 1974.

58   Porter B. R., Rollins M. L., *J. App. Polym. Sci.*, **16**, 217 (1972).

4. AN INVESTIGATION OF THE EFFECTS OF SWELLING AND CROSSLINKING ON THE SURFACE AREA, PORE STRUCTURE AND PROTEIN CAPACITY OF A CELLULOSE BASED BIOSEPARATION MEDIUM.

4.1. INTRODUCTION

Cellulose can be employed as an effective, low cost chromatography medium for protein separation[1-4], and as was described in the introduction to this thesis the performance of a bioseparation material is ultimately determined by the fundamental properties of the solid phase. We have already examined the effect of the microstructural nature of cellulose with particular reference to the short range crystallinity of the matrix and its effects upon the accessibility of a gaseous labelling agent. In this chapter we intend to demonstrate the significance of the pore structure and its direct relationship to protein uptake in the case of a quaternary methyl functionalised cellulose matrix.

Pore structure studies in the past have explained macroscopic pore structure parameters in terms of microscopic structure models[5], i.e. using microstructural bonding characteristics of the polymer network to explain permeability, specific surface area and porosity characteristics. Consequently modifications to the microstructural nature of an extended cellulose sponge matrix would be expected to have a concurrent effect on the pore structure and surface area of the material.

In this chapter we have examined the effect of crosslinking and alkali swelling on the pore structure of a regenerated cellulose. The alteration of the pore structure has then been related to the binding of Bovine Serum Albumin (BSA) to the quaternary methyl derivatised form of the regenerated cellulose.

4.1.1. Porosity and Specific Surface Area

Porosity is defined as the fraction of the bulk volume of the porous sample that is occupied by a pore of void space. The voids can be described as interconnected or effective pore space, non-interconnected or isolated pore space and dead end or blind pore space. The isolated pores cannot contribute to matter transport through the matrix and dead end pores are able to contribute only negligibly. The pore structure can strongly influence the access of large and small molecules to the internal surface of the material.

The specific surface area of a porous material is defined as the interstitial surface area of the voids and pores per unit mass of the porous material. There is an inverse relationship between surface area and pore diameter size.

4.1.2. The Pore Structure of Cellulose

The cellulose microstructure was described in chapter 3, as a hydrogen bonded semicrystalline fibrillar network. These microfibrillar units bond together in a lamellar structure to constitute cellulose fibres[6].

In a similar way that amorphous sections of the cellulose microfibril were attributed to imperfections in the packing of the cellulose chains, porosity arises due to imperfect packing of the microfibrils within the cellulose fibres[7]. The fibrillar nature of cellulose results in a huge range of pore sizes from micropores a few angströms in diameter to macropores with diameters approaching several microns.

Pores with diameters less than 25Å are referred to as micropores, and result from extremely small imperfections in the bonding of the cellulose chains on a molecular level. Mesoporosity arises due to inefficient packing of the cellulosic microfibrils yielding intrafibrillar (or intralamellar) pores, 25-75 Å in diameter. Macropores with diameters greater than 75Å are present in-between the hydrogen bonded fibrillar network.

Conventional methods used for probing the porosity of cellulose are selected on the basis of pore sizes of interest. Water[8,9], benzene[10], ethanol[11], and nitrogen[12] sorption techniques have been used to evaluate pores in the 10-100 Å regime. Distinct relationships have been observed between the micro and meso porosity of cellulose and chemical accessibility studies, Nelson and Oliver[13] attributed a large proportion of the reactive surface of a range of celluloses to their micro and meso porous structure. The micro and meso pores determine the accessibility of small molecules to the matrix, for example this has important ramifications in terms of derivatisation reactions. Larger meso and macropores control the accessibility of the potential adsorbate molecule in a bioseparation system.

Fewer studies have considered macropores between 75-1000Å in diameter, since they have proved much more difficult to characterize. Cross-sectional electron

microscopy of alkali swollen cellulose fibres have suggested a 'honey-comb' structure of cylindrical pores[14] extending down the length of the fibre. Pores up to 0.1 μm in diameter were observed by this method, larger pores are located nearer to the edges of the fibre whilst the smallest pores are present in a central core region[6]. The solute exclusion method pioneered by Aggebrandt and Samuelson[15], and further developed by Stone et al[16] enabled pores in the 100-1000 Å range to be characterized, but this is subject to only a limited degree of accuracy.

Mercury porosymmetry[7, 17, 18] has been used to measure cellulose pore apertures between 0.1-100 μm.

4.1.3. Matrix Processing

Chemical treatment of the base material can disrupt the hydrogen bonding in cellulose, and thereby reduce interfibrillar cohesion, which causes structural rearrangement and redistribution of pore architecture[19, 20].

4.1.3.1. *Swelling*

The swelling[12, 14, 21 - 24] of cellulose is generally the first reaction step in a large scale derivatization of cellulose[25], and can be achieved using a range of reagents including water[9, 24, 26], methylamine[23], and liquid ammonia, though alkali hydroxide solutions are the most widely used. The term 'mercerization'[6, 23, 24] has been employed to describe swelling with alkali hydroxide solutions, and has been shown to increase the micro/meso-porous nature of the matrix[10, 12] and improve the efficiency of derivatization

reactions[23]. Alternative studies have demonstrated that hydrophobic folding of the matrix at a high pH gives rise to macropore shrinkage in conjunction with a concomitant decrease in accessibility to the charged centres for protein attachment[2]. The derivatization of cellulose has also been shown to cause swelling of the matrix.

4.1.3.2. *Crosslinking*

Highly crystalline cellulose consists of a close packed supramolecular microfibrillar structure, which hinders the penetration of large and/or poorly charged species into the cellulose matrix; this results in a small number of readily accessible reactive sites, and therefore ultimately a low protein binding capacity[4]. In order to maximise accessibility a cellulose with a high amorphous content should be used, however amorphous celluloses have relatively poor mechanical properties[6], and require strengthening via crosslinking reactions.

The basis for the crosslinking chemistry of cellulose had its foundations in the 1950's, driven by the demand for wrinkle free[6], shrink proof textiles and fabrics. There are a huge number of di and tri-functional reagents[6, 27] capable of bridging the gap between the hydroxyls on neighbouring fibrillar units. A few studies have shown a reduction in mesoporosity following the crosslinking of cellulose[12, 28], though no studies have been found that consider the effect of crosslinking on the macropore region.

4.1.3.3. *Drying*

The cellulose network is extremely sensitive to drying, the hydrogen bonded

structure can be swollen as described above and is stabilised through interactions with aqueous molecules in the microfibrillar structure[26]. The presence of water molecules is therefore crucial to the mechanical stability of the matrix and lowering the water content can lead to collapse of the pore structure[11, 29] resulting in a loss of surface area and available pore volume[10].

4.2. EXPERIMENTAL

4.2.1. Sample Preparation

Regenerated sponge cellulose, derived from wood pulp and made via the *viscose* process[30] was used as the base material for the following investigation. Prior to examination each sample was rinsed in water, freeze dried and stored under vacuum (~0.1 Torr) at 50 °C for two weeks prior to analysis. Freeze drying has been shown to minimise pore shrinkage, and the collapse and distortion of the supramolecular structure of the polymer which occurs during dehydration.

4.2.1.1. *Swelling with NaOH*

Swelling of the untreated regenerated cellulose (sample 1) was attempted by immersing it in 2M NaOH for 2hrs at 100 °C, the resulting material was designated sample 2.

4.2.1.2. *Crosslinking*

Cross-linked samples were prepared from the sodium hydroxide swollen regenerated cellulose (sample 2) by BPS Separations Ltd. using 0.5%, 1.0%, 1.5%, and 2.0% by volume concentrations of epichlorohydrin in accordance with the Scheme 1 shown below. We can see in Scheme 1 below that the crosslinking of the cellulose matrix is achieved by the acid induced ring opening of the epoxide on the epichlorohydrin molecule (Scheme 1a). This takes place via the attack of the nucleophilic hydroxyls on the cellulose molecule on the protonated epoxide (Scheme 1b) and leads to the product (Scheme 1c). Under basic conditions intermolecular substitution can occur and the chlorine atom acts as a good leaving group (Scheme 1d) which leads to the formation of another epoxide ring (Scheme 1e). Further reaction of this ring can be achieved under acidic conditions as discussed previously leading to the crosslinking of the cellulose matrix (Scheme 1f). For future reference these are referred to as samples 3, 4, 5, and 6 respectively.

4.2.2. Specific Surface Area and Pore Structure Analysis

Nitrogen adsorption isotherms were measured for each cellulose sample using a PMI Brookhaven Sorption apparatus, each sample was outgassed at 0.1 Torr and room temperature for 48hrs prior to analysis. Pore size distributions were calculated from the adsorption region of the isotherm using the modified[31] procedure developed by Pierce[32]. The Brunauer, Emmett and Teller (BET)[33,34] method for specific surface area determination was employed. A detailed description of the theory outlining calculation of the BET surface area and pore distribution can be found in chapter 2, section 2.4.
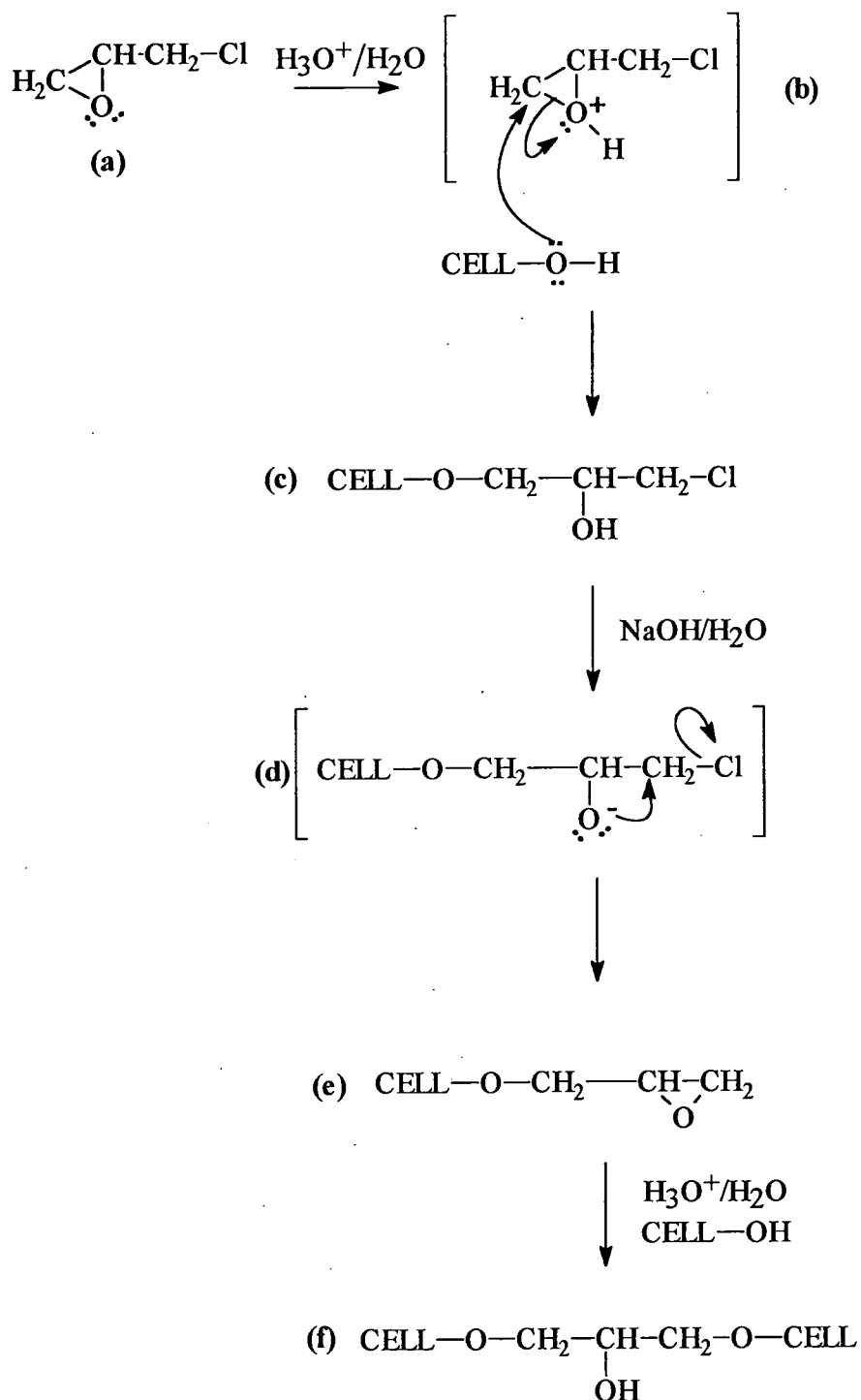
SCHEME 1: The crosslinking of cellulose using epichlorohydrin.

4.2.3. Scanning Electron Microscopy (SEM) study of the Cellulose Matrix

SEM images of the untreated cellulose matrix was obtained on our behalf by BPS Separations Ltd. using a Jeol JSM-6400 WinSEM at a voltage of 10 keV with electron beam spot sizes ranging from 10 - 100 nm in diameter. The samples were prepared for SEM analysis by attaching them to a 3 cm diameter aluminium disc using conductive carbon based adhesive. The sample was then coated with gold using an SC510 sputter coater (V.G. Microtech, Uckfield, UK) operating at 0.1 mbar pressure of Argon and with a sputtering current of 30 mA. A three minute sputtering treatment was found to give the best gold coating for optimum imaging.

4.2.4. Protein Uptake Measurements

Protein uptake measurements were performed by BPS Separations Ltd. in order to quantify the effects of swelling and crosslinking upon the binding of a biomolecule. The measurements were based upon the selective adsorption of Bovine Serum Albumin (BSA) from a solution of known concentration. Epichlorohydrin in aqueous base solution was used as a crosslinking reagent for cellulose[27, 35 37], and subsequently derivatised to attach quaternary methyl ligands (QM)[1]. Quaternary methyl ligands have specific activity towards BSA and matrices derivatized in this manner are often employed as hydrophobic interaction chromatography matrices[38]. The adsorbed BSA was then eluted from the matrix with a known quantity of 0.1 M NaCl. The amount of BSA in the eluate was determined using High Performance Liquid Chromatography (HPLC) and a comparison of the effect of increasing levels of crosslinker upon the levels of protein uptake was made.

4.3. RESULTS

4.3.1. The Cellulose Nitrogen Adsorption Isotherm

A typical nitrogen adsorption isotherm is shown in Figure 4.1, and it is clear from this that cellulose exhibits an unusual type of isotherm which does not fall in to the five types listed in the BET classification (see chapter 2, section 2.4). Closer examination of the adsorption isotherm shown in Figure 4.1 reveals the presence of step features or kinks at partial pressures in the standard state of nitrogen ranging from 0.3 to 0.7.

The point where completion of a monolayer occurs can be observed at a partial pressure of nitrogen between 0.05 and 0.1 and hence we are able to determine the monolayer capacity and furthermore the specific surface area of these materials. At higher partial pressures of nitrogen the deviation of the adsorption isotherm from the BET classification indicates the porous nature of the cellulose sponge. The step features labelled A, B and C in Figure 4.1 can be attributed to the filling of pores of a particular diameter. For example the step feature marked A in Figure 4.1 can be attributed to a larger number of pores with diameters ranging from 300 to 500 Å, therefore the increase in amount of gas adsorbed in for each increment in the partial pressure of nitrogen is due to the effect of capillary forces which enhance the tendency of the nitrogen to condense within the pore. The step feature corresponds to the point were the maximum number of nitrogen molecules have condensed in the pore, leading to a complete filling of the pore and a reduction in the available surface area. Hence in the next increment in partial pressure we observed a reduction in the amount of adsorbed gas.

4.3.2. Specific Surface Area

A BET plot for the unmodified cellulose (sample 1) is shown in Figure 4.2, the BET treatment of the adsorption data is particularly applicable in this case and the specific surface area of the sample can be calculated from these data with good accuracy. The specific surface area values for samples 1-7 are shown in Table 4.1 below. The third column shows the variance in the measurements to one standard deviation.

Swelling of the matrix with NaOH resulted in a large increase in surface area, from 35.7 m^2/g (sample 1) to 55.4 m^2/g (sample 2). However, statistically insignificant differences in the surface areas were observed for the cross-linked samples (3-6), each cross-linked material having a surface area ≈ 50 m^2/g, which compares well with the areas of dried cellulose materials found in the literature[29].

Table 4.1   Specific Surface Area Values for Samples 1-6

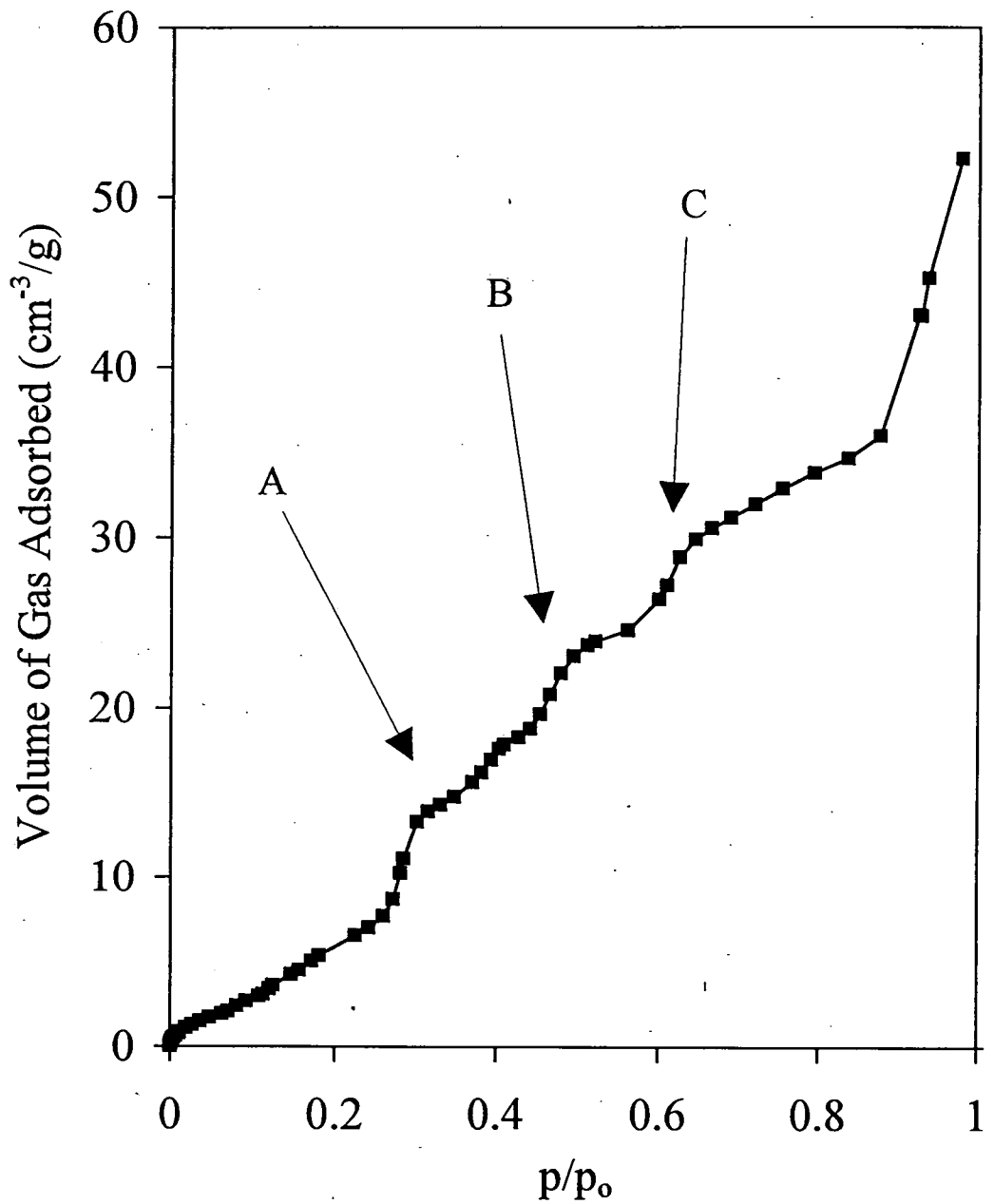| Sample	Specific Surface Area (m^2/g)	σ_x $(\sigma_x = 1\ s.d)$
1	35.7	1.5
2	55.4	0.17
3	57.5	4.6
4	53.5	0.9
5	48.7	1.0
6	51.2	2.7

Figure 4.1   A typical nitrogen adsorption isotherm plot obtained from the unmodified cellulose membrane (Sample 1), the labels A, B and C refer to the step features in the adsorption isotherm which deviate from typical BET classification.
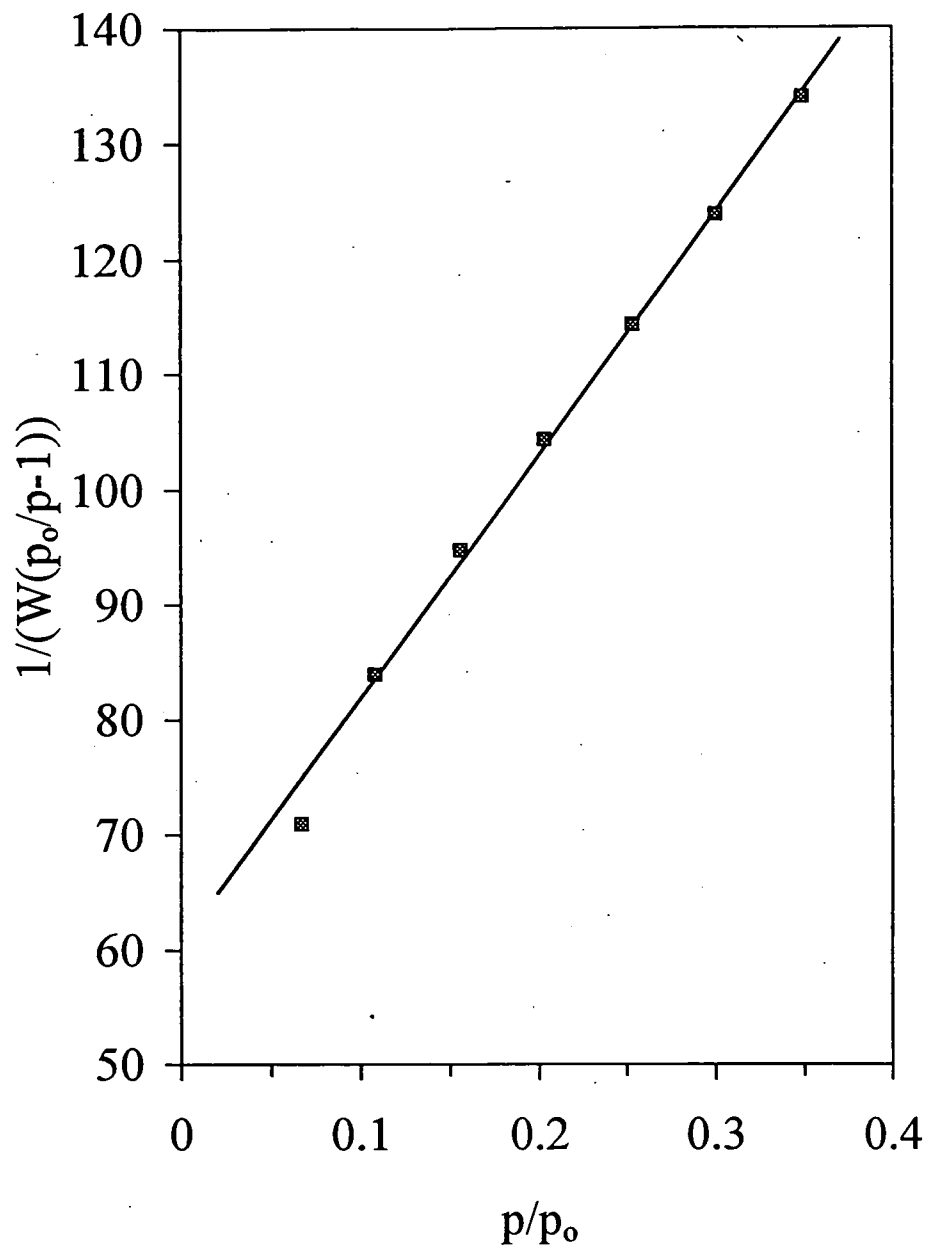
Figure 4.2   **A BET plot obtained from the unmodified cellulose membrane (Sample 1).**

4.3.3. Pore Structure

4.3.3.1. *Untreated Cellulose*

The long range pore structure of the untreated regenerated cellulose material is shown in the Scanning Electron Microscope (SEM) image in Figure 4.3. The 'sponge-like' nature of the material is clearly demonstrated and the pores have sizes ranging from 20 μm to 400 μm in diameter. The large pores shown in Figure 4.3 however, contribute almost negligibly to the total pore volume of the material as a whole and if we examine the SEM image more closely the presence of smaller pores on the surface of the cellulose can just be distinguished although the resolution of the image is not sufficient to determine their sizes.

In common with many porous membranes used for bioseparation it is the internal pore structure that contributes in the main to the total pore volume of the material. The pore size distribution for untreated cellulose (sample 1) is shown in Figure 4.4 and this is typical of pore distributions observed for other cellulose based materials[10, 13]. It is noticeable that most of the pore volume is located at less than 300 Å aperture diameter, whilst the majority of pores are located around 30 Å.

4.3.3.2. *Swelling with NaOH*

Comparing the overall pore distributions for the untreated cellulose (sample 1) and the sodium hydroxide swollen cellulose (sample 2) in Figure 4.3 we can see that the action of the sodium hydroxide on the base material leads to an increase in the

mesoporosity of the sample. Examining the pore distribution for sample 2 more closely reveals the majority of pores with diameters of 30Å followed by a broad shoulder extending to around 100Å before the distribution falls.

The macroporous structure of samples 1 and 2 were also examined and are shown in Figure 4.5. In this case pronounced differences can be seen in the 300 to 1100Å region. In the case of the untreated cellulose (sample 1) there is a lack of significant pore structure in this region, whereas in the case of the swollen material (sample 2) a larger number of pores are present with diameters of 500 - 600 Å and 600 - 800 Å.

4.3.3.3. *Cross-linked Cellulose*

The reaction of the swollen cellulose with 0.5%, 1.0%, 1.5% and 2.0% by volume of epichlorohydrin crosslinking solution (samples 3, 4, 5 and 6 respectively) causes a reduction in macroporosity with increasing crosslinker concentration. Figure 4.6 shows that as the crosslinking reagent concentration is increased, the number of pores at 600 Å are reduced to approximately one third of their original value, beyond which they experience no further perturbation. The pores in the 800 Å range virtually disappear at low crosslinker concentrations. The pore volume corresponding to 1100 Å apertures is slightly lowered by 0.5% crosslinking reagent, however there is a rapid attenuation of these macropores at higher concentrations. In contrast the meso and microporosity region remains virtually unperturbed by the epichlorohydrin solution with respect to the uncross-linked swollen cellulose material (sample 2).
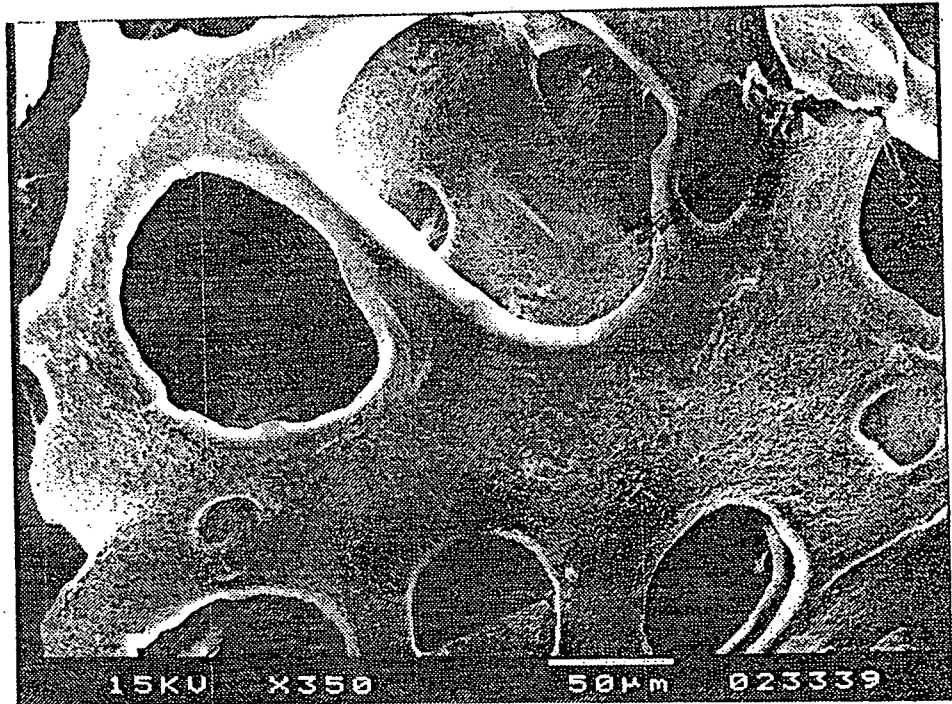
Figure 4.3 **SEM image of the untreated cellulose matrix[39], the scale bar represents 50 μm.**
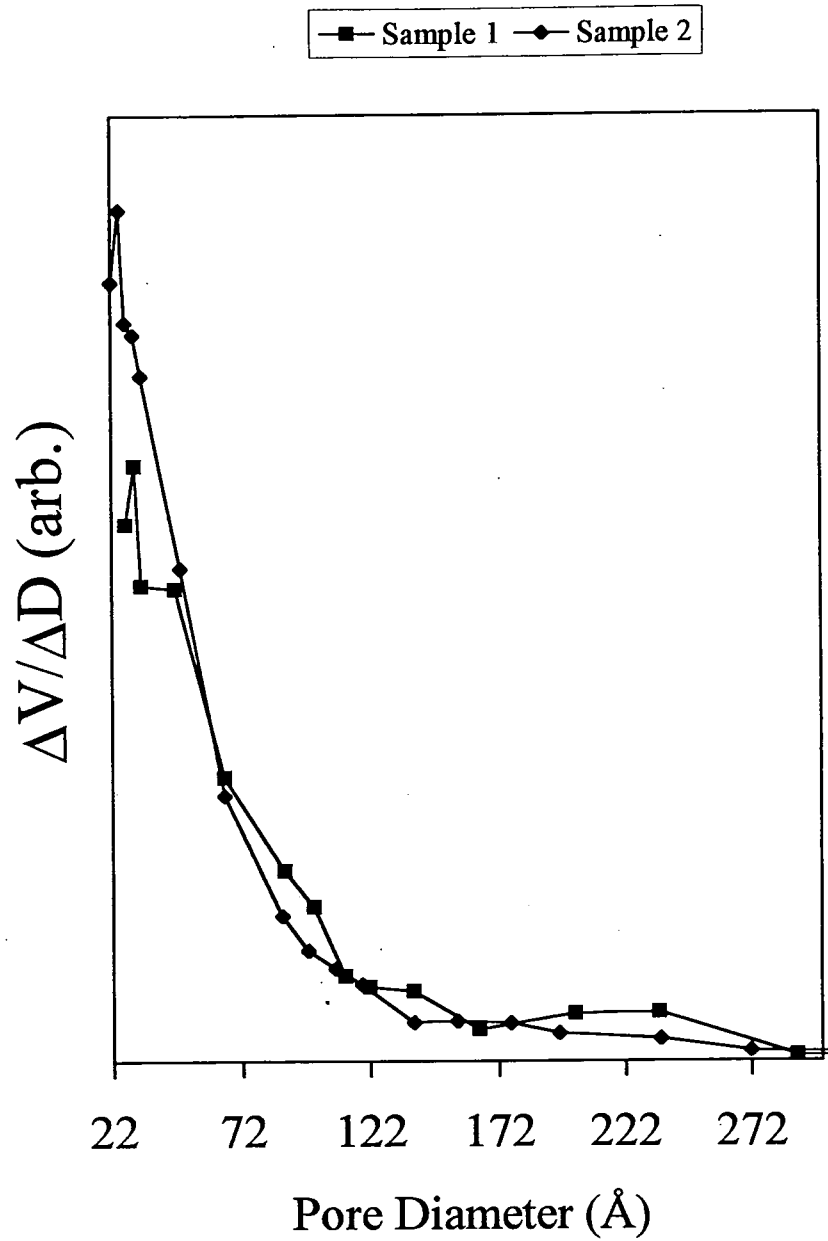
Figure 4.4   A comparison of the overall pore size distribution of untreated cellulose (sample 1) and cellulose swollen in 2M NaOH (sample 2).
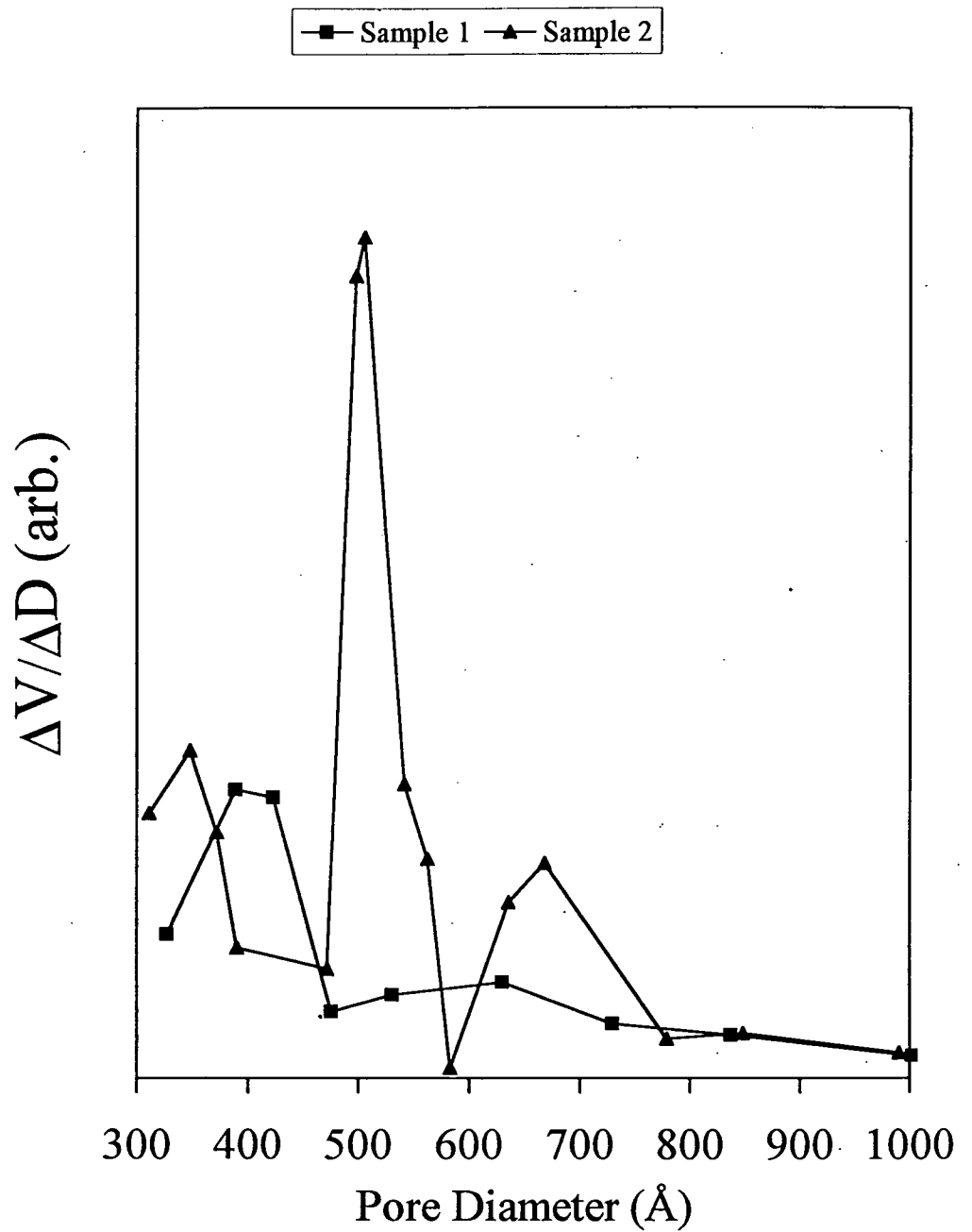
Figure 4.5   **Macropore size distributions of untreated cellulose (sample 1) and cellulose swollen in 2M NaOH (sample 2).**

Figure 4.6   Macropore size distributions of sodium hydroxide swollen cellulose having undergone differing degrees of crosslinking obtained by using 0.0%, 0.5%, 1.0%, 1.5%, and 2.0% by volume concentrations of epichlorohydrin (corresponding to samples 2, 3, 4, 5, and 6 respectively).

4.3.4. Protein Uptake Experiments

In order to rationalise the behaviour of the behaviour of the cellulose matrix in terms of its performance as a bioseparation media it was necessary to compare the effect of the swelling and crosslinking treatments on the protein capacity of the quaternary 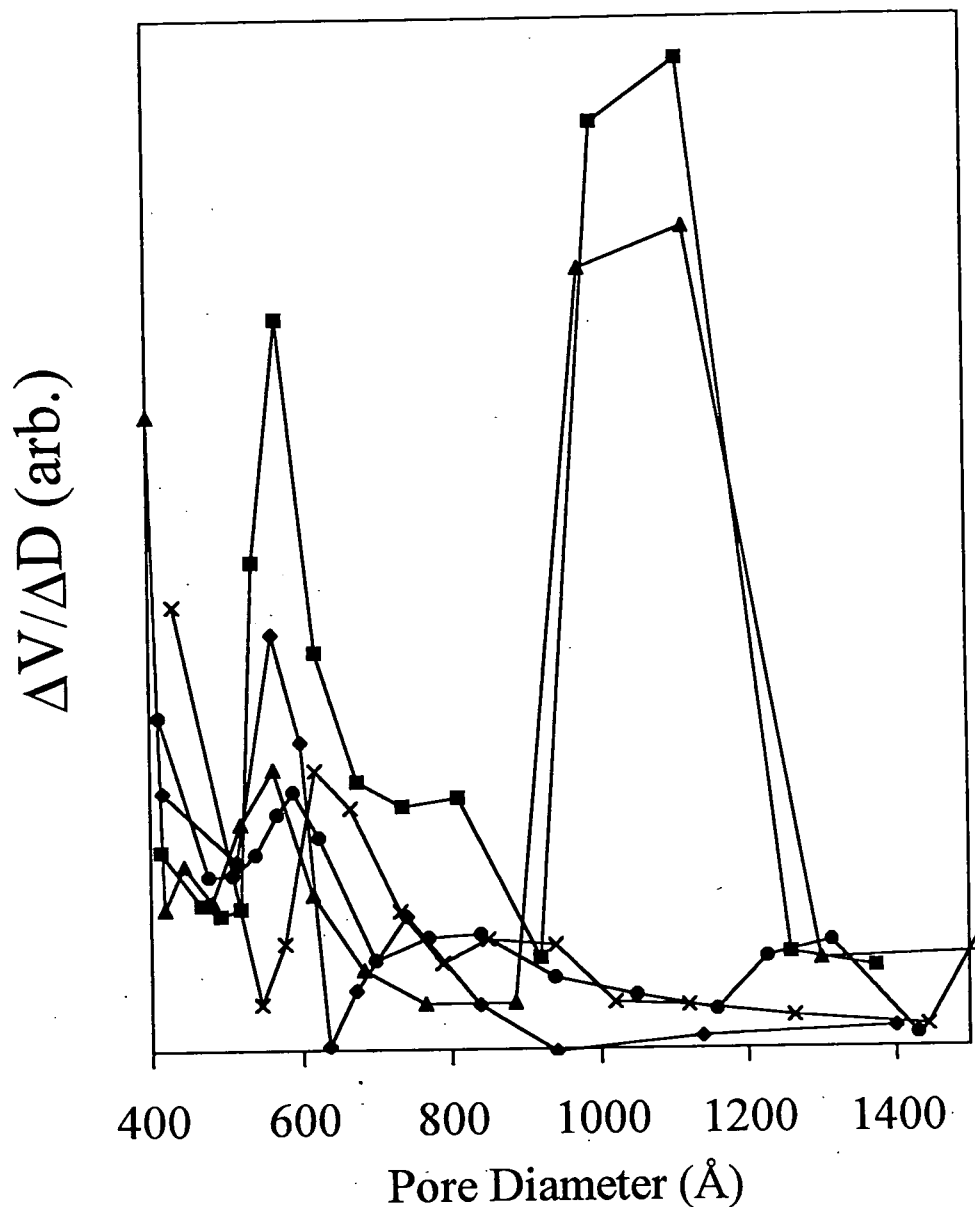methyl derivatised celluloses. The data for the binding of BSA on the cross-linked cellulose base material (sample 1) and the sodium hydroxide swollen cellulose (sample 2) is summarised in Figure 4.8 below.

We can see that the swelling treatment increases the total amount of BSA bound to the matrix for each of the crosslinker levels. For example, following the addition of 1% v/v epichlorohydrin to sample 1 the BSA capacity was measured at 55 mg/ml of eluate, whereas for sample 2 following the same crosslinking treatment the capacity was 110 mg/ml. Unfortunately we were unable to determine the BSA capacity of the celluloses at 0% v/v epichlorohydrin treatment because the mechanical strength of the matrix was found to be too low. This resulted in the compression of the matrix and the formation of blockages in the separation column under the flow conditions required during the determination of the BSA capacity.

Crosslinking reduces the amount of BSA bound to the QM derivatized matrix. A linear correlation is observed between the crosslinker concentration and the amount of BSA in the eluate. Protein binding reaches zero for samples 1 and 2 at 2.5% and 3.7% v/v concentration of epichlorohydrin respectively.
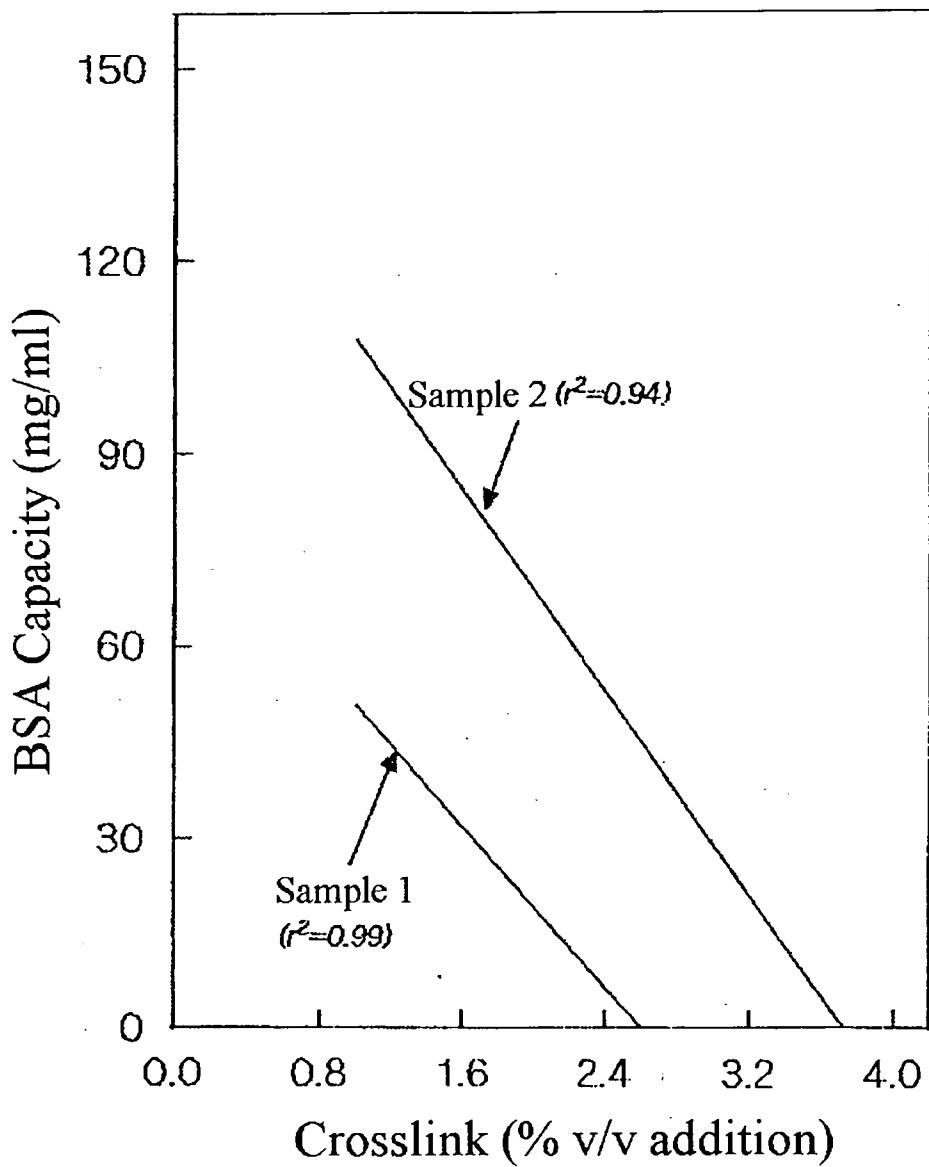
Figure 4.7   **Variation in Uptake of Bovine Serum Albumin on differing cellulose matrices with increasing crosslinker concentration.**

4.4. DISCUSSION

The nitrogen sorption technique has proven invaluable in probing the pore structure of the cellulose materials used in this study, it is the only technique suited to the analysis of pores in the range of 10 - 1500 Å. However, accurate detection of pores above 1000 Å in diameter pushes the sensitivity of this technique to the limit.

4.4.1. Swelling with NaOH

The general increase in the mesoporosity of cellulose fibres resulting from NaOH treatment has been described in previous articles[10] and the swelling effect of NaOH on celluloses has been well documented[7, 24]. NaOH has been said to improve the reactivity[23] of cellulose fibres, however the increased reactivity of the cellulose matrix can be attributed to greater accessibility of the hydroxyl groups. Therefore the increased mesoporosity enables the reagent molecules to penetrate in to more narrow pores. This leads to an associated increase in total surface area available for reaction and gives the impression of increased reactivity at the cellulose surface.

We can be confident that the affect of NaOH on the cellulose matrix can be attributed to the disruption of the hydrogen bonded network because the degradative effects of NaOH on cellulose are known to be negligible[40]. The glycosidic bond in the polymer backbone is stable up to 170 °C, endwise degradation of the polymer chain can occur but is thought to be an unfavourable degradation pathway. However a loss of weight has been observed during scouring, consistent with the dissolution of short chain material from the cellulose[40]. The effects of NaOH on the macropore structure of

cellulose appears to be due to interfibrillar swelling and whereas the intrafibrillar swelling associated with mesopore formation is well known, the swelling of the pores between 600 and 1200 Å in diameter has not been widely reported. However, one study involving electron microscopy of cross sections of cotton fibres[14] swelled in solutions of alkali hydroxides did show the formation of cylindrical pores in parallel with the length of the fibre with diameters of 0.1μm. These pores could be similar in nature to the 600-1100Å diameter pores measured in this study.

4.4.2. Cross-linked Cellulose

Crosslinking with epichlorohydrin solution can strongly alter the macroporous nature of cellulose, whilst the mesopore structure remains intact. In the macroporous range, the 600 Å pores partially disappear during crosslinking, whereas the 800 Å and 1100 Å pores completely collapse at higher crosslinker concentrations. An explanation for this can be found if we take in to account that the cross sectional area associated with a cylindrical 1100 Å diameter pore is approximately 3 times greater than a pore with a diameter of 600 Å. It would therefore be reasonable to assume that the bonding required to sustain a specific pore structure increases rapidly with increasing pore diameter size[10]. As a consequence of this the smaller pores tend to be far more robust, since they comprise microfibrillar voids, and are stabilised by short range hydrogen bonding. This is confirmed experimentally in this study by the minimal effect of the cross-linking reaction on the mesoporous structure of cellulose. In contrast macropores are formed by fibrillar packing, this is a more loosely bound type of structure, which leads to weaker fibrillar association. Displacement of the fibrillar structure is usually associated with swelling of cellulose in various solutions[24], and can give rise to large pore collapse during

drying[11, 10]. Crosslinks within the larger pores may be expected to have a much more detrimental effect on the pore stability compared to a similar number of crosslinks introduced into a microfibrillar environment. As well as restricting the swelling of cellulose fibres in the wet state, the crosslinking process can also be expected to influence the mechanical[27] and poly-electrolyte (e.g. protein) adsorption characteristics of the cellulose matrix[41]. For instance Martin and Rowland[28] used partial separation of pairs of sugars with differing molecular weights as a measure of the effect of crosslinking upon cellulose. After crosslinking with formaldehyde the amorphous cellulose showed reduced permeability to larger molecules but increased permeability to molecules with molecular weights less than 1000 gmol[-1].

4.4.3. Protein Uptake Measurements

We have already shown that we are able to improve the protein capacity of the unswollen cellulose by heating the sample in 2M NaOH at 100°C for 4 hrs. This increases the mesoporous structure of the material as shown in the case of sample 1 and sample 2. The efficiency of cross sectional attack of a large molecular reactant has been found to increase with increasing severity of the scouring process and if we consider the dimensions of the BSA protein used in this study which are approximately 5 nm in diameter and 40 nm in length[42], in conjunction with the increase in the macropore structure around 1000 Å it seems reasonable that it may be the opening of the macropores that leads to the improved protein capacities since the mesopore structure discussed above is too small to allow the penetration of BSA.

In addition, the protein uptake measurements show decreasing activity of the

cross-linked and QM derivatised cellulose matrix towards BSA with increasing crosslinker concentration. Upon initial consideration several possible explanations for these observations could be deduced. Firstly, the crosslinking reaction consumes hydroxyl functionalities, and this could be responsible for less efficient quaternary methyl derivatization of the matrix, leading to fewer available binding sites for the adsorbate molecule. However estimations of the number of crosslinks present in the cellulose matrix based upon mechanical stress and compression studies[43] have indicated that the degree of crosslinking, even at epichlorohydrin concentrations up to 5% v/v is surprisingly low, with as few as 1 crosslink per 30000 cellulose repeat units.

In order to support these data [1]H Nuclear Magnetic Resonance (NMR) analysis[43] was used to quantify the degree of derivatisation of matrices exposed to 1 % and 5 % v/v solutions of epichlorohydrin. The NMR resonance of the protons on the quaternary methyl ligands could be clearly observed in the NMR spectra of cellulose, and the intensity of that resonance allowed a comparison of the degree of derivatization. The material exposed to high crosslinker concentration exhibited no difference in the proportion of QM ligands and hence we can conclude that the degree of derivatization was not affected by the crosslinking process. This further suggests that accessibility of the adsorbate molecule to the adsorption site and not the total number of adsorption sites is a governing factor in this case.

Previous workers have demonstrated a relationship between porosity and reactivity of cellulose, Nelson et al[13] investigated the acetylation of the cellulose hydroxyl groups and Focher et al[44] demonstrated the relationship between the enzymatic hydrolysis of a cotton cellulose with respect to its mesoporosity. The enzymatic

degradation decreased with increasing density of packing of cellulose and this was due to steric hindrance of the enzyme by the fibrillar structure of the cellulose. This can be understood considering the size of the molecules involved, an enzyme with a molecular weight of 63000 gmol^{-1} has dimensions of 20 nm length and 3 nm width[45], this will be smaller than the macroscopic pore structure of cellulose, cell lumina, pit apertures and membrane pores which can be from 200 nm to greater than 10 m in diameter, but much larger than the pores between microfibrils which are usually less than 20 nm. We would therefore expect protein molecules with molecular weights in the hundred thousands or millions gmol^{-1} to be very sensitive to the distribution of macropores in the cellulose matrix.

4.5. CONCLUSIONS

Nitrogen adsorption isotherms have shown that the pore structure of cellulose is very sensitive to chemical swelling and cross-linking treatments. Swelling with NaOH was shown to disrupt both the meso and macroporous structure of the material whereas cross-linking caused a preferential disruption of the macropores contained within the host matrix. It is far from clear what determines the initial macropore structure of a particular batch of cellulose, initial suggestions point towards the source of the fibrous wood pulp and the processing conditions used during the formulation of the matrix.

The protein capacity has been shown to be dependent upon the macroporous structure of the cellulose and this is thought to be due to the availability of active binding sites. Consequently protein capacity is governed by access of the protein molecules through pores of suitable diameter to the internal surface of the cellulose. Provided the

reacting molecule is small enough to enter all of the pores the reactivity can be related to the total surface area. However the porosity becomes a critical factor when the size of the reacting species approaches the size of the pore in to which it is attempting to penetrate and that part of the total surface area becomes inaccessible. The level of matrix crosslinking was found not to affect its level of functionalisation. Furthermore this suggests that provided the degree of derivatization does not fall below a minimum level, then the binding of a protein molecule to the stationary phase will be independent of the level of derivatisation[46] and closely associated with the macroporous nature of the material.

4.6. REFERENCES

1   Kennedy J. F., Paterson M., *Polym. Internat.*, **32**, 71, (1993).

2   Chen H-L., Hon K. C., *Reactive Polymers*, **5**, 5, (1987).

3   Callstrom M. R. , Bednarski M. D., *MRS Bulletin*, **Oct**, 54 (1992).

4   Kremer R.D., Tabb D., *Internat. Lab.*, **July/August**, 40 (1989).

5   Dullien F. A. L., *Porous Media: Fluid Transport and Pore Structure*; Academic Press, New York, 1979.

6   Nevell T. P., Zeronian S. H., *Cellulose Chemistry and its applications*, John Wiley, New York, 1986.

7   Jeffries R.; Jones D. M.; Roberts J. G.; Selby K.; Simmens S. C.; Warwicker J. O., *Cellulose. Chem., Technol.* **3**, 255 (1969).

8   Zeronian S. H.; Coole M. L.; Alger K. W.; Chandler, J.M. *J. App. Polym. Sci.: Appl. Polym. Symp.*, **37**, 1053 (1983).

9   Weatherwax R. C., *J. Colloid Int. Sci.*, **49**, 40 (1974).

10   Alince B., *Colloid and Polymer Sci.*, **253**, 720 (1975).

11   Weatherwax R. C., *J. Colloid. Int. Sci.*, **62**, 3, 432 (1977).

12   Porter B. R., Rollins M. L., *J. Appl. Polym. Sci.*, **16**, 217 (1972).

13   Nelson R., Oliver D. W., *J. Polym. Sci.: Part C*, **36**, 305 (1971).

14   Aravindanath S., Bhama Iyer P., Sreenivasan S., J. Appl. Polym. Sci., **46**, 2239 (1992).

15   Aggebrandt L., Samuelson O., J. Appl. Polym. Sci., **8**, 2801 (1964).

16   Stone J. E.; Trieber E. E.; Abrahamson B., *Tappi*, **52**, 108 (1969).

17   Gregg S. J., Sing K. S. W., *Adsorption, Surface Area and Porosity*; Academic Press, London 1967.

18   Ström G., Carlsson G., *J. Adhesion Sci. and Technol.*, **6**, 745 (1992).

19   Rowland S. P., Wade C. P., Bertoniere N. R., *J. Appl. Polym. Sci.*, **29**, 3349 (1984).

20   Rowland S. P., Wade C. P., Bertoniere N. R., *J. Appl. Polym. Sci.*, **31**, 2769 (1986).

21   Gert N. V., Torgashov V. I.; Shishonok M. V., Sinyak S. J., Kaputsii F. N., *J. Polym. Sci.: Part B: Polym. Phys.*, **31** 567 (1993).

22   Lokhande H. T., Thakare A. M., *J. Polym. Sci.: Part C: Polym. Lett.*, **28**, 21 (1990).

23   Buschle-Diller G., Zeronian S. H., *J. Appl. Polym. Sci.*, **45**, 967 (1992).

24   El-Din N. M. S., *Polym. Internat.*, **32**, 13 (1993).

25   Laszkiewicz B., Wcislo P., *J. Appl. Polym. Sci.*, **39**, 415 (1990).

26   Rowland S. P., ACS Symp.Ser. **49**, 20 (1977).

27   Deering Milliken Research Corp.; British Patent No. 8834/57, 1960.

28   Martin L. F., Rowland S. P., *J. Polym. Sci.: Part A: Polym. Chem.*, 5, 2563 (1967).

29   Weatherwax R. C., Caulfield D. F., *Tappi*, 54, 985 (1971).

30   Trieber E. E. in *Cellulose Chemistry and its Applications*; T. P. Nevell, S. H. Zeronian, Eds., Wiley, New York, 1985.

31   Orr C., Dalla Valle J. M., *Fine Particle Measurement*; Macmillan, London; p271 (1959)

32   Pierce C., *J. Phys. Chem.*, 57, 149 (1953).

33   Brunauer S., Emmet P.H.; Teller E., *J. Amer. Chem. Soc.*, 60, 309 (1938).

34   Brunauer S., Deming L. S., Deming W. S., Teller E., *J. Amer. Chem. Soc.*, 62, 1723 (1940).

35   BPS Separations Ltd, Eur. Pat. Appl. 91909759.2.

36   Guthrie J. D., Bullock A. L., *Ind. Eng. Chem.*, 52, 11 (1960).

37   Guthrie J. D., *Ion Exchangers in Organic and Biochemistry*; Interscience; Chapter 30, 1957.

38   Hearn M. T. W., *HPLC of Proteins Peptides and Polynucleotides*, VCH, New York 1991.

39   Courtesy of BPS Separations Ltd., unpublished work, 1992.

40   Zeronian S. H. in *Cellulose Chemistry and its Applications*, T. P. Nevell and S. H. Zeronian, Eds., Wiley, New York, 1985.

41   Peterson E. A., *Cellulosic Ion Exchangers*; Elsevier, Chapter 2 1980.

42   Wold F., *Macromolecules: Structure and Function*, Prentice Hall Inc., New Jersey, 1971.

43   Thomas D., Durham University Industrial Research Laboratories, personal

communication, 1992.

44   Focher P. O., Marzetti A., Sarto V., Beltrame P. L., Carniti P., *J. App. Polym. Sci.*, **29**, 3329 (1984).

45   French A. D., in *Cellulose Chemistry and its Applications*, T. P. Nevell and S. H. Zeronian, Eds., Wiley, New York, 1985.

46   Woffindin C., Hoenich N. A., Matthews J. N. S., *Nephrol. Dial. Transplant*, **7**, 340 (1992).

5. SURFACE MODIFICATION OF PTFE FILM.

5.1. INTRODUCTION

The robust physical properties of poly(tetrafluoroethylene) (PTFE)[1] make it an attractive polymer for use as a stationary phase in a bioseparation system, however its inert chemical properties have prevented its widespread use. Reduction of the PTFE surface using alkali metals[2,3] in conjunction with derivatisation has allowed the chemical and physical nature of the surface to be modified[4-14] whilst the properties of the underlying PTFE matrix can be maintained.

We have investigated the effect the alkali metal reducing agent on the chemical and physical properties of the PTFE surface, and subsequently attempted to introduce specific functionality in to the activated layer.

5.1.1. Background

PTFE is the most important fluorine containing polymer and possesses the structure shown in Figure 5.1. It accounts for 90% of the world's fluoropolymer consumption which has been estimated at over 5000 tonnes per annum[15]. Large scale production of PTFE began during the Second World War, following which it was released for general commercial exploitation. PTFE is produced from the rapid exothermic polymerization of tetrafluoroethylene at moderate pressure using aqueous ammonium persulphate[15] as an initiator. Commercially available PTFE has a molecular

weight between 500,000 and 5,000,000 gmol^{-1} and a specific gravity of between 2.1-2.3 gcm^{-3}.

PTFE has been of valuable use in many areas due to its predominantly inert characteristics. It possesses a high working temperature (~250°C), is stable to the majority of chemicals, has low dielectric loss factor[16], exhibits small coefficients of friction[1] and has a high resistance towards penetration of water vapour[17]. These qualities have led to the widespread use of PTFE in industry as gaskets, expansion joints and sleeving for electrical cables[15], and in surgical and medical areas as replacement joints and biocompatible membranes[18].

The demand in the 1950s and 60s for a wider range of materials with non stick properties prompted research in to methods of bonding PTFE to other surfaces. A range of adhesives[19] were developed that were able to bond PTFE, although with a degree of difficulty. Later work concentrated on the modification of the polymer surface itself, enabling more conventional adhesives to bond the material, the chemical and physical properties of PTFE can be altered using highly reactive alkali metal reducing agents, three of which are described in the following section.

5.1.2. Alkali Metal Routes To Activated PTFE

5.1.2.1. *Sodium/Ammonia Complex*

Sodium is well known for its behaviour as a reducing agent. In 1824 it was discovered that sodium could reduce aluminium chloride to pure aluminium and sodium

has since been exploited as a chemical reagent[20] in many organic syntheses. The soluble complex of sodium in ammonia[21], consists of a solvated or co-ordinated form of sodium to several ammonia molecules[22] as shown in Figure 5.2. The complex has an unshared electron, and the group of atoms can be considered as a free radical, hence in this form the sodium reacts rapidly with a large number of weakly acidic compounds.

The sodium/ammonia complex acts effectively as a Lewis base donating its lone electron to the acidic fluorine atoms bound in the polymeric chain of PTFE This has the effect of leaving the surface of the material fluorine deficient, the lone electrons on the surface combine to form double carbon-carbon bonds, and therefore the reactivity of the surface is modified.

5.1.2.2. *Sodium/Naphthalene Complex*

In 1932 the discovery by Scott et al[23] of the sodium-naphthalene-ether complex led to its use as a substitute for the sodium/ammonia system in organic synthesis because it was as efficient and easier to handle. Combination of sodium and naphthalene results in the formation of a 1:1 adduct, Figure 5.3. In the presence of an ether of high oxygen content the complex when was able to reduce PTFE. This has led to its widespread use as a defluorinating agent in the surface modification of PTFE[5- 10, 26]. The ether based solvent is thought to solubilise the sodium atom[24] (for example, the reaction would not work with diethyl ether, but would with THF or dimethylether).
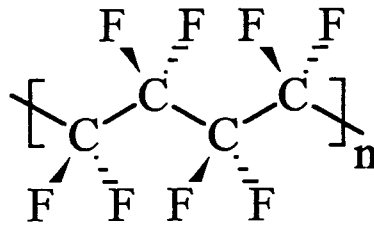
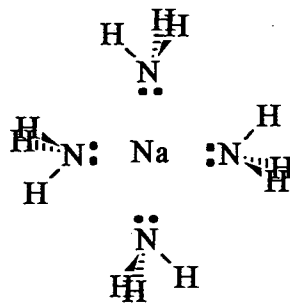**Figure 5.1**   **Representation of the Bonding within PTFE**

Figure 5.2   **The Sodium/Ammonia Complex.**

In this form the sodium atom is more tightly bound than in liquid ammonia, and this can be demonstrated by the ability to perform carrier and addition reactions of sodium on the naphthalene ring. The sodium is stabilised by the introduction of its valence extra electron in to the naphthalene π system[25]. This however does not produce large changes in the positions of the energy levels of the π system and the naphthalene is able to exist as a negative ion free radical in the complex form.

The mechanism by which this sodium naphthalenide complex reacts is poorly understood. However the exposure of a fluoropolymer to the complex leads to rapid surface defluorination and unsaturated bond formation, the reaction is probably as shown in Figure 5.4.

5.1.2.3. *Lithium/Mercury Amalgam*

Another method for defluorinating the surface of PTFE, involves the use of alkali metal amalgams such as Li in Hg. The mechanism of defluorination has been described in terms of an electrochemical cell Li│C+LiF│PTFE. The Li amalgam behaves as the anode and PTFE. as the cathode, with the C + 2 Li layer acting as a mechanical separator of both reaction partners, whilst also functioning as a solid electrolyte and electron conductor.

The ionic current between amalgam anode and C-PTFE cathode is transferred exclusively by the Li^+ cations in the solid phase which forms between either electrode as a continuously growing layer. Various alkali metals can be used with decreasing

reactivity from Li to Na to K, the reaction with each of these proceeds in much the same way, although at progressively slower rates.

The product obtained from this treatment has been found to be a mixture of carbon and LiF in the surface region, with a small amount of LiF chemically bonded to the carbon[3], although this can be removed by washing with water.

5.1.2.4.   *Benzoin Dianion Route.*

This method[4, 26] is one of the more recent chemical routes to an activated PTFE surface and avoids the use of an alkali metal reducing agent the mechanism is outlined in Figure 5.5.

5.1.3. Functionalisation of the Activated PTFE

McCarthy et al[6- 11, 26] have pioneered much of the organic modification of the activated PTFE surface which results from the alkali metal treatment. To date -OH, -CO_2H, -Br and -NH_2 are amongst some of the groups that have been introduced on to the PTFE surface. Problems in obtaining a uniformly functionalised PTFE surface have been encountered and this can be attributed to the 'dirty' nature of the etching reaction and the high reactivity of the etched layer.   This leads to the presence of surface contaminants and oxidised species prior to the attempted functionalisation reaction. More recently, greater success has been observed using poly(chlorofluoroethylene) PCTFE as a starting material which because of its higher reactivity can be directly functionalised using organo-lithium compounds without the initial activation step[27].
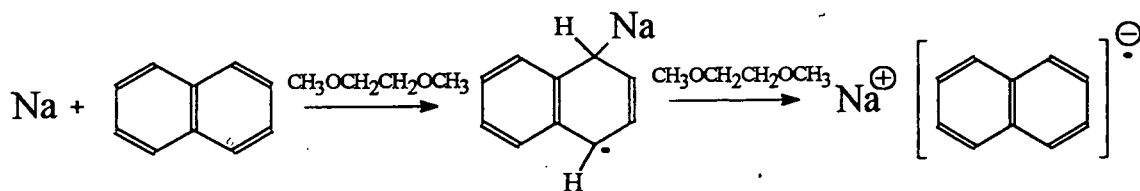
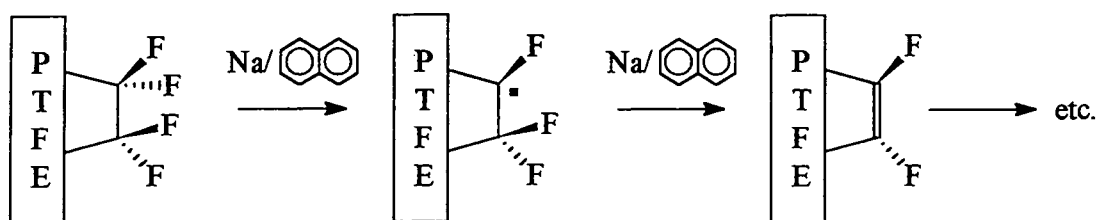**Figure 5.3**   **Sodium/Naphthalene Adduct.**

Figure 5.4   **Activation of PTFE Surface using the Sodium/Naphthalene**
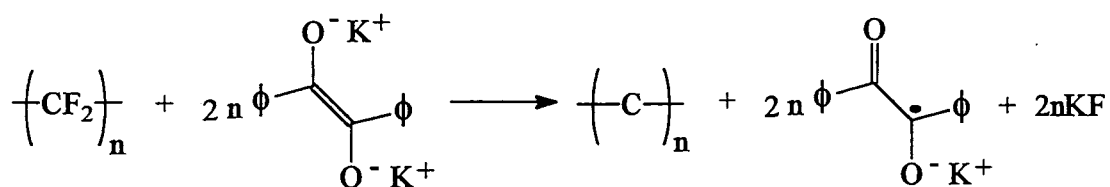
complex.

Figure 5.5   **Reaction Scheme for the Benzoin Dianion Route**

5.1.4. Uses of Functionalised PTFE

The interest generated from these types of surfaces stems from the properties imparted upon the PTFE once it has been functionalised, derivatised PTFE can be used as a matrix base[28], on to which proteins[29] can be attracted, provided the correct functionality is present on the surface of the polymer, as outlined in chapter 1. The activated and functionalised material has already found limited application in affinity[30,31] and reversed phase[32] chromatography applications. A further benefit of PTFE is that it is able to operate outside normal elution conditions (the pH being between the values of 2 and 4) and so separations requiring more harsh conditions could be performed.

5.2. EXPERIMENTAL AND RESULTS

5.2.1. Materials

The poly(tetrafluoroethylene) (PTFE) used in this chapter was in the form of a continuous polymer film (99% pure, Goodfellows Ltd.). The activation of the polymer surface was achieved by using 'Tetra-etch' (a solution of sodium naphthalenide in glycol ether) supplied by Gore Ltd. Washing of the samples was performed as indicated in the following sections using distilled water (99.5% pure), analar grade (99% pure) acetone and hexane, and dry (<7ppm H_2O) tetrahydrofuran (THF). Functionalization was attempted by reaction with bromobenzene (99% pure) obtained from Aldrich Chemical Co. Ltd., and 10% LiOH in distilled water.

5.2.2. Sample Analysis

X-ray photoelectron spectroscopy (XPS) analysis was carried out on a Kratos ES200 X-ray photoelectron spectrometer operating in the fixed analyser transmission (FAT) mode, at a pass energy of 65 eV, and an electron take-off-angle of 30° from the substrate normal. Mg $K_{\alpha 1,2}$ (1253.6 eV) ionising radiation was used as the photoexcitation source. A PC computer was used for XPS data accumulation and component peak analysis, assuming linear background subtraction and Gaussian fits with fixed full width at half maximum (FWHM)[33]. All spectra are referenced to the C(1s) core level shift for adventitious hydrocarbon at 285.0 eV[34].

Attenuated total reflection infrared (ATR-IR) measurements were taken on a Mattson Polaris FTIR instrument, equipped with a Specac optical table and a KRS-5 ATR crystal. Infrared spectra were accumulated at 4 cm^{-1} resolution in the range 400 cm^{-1} to 4000 cm^{-1} over 100 scans.

AFM analysis was performed using a Polaron SP300 atomic force microscope (VG Microtech, Uckfield, UK), using prefabricated cantilevers (Park Scientific, California, USA) with theoretical spring constants of 0.01 and 0.03 nN/m. The AFM images were acquired in contact mode with nominal applied force of 0.2 nN at a scan frequency of 10 Hz. The images are presented as three-dimensional greyscale representations.

5.2.3. The Activation of PTFE Film in Air and the Effect of Reaction Time.

Samples of film were cut in to strips, 0.5 cm by 2 cm in size suitable for mounting on an XPS probe sample stub, and 1 cm by 4 cm for ATR-FTIR analysis. The strips of PTFE were immersed in a cyclohexane/iso-propyl alcohol solution and ultrasonically cleaned for approximately 5 minutes. Each sample was activated in 20 ml of undiluted 'Tetra-etch' solution at room temperature for 1, 5, 10, 20, and 30 minute period respectively, and washed with four 20 ml aliquots each of water, acetone and hexane in order to remove as much of the unreacted material as possible. The sample was then allowed to dry in a covered vessel in air for several hours prior to analysis.

5.2.3.1. *XPS Analysis.*

XPS of unactivated PTFE film resulted in single peaks in the C(1s) spectra corresponding to the -(CF$_2$)- environment (291.2 eV), and the F(1s) spectra (689.9 eV) which were in good agreement with literature values[35]. An example of the C(1s) spectra for unactivated PTFE film is shown in Figure 5.6 and the single environment attributable to carbon bound to two fluorine atoms (CF$_2$ 291.2 eV)[36] can be clearly distinguished.

The C(1s) XP spectra of PTFE film activated for 30 minutes are shown in Figure 5.7. Initially we were led to conclude that there were no fluorocarbon environments in the C(1s) spectra because no F(1s) signal was detected within the reacted layer. However this is not wholly conclusive proof since account must be made for the differing attenuation lengths of photoelectrons from the F(1s) and C(1s) core energy levels. Seah and Dench[37] analysed the inelastic mean free paths of electrons from a wide range of

elements and the attenuation length of a F(1s) photoelectron was shown to be approximately 4 monolayers whereas a C(1s) photoelectron was typically 7-8 monolayers in depth. This can be attributed to the lower kinetic energy of F(1s) electrons compared to C(1s) and this means that the photoelectrons which we attribute to the C(1s) environment originate on average from a greater depth in to the PTFE sample compared to the F(1s). This problem can be overcome by analysing the alternative fluorine photoelectron line, the F(2s) which occurs at a low binding energy of (23 eV)[35] and has a particularly high attenuation length of 10 monolayers[37]. This line was found to be absent and we can therefore be confident that a complete defluorination of the layer sampled by XPS analysis had occurred. The C(1s) spectra in Figure 5.7 can therefore be fitted to the following range of carbon environments : hydrocarbon, crosslinked or unsaturated carbon species (285.0 eV)[36], carbon singly bond to an oxygen atom (C-O 286.6 eV)[36], carbonyl or carbon bound to two oxygen atoms (C=O, O-C-O 287.7 eV)[36] and carboxylate groups (O-C=O)[36].

Figure 5.8 shows the percentage composition of the surface layer with increasing activation times, from which it is apparent that the majority of defluorination of the surface layer was completed within 1-2 minutes of immersion in the sodium naphthalenide solution and complete defluorination was achieved within 30 minutes. The washing procedure employed was effective in removing all unreacted material since no Na (2s) signal was observed in the XP spectra.

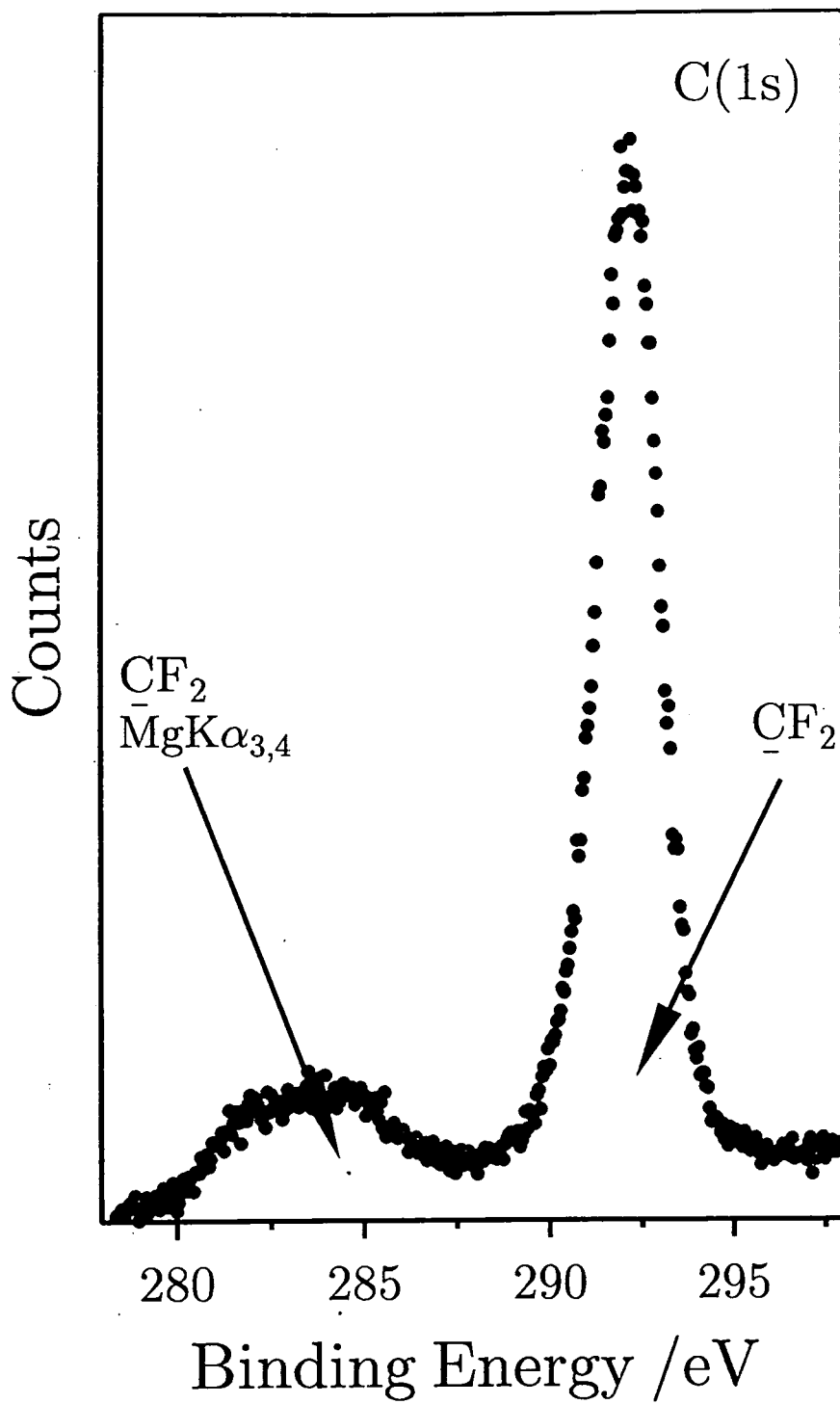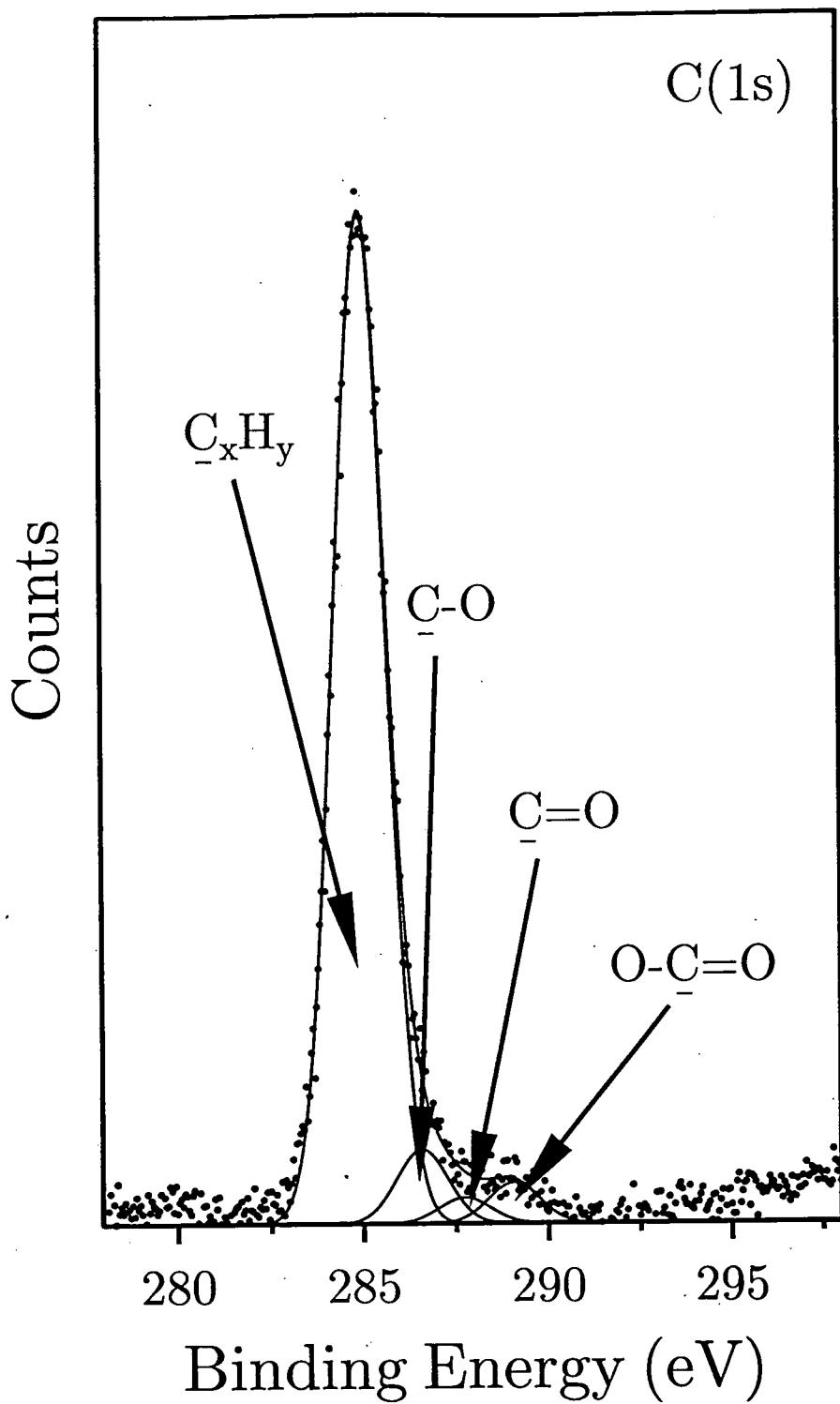**Figure 5.6**   **C(1s) XP Spectra of Untreated PTFE Film.**

Figure 5.7   **C(1s) XP Spectra of PTFE Film Activated for 30 Mins.**
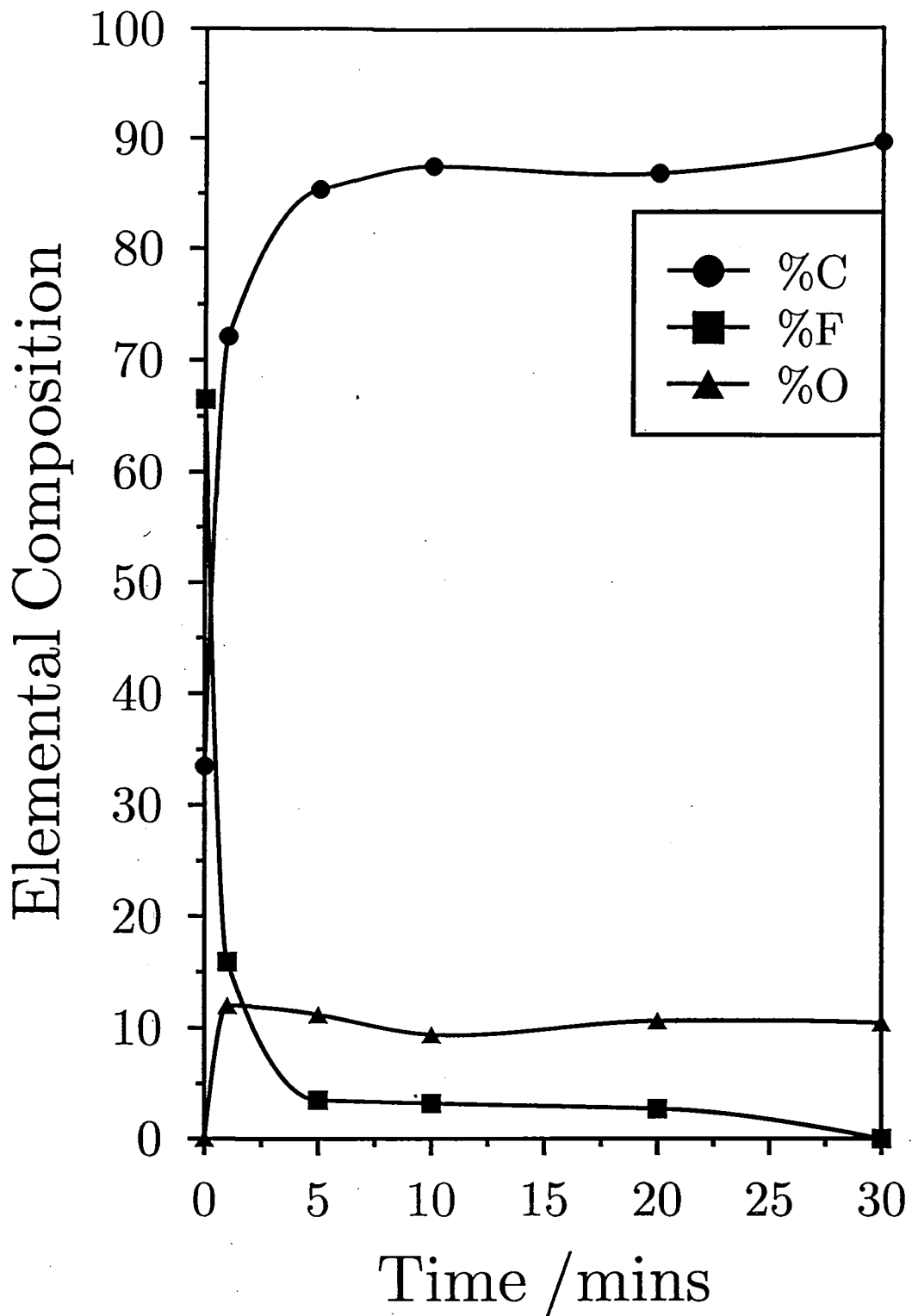
Figure 5.8   **Elemental composition of surface layer determined by XPS analysis vs. reaction time.**

5.2.3.2. *ATR-FTIR Analysis.*

Figure 5.9 represents the ATR-FTIR spectra for PTFE film with increasing activating times in the 1300-400 cm^{-1} region. The major peaks for unreacted PTFE occur at the characteristic frequencies shown in Table 5.1 and as the activating time increases in Figure 5.9 we observe a decrease in the peaks which can be attributed to PTFE. The ATR-FTIR technique can also give some general indication to the depth of penetration of the activating procedure because the infra-red radiation is able to sample to a depth of around 1μm[38]. This is a much greater depth than XPS and we can deduce that the reaction etches several hundred nanometres in to the PTFE surface. The reduction of the characteristic PTFE peaks is also accompanied by the formation and growth of two broad adsorption bands at 1430 and 1600 cm^{-1} respectively, see Figure 5.10. These can be assigned to aromatic and unsaturated carbon-carbon stretching modes[40,39].

Table 5.1   Characteristic IR Frequencies for PTFE

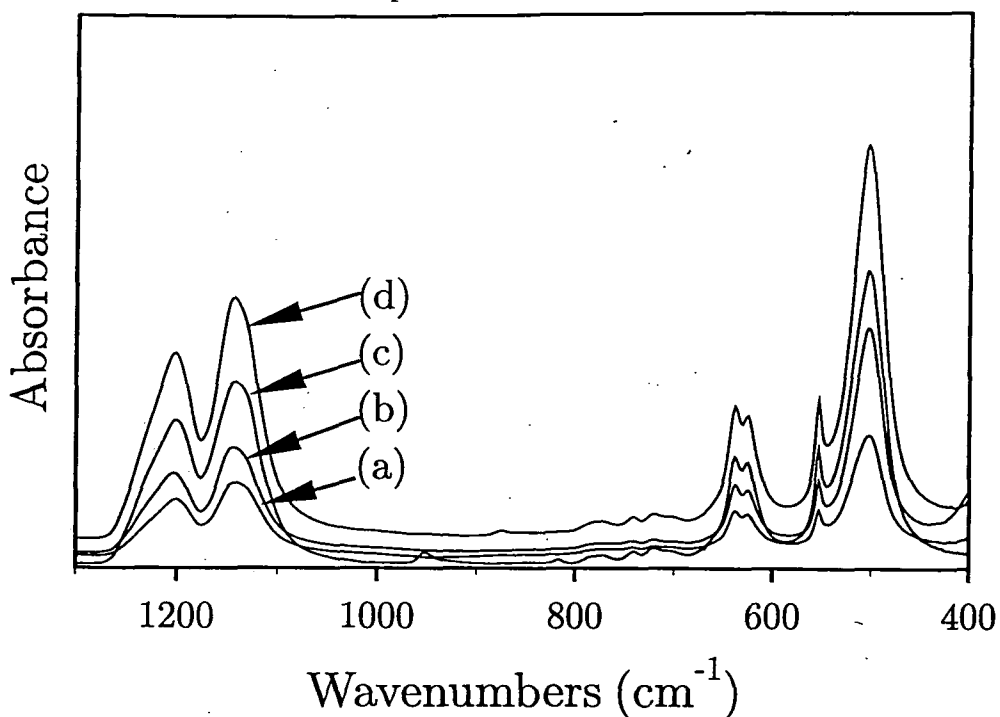| Wavenumbers (cm^{-1})	Assignment[40]
506	CF$_2$ wag
556	CF$_2$ rock
625	helix reversal
639	CF$_2$ rock
1147	assym. CF$_2$ stretch
1204	sym. CF$_2$ stretch

Figure 5.9 **ATR-FTIR spectra (overlayered 1300-400 cm^{-1} region) of PTFE film reacted for 30 Mins (a), 10 Mins (b), 1 Min (c) and 0 Mins (d).**
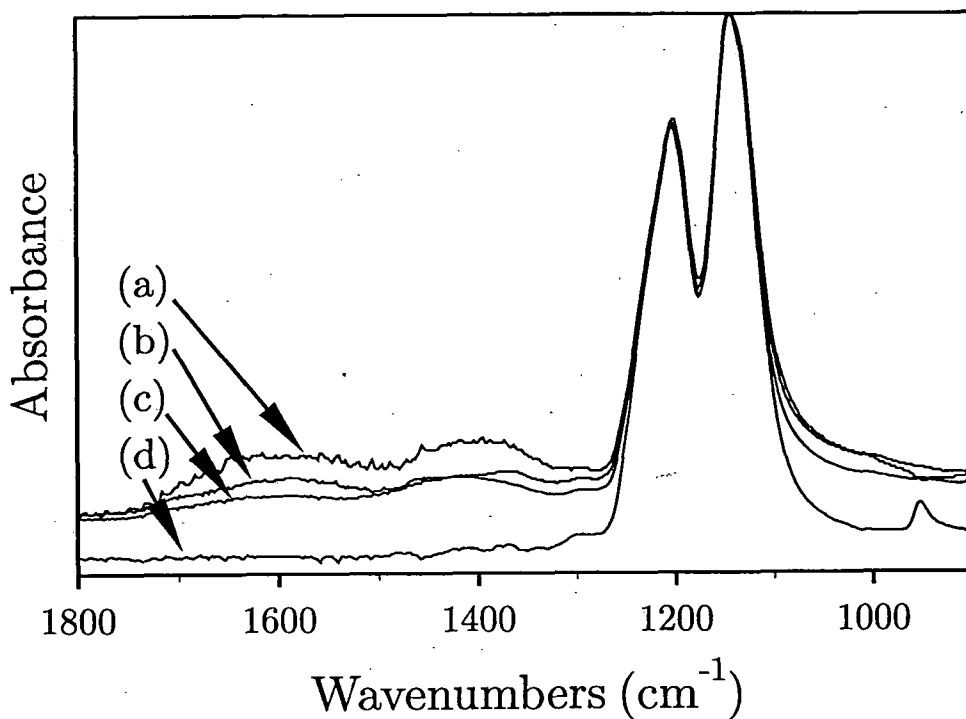

Figure 5.10 **ATR-FTIR spectra (1800-900 cm^{-1} region normalised to the CF$_2$ peak at 1147 cm^{-1}) of PTFE film reacted for 30 Mins (a), 10 Mins (b), 1 Min (c) and 0 Mins (d).**

5.2.3.3. *AFM Analysis.*

Large differences were observed in the morphology of the PTFE film before and after reacting for 30 minutes. Five areas of each film were selected at random for analysis to try and provide a representative picture of each sample. In Figure 5.11(a) is shown a typical 1 μm by 1μm three dimensional greyscale image of the unreacted surface and in Figure 5.11(b) is shown a line profile of a section across the image. Prior to reaction the PTFE film surface consists of large undulating features which have dimensions of the order of 300-400 nm diameter and range from 50 - 150 nm in height, the average RMS roughness value was 15.8 ± 2.5 nm. The analysis of larger (5 μm x 5 μm) areas of the untreated sample revealed striations which appeared to extend for several microns across the sampled area, this may be attributable to orientation of the polymer fibres[41] during the processing of the film during manufacture.

Analysis of the activated PTFE revealed a remarkably different morphology by comparison, a 1 μm x 1 μm representation is shown in Figure 5.11(c) and the line profile is shown in Figure 5.11. We can immediately see that the activation process has caused a noticeable roughening of the surface. The average RMS roughness value in this case was 21.5 ± 1.7 nm. The features present on the activated PTFE surface were found to be 50-100 nm in width and up to 100 nm in height. Direct comparison of the cross section line profiles clearly demonstrates the large change in the morphology of the PTFE sample following the reaction with the sodium naphthalenide reagent.

(a)
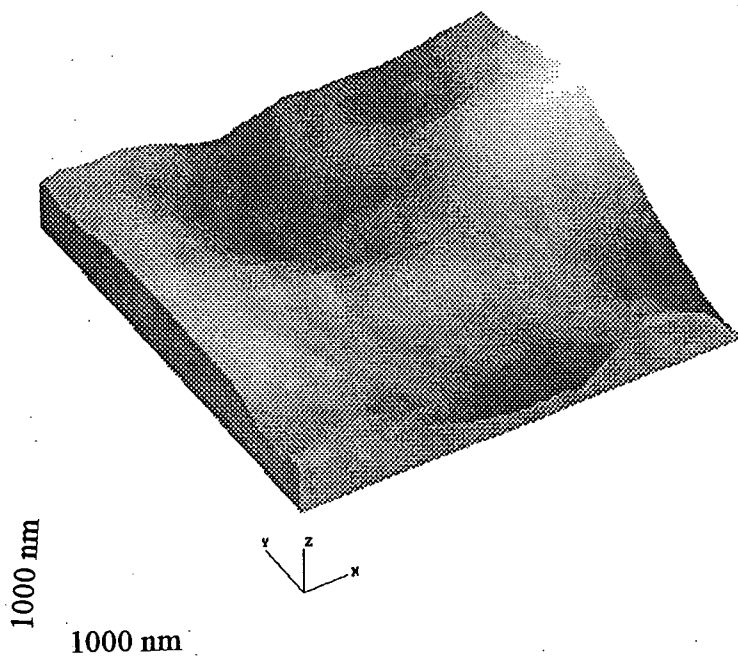
(b)
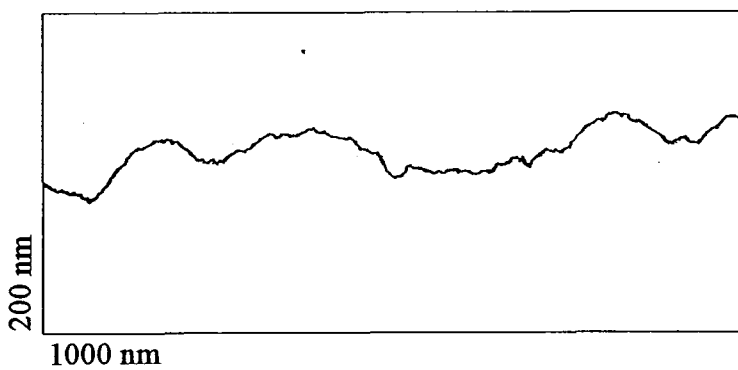
Figure 5.11   **AFM image of untreated PTFE film (a) and its corresponding**

cross section line profile(b).

(c)

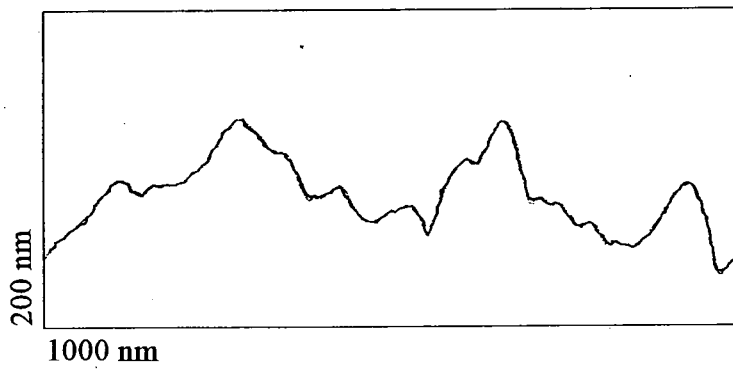1000 nm

1000 nm

(d)

200 nm

1000 nm
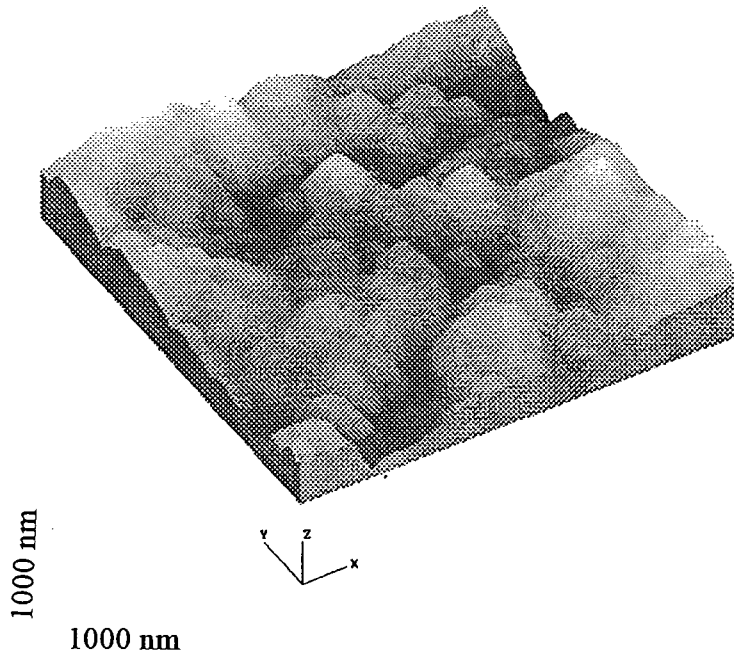
Figure 5.11   **AFM image of PTFE film reacted for 30 Mins (c) and its corresponding cross section line profile (d).**

5.2.4. The Activation of PTFE Film in a Nitrogenous Atmosphere and the Effect of Reagent Concentration

The sodium naphthalenide in glycol ether was diluted using dry (< 7 ppm H_2O) THF (tetra-hydrofuran). The reaction conditions were varied by increasing the dilution of the 'Tetra etch' (TE) with tetra-hydrofuran (THF), each of the samples were immersed in a total volume of reactant equal to 20 ml for 5 Mins, and then repeatedly washed in dry THF. Activation was accomplished under a nitrogen atmosphere in a Faircrest glovebox (<20ppm H_2O), XPS analysis of the activated samples was performed directly from the glovebox chamber thereby preventing any contact with air or atmospheric moisture.

5.2.4.1. *XPS Analysis.*

Figure 5.12 illustrates the effect of reducing the concentration of the etchant solution on the composition of the near surface layer. The degree of defluorination increases very rapidly once the volume fraction of etchant in the THF solvent increases above 0.05. This is manifest as a large reduction in the proportion fluorine bound to carbon (689.0 eV), combined with a growth in the fluoride signal (686.0 eV). This indicates that washing the surface in THF alone is inefficient at removing NaF formed by the defluorination reaction, the quantity of sodium in the surface layer is approximately twice the amount of fluoride present. An increase in the proportion of oxygen was also noted which we were unable eliminate
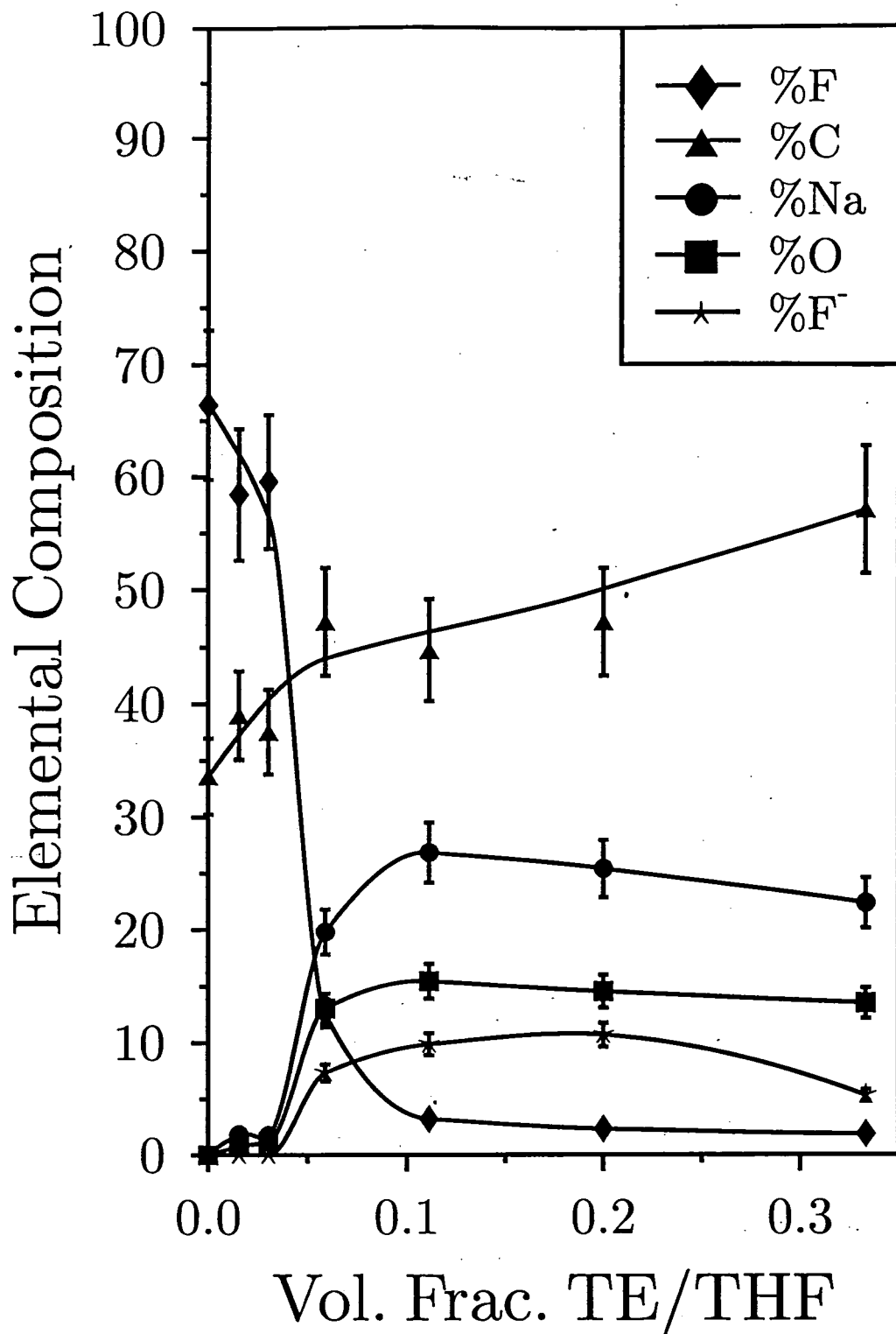
Figure 5.12   Elemental composition of surface layer determined by XPS

analysis Vs volume fraction of sodium naphthalenide in THF.

5.2.5. Functionalisation of the Activated PTFE Film.

In this section we intend to demonstrate the reactivity of the defluorinated layer which results from the activation process and the ease with which it can be crudely functionalised. Samples of PTFE film were prepared as described earlier, and reacted with 20 ml of undiluted sodium naphthalenide solution at room temperature for 30 minutes in order to form an activated layer of the PTFE surface. Functionalisation of the PTFE film was accomplished by placing the activated material in to 50 ml of bromobenzene in order to attach phenyl groups, or a 50 ml solution of 10% LiOH(aq) in an attempt to form -OH groups at the surface. The reagent was allowed to mix with the activated sample and reacted for one hour. Following the reaction the samples were thoroughly washed as before, with four 20 ml aliquots each of water, acetone and hexane, and then allowed to dry in a covered container in air for several hours prior to analysis

5.2.5.1.   *Reaction of Activated PTFE Film with Bromobenzene.*

The atomic composition of the activated PTFE reacted with bromobenzene determined by XPS analysis is shown in

Table 5.2 and we can see that 81% of the surface is of carbonaceous origin. No indication of π-π^* shake up transitions were observed to higher binding energy which is usually a good indication for the presence of unsaturated groups[42]. However π-π^* transitions are typically of low intensity ~6% of total C(1s) area for a polymer such as poly(ethyleneterapthalate) (PET), and since chemical binding energy shifts of crosslinked or unsaturated carbon-carbon species are inherently small unambiguous characterisation

of phenyl groups is difficult.

The ATR-FTIR of the activated film reacted with bromobenzene is shown in Figure 5.13, an increase in the intensity of the peaks centred at 1566 and 1400 cm^{-1} is observed which can be assigned to aromatic C-C stretching within a ring[40, 43] structure. The appearance of a doublet shaped shoulder at 1041 and 1022 cm^{-1} beside the main C-F stretching frequency at 1147 cm^{-1} can be assigned to in plane bending bands of aromatic ring hydrogens[40], and extremely weak features at ~3000 cm^{-1} (which are difficult to observe in Figure 5.13) indicate C-H stretching[40]. These peaks can be taken as a tentative indication that the attachment of phenyl rings was achieved.

Table 5.2   **Atomic Composition of the Surface of Activated PTFE Film Following by Reaction with Bromobenzene Determined by XPS.**

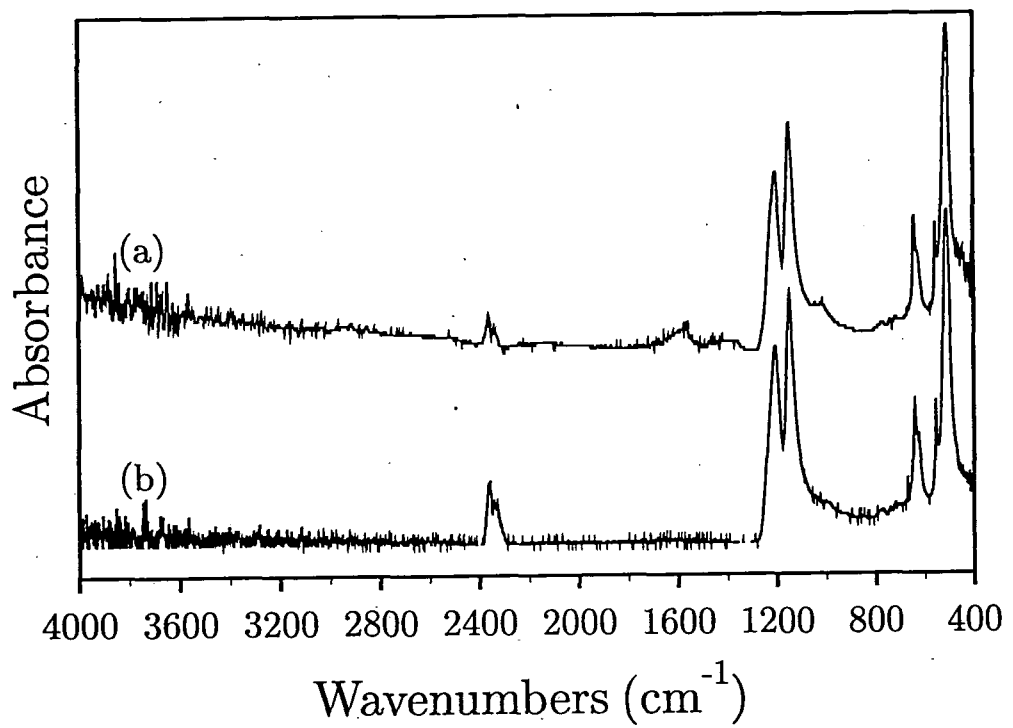| Percentage Composition	Untreated	Activated and reacted in bromobenzene
%C	33.5	81.0
%F	66.5	5.7
%F⁻	0	0.2
%O	0	13.1
%Na	0	0

Figure 5.13   ATR-FTIR spectra of PTFE film (a) activated for 30 Mins and

Reacted with Bromobenzene, (b) untreated.

5.2.5.2. *Reaction of Activated PTFE Film with 10% LiOH(aq).*

XPS analysis of the activated PTFE film reacted with a solution of 10% LiOH(aq) has a relatively high proportion of oxygen in the surface layer, see Table 5.3. Though it is noticeable that the degree of defluorination in this case was not as high as in previous samples a good indication of the oxidation of the activated layer is the oxygen/carbon ratio, this suggests a 1:4 ratio of oxygen to carbon following the reaction with LiOH (aq) compared to 1 in every 7 for activated PTFE following air exposure.

The ATR-FTIR spectra shown below, Figure 5.14 indicates the presence of oxygenated species from the following features: a broad absorption centred at ~3200 cm^{-1} is indicative of intermolecularly hydrogen bonded -OH stretching modes[40], 1668 cm^{-1} can be attributed to C=O stretching[40], a growth in the intensity of the peak at 1430 cm^{-1} which had previously been assigned to aromatic or unsaturated C-C stretching could instead be associated with -OH in plane bending vibrations[40].

Table 5.3   Atomic Composition Determined by XPS of Activated PTFE Film Followed by Reaction 10% LiOH(aq).

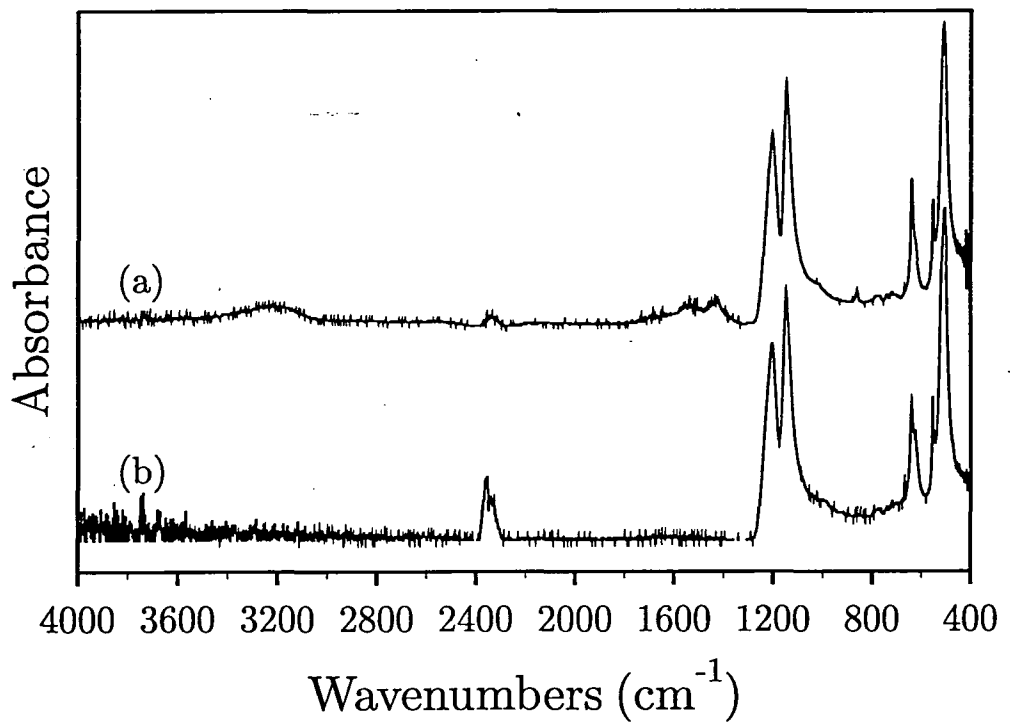| Percentage Composition	Untreated	Activated and reacted in 10% LiOH (aq)
%C	33.5	68.2
%F	66.5	15.2
%F	~	0
%O	~	16.6
%Na	~	0

Figure 5.14   **ATR-FTIR spectra of PTFE film (a) etched for 30 Mins followed by reaction with 10% LiOH(aq), (b) unetched.**

5.3. DISCUSSION

5.3.1. Chemical Structure of Activated PTFE

The results presented above confirm that the reaction of PTFE with sodium naphthalenide etchant leads to the rapid defluorination of the PTFE surface layer extending to several hundred nanometres in depth. The surface layer was composed predominantly of carbonaceous material and contained a small proportion of oxygenated functionalities. Other studies however, have shown these to be localised in the top few nanometres of the activated surface layer[12] and this suggests that the oxygenated species result from exposure to atmospheric oxygen and water, post etch washing[5] or due to the oxidation of unreacted etchant[44]. The attempt to minimise the oxidation of the activated surface by performing the reaction under a dry nitrogen atmosphere did not significantly reduce the levels of oxidised species measured by XPS analysis. This suggests that air oxidation is less important than intimated by the literature, either the oxygen/moisture levels were sufficiently high enough to react with a significant proportion of the active centres, or oxygen incorporation is occurring due to a reaction with the ether solvent.

It is generally accepted that the defluorination reaction results in the formation of reactive radical centres on the surface which then react further to form crosslinked C-C bonds, unsaturated C=C and C≡C and graphitic structures[13, 14]. This yields a diffuse PTFE/PTFE-C interface[7], which has been identified using scanning electron microscopy. Most of these observations[45] have been supported by X-ray scattering, electron microscopy and XPS[13] data, though EPR[46] has put the existence of the graphitic ring structures in to doubt. Unfortunately XPS analysis is unable to give detailed information

about the bonding characteristics of the carbon-carbon species in the defluorinated layer and we have had to rely upon ATR data to give an insight in to the chemical structure of the etched layer. The growth of unsaturated carbon-carbon stretching modes in the infra-red spectra at higher etching agrees with the observations of other groups. Even so, it is noticeable from the ATR-FTIR analysis that the large reduction in the CF_2 stretching bands with increasing etching times is not matched by a correspondingly large increase in the peaks attributable to aromatic or unsaturated C-C stretching modes as expected. This leads to the conclusion that perhaps unsaturated bond formation is not the dominant pathway and crosslinking is more common. Crosslinking would lead to the formation of non infra-red active carbon bonding modes for example in graphitic or diamond-like structures. Raman studies[4, 26] of PTFE defluorinated via the benzoin dianion method have shown a significant proportion of raman active saturated carbon-carbon stretching modes, and ^{13}C CPMAS NMR[8] has demonstrated the presence of sp, sp^2 and sp^3 hybridised carbon environments in etched material.

5.3.2. Mechanistic Considerations

5.3.2.1. *Defluorination Reaction*

Several mechanisms have been proposed in an attempt to explain the defluorination of PTFE via the alkali etching, however a thorough understanding has not yet been achieved. Rapid kinetics and unusually deep modification has been taken as evidence for the corrosion[2] based mechanism of defluorination. The Li/Hg amalgam system has been described in terms of a $Li | C+LiF | PTFE$ electrochemical cell, where corrosion of the PTFE occurs by the donation of the valence electron of the Li in to the

conjugated system of the etched layer. This enables the reaction to proceed at a much faster rate than expected if the Li had to diffuse through the etched layer to the reaction front. Kinetic studies showed that the rate of etching in this case had no connection with the concentration of Li in the Hg amalgam[2]. In the sodium naphthalenide system we found that the dilution of the 'Tetra-etch' caused little change in the composition of the surface layer measured by XPS until the etchant was at a very low concentration.

An equation relating the thickness of the layer formed to the time of the reaction was devised by Jansta et al[2] and the relationship (5.1) is shown below.

$$l' = K\sqrt{t} \qquad (5.1)$$

where l' = thickness of reacted layer, t = time and K is a constant which was found to be dependent upon the reaction temperature.

If we follow the diminution of the CF_2 peaks in the infra-red spectra with time as shown Figure 5.15, we can also make some deduction about the rate of the etching process. This shows excellent agreement with gravimetric determinations of etching rates[5,8] in other studies. However plotting these data against $\sqrt{t}$ in accordance with expression suggested by Jansta et al[2] gave only moderate agreement, which demonstrates that the corrosive mechanism for defluorination is inadequate when applied to the defluorination of PTFE with sodium naphthalenide.

Kavan et al[47] proposed an alternative to the corrosive mechanism involving the diffusion of the reactants and products to and from the reaction front. It was further

suggested that the resistivity of the C/LiF layer formed during the defluorination reaction, to Li^+ transport was the rate determining step and he concluded that the slower rate observed by Jansta[2] for defluorination using Na and K amalgams compared to Li could be explained by the higher resistivities to cation transport of the NaF and KF formed in the interfacial layer.

In contrast Marchesi et al[5] in considering the sodium naphthalenide etching system supported the corrosive electron transfer mechanism but suggested that the migration of fluoride ions from the reaction front was the rate limiting step. This explanation seems to best explain the results observed in this case.

5.3.2.2. *Functionalisation*

The reactions by which the groups are bonded to the polymer surface are very dependent upon the composition of the activated surface. The functionalisation of the activated surface can be considered in terms of a radical addition reaction or nucleophilic addition to unsaturated carbon carbon bonds.

The functonalisation of the material met with limited success, hydroxylation was quite effectively demonstrated, however unambiguous evidence illustrating the presence of phenyl groups in the defluorinated layer proved much less convincing. This may be due to the low surface sensitivity of ATR-FTIR analysis and the inability of XPS to distinguish between the forms of carbon in the etched layer and attached phenyl groups. Alternatively the results may simply indicate poorer functionalisation in the case of reaction with bromobenzene.

Polymer surface reactions occur under sterically hindered conditions, due to the close packing packing of the molecular chains and the two dimensional environment. This may prevent the phenyl groups from closely spaced reaction sites leading to a more widely spaced distribution of functionality. A large proportion of the available active sites could be within the activated layer, which may mean that the majority of the activated surface is inaccessible to larger molecules such as bromobenzene.

Reactions of aromatic halides are generally based upon electrophilic substitution of the halogen from the ring[24, 48]. The surface of defluorinated PTFE is highly unsaturated and has a high proportion of radical species[46] present thus electrophilic attack on to the aromatic ring would be unlikely. Nucleophilic mechanisms have been postulated, Figure 5.16, but the reaction is not favourable unless the intermediate transition state is stabilised by electron withdrawing groups.

Radical addition of the phenyl group to the activated surface could arise through the initiation step illustrated in Figure 5.17 which occurs by way of a radical ion intermediate and involves the donation of an electron from the activated surface to an unfilled π orbital of the aromatic ring and the ejection of a bromide ion[24]. The phenyl radical can then undergo a radical addition as indicated in Figure 5.18. Steric considerations favour the radical mechanism proposed above, Figure 5.17 which is able to progress via unimolecular transition states. The bimolecular transition states involved in Figure 5.16 will be a higher energy pathway.

The reaction of hydroxide ions with the activated PTFE will be subject to less steric hindrance than the phenylation reaction and a larger proportion of the activated

surface may be accessible to the hydroxide ions. The mechanism of hydroxylation is not clear in this case. Defluorination of poly(vinyldifluoride) (PVDF), a partially fluorinated saturated polymer with the following structure $-(CH_2-CF_2)_n-$ was demonstrated by Crowe et al[49] using a saturated solution of LiOH. Unlike PVDF however, PTFE is not normally affected by concentrated alkali hydroxide, but the unsaturated partially defluorinated PTFE functionalities will be susceptible to the nucleophilic attack of hydroxide anions due to the high electronegativity of the fluorinated substituents which stabilise the anionic intermediate. A possible mechanism of the hydroxylation reaction is shown in Figure 5.19.
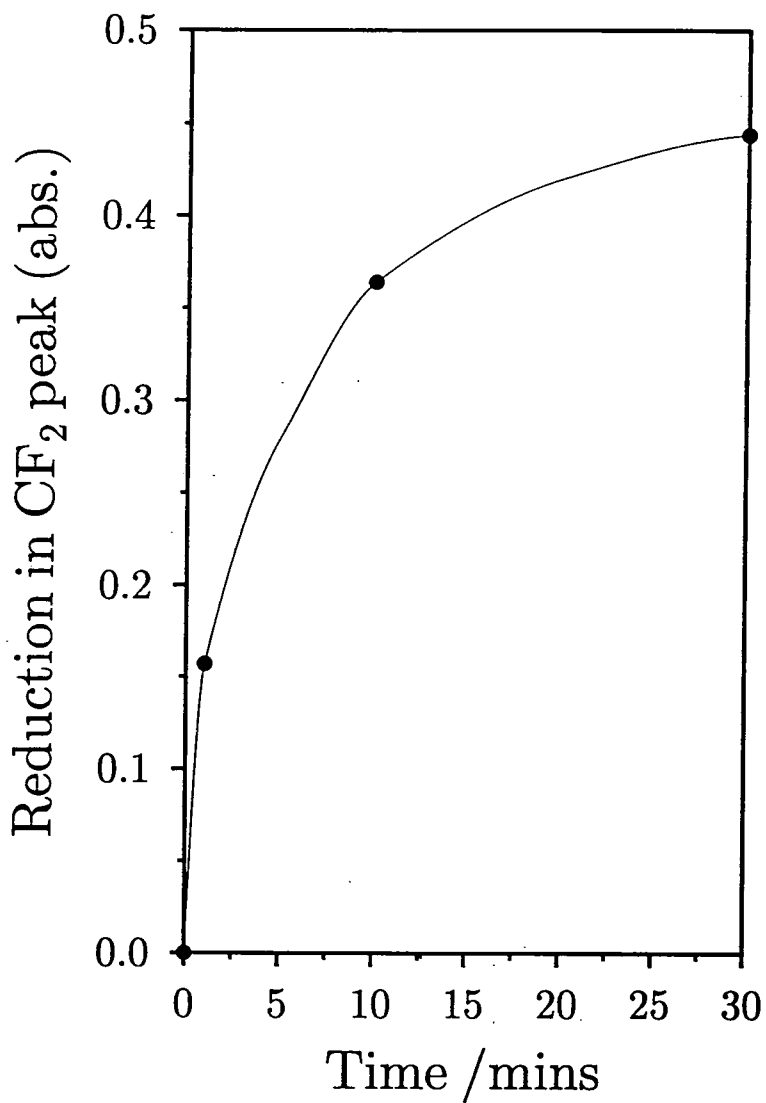
Figure 5.15   **Variation in Intensity of CF₂ peaks with Reaction Time**
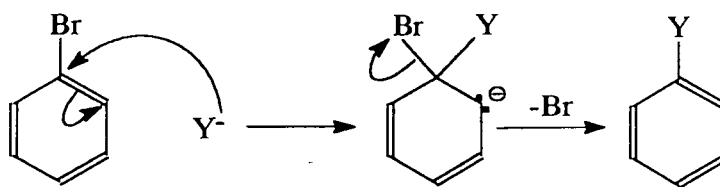
Figure 5.16   Nucleophilic Substitution of Bromine in Bromobenzene (Y = nucleophile).
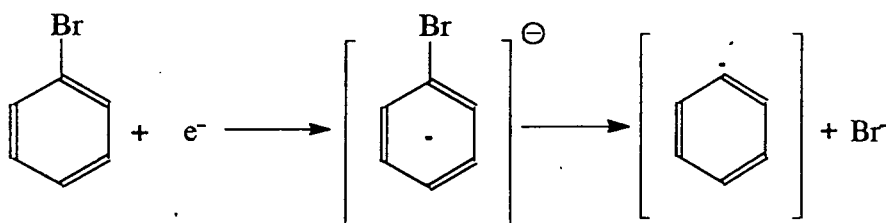

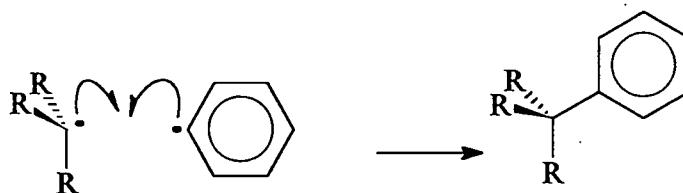**Figure 5.17**   Initiation of the Radical reaction with Bromobenzene

Figure 5.18   Addition of the Phenyl Radical to the Activated PTFE (R= sp, sp^2 or sp^3 hybridized carbon)
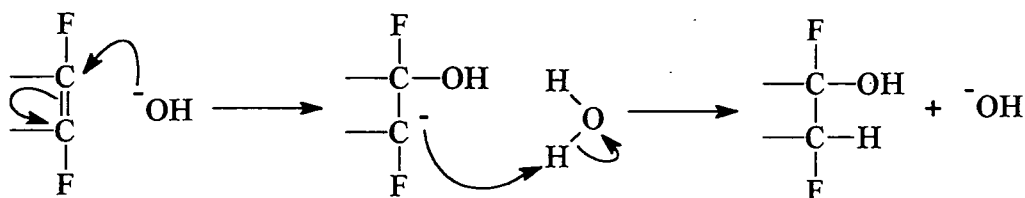

Figure 5.19   Possible Mechanism for Hydroxylation of the Interfacial Layer.

5.4. CONCLUSIONS

The reaction of sodium naphthalenide with PTFE leads to rapid defluorination of the near-surface region, and the formation of a partially crosslinked and unsaturated carbonaceous network. There is also some roughening of the surface as evidenced by AFM analysis. The results presented here seemed to support the combined corrosion/diffusion based mechanism proposed by Marchesi[5]. Hydroxylation of the activated PTFE layer has been demonstrated, although the phenylation of the surface was not proven.

5.5. REFERENCES

1   *Encyclopedia of Polymer Science and Engineering*, Vol. 16, Wiley, New York, 1991.

2   Jansta J., Dousek F. P., Riha J., *J.Appl. Polym. Sci.*, **19**, 3201 (1975).

3   Kavan L., Dousek F. P., *Electrochim. Acta.*, **26**, 233 (1981).

4   Iqbal Z., Ivory D. M., Szobota J. S., Elsenbaumer R. L., Baughman R. H., *Macromolecules*, **19**, 2992 (1986).

5   Marchesi J.T., Ha K., Garton A., *J. Adhesion*, **36**, 55 (1991).

6   Bening R. C., McCarthy T. J., *Macromolecules*, **23**, 2648 (1990).

7   Schoichet M. S., McCarthy T. J., *Macromolecules*, **24**, 982 (1991).

8   Costello C. A., McCarthy T. J., *Macromolecules*, **20**, 2819 (1987).

9   Dias A. J., McCarthy T. J., *Macromolecules*, **17**, 2529 (1984).

10   Dias A. J., McCarthy T. J., *Macromolecules*, **18**, 1826 (1985).

11   Gagnon D. R., McCarthy T. J., *J. Appl. Polym.* Sci., **29**, 4335 (1984).

12   Ha K., McClain S., Suib S. L., Garton A., *J. Adhesion, 33*, 169 (1991).

13   Kavan L., Dousek F. P., Jansta J., *Carbon*, **22**, 77 (1984).

14   Kavan L., Dousek F. P., *Carbon*, **24**, 61 (1986).

15   Banks R. E., *Fluorocarbons and their Derivatives*, Oldbourne Press, London, 1964.

16   Chang C-A., Baglin J. E. E., Schrott A. G., Lin K-C., *Appl. Phys. Lett.*, **51**, 103 (1987).

17   Nelson E. R., Kilduff T. J., Benderley A. A., *Ind. Eng. Chem.*, **50**, 329 (1958).

18   Dumitriu S., *Polymeric Biomaterials*, Dekker Inc., New York, 1994.

19   Tefal Co., British Patent 1358428, (1971)

20   Hansley V. L., *Ind. Eng. Chem.*, **43**,1759 (1951).

21   Vaughan T. H., Hennion G. F., Vogt R. R., Nieuwland J. A., *J. Org. Chem.*, **2**, 1 (1937).

22   Yost D. M., Russell H., *Systematic Organic Chemistry*, pp 145-7, NewYork, Prentice Hall, 1944.

23 . Scott N. D., Walker J. F., Hansley V. L., *J. Am. Chem. Soc.*, **58**, 2442 (1936).

24   Roberts J. D., Caserio R., *Basic Principles of Organic Chemistry*, 2nd Ed., Benjamin Inc., California, 1977.

25   Paul D. E., Lipkin D., Weissman S. I., *J. Am. Chem. Soc.*, **78**, 116 (1956).

26   Costello C. A., McCarthy T. J., *Macromolecules*, **17**, 2940 (1984).

27   Bee T. G., Dias A. J., Franchina N. L., Kolb B. U., Lee K.-W., Patton P. A., Schoichet M. S., McCarthy T. J., in *Polymer Surfaces and Interfaces II*, Feast W. J., Munro H. S., Richards R. W., (Eds.), John Wiley, Chichester, pp 1-25, 1992.

28   Stewart D. J., Hughes P., Lowe C, R., *J.Biotech.*, **11**, 253 (1988).

29   Young B. R., Pitt W. G., Cooper B. S., *J. Colloid Int. Sci.*, **125**, 246 (1988).

30   Kirkland J. J., *Anal. Chem.*, **35**, 2003 (1963).

31   Scopes R. K., *Protein Purification - principles and practice,* 2nd Ed., Springer

      Verlag, New York, 1988.

32   Kervalage A. R., Hasan T., Cooperman B. S., *J. Biol. Chem.*, **258**, 6313 (1982).

33   Evans J.F., Gibson J.H., Moulder J.F., Hammond J.S., Goretzki H., *Fresenius Z.*

      Anal. Chem., **319**, 841 (1984).

34   Johansson G., Hedman J., Berndtsson A., Klasson M., Nilsson R. J., *Electron*

      Spectr., **2**, 295 (1973).

35   Clark D. T., Feast W. J., Kilcast D., Musgrave W. K. R., *J. Polym. Sci.*, **11**, 398

      (1973).

36   Lopez G. P., Castner D. G., Ratner B. D., *Surf. Int. Anal.*, **17**, 267 (1991).

37   Seah M. P., Dench W. A., *Surf. Int. Anal.*, **1**, 2 (1979).

38   Mirabella F. M. Jr.,*Applied Spectroscopy Reviews*, **21**, 45 (1985).

39   Adams M. R., Ha K, Marchesi J., Yang J., Garton A., in *Structure-Property*

      Relations in Polymers, Urban M. W., Craver C. D., Eds., ACS **236**, 333 (1991).

40   Silverstein R. M., Bassler G. C., Morill T. C., *Spectrometric Identification of*

      Organic Compounds, 4th Ed., John Wiley, New York, 1981.

41   Dietz P., Hansma P. K., Ihn K. J., Motamedi F., Smith P., *J. Mater. Sci.*, **28**,

      1377 (1993).

42   Beamson G., Briggs D., *High Resolution XPS of Organic Polymers-The Scienta*

      ESCA 300 Database p. 236. John Wiley, Chichester, 1992.

43   Bellamy L. J., *The Infra-red Spectra of Complex Molecules*, Chapman and Hall,

London, 1986.

44   Rye R. R., Arnold W. W., *Langmuir.*, **5**, 1331 (1989).

45   Peltzbauer Z., Baldrian J., *Carbon*, **17**, 317 (1979).

46   Kavan L., Klima J., Pseidlova M., *Carbon*, **23**, 45 (1985).

47   Kavan L., Dousek F. P., Micka K., Weber J., Carbon **26**, 235 (1988).

48   Graham Solomons T. W., *Organic Chemistry*, 2nd Ed., Wiley, New York, 1980.

49   Crowe R., Badyal J. P. S., *J. Chem. Soc. Chem. Comm.*, 958 (1991).

6. DYNAMIC SURFACE PROPERTIES OF CHEMICALLY ACTIVATED PTFE PARTICLES.

6.1. INTRODUCTION

The chemical modification of PTFE using an alkali metal reduction[1] step in order to make the surface more reactive, followed by the introduction of specific functionality[2,] using conventional organic chemistries was presented in the previous chapter as an attractive potential route leading to stationary phases which could be 'tailored' to the specific requirements of the end user.

In the introductory chapter to this thesis we emphasised the importance of the dynamic aspects of polymer surfaces. The activated PTFE surface which results from the alkali metal defluorination has been shown to be inherently unstable, which is reflected in its highly reactive nature. Dwight et al[4] examined the mobility of an etched PTFE film. XPS analysis showed a reversion of the etched layer back to its original fluorinated composition following the heating of the sample. In order to consider the activated PTFE surface for use as a bioseparation media it is important to understand the surface dynamics of the material. For example the thermal properties which influence the mobility of the surface; Tm (melting temperature) and Tg (glass transition temperature) are much lower in the case of polymers compared to say, inorganic materials and consequently polymeric systems enjoy a much greater degree of molecular freedom especially at their surfaces. This will be of major importance in understanding the

179

behaviour of the activated and functionalised PTFE upon it exposure to a biological fluid phase.

We have already discussed the effects of the sodium naphthalenide reagent on the chemical properties of a PTFE film. Even so, despite the relatively large amount of information concerning the chemical properties of the etched layer very few studies have investigated the physical properties. We have also shown by comparing AFM analysis of the film before and after the reaction, that the morphology of the material is significantly altered during the activation process. It is this roughening of the surface that is thought to contribute to the ease with which the etched material can be bonded to other substrates using conventional adhesives[3].

It has been suggested by several groups that the alkali etching process renders the surface highly porous[4] and that this porosity can extend in the most extreme of circumstances to a depth of 10 000Å[5-7], however many of these observations are based upon Scanning Electron Microscopy (SEM) studies of the etched PTFE film, and although the technique is well suited to characterising the morphology of these films it is questionable whether the technique is able to positively identify the presence of porous structures extending deeply in to the etched layer.

In this chapter we have studied granulated PTFE material which more accurately reflects the form of the material as it would be employed as a bioseparation media. Nitrogen sorption has been employed in an attempt to investigate the physical nature of the etched layer, since as we have shown earlier in this thesis it is a versatile technique for the measurement of internal pore structure in solids. In addition we intend to

characterise the dynamic properties of the interface between the defluorinated PTFE and the bulk PTFE by examining the thermal stability of the etched layer in relation to both its chemical and physical properties.

6.2. EXPERIMENTAL

6.2.1. Materials

The samples of poly(tetrafluoroethylene) (PTFE) used in this chapter were in the form of a powder (50 µm average particle size) supplied by Mupor Ltd. The activation of the polymer surface was achieved by using 'Tetra-etch' (a solution of sodium naphthalenide in glycol ether) supplied by Gore Ltd. Washing of the samples was performed as indicated below distilled water (99.5% pure), analar grade (99% pure) acetone and hexane, and dry (<7ppm H_2O) tetrahydrofuran (THF).

One gram of granulated PTFE was accurately weighed out and used as received. Activation of the material was performed using 40 ml of 'Tetra-etch' at room temperature for 30 minutes in a continuously stirred reaction vessel. The resulting activated powder was washed with four 40 ml aliquots of water, acetone and hexane. Drying was achieved in a covered vessel in air for two hours.

Thermal treatments were performed in a vacuum oven at 0.1 mbar (in order to minimise atmospheric surface contamination) at room temperature (~23 °C), 50 °C and 100°C for 12 hours respectively prior to analysis.

6.2.2. Sample Analysis

The powdered samples were prepared for XPS analysis by using double sided tape to attach the material to a metallic stub. XPS analysis was carried out on a Kratos ES200 X-ray photoelectron spectrometer operating in the fixed analyser transmission (FAT) mode, at a pass energy of 65 eV, and an electron take-off-angle of 30° from the substrate normal. Mg $K_{\alpha 1,2}$ (1253.6 eV) ionising radiation was used as the photoexcitation source. A PC computer was used for XPS data accumulation and component peak analysis, assuming linear background subtraction and Gaussian fits with fixed full width at half maximum (FWHM)[8]. All spectra are referenced to the C(1s) core level shift for adventitious hydrocarbon at 285.0 eV[9].

Attenuated total reflection infrared (ATR-IR) measurements were taken on a Mattson Polaris FTIR instrument, equipped with a Specac optical table and a KRS-5 ATR crystal. The powdered material was pressed into flattened discs which could then be mounted in to the ATR cell. Infrared spectra were accumulated at 4 cm^{-1} resolution in the range 400 cm^{-1} to 4000 cm^{-1} over 100 scans.

Nitrogen adsorption isotherms were performed on the powdered PTFE samples using a PMI Brookhaven Sorption apparatus. Each sample was outgassed at 0.1 Torr and room temperature for 24hrs prior to analysis to remove any physisorbed moisture. A detailed description of the theory outlining the BET surface area and pore distribution determination can be found in chapter 2, section 2.4.

6.3. RESULTS

6.3.1. XPS Analysis.

In common with the air etched PTFE films described above, the C(1s) XP Spectra of the etched powder is dominated by a carbonaceous peak with a range of oxygenated functionalities at higher binding energies. Table 6.1 shows the percentage composition of the surface layer, around 10% is attributed to oxygenated species and it is apparent that etching for 30 minutes has led to incomplete defluorination of the surface layer sampled by XPS which manifests itself in a small (~4 atomic percent) but important contribution to the F(1s) environment. The washing procedure in this case has not been completely successful in removing NaF and unreacted etchant, this may be an indication of the porous nature of the etched powder which will hinder the dissolution of the inorganic NaF produced from the reaction. In Figure 6.1 the F(1s) to C(1s) ratio gives an indication of the degree of fluorination of the layer sampled by XPS. A small increase is observed in the F/C ratio.

6.3.2. ATR-FTIR Analysis.

ATR-FTIR analysis provides a contrasting picture of the etched samples which have been subjected to heating compared to the one presented by the XPS data. Etching for 30 minutes followed by evacuation at room temperature for 12 hours significantly reduces the intensity of the asymmetrical and symmetrical CF_2 stretching modes at 1147 and 1201 cm^{-1}. Heating at 50°C causes a gradual increase in these bands, heating at 100 °C has a more pronounced affect and the peaks are restored almost to the intensity of

untreated PTFE film as shown in Figure 6.2.

Aromatic and unsaturated carbon-carbon stretching frequencies at 1430 and 1600 cm^{-1} are also present in the surface layer of the etched powder, Figure 6.3. These are accompanied by a weak shoulder present at approximately 1700 cm^{-1} which may be due to C=O stretching[10] modes of the oxygenated functionalities. Heating in this case reduces the ratio of the peaks assigned to defluorinated unsaturated carbon with respect to the PTFE peaks.

Table 6.1   **Percentage Composition Determined by XPS of the Surface of Etched PTFE Powder and the Effect of Heat Treatment.**

Percentage Composition	Treatment Conditions			
	Untreated	Etched	Etched and heated for 12hrs at 50°C	Etched and heated for 12 hrs at 100°C
%C	33.5	72.4	76.7	64.4
%F	66.5	4.3	3.8	4.6
%F	0	4.6	5.1	7.8
%O	0	10.2	7.0	10.3
%Na	0	8.4	7.5	13.0
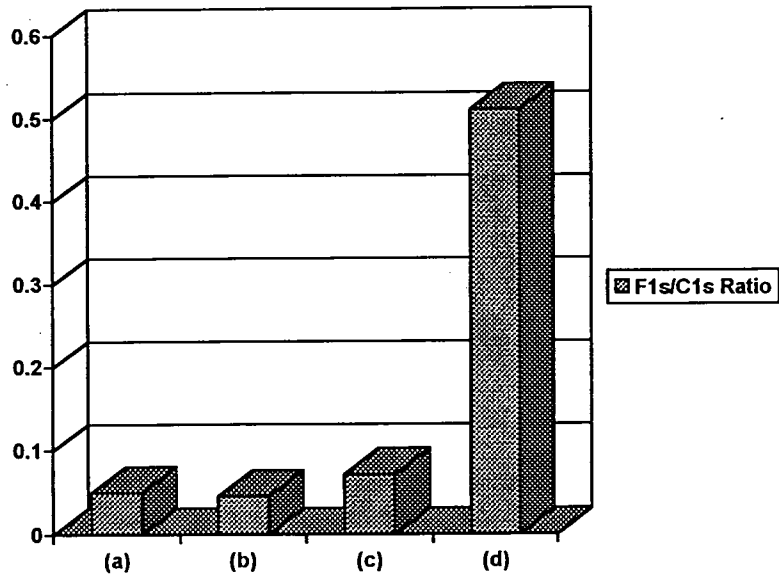
Figure 6.1   Chart showing the Fluorine 1s /Carbon 1s ratio of PTFE (a) etched for 30 Mins, with no heating, (b) etched for 30 Mins, heated at 50 °C for 12hrs, (c) etched for 30 Mins, heated at 100 °C for 12 hrs and (d) untreated PTFE powder.
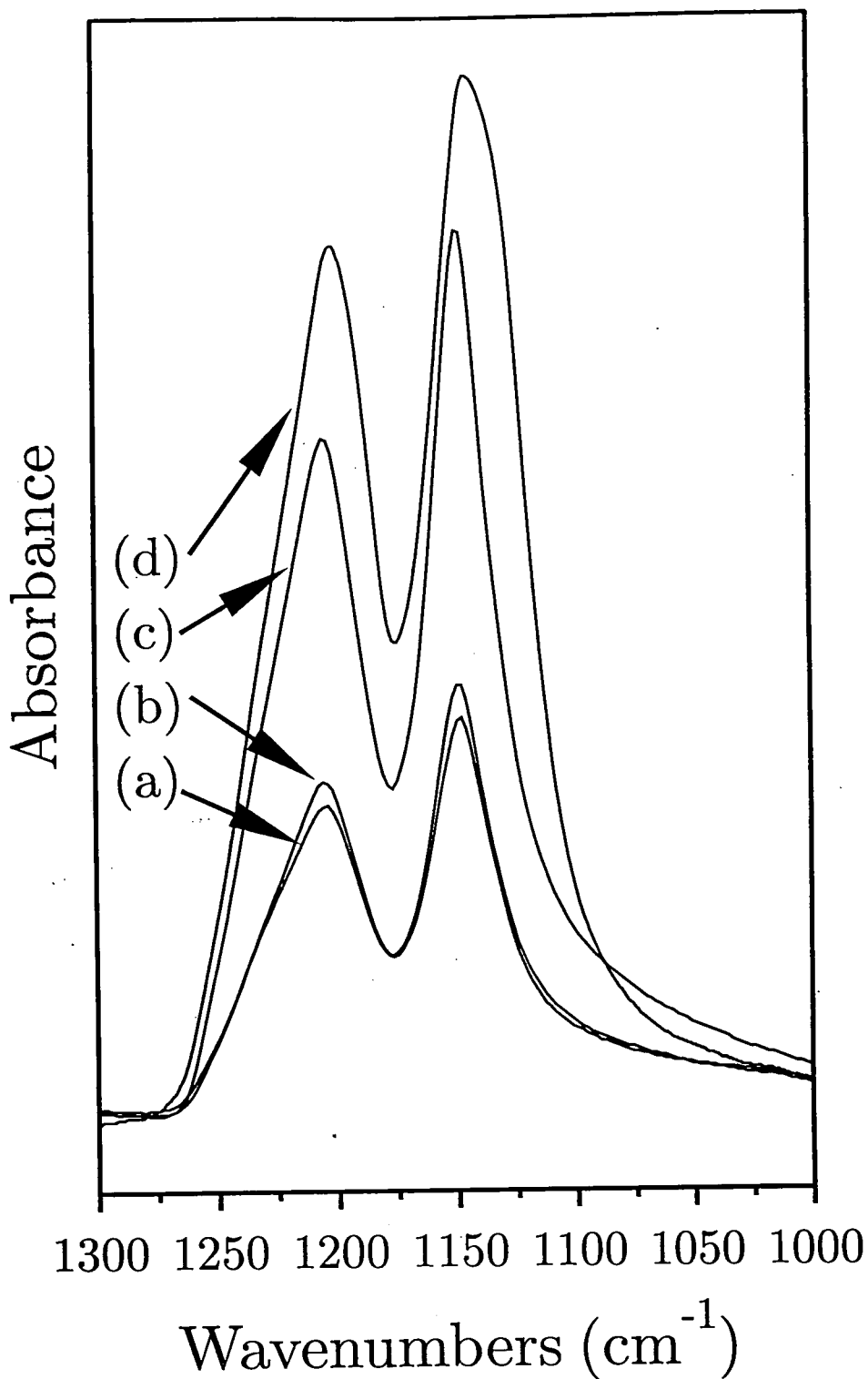
Figure 6.2　　Variation in the intensity of the asymmetrical and symmetrical stretching modes of CF_2 for (a) etched for 30 Mins with no heating, (b) etched for 30 Mins, heated at 50°C for 12hrs, (c) etched for 30 Mins, heated at 100°C for 12 hrs and (d) untreated PTFE powder.

Figure 6.3   ATR-FTIR (1800-900 cm^{-1} region normalised to the CF$_2$ peak at 1147 cm^{-1}) for (a) etched for 30 Mins, with no heating, (b) etched for 30 Mins, heated at 50°C for 12hrs, (c) etched for 30 Mins, heated at 100°C for 12 hrs and (d) untreated PTFE powder.
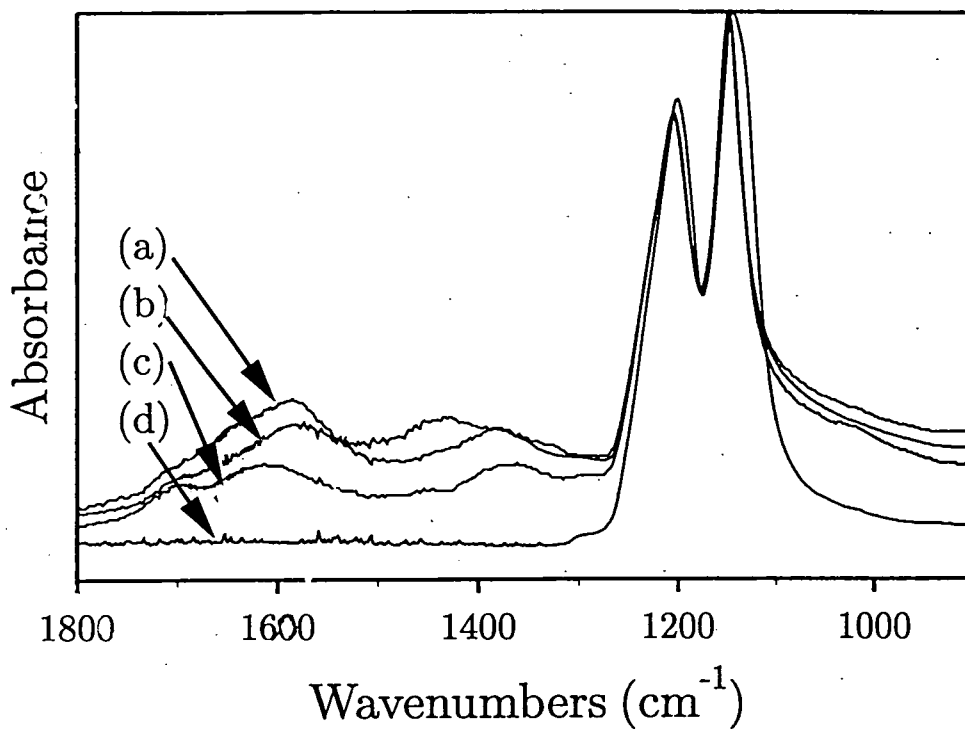
6.3.3. Nitrogen Gas Sorption Determination of Specific Surface Area and Pore Distribution.

PTFE powder adopts the Type II adsorption isotherm in the BET classification[11,12] as shown in Figure 6.4. This is common in materials exhibiting little or no porosity. The nitrogen adsorption isotherm for the etched material in Figure 6.5, exhibits an adsorption isotherm which appears to be a combination of Type I and Type II. The type I isotherm is characteristic of microporous solids such as activated carbons[13] and this isotherm represents the formation of a highly microporous etched layer around the non-porous PTFE particle.

A large increase in surface area is observed upon etching see Table 6.2 from 3.5 m²/g in virgin PTFE to 49.0 m²/g in the material etched for 30 minutes. The action of heat causes a reduction in the specific surface area. The data show that the 50 °C treatment reduces the surface area only slightly whereas heating for 12 hrs at 100 °C reduces the surface area almost to the level of the unetched PTFE surface.

Table 6.2   **Surface Area of Etched and Heat Treated PTFE Powder.**

	Treatment Conditions			
	Untreated	Etched	Etched and heated for 12hrs at50°C	Etched and heated for 12 hrs at 100°C
Surface Area (m²/g)	3.5	49.0	46.1	9.2

Calculations of pore structure distributions from the nitrogen adsorption isotherms are shown in Figure 6.6 (microporous region) and Figure 6.7 (meso/macroporous region). Figure 6.6 shows quite clearly the formation of a highly microporous structure in the etched samples which is indicated by the increased uptake of nitrogen between 3-8 Å. The change in the rate of adsorption of N_2 suggests pore filling and closure at a diameter corresponding to between 5 and 8Å. There is also an increase in the number of mesopores in the sample as shown in Figure 6.7 and this increase is particularly prominent in the 20-50 Å range.

Heating at 100°C leads to a significant reduction of the microporous nature of the surface layer, whereas at 50°C the reduction in microporosity is less marked. These observations support the specific surface area calculations above, and suggest that the majority of extra surface created during the etching process is contained in the internal microporous structure of the carbonaceous layer. The meso/macropores are much more stable than the micropores. Figure 6.7 shows a small reduction in the pore distributions of the etched samples at 50° and 100°C.
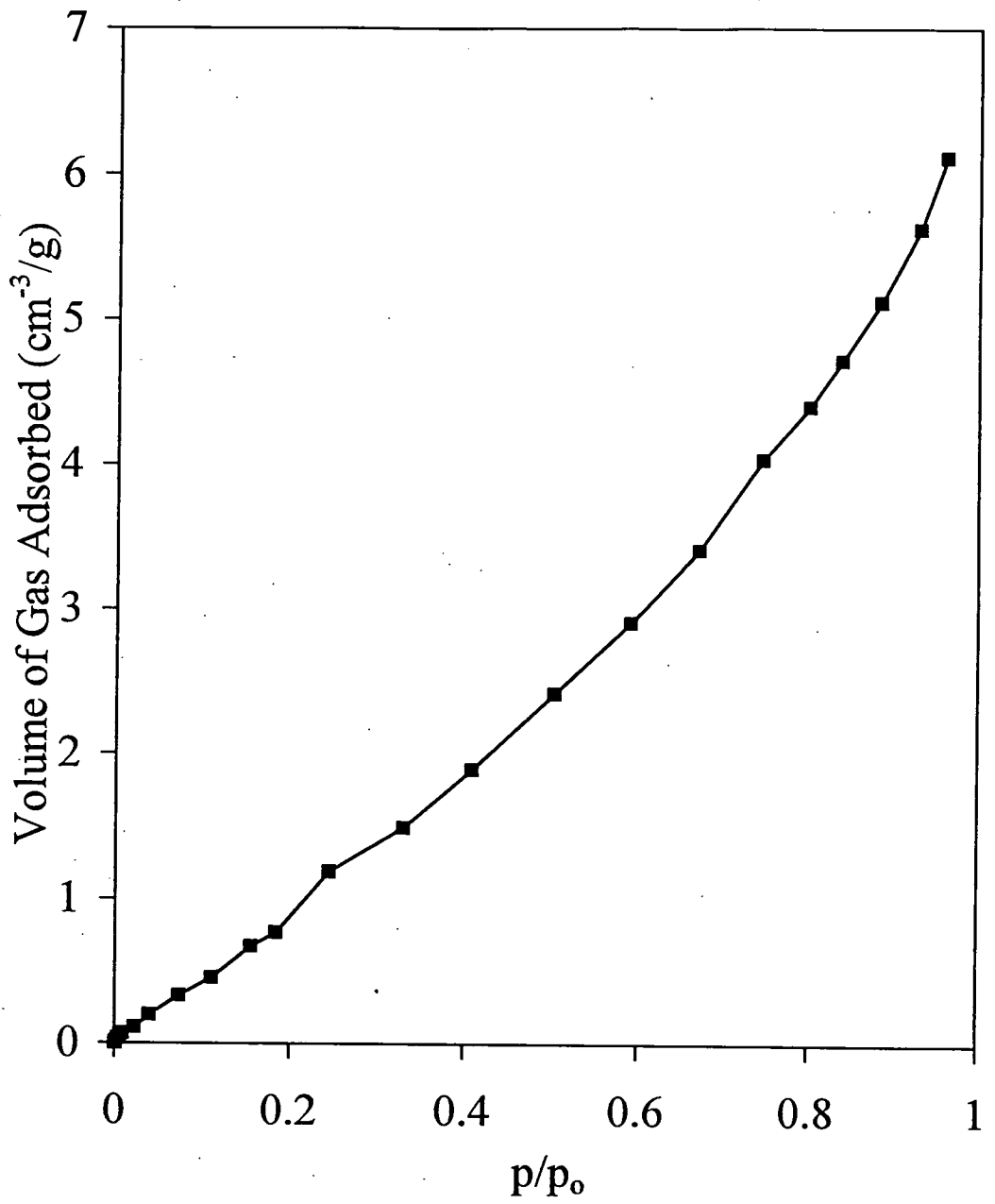
Figure 6.4   **A nitrogen adsorption isotherm plot for untreated PTFE powder.**
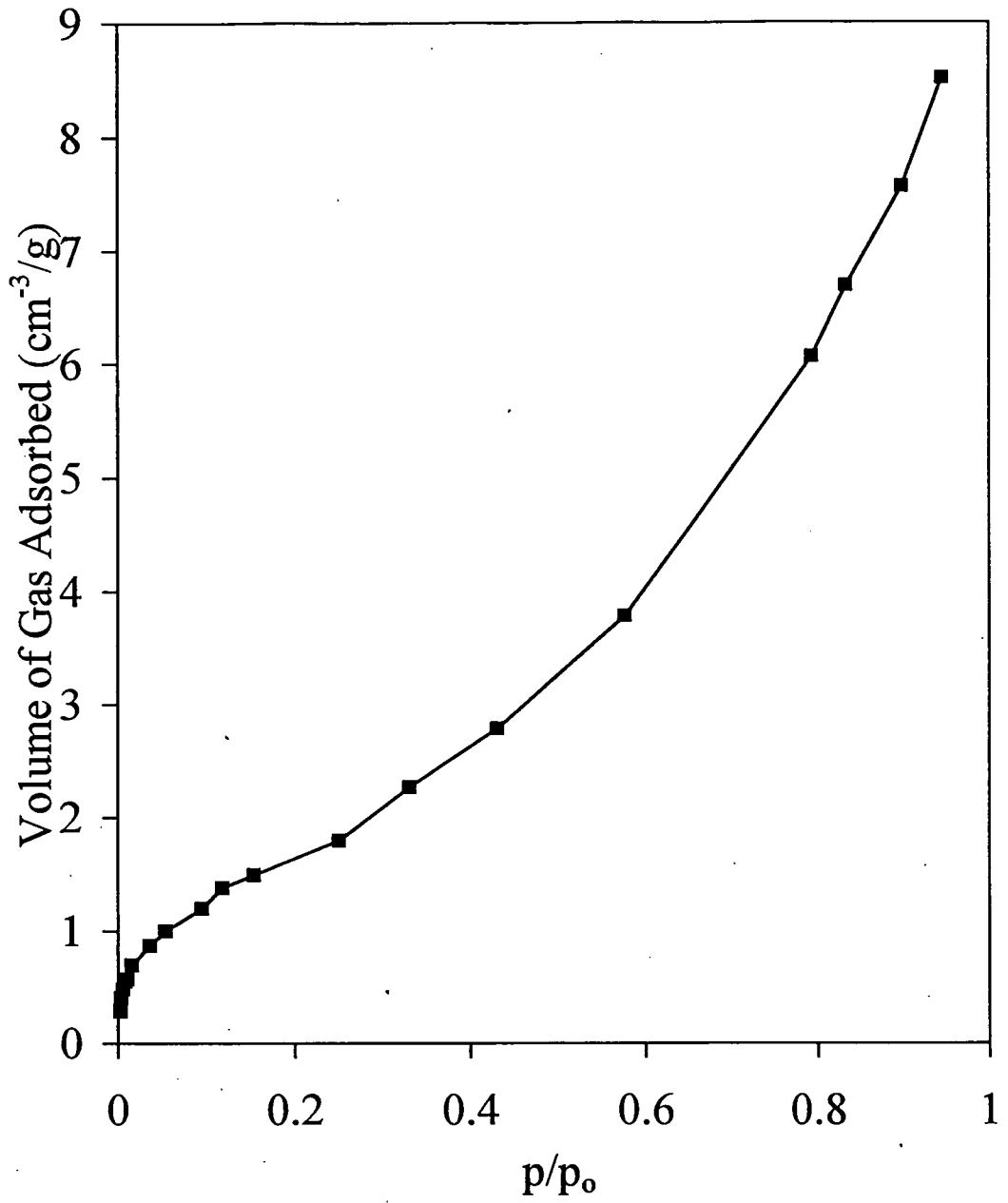
Figure 6.5   **A nitrogen adsorption isotherm plot for PTFE powder which has been etched for 30 Mins.**
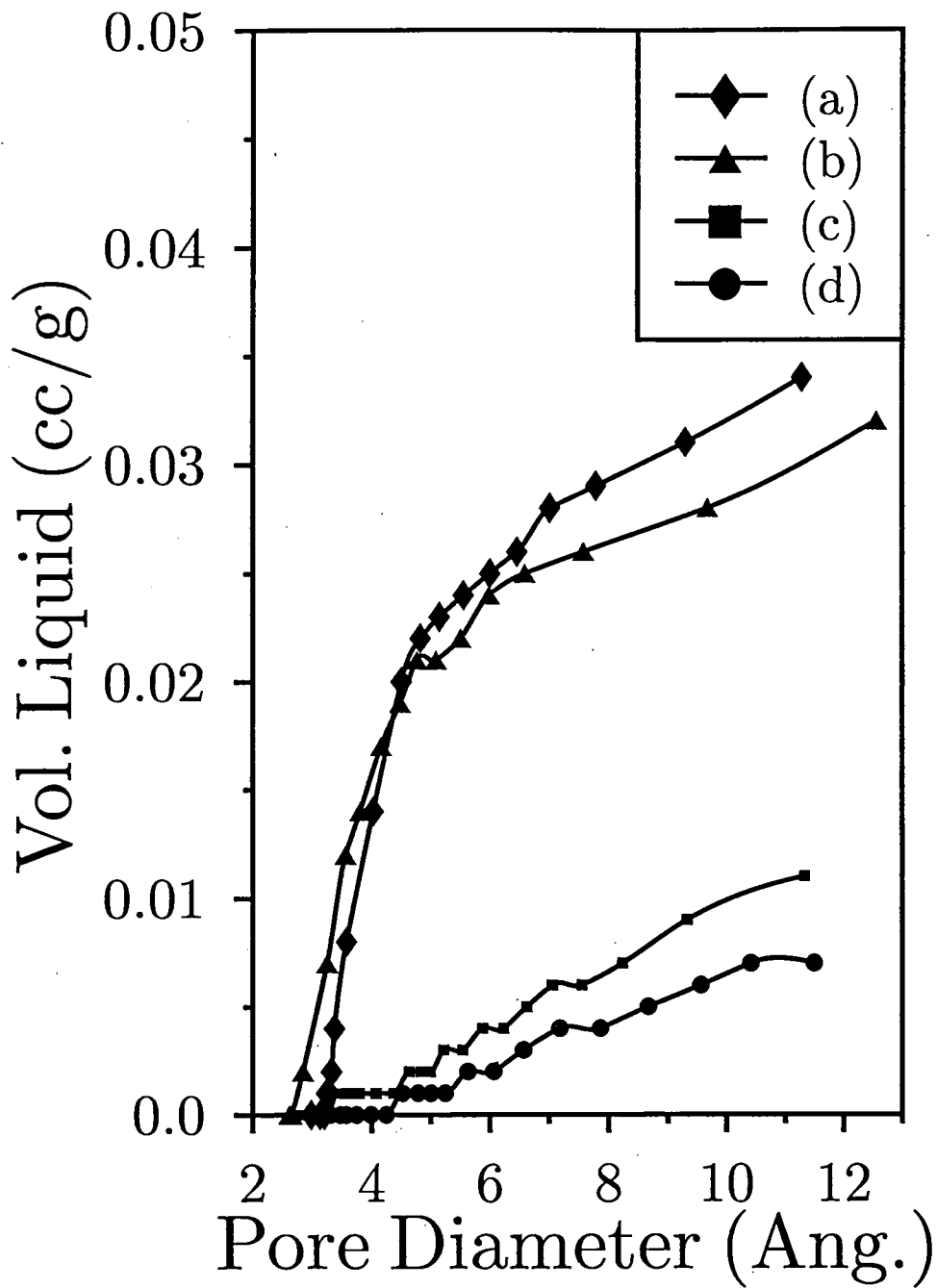
Figure 6.6   **Microporosity of: PTFE powder (a) etched for 30 Mins, unheated, (b) etched for 30 Mins, heated at 50°C for 12 hrs, (c) etched for 30 Mins, heated at 100°C for 12 hrs and (d) untreated PTFE powder.**

Figure 6.7   Mesoporosity of: PTFE powder (a) etched for 30 Mins, unheated, (b) etched for 30 Mins, heated at 50°C for 12 hrs, (c) etched for 30 Mins, heated at 100°C for 12 hrs and (d) untreated PTFE powder.

6.4. DISCUSSION

6.4.1. Physical Structure of Etched PTFE

The significant improvement in the adhesion to etched PTFE surfaces has been attributed to the mechanical interlocking of the adhesive with the sponge like pore structure of the surface[6]. Even so, SEM studies of the etched film surfaces have shown no evidence of 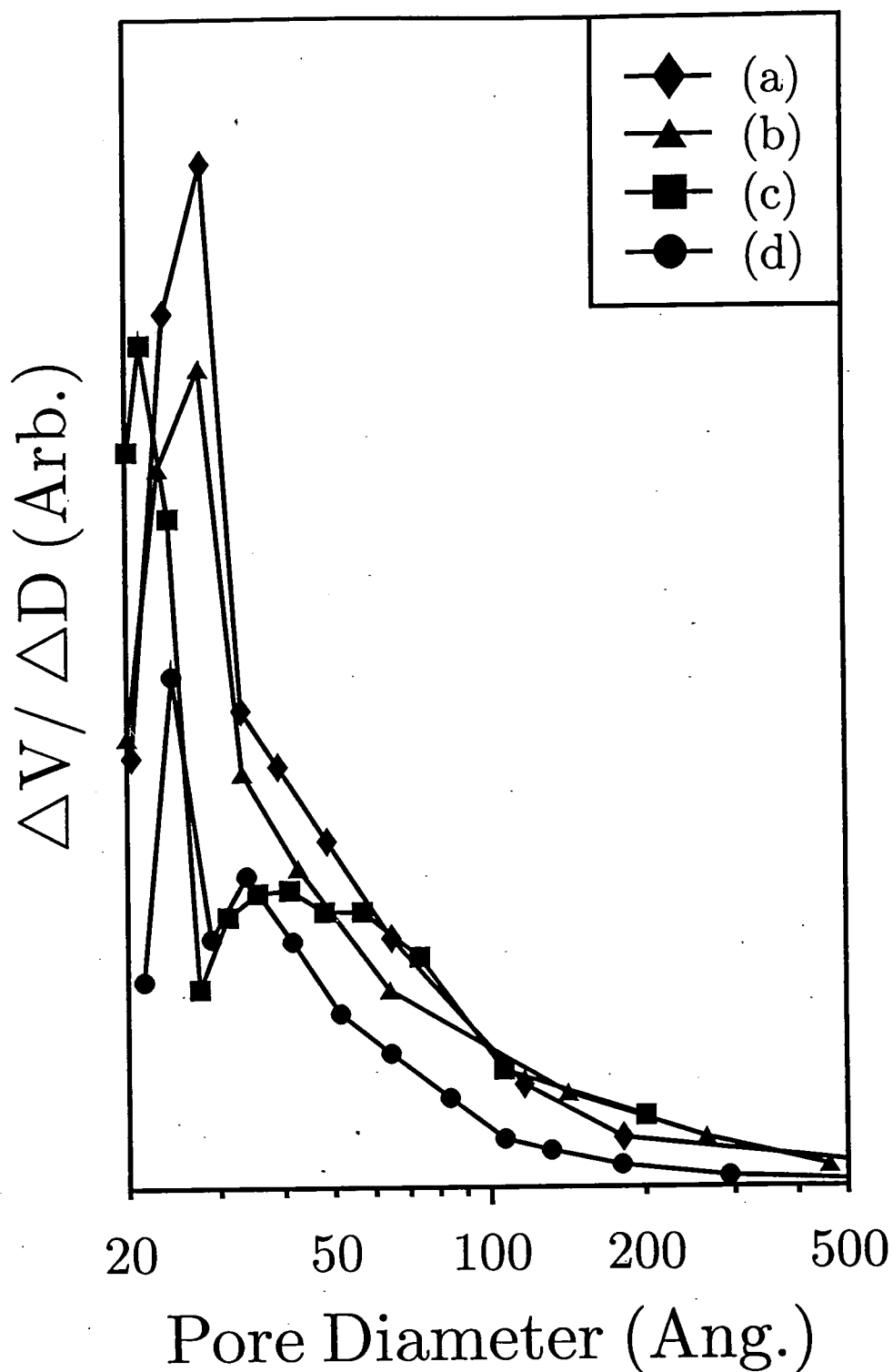pore formation[3] and the rapid dissolution of the alkali metal fluoride formed during the etching reaction was said to exclude the formation of a pore structure since the process would be diffusion based[1] and therefore much slower than observed.

The gas sorption results suggest that defluorination of the PTFE powder particles renders them highly microporous and this manifests itself in a much greater specific surface area as shown in Table 6.2. The mechanism leading to the formation of a porous structure in the carbonaceous layer of PTFE has been debated for some time. Pore formation in Li/Hg amalgam activated PTFE surface was attributed to the growth of LiF crystallites[14] within the PTFE structure during the reaction which were thought to cause deformation and compression of the polymer chains. Subsequent washing, removes these crystallites, leaving behind an extensive pore structure.

An alternative explanation could be due to the presence of crystalline and amorphous phases in the PTFE particle. Unfortunately we have no data concerning the proportion of crystalline material in these samples of PTFE but if preferential etching of the less densely packed and therefore more accessible amorphous regions of the sample were to occur then it is possible that this could result in the formation of a porous layer.

Referring to the AFM data of the etched PTFE film in Chapter 5 we observed a noticeable roughening and pitting of the surface, this could indicate more rapid etching of the amorphous regions also.

6.4.2. The Surface Dynamics of the Activated PTFE

Heating of the etched PTFE powder appears to cause the reversion of the etched layer in to a more PTFE 'like' material. XPS[4] analysis of etched PTFE films treated at high temperatures (~200°C) have shown a sharp increase in the F(1s) peak with an accompanied reduction in the oxygenated environments and this was interpreted as a removal of some of the etched layer exposing more of the unreacted PTFE. Temperature program desorption studies have shown that heat induced modification of the etched surface cannot be explained by the desorption of an overlayer from the surface of the etched material, but results from processes occurring in the solid phase[15]. The XPS data presented in this chapter, Table 6.1 do not give as strong an indication of this behaviour, which is probably as a result of the lower temperatures used in this study and the greater thickness of the etched layer. The growth in the infra-red CF_2 peaks however does allow us the follow the change in the etched layer resulting from the heat treatment see Figure 6.2. Since the loss of material has been discounted as an explanation for the change in the etched surface then this indicates that a rearrangement of the PTFE/PTFE-C interface must have occurred, perhaps via a diffusion mechanism of the PTFE polymer chains through the interfacial boundary layer.

Table 6.3   **Transition Temperatures for PTFE**

Temperature (°C)	Region affected
1st order	
19	crystalline, angular displacement[16]
30	crystalline, crystal disordering[16]
90 (80 to 110)	crystalline[17]
2nd order	
-90 (-110 to -73)	amorphous, rotational motion around C-C bond
-30 (-40 to -15)	amorphous[17]
130 (120 to 140)	amorphous[17]

In order to find a suitable explanation for this phenomenon we must consider the surface molecular dynamics of PTFE. The most appropriate indicator as to the molecular mobility of PTFE is the glass transition temperature (Tg)[18] for the bulk PTFE polymer. In Table 6.3 are a list of the temperatures at which the bulk PTFE chains possess enough thermal energy to overcome the barrier to molecular motion.

If we compare the data in Table 6.3 to the temperatures which we have subjected the etched PTFE powders then we can see that at 50 °C there will be enough thermal energy to allow 1st order crystalline displacements and 2nd order rotations of the PTFE chain to occur. A further point to note is that the values quoted in Table 6.3 are for bulk molecular motions. A theoretical study of a glassy poly(propylene) (PP)[19] polymer showed that the surface motions of the polymer chains were much enhanced compared to the bulk at its Tg. The enhanced mobility of the surface suggests that there would be a high probability of the surface reorientation under these conditions. At 100 °C we

would expect the surface and sub-surface regions of PTFE to adopt a polymer melt configuration, and in order to minimise the interfacial energy of the system the PTFE chains migrate to the surface.

A greater degree of molecular motion may be accompanied by an increase in the specific volume of the polymer, which is especially noticeable in more crystalline samples where the more efficiently packed structure is disrupted. Leading to a migration of the PTFE polymer chains outwards from the centre of the particle in to the etched layer. We have already shown that the majority of the surface area of the etched layer is present in the microporous structure of the material with pore diameters of between 5-10 Å. The reduction in surface area is believed to be due to the filling of micropores with material diffusing from within the particle as the molecular mobility of the PTFE increases. As we have shown the micropores are most effected by the thermal treatment of the etched particles.

6.5. CONCLUSIONS

The sodium naphthalenide defluorination of PTFE leads to the formation of a highly microporous etched layer and an approximately fifteen-fold increase in the surface area of the material. Reorientation of the interface between the virgin PTFE and the etched material as a function of the temperature, which we have been able to monitor using infra-red analysis leads to the disruption of the pore structure and loss of specific surface area.

6.6. REFERENCES

1   Jansta J., Dousek F. P., Riha J., *J.Appl. Polym. Sci.*, **19**, 3201 (1975).

2   Iqbal Z., Ivory D. M., Szobota J. S., Elsenbaumer R. L., Baughman R. H., *Macromolecules*, **19**, 2992 (1986).

3   Marchesi J.T., Ha K., Garton A., Swei G. S., Kristal K. W., *J. Adhesion*, **36**, 55 (1991).

4   Dwight D. W., Riggs W. M., *J. Colloid. Int. Sci.*, **47**, 650 (1974).

5   Benderley A. A., *J. Appl. Polym. Sci.*, 20, 221 (1962).

6   Rye R. R., Arnold W. W., *Langmuir.*, **5**, 1331 (1989).

7   Costello C. A., McCarthy T. J., *Macromolecules*, **17**, 2940 (1984).

8   Evans J.F., Gibson J.H., Moulder J.F., Hammond J.S., Goretzki H., *Fresenius Z. Anal. Chem.*, **319**, 841 (1984).

9   Johansson G., Hedman J., Berndtsson A., Klasson M., Nilsson R. J., *Electron Spectr.*, **2**, 295 (1973).

10   Silverstein R. M., Bassler G. C., Morill T. C., *Spectrometric Identification of Organic Compounds*, 4th Ed., John Wiley, New York, 1981.

11   Brunauer S., Emmett P. H., Teller E., *J. Amer. Chem. Soc.*, **60**, 309 (1938).

12   Brunauer S., Deming L. S., Deming W. S.Teller E., *J. Amer. Chem. Soc.*, **62**, 1723 (1940).

13   Gregg S. J., sing K. S. W., *Adsorption, Surface Area and Porosity*, Academic Press, London, 1967.

14   Peltzbauer Z., Baldrian J., *Carbon*, **17**, 317 (1979).

15   Rye R. R., Kelber J. A., *Appl. Surf. Sci.*, **28**, 397 (1987).

16   Starkweather H. W. Jr., Kampert W. G., *Macromolecules*, **23**, 2715 (1990).

17   Araki Y., *J.Appl. Polym. Sci.*, **9**, 3585 (1965).

18   Cowie J. M. G., *Polymers:Chemistry and Physics of Modern Materials*, Bell and

Bain Ltd., Glasgow, 1973.

19   Mansfield K. F., Theodorou D. N., *Macromolecules*, **24**, 6283 (1991).

7. A MECHANISTIC STUDY OF THE DEFLUORINATION OF PTFE AND PVDF BY Na ATOMS.

7.1. INTRODUCTION

7.1.1. Alkali Deposition on to PTFE

Although studies of alkali metal adsorption onto metallic[1-5] and semiconducting[6-9] substrates are widespread, until now there have been no well defined investigations published which address the mechanistic aspects of alkali metal deposition onto polymeric surfaces.

Polytetrafluoroethylene (PTFE or Teflon) consists of a fluorinated straight chain polymer, $(-CF_2CF_2-)_n$; the stable C-F bond gives rise to its chemical inertness. Metallization of polytetrafluoroethylene has been the subject of numerous studies; this is important for electronic device manufacture[10], for the improvement of polymer wear characteristics[11-13], and packaging technology[14,15]. A variety of methods are available for the metallization of PTFE, these include: hot wall chemical vapour deposition (CVD)[16], electron beam evaporation[17], resistive evaporation[13], mechanical transfer[13], and catalytic or thermal reduction of mineral salt supported on a PTFE substrate[13]. Electron beam[16], X-ray irradiation[18,19], ion beam sputtering[10], and wet chemical[16,20,21] treatments of the PTFE substrate prior to deposition, and X-ray irradiation[22], ion bombardment[23], and thermal treatments following metallization can also be employed to achieve the desired physicochemical characteristics at the

metal/polymer interface. Despite the relative chemical inertness of PTFE, most metal fluxes do adhere to the PTFE surface, usually forming a boundary layer with a mixed metal / metal fluoride / defluorinated PTFE / PTFE composition[24]. The adhesion strength of the metal layers bonded to PTFE is reported to be primarily dependent upon the reactivity and size of the metal ad-atom[10]. Less reactive metals such as gold tend to form metallic overlayers[17, 22]. In the case of more electropositive metals, a breakdown in the polymer substructure is more likely. An important example of the latter category is Na/NH₃ wet chemical defluorination of PTFE, this treatment is used industrially to improve the bonding characteristics of PTFE[25].

7.1.2. Metallization of PVDF

Polyvinyldifluoride is also a straight chain polymer akin to PTFE, two fluorine groups on each alternating carbon atom have been replaced with hydrogen atoms, -(CH₂-CF₂)ₙ- and as such it possesses some of the properties exhibited by PTFE. Generally though it tends to be much more vulnerable to chemical attack, and has found many applications as a membrane material[26]. Metallization studies involving PVDF are much less common than in the case of PTFE, PVDF does not possess the excellent di-electrical properties exhibited by PTFE. Crowe et al[27] have shown defluorination of the PVDF surface using saturated LiOH solution, however the majority of surface treatments have involved in situ radiation, electron and heavy atom bombardment[28 - 30].

7.1.3. Mechanistic Aspects of Sodium Deposition on to Polymers

In this chapter, sodium metallization of PTFE under ultra high vacuum conditions is used to model the wet chemical sodium naphthalenide defluorination of PTFE, which arose as a result of the experiments conducted in chapter 5. Current understanding of the sodium naphthalenide chemical etch reaction is limited due to the presence of surface oxidation[19] following the etching process. Originally this was intended as a systematic study to include (poly)tetrafluoroethylene -$(CF_2)_n$-, poly(vinyldifluoride) -$(CF_2\text{-}CH_2)_n$- and finally (poly)ethylene -$(CH_2)_n$- however problems with equipment have limited the study to PTFE and PVDF.

7.2. EXPERIMENTAL

Additive-free PTFE film (Goodfellows Ltd) was washed in a 50:50 isopropyl alcohol / hexane mixture, and then dried in air. PVDF film (Goodfellows Ltd.) was cast in water from a 30% w/w solution of PVDF in 99% pure N-methyl-2-pyrollidinone (Aldrich Chemical Co. Ltd) prepared at 60°C. The films were washed in a 50:50 isopropylalcohol / hexane mixture and dried in air for several days prior to insertion in to the spectrometer.

A sodium metal vapour source (SAES Getters Ltd.) was mounted on to a Vacuum Generators ESCALAB spectrometer (base pressure 2 x 10^{-11} mbar), Figure 1. The sodium source was thoroughly outgassed prior to deposition. Metal dosage was controlled by using a rotatable shutter arrangement, deposition rates were dependent upon the current passing through the source, and constant deposition rates were

maintained using an accurate steady current power supply. The current was typically 6.5 Amps for each deposition experiment.

X-ray photoelectron spectroscopy (XPS) studies were performed using an unmonochromatized Mg K_α X-ray photoexcitation source and a hemispherical analyser operating in the constant analyser energy mode (CAE, 50 eV pass energy), with an electron take-off-angle of 30° from the substrate normal. An IBM PC compatible computer was used for XPS data accumulation and component peak analysis, assuming linear background subtraction and Gaussian fits with fixed full width at half maximum (FWHM)[31]. All binding energies are referenced to the C(1s) core level at 291.2 eV for the (-$\underline{C}F_2$-) linkage contained in PTFE[32,33] and PVDF[27].

Instrumentally determined sensitivity factors for unit stoichiometry were taken as C(1s) : F(1s) : Na(1s) equals 1.00 : 0.20 : 0.18. These were measured by analysing the XP spectra of several ideal compounds of known stoichiometry and calculating an average set of sensitivity factors based upon these data. The samples included NaF (Aldrich Chemical Co.), Na_2CO_3 (Aldrich Chemical Co.), PTFE (Goodfellows Ltd.) and PVDF (Goodfellows Ltd.), each of the compounds were thoroughly cleaned using isopropyl alcohol and hexane prior to analysis to minimise any adsorbed contaminants.
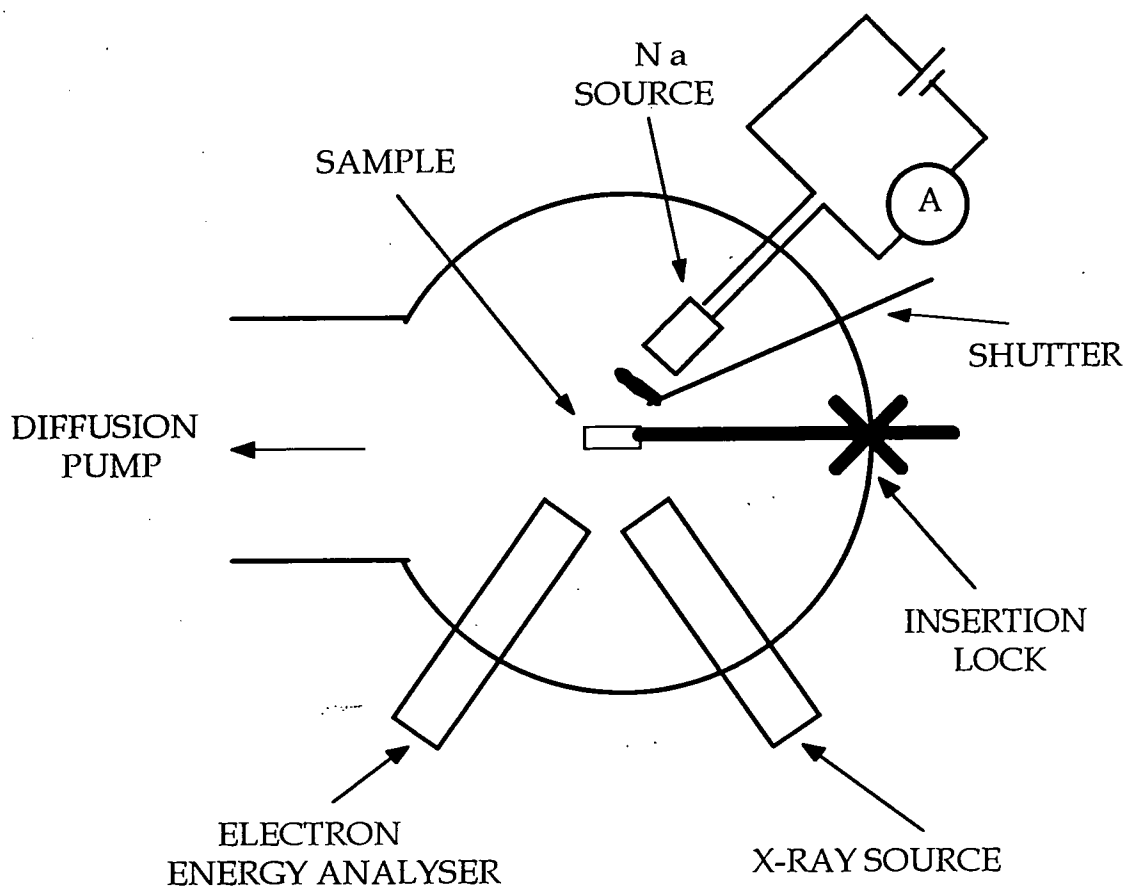
Figure 7.1   **Schematic Diagram of the CLAM spectrometer and Na Getter Source.**

7.3. RESULTS

7.3.1. PTFE

The variation in elemental concentration at the polymer surface with increasing sodium dosage is summarised in Figure 7.2. No oxygenated species were observed during metal uptake. The overall attenuation in C(1s) intensity is associated with the surface build-up of sodium species, however it is of interest to note that there is an initial increase in C(1s) peak area with sodium exposure.

Clean PTFE displays a main C(1s) peak at 291.2 eV, and a weak Mg $K_{\alpha 3,4}$ satellite at lower binding energy, Figure 7.3a. Sodium metallization of PTFE resulted in a marked change in the appearance of the C(1s) envelope. This can be fitted to six MgK $\alpha_{1,2}$ component peaks, Figure 7.4a, corresponding to [13, 32-34] : $-\underline{C}_x-$ (284.6 eV), $\equiv\underline{C}-CF_n-$ (286.6 eV), $=F\underline{C}-C\equiv$ (288.3 eV), $=\underline{C}F-CF_n-$, (289.5 eV), $-\underline{C}F_2-$ (291.2 eV) and $-\underline{C}F_3$ (293.6 eV). Additional Mg $K_{\alpha 3,4}$ satellites (with a different fixed FWHM) were also taken into consideration. The relative variation of these component peaks is consistent with sodium atoms defluorinating the PTFE surface to form predominantly crosslinked / graphitic / olefinic carbon species[34], partially fluorinated carbon moieties, and $-\underline{C}F_3$ groups at the expense of $-\underline{C}F_2-$ centres, Figure 7.5.

Two components are discernible in the F(1s) peak which correspond to covalently bonded fluorine atoms in the 688-689 eV range and fluoride ions at approximately 685 eV[35], see Figure 7.4b. The latter species increases in concentration with sodium exposure, Figure 7.2.

There is a shift in the Na(1s) core level binding energy from 1070.3 eV (8 Mins deposition) to 1071.5 eV (95 Mins deposition), shown in Figure 7.6. This compares with quoted Na(1s) binding energies of 1071.8 eV and 1071.2 eV for sodium metal and sodium fluoride respectively[35]. It is interesting to note that the formation of the plateau in the elemental composition plot shown in Figure 7.2 and the reduction in the rate of change of the Na(1s) shift coincide at around 55 Mins total deposition time. Further deposition leads to an increasingly metallized surface layer, and a Na(1s) binding energy approaching that of metallic sodium at 1071.8 eV[35].

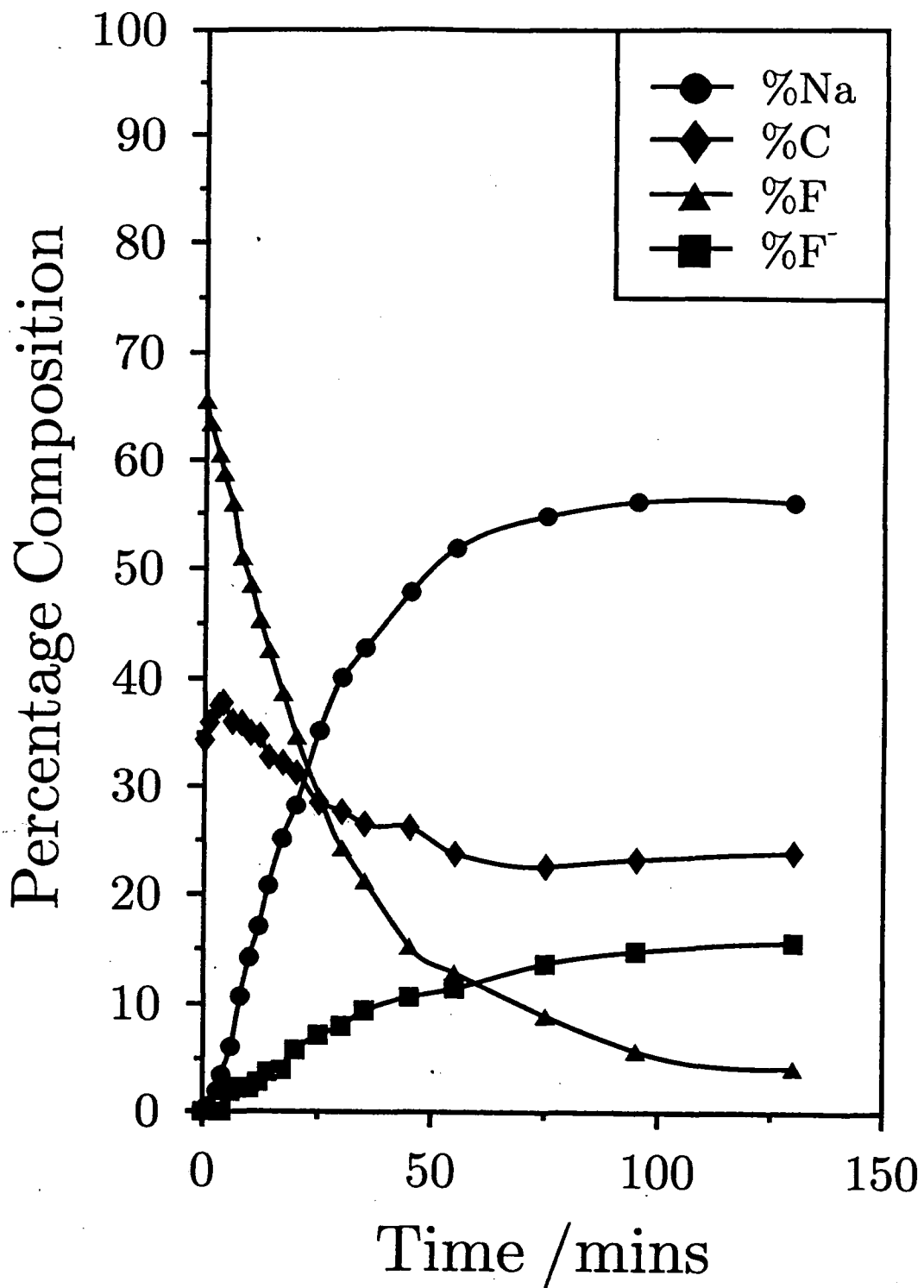**Figure 7.2**   **Elemental composition of PTFE as a function of sodium metal exposure.**

Figure 7.3a   C(1s) XPS spectra of PTFE as a function of sodium metal dosage.
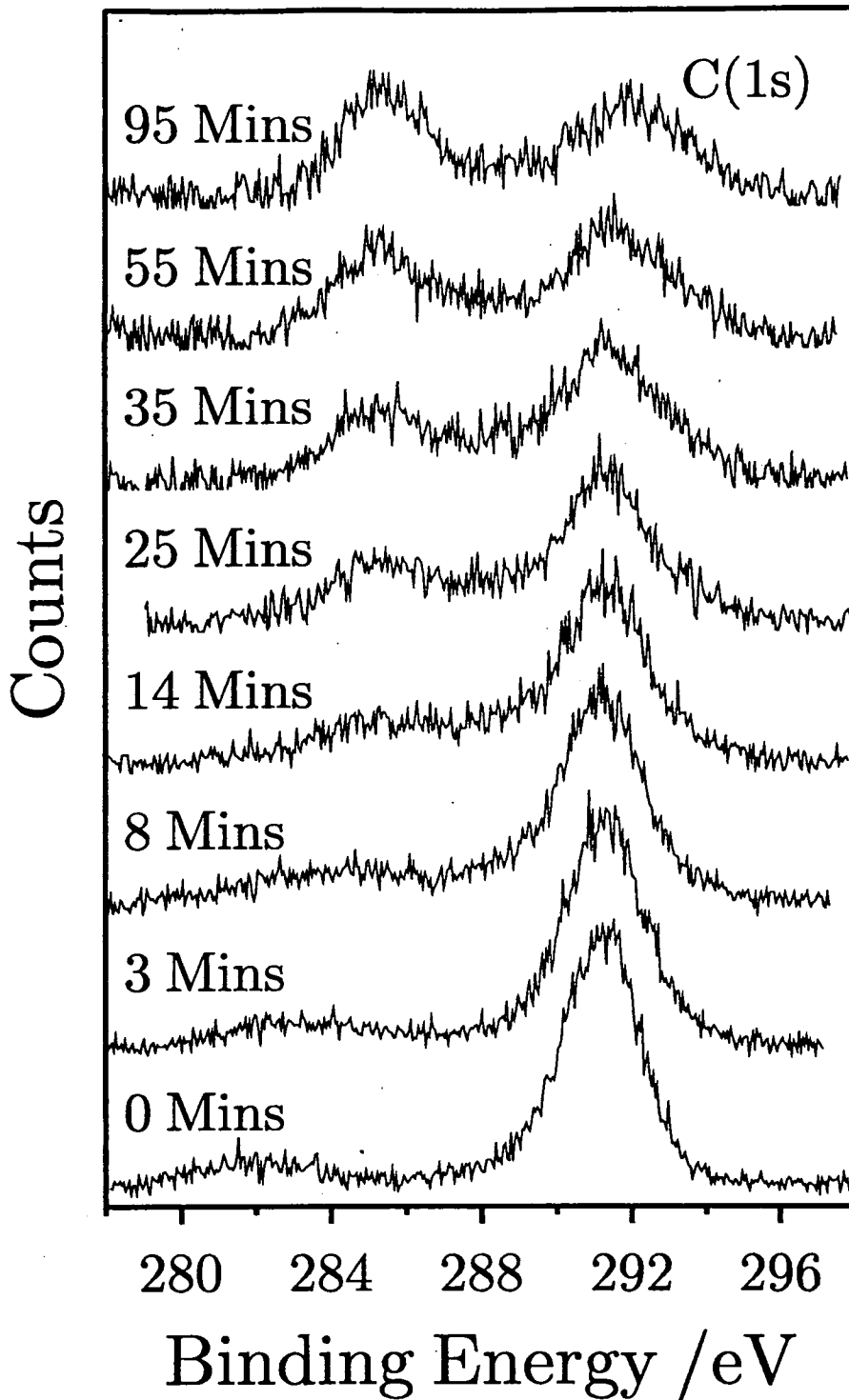
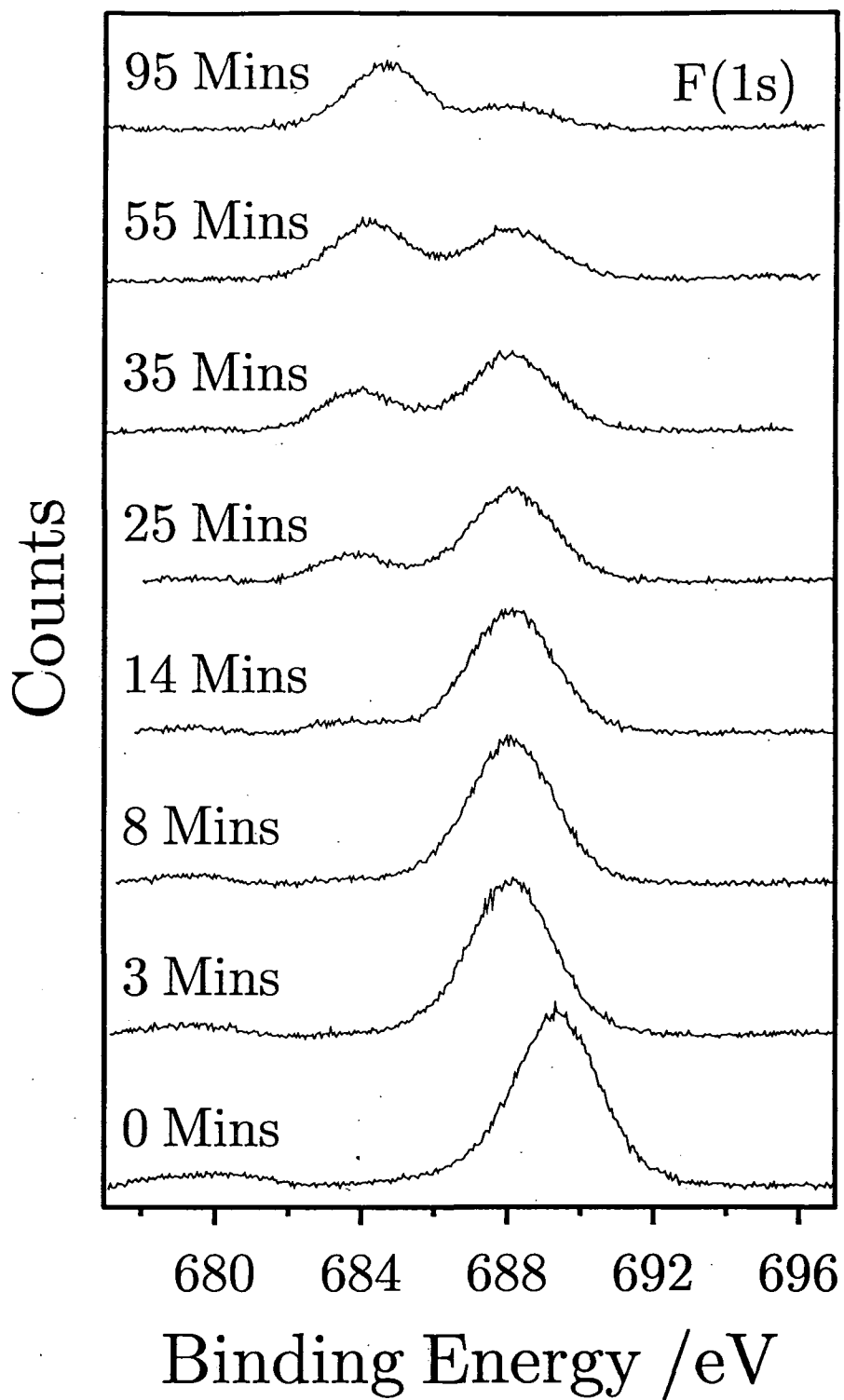**Figure 7.3b**   **F(1s) XPS spectra of PTFE as a function of sodium metal dosage.**

Figure 7.3c   **Na(1s) XPS spectra of PTFE as a function of sodium metal dosage.**

Figure 7.4a   **C(1s) Core level peak fit of metallized PTFE (130 Mins).**

Figure 7.4b   **F(1s) Core level peak fit of metallized PTFE (130 Mins).**
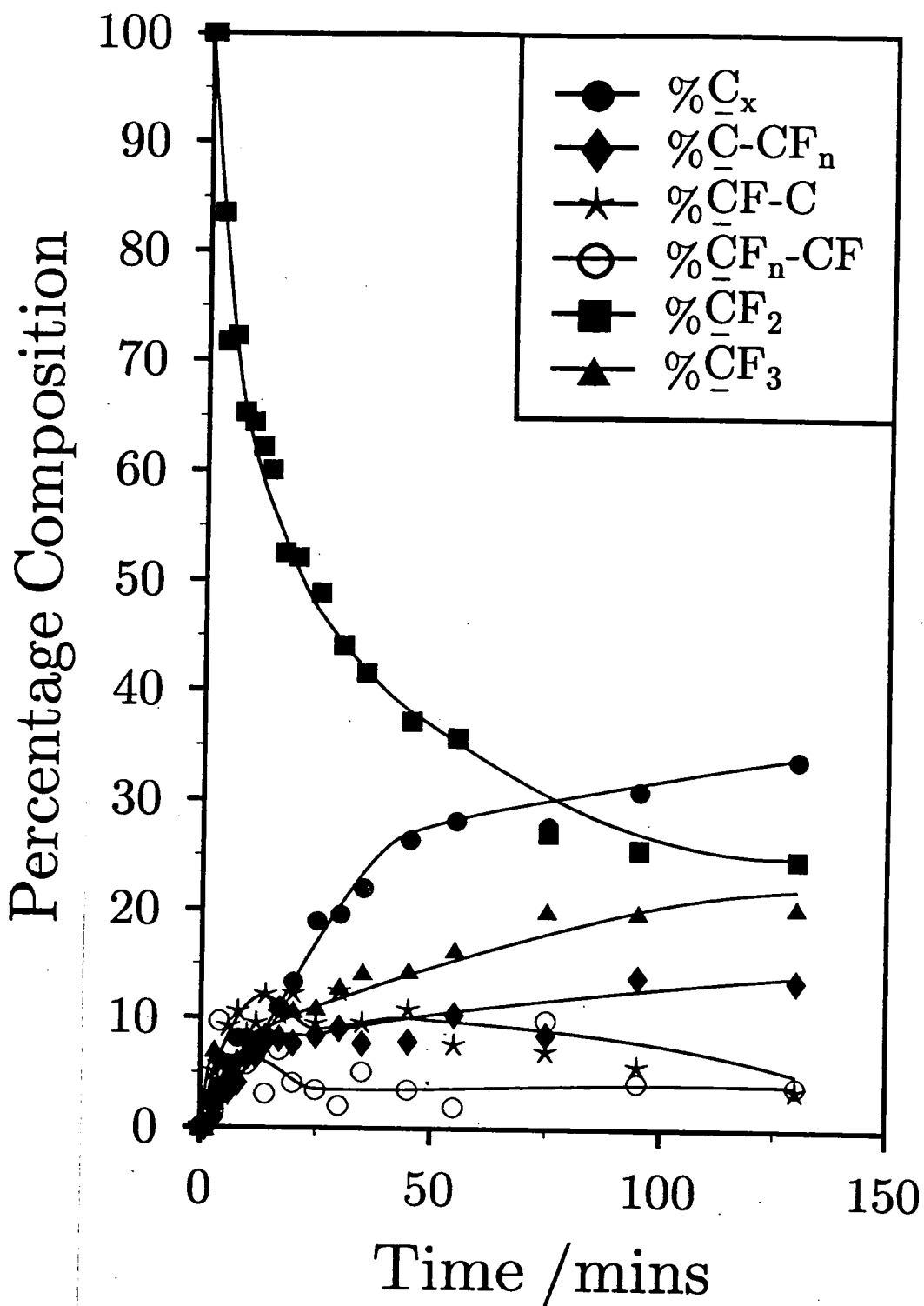
Figure 7.5. Variation of C(1s) environments on PTFE with increasing sodium

metal dosage.
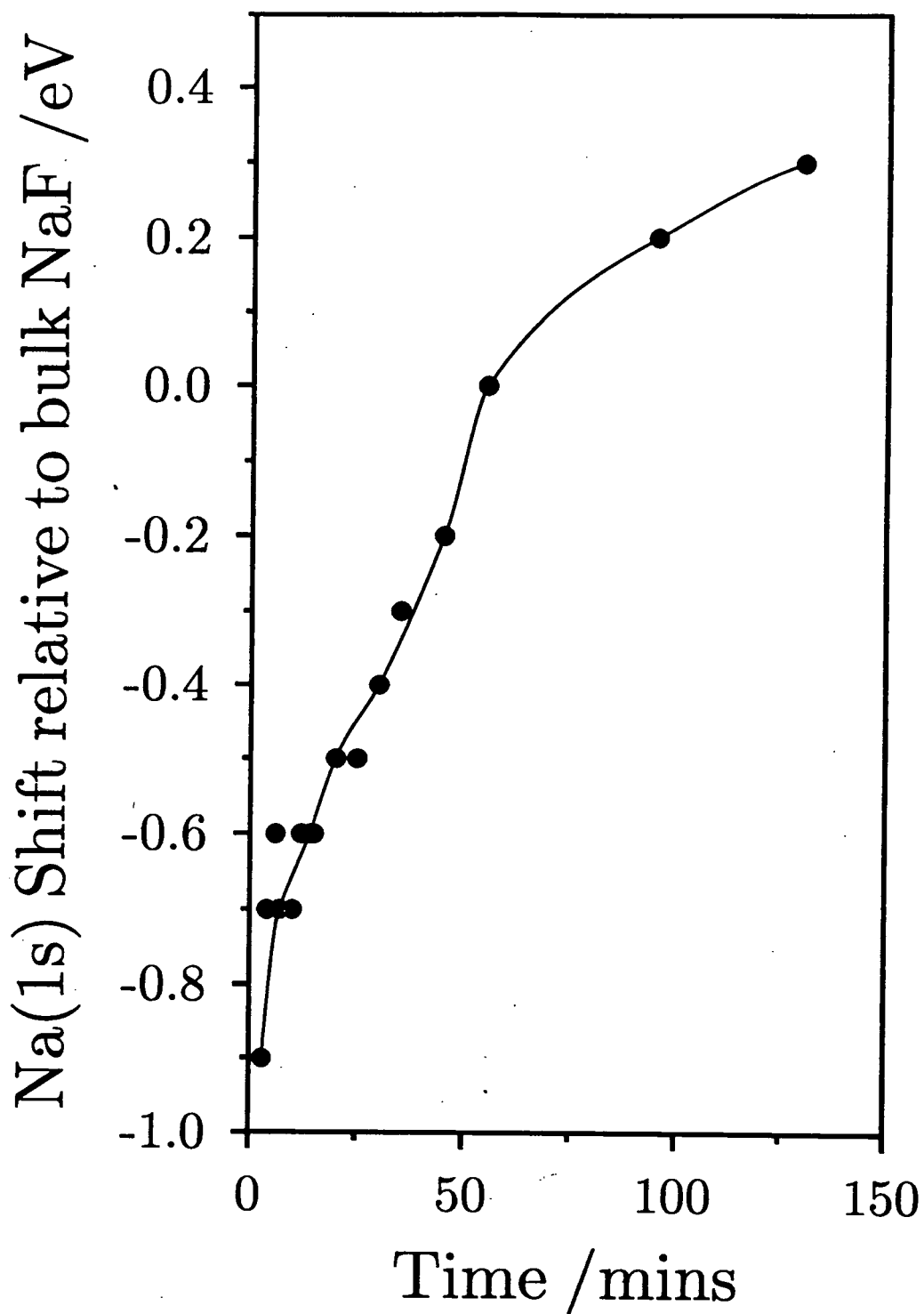
Figure 7.6   Variation of Na(1s) core level binding energy on PTFE with increasing sodium exposure (referenced with respect to the Na(1s) binding energy of 1071.2 eV for NaF solid), ± 0.05 eV.

7.3.2. PVDF

The C(1s) XP Spectra of the cast PVDF film could be fitted with two environments in a 1:1 intensity ratio, the CF_2 peak at 291.2eV and CH_2 peak at 286.6 eV[27, 36], only carbon and fluorine signals could be observed in the XPS analysis indicating that the PVDF was clean. The variation in the elemental composition of the PVDF surface during sodium deposition is shown in Figure 7.7. Hydrogen atoms do not possess a sufficiently large enough photoelectron cross section to be ionised by x-ray irradiation and consequently cannot be quantified by XPS. In common with the elemental composition of PTFE we observe a decrease in the proportion of fluorine containing species, an increase in the fluoride and sodium signals, and a decrease in the carbon content, although in this case the initial increase in carbon is not observed at low deposition times.

The C 1s spectra of sodium metallized PVDF is shown in Figure 7.9a and the carbon environments have been fitted to the following binding energies[32, 33, 36]: $-\underline{C}_xH_n-$ (284.6 eV), $\underline{C}H_n-CF_2-$ (286.6 eV), $\underline{C}F-CH_n$ (288.3 eV), $-\underline{C}F_2-CH_n-$ (291.2 eV) and $-\underline{C}F_3$ (293.6 eV). The F 1s region, Figure 7.9b exhibits covalently bonded fluorine at 688-689eV and fluoride ions at 685eV[35]. Na(1s) core level binding energy shifts, Figure 7.11 shows significant difference to the shifts observed during deposition of Na on to PTFE. The Na(1s) binding energy shifted from was 1071.0 eV (10 Mins deposition) to 1071.8 eV (150 Mins deposition). This suggests that in contrast to the deposition of sodium on to PTFE, the sodium species reacting with PVDF are forming crystalline NaF almost immediately which becomes more metallic as the build up of a Na overlayer occurs at higher deposition times.
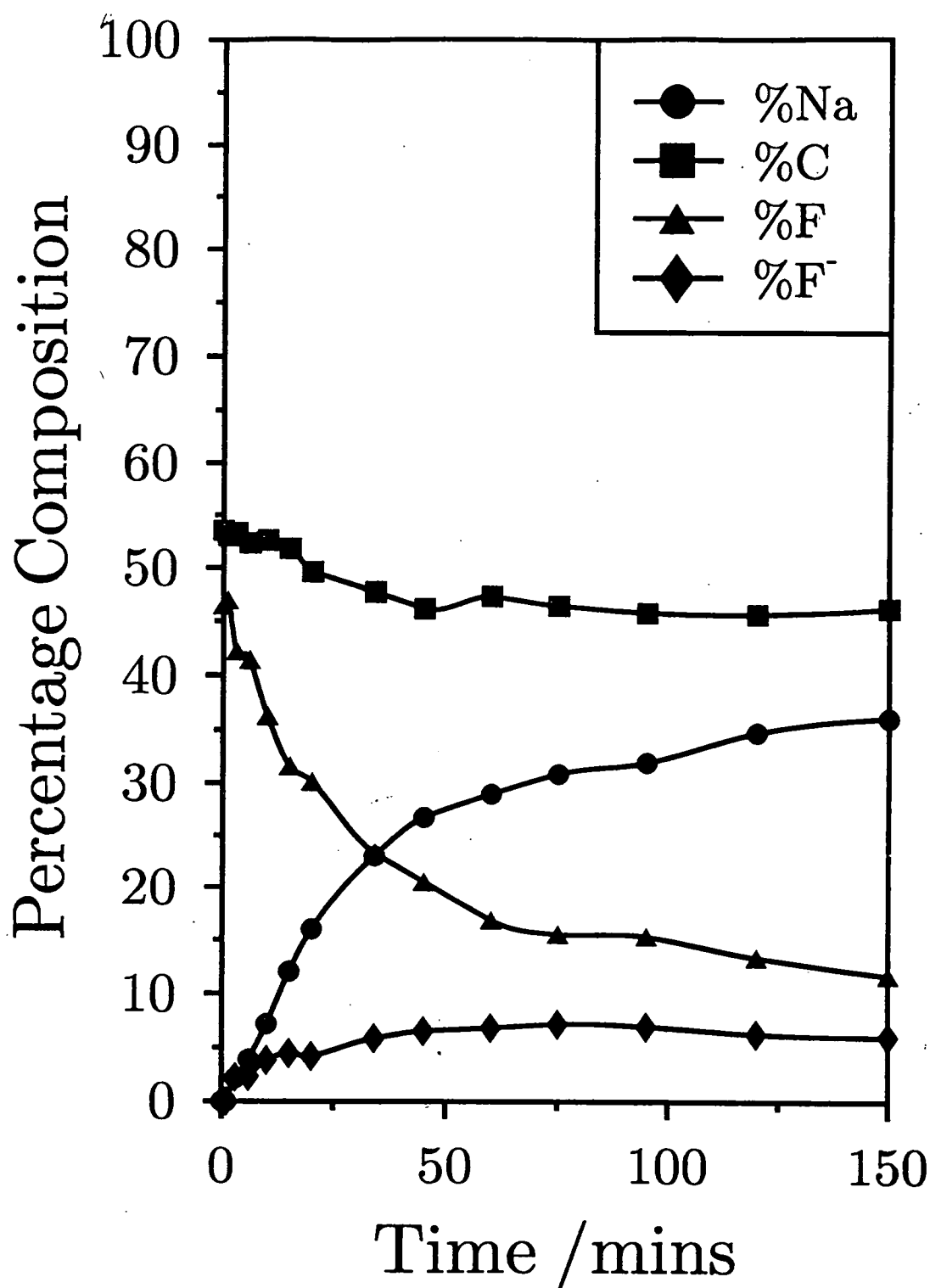
Figure 7.7   **Elemental composition of PVDF as a function of sodium metal exposure.**
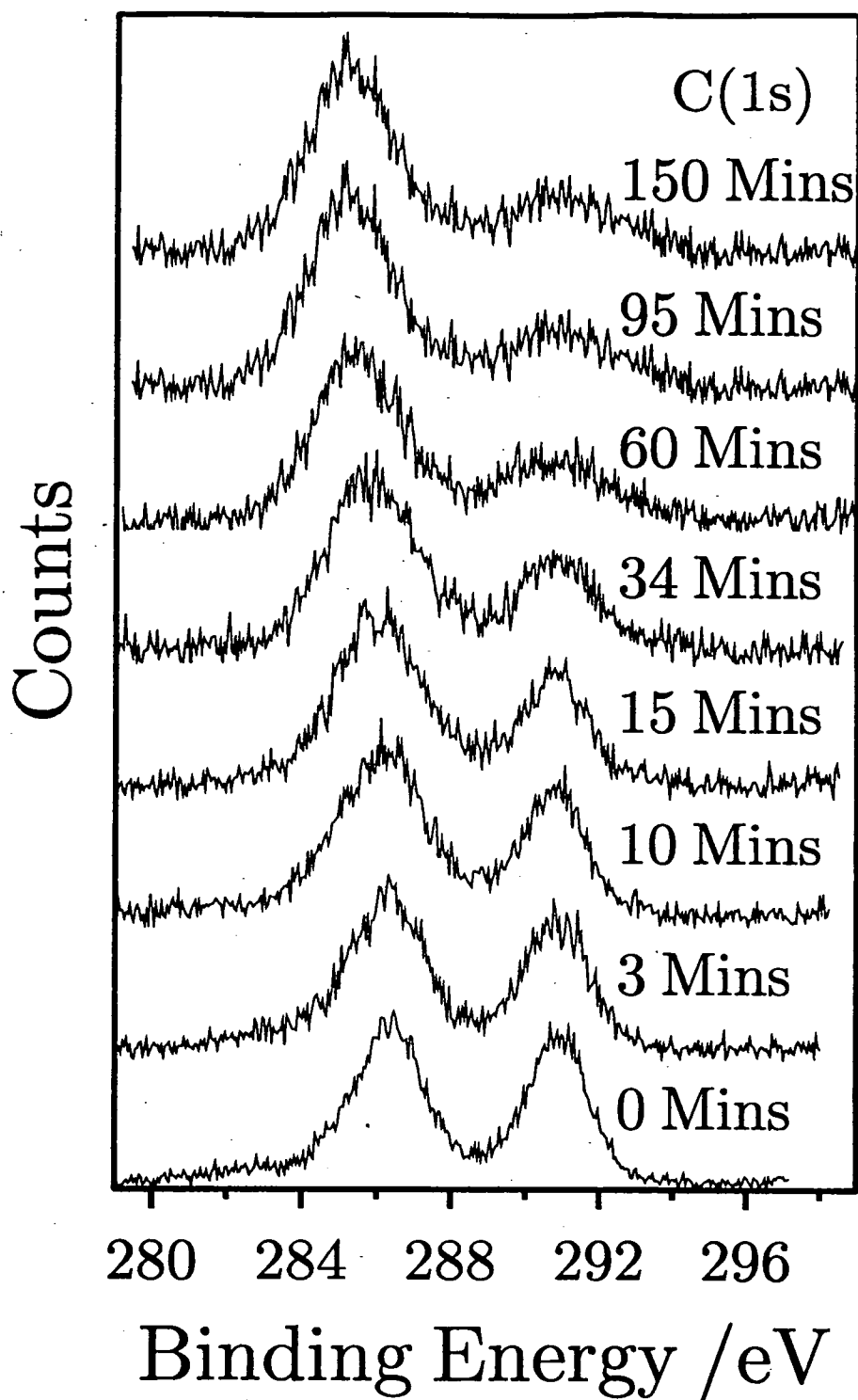
Figure 7.8a   C(1s) XPS spectra of PVDF as a function of sodium metal dosage.
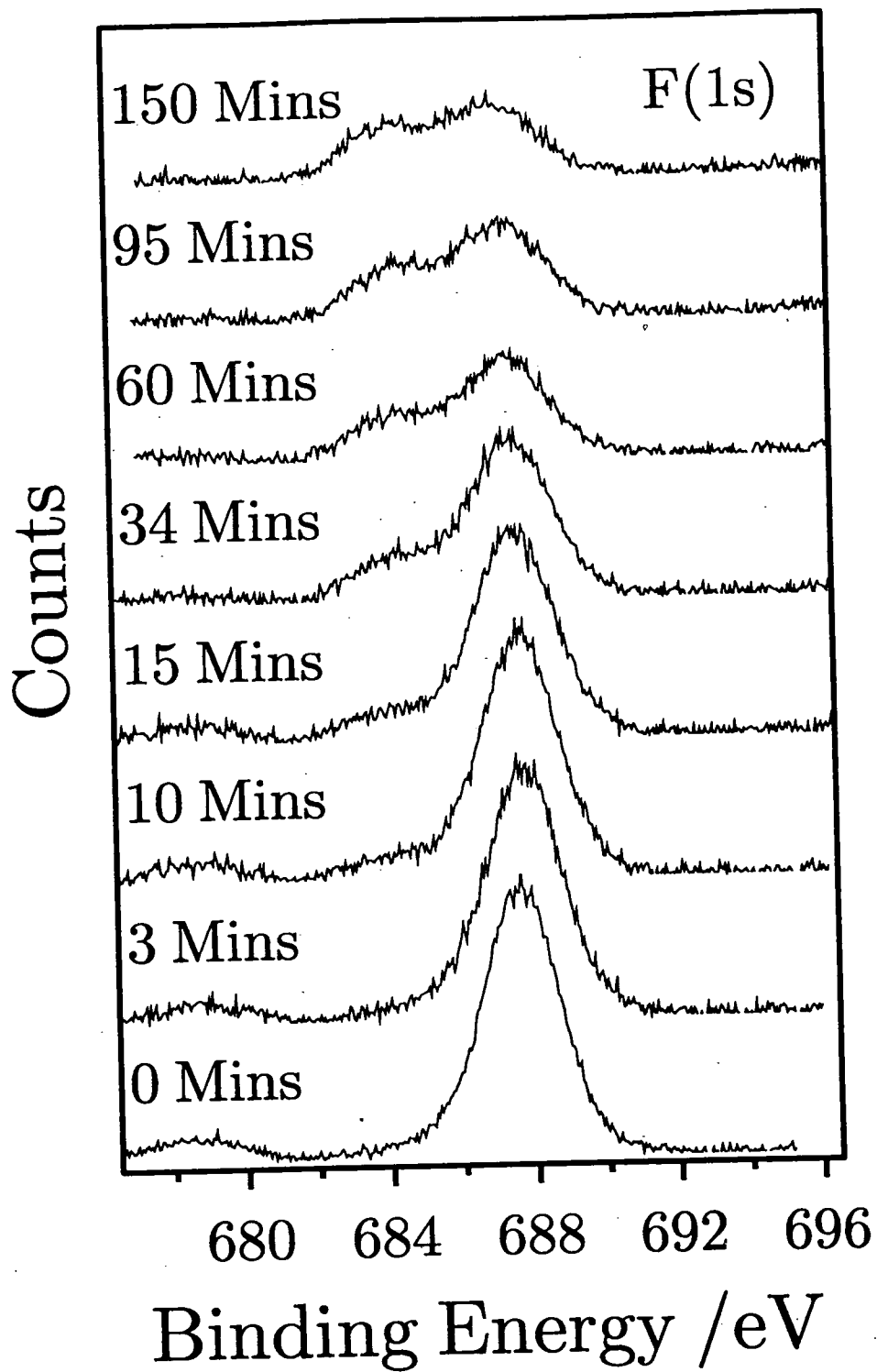
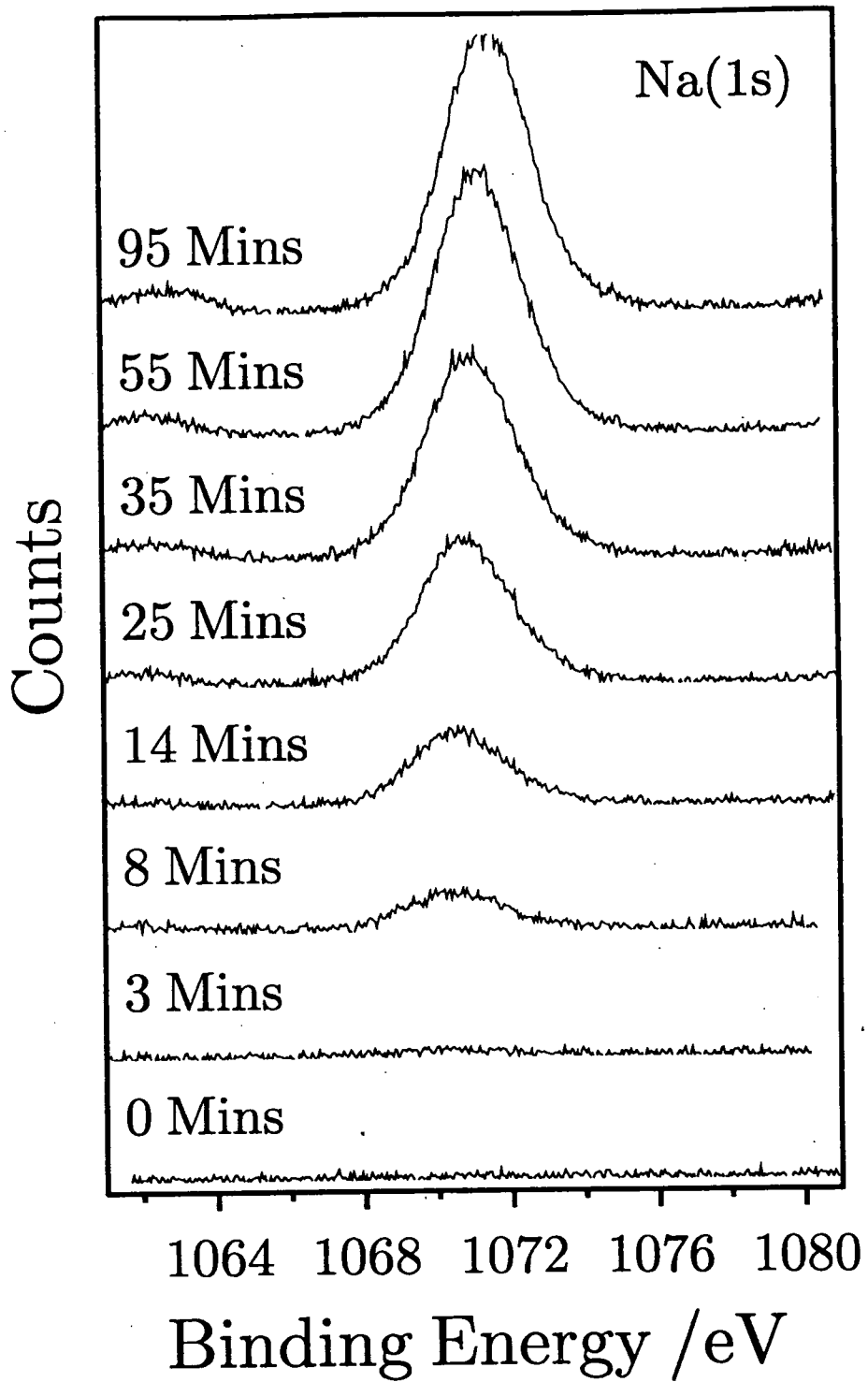**Figure 7.8b**   **F (1s) XPS spectra of PVDF as a function of sodium metal dosage.**
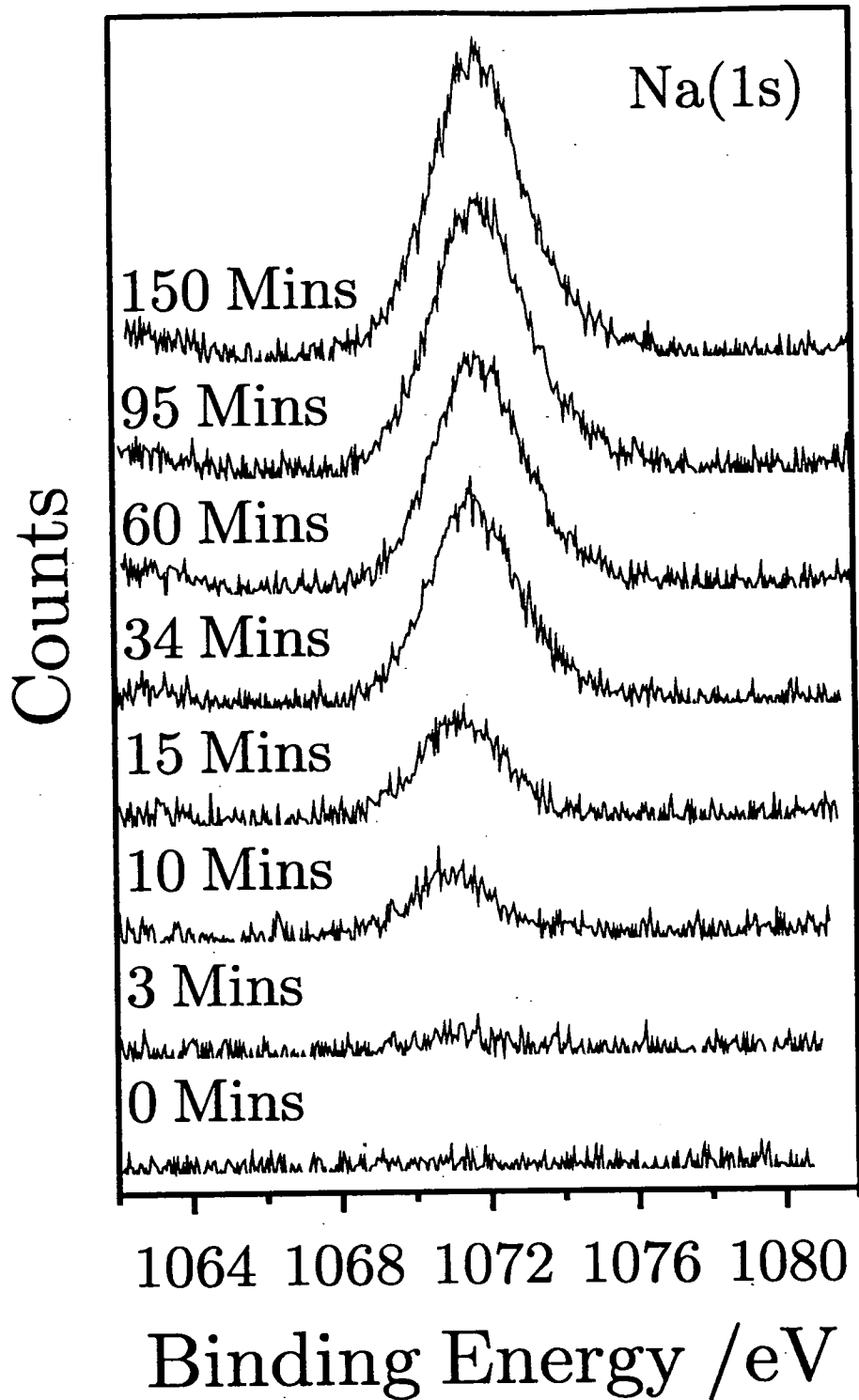
Figure 7.8c   Na (1s) XPS spectra of PVDF as a function of sodium metal
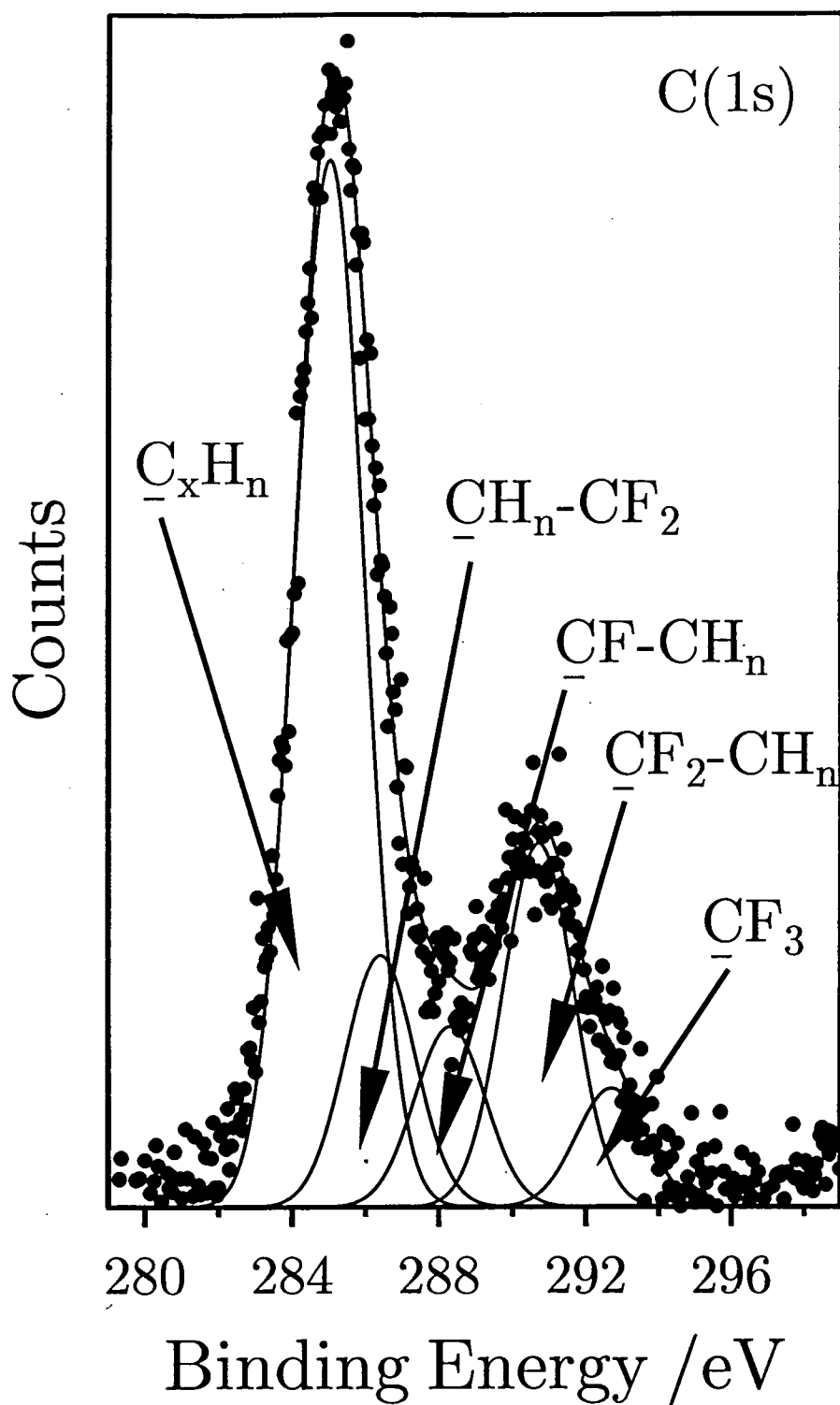
dosage.
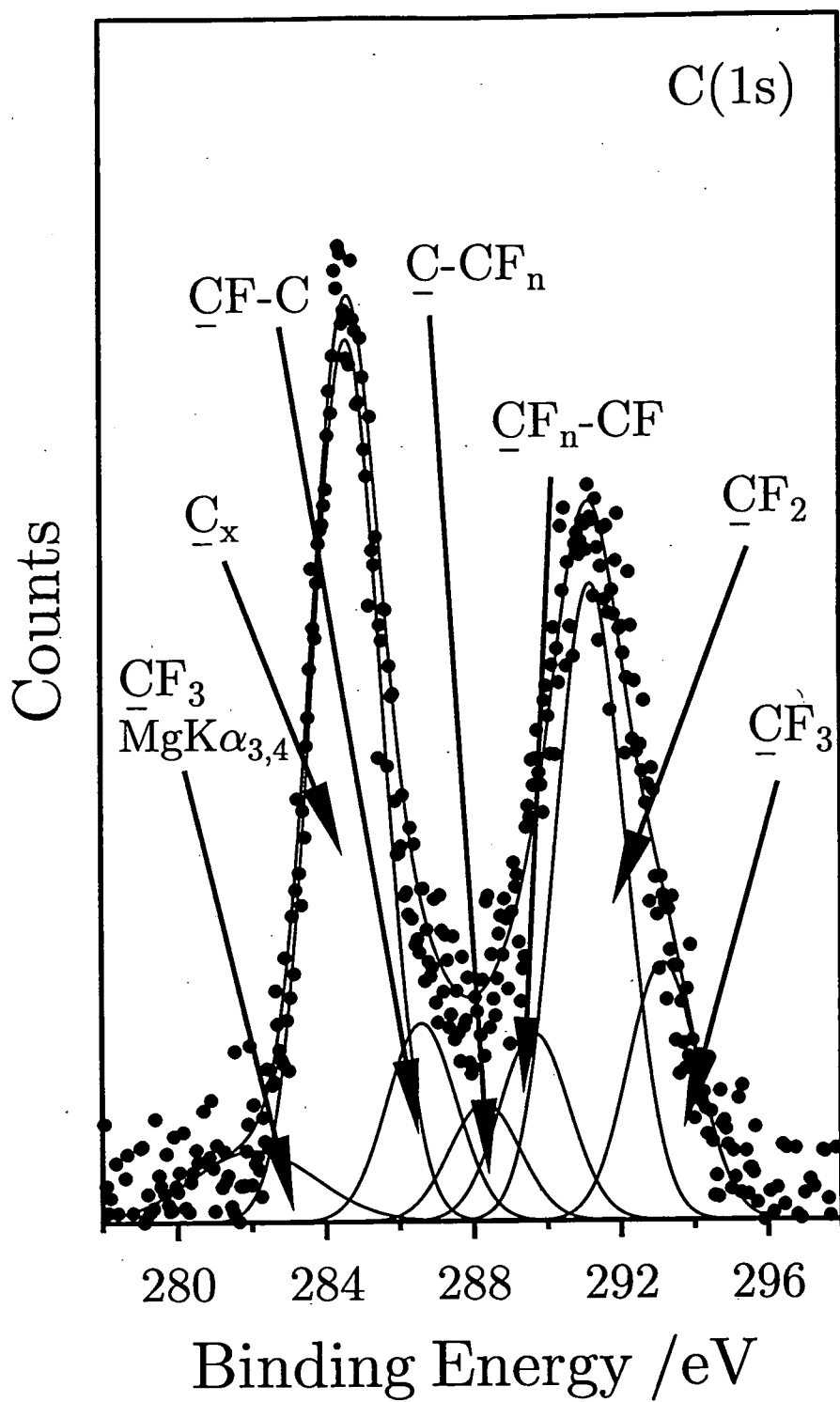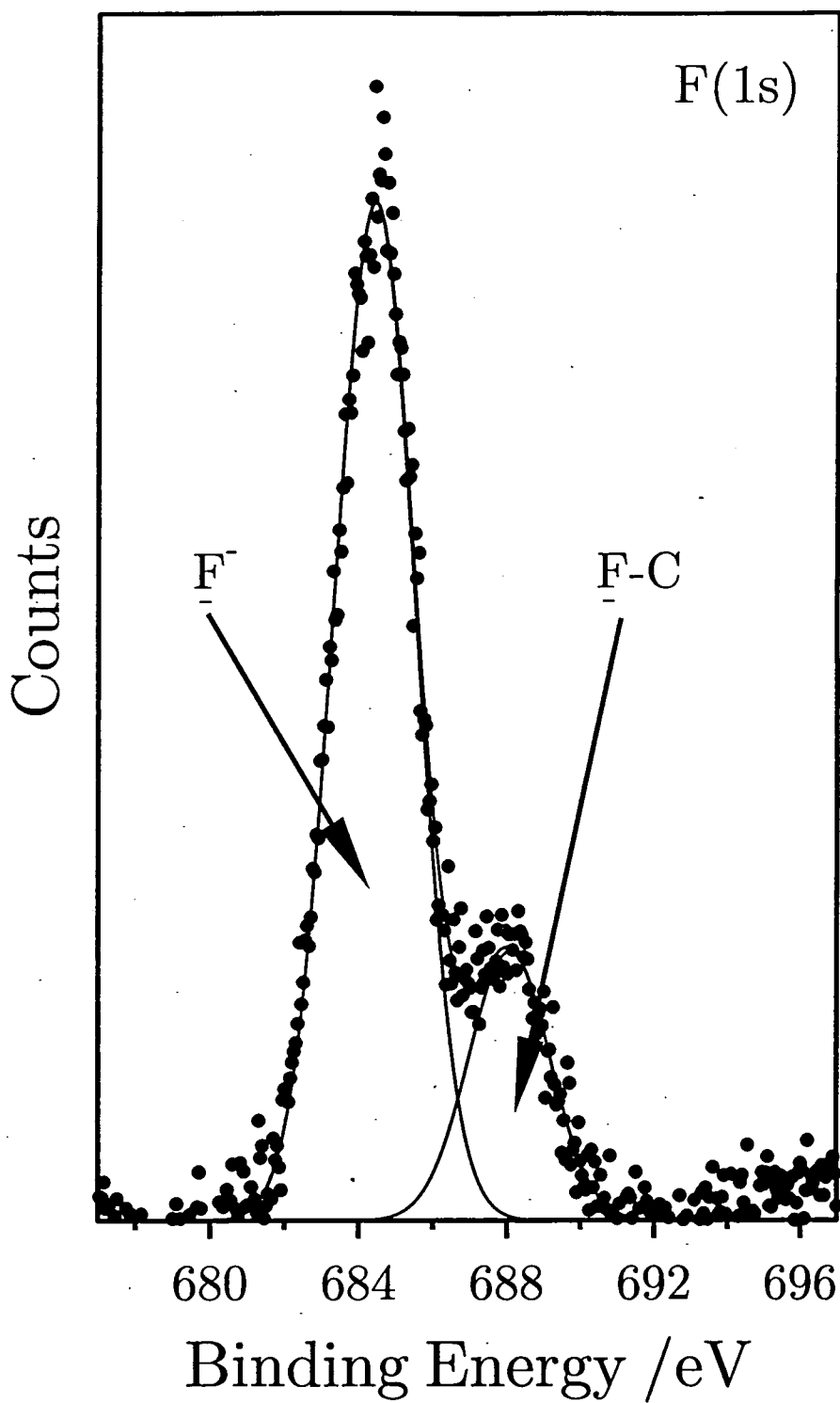
Figure 7.9a   **C(1s) Core level peak fit of metallized PVDF (120 Mins).**
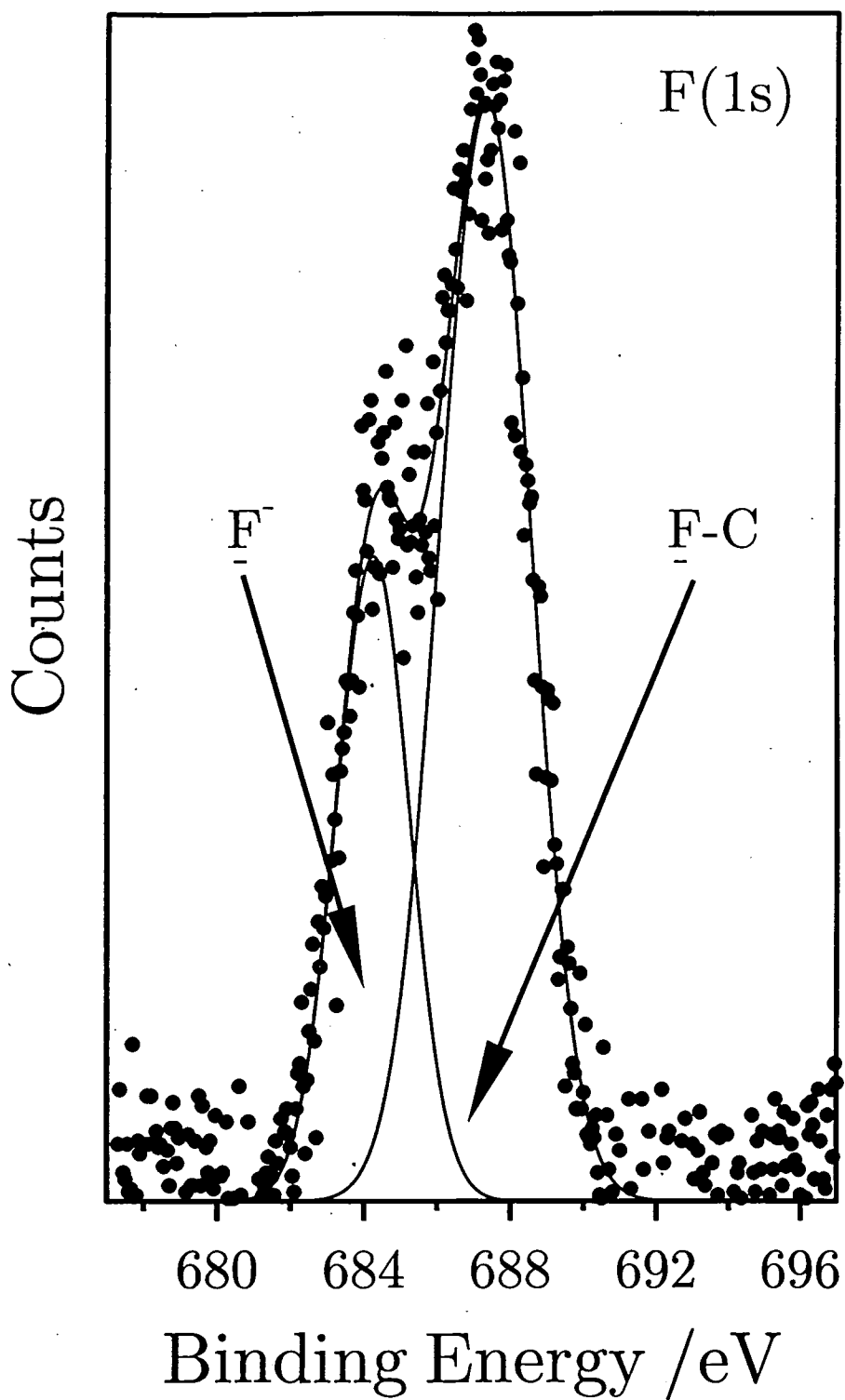
Figure 7.9b F(1s) Core level peak fit of metallized PVDF (120 Mins).
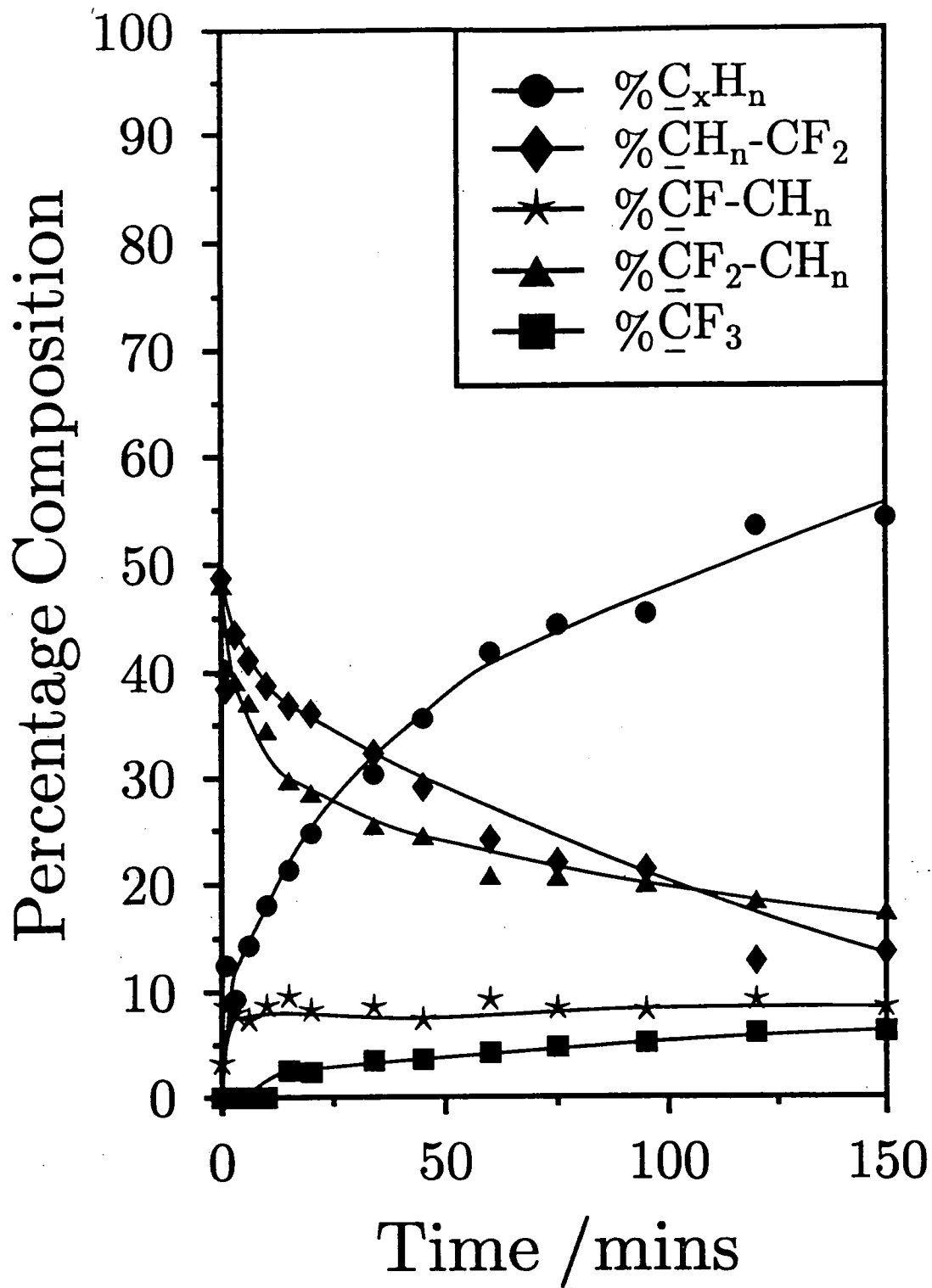
Figure 7.10 Variation of C(1s) environments on PVDF with increasing sodium metal dosage.
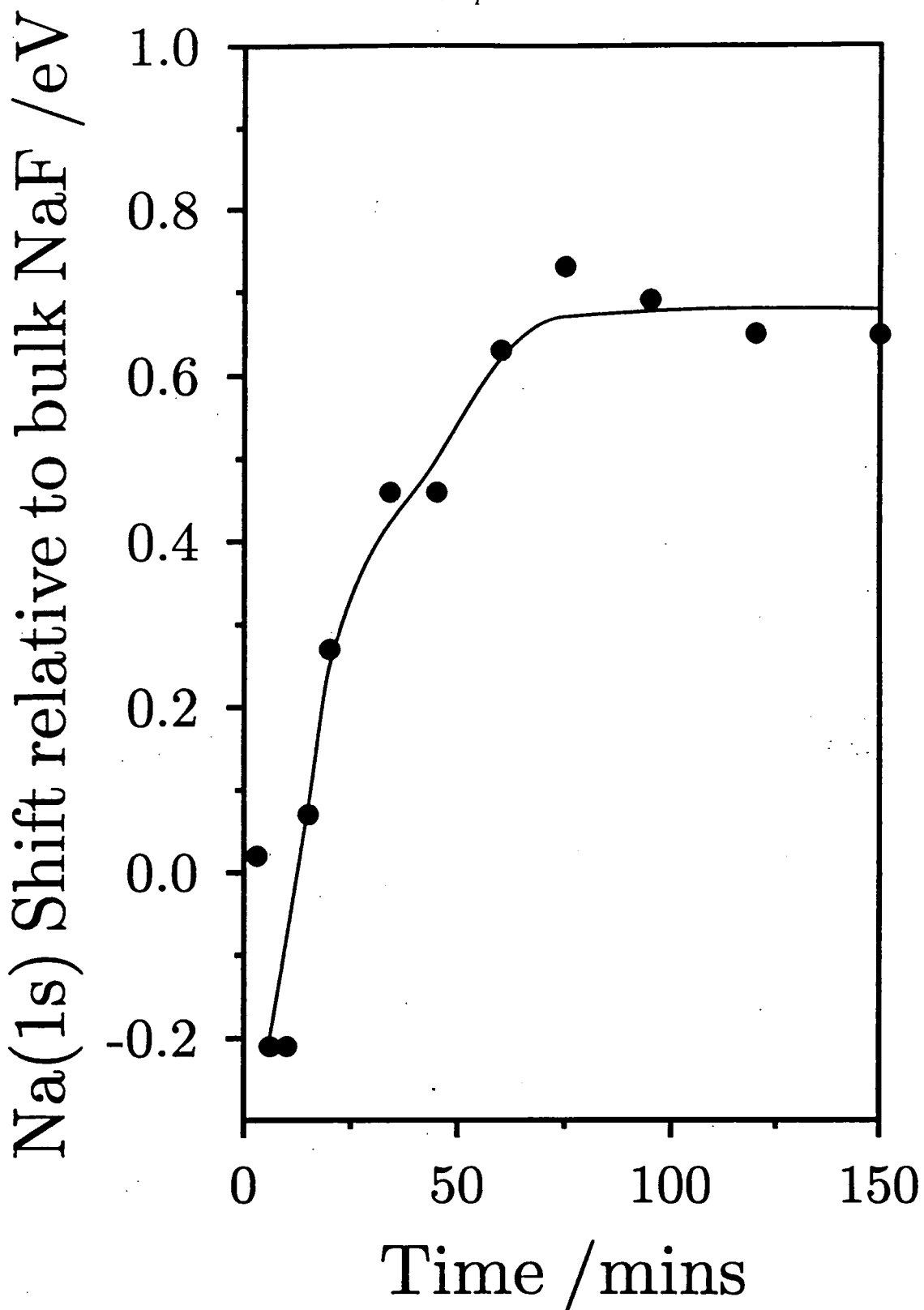
Figure 7.11   Variation of Na(1s) core level binding energy on PVDF with increasing sodium exposure (referenced with respect to the Na(1s) binding energy of 1071.2 eV for NaF solid), ± 0.05 eV.

7.4. DISCUSSION

7.4.1. PTFE

The reaction of sodium atoms with the PTFE surface is primarily governed by the thermodynamic driving force for the formation of NaF:

$$-(CF_2-CF_2)_n-(s)+ 2nNa(g) \quad \rightarrow \quad -(CF=CF)_n-(s) + 2nNaF(s)$$
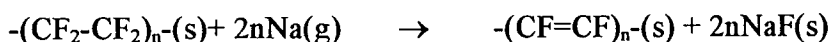
$$\Delta H \approx -1400 \text{ kJmol}^{-1} \quad (\text{where } n = 1)$$

Therefore the enthalpy change for the reaction of Na(g) with PTFE to yield NaF is extremely favourable. Hence the initial stages of reaction of sodium atoms with the PTFE surface can be expected to produce NaF molecules and free radical centres along the polymer backbone, Scheme 1. At the polymer surface, the NaF molecules experience low attractive forces with the underlying substrate, and therefore will desorb under ultra high vacuum conditions to leave behind a carbon-rich surface. This description is consistent with the observed rise in elemental carbon concentration at the PTFE surface for short sodium exposures, in conjunction with the loss of covalent fluorine centres, and the absence of fluoride ions, as was shown in Figure 7.2.

SCHEME 1: Initial defluorination of PTFE.

$$\text{Na} \quad\quad \overset{\cdot}{\text{—CF}}\text{—CF}_2\text{—CF}_2\text{-} \quad + \quad \text{NaF}$$
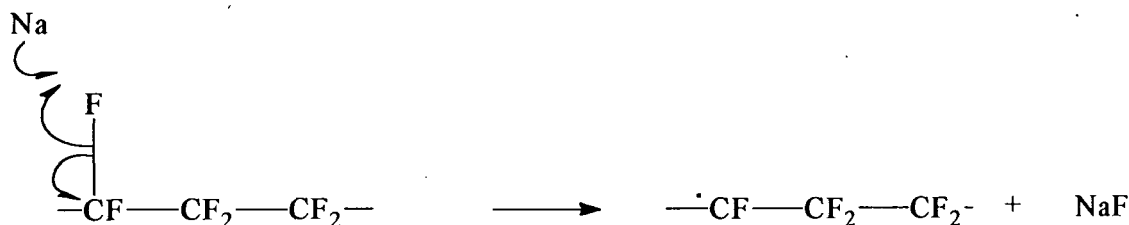
It is important to realise that one of the major physicochemical differences between polymers and bulk metals or inorganic materials is that the former class of materials are much less rigid, and therefore allow permeation of species into the bulk. The core level electron escape depths[37] [Na(1s) 5 Å, F(1s) = 10 Å, and C(1s) = 20 Å] are sufficiently large that there will also be some sampling of the polymer subsurface during XPS analysis. Larger doses of sodium can result in the permeation of metal atoms through the defluorinated surface and into the subsurface region where they undergo reaction with C-F bonds to form buried NaF molecules, the relatively larger size of this product species will attenuate its mobility, thereby causing it to become trapped in the subsurface. As a consequence, these NaF molecules will now be detected by XPS. On this basis, one can also account for the observed trend in Na(1s) core level binding energies, Figure 7.6: isolated NaF molecules will possess a degree of covalent character[38] thereby yielding a lower Na(1s) core level binding energy around 1070.6 eV. As the subsurface concentration of NaF molecules builds up, (NaF)$_n$ clusters[39] will start to form, and eventually NaF crystallites, this will in turn cause an increase in Na(1s) core level binding energy approaching the literature value for bulk NaF of 1071.2 eV, see Figure 7.6. Prolonged exposure of Na atoms will eventually lead to a metallic layer

being formed on top of the carbon-rich surface layer, hence the Na(1s) core level binding energy will finally reach the reported value for bulk sodium metal[35]. Growth of the sodium metal overlayer begins at approximately 50 Mins deposition, where an attenuation in the rate of change of Na(1s) signal intensity and Na(1s) binding energy is seen, Figures 6.2 and 6.6 respectively.

The observed defluorination of PTFE by sodium atoms is in agreement with previous metallization studies Pb[11, 12], Zn[11, 12], Cr[10-12, 14], Sn[11, 12], Cd[10], In[13], Sn[13], Cu[10, 14, 16, 20], Ti[10, 14], Al[10, 3, 14], Au[10, 14, 23], Ag[13], and Ni[13,40]. In all of the aforementioned cases, except for Au, a mixed metal fluoride/polymeric interfacial region is reported. Carbides with a C(1s) XPS binding energy of 282.0 eV[14] tend to form for the more reactive multivalent metals, e.g. Cr and Ti deposition[22, 34].

It is interesting to note that carbide species are not generated during the exposure of sodium atoms to PTFE polymer, instead the carbonaceous species formed are more akin to those observed following radiation induced crosslinking of PTFE[20]. We can explain this in the case of a monovalent atom such as sodium by pointing out that there is only one valence electron available for transfer to the fluorine atom in the C-F bond, which leaves a free radical site behind on the polymer backbone. In contrast, multivalent metal ad-atoms possess a large number of valence electrons and there exists the possibility of any surplus valence electrons participating in carbide formation.
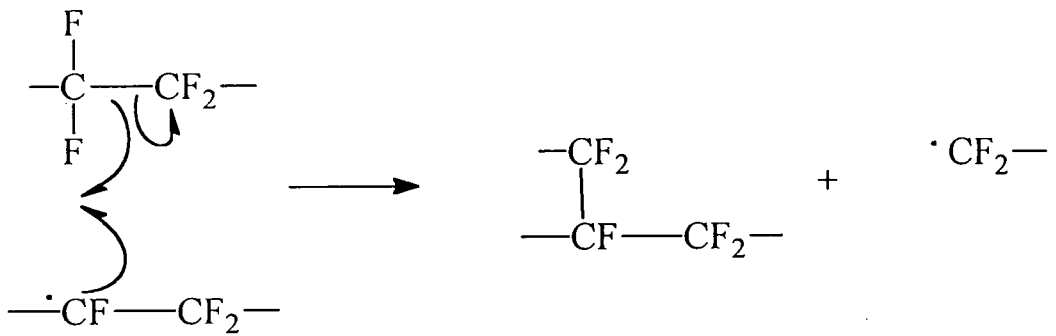
Mechanistic theories have emphasised the importance of electron transfer processes during the reaction of Na/NH$_3$ with PTFE[41]. Also there are a wealth of studies concerned with surface induced crosslinking of PTFE by various methods which

include: electron beam irradiation[20, 41-44] X-ray irradiation[20, 22, 24, 34, 45, 46], RF induced plasma[47-49], chemical treatments[34, 50, 51], electrochemical reduction[52, 53] and ion beam bombardment[23, 49, 53, 54]. The resultant chemical functionalities are similar in nature to those observed in this study (although in some cases to differing degrees). In these studies, reaction is generally considered in terms of radiation induced free radical chemistry[20], the first step of which has been suggested to be the cleavage of the C-F bond due to low energy valence excitations[17], forming -CF$^\bullet$ + F$^\bullet$ radical species. The complexity of the subsequent reactions has prevented a thorough understanding of the chain reaction, but the free radical centres on the polymer surface are believed to undergo branching and crosslinking to yield C_x, $\equiv CF$, $>CF_2$ and -CF$_3$ groups as identified by XPS[34]. Some examples of such crosslinking mechanisms are illustrated in Scheme 2 and we are able to draw parallels between the radiation induced chemical modification of the PTFE surface with the species observed to form following the defluorination of the surface by Na atoms.

In the present study, clearly there is also a significant amount of -CF$_3$ group generation during sodium exposure. The likely absence of F$^\bullet$ species due to the energetically favourable formation of NaF, shown in Scheme 1, means that -CF$_3$ groups are unlikely to form via the conventional recombination[54, 55] of a -CF$_2$$^\bullet$ radical species with a F$^\bullet$ radical. A more plausible reaction pathway may involve nucleophilic attack by the NaF molecule (or effectively the fluoride ion[56]) on the PTFE chain, leading to the formation of an unsaturated fluorinated chain and -CF$_3$ species, see Scheme 3A. It is worth emphasising that molecular NaF would offer a fluoride ion in an unsolvated form, which is devoid of a bulk crystal lattice and consequently NaF would possess an inherent reactivity that could not be realised under conventional synthetic organic chemistry

conditions, giving rise to extremely strong nucleophilic behaviour. Following the initial nucleophilic attack of the fluoride ion and the cleavage of the PTFE polymer backbone, the resulting unsaturated bond is susceptible to further nucleophilic attack. This becomes catalytic in nature and this could possibly explain the relatively large proportion of -CF$_3$ containing moities from XPS analysis.

An alternative mechanistic explanation for -CF$_3$ formation could encompass a 1,2 fluorine atom shift during the rearrangement of a -CF$_2$$^{\bullet}$ end group, Scheme 3B. This reaction would confer greater stability to the free radical by the strongly electron withdrawing effect of the -CF$_3$ group and the reduction of repulsive interactions between the free radical and neighbouring fluorine valence electrons.

SCHEME 2: Crosslinking of PTFE.

OR
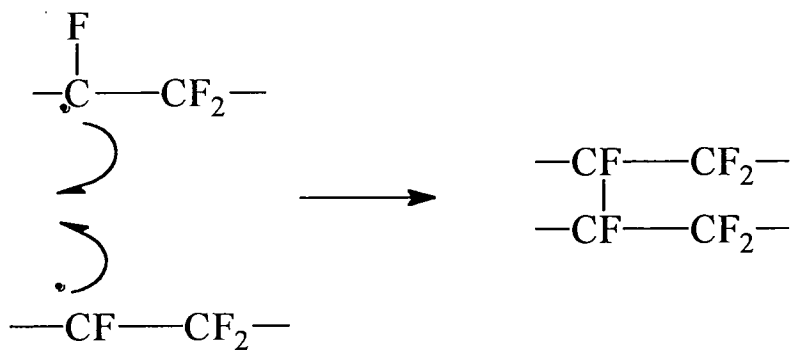
SCHEME 3: CF$_3$ formation on PTFE.

(A)

$$Na-F$$

$$-CF_2-CF_2-CF_2-CF_2-$$

$$-CF_3 + {}^-CF_2-CF-CF_2{}^- + Na^+$$
$$\qquad\qquad\qquad |$$
$$\qquad\qquad\qquad F$$

$$-CF_3 + CF_2=CF-CF- $$
$$\qquad\qquad\qquad\quad |$$
$$\qquad\qquad\qquad\quad F$$

$$Na-F$$

$$-CF_3 + CF_3-CF=CF- + NaF$$

etc

(B)

$$\cdot CF_2-\overset{F}{\underset{F}{C}}- \longrightarrow CF_3-\overset{\cdot}{\underset{F}{C}}-$$
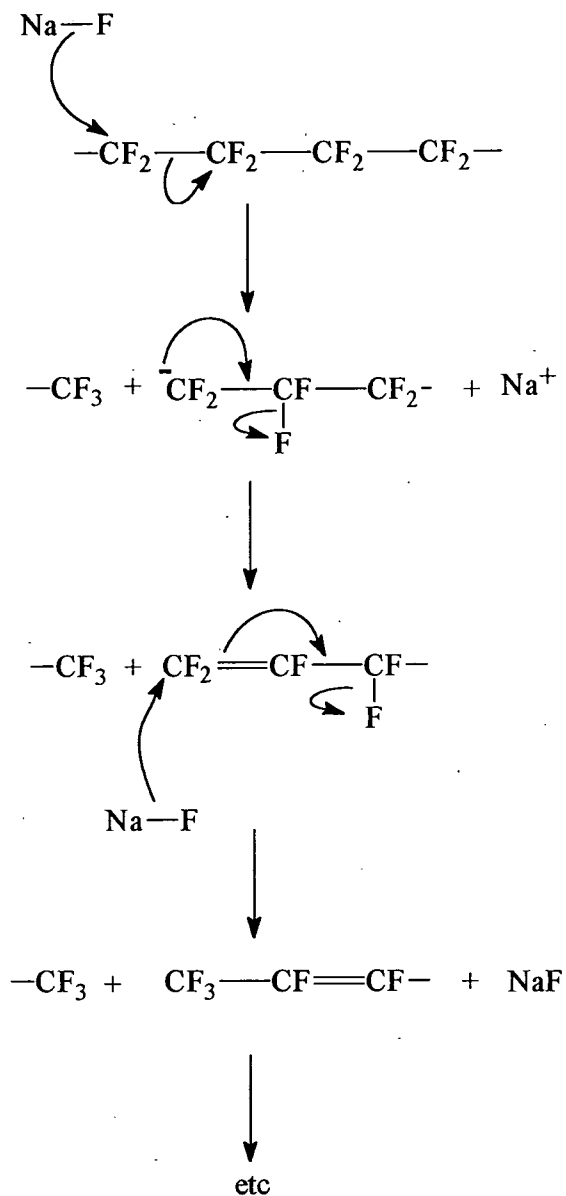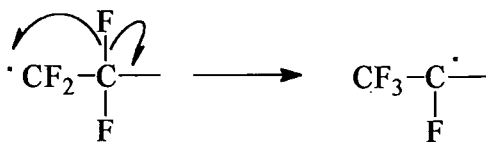
7.4.2. PVDF

The mechanism of the initial reaction of Na at the PVDF surface offers the possibility of defluorination forming NaF, or dehydrogenation forming NaH. The likelihood of either reaction can be assessed by comparing the energy of the initial bond breaking step, and it is evident that the bond energies of C-F and C-H are similar, though C-H is more easily broken than C-F by ~30 kJmol^{-1}, Table 6.1. This indicates that the dehydrogenation of the surface should be the most likely initial step. However, comparing the heats of formation of NaF and NaH lattice structures an extremely large difference -572 kJmol^{-1} compared to -56.8 kJmol^{-1} respectively is observed, Table 6.2 favouring the formation of the NaF as a more stable product compared to NaH.

Table 6.1   **Bond Energies of C-F and C-H.**

Bond (in CH$_3$CH$_2$-X)	Energy (kJmol^{-1})
(X =) F	443[57]
(X =) H	410[57]

Table 6.2   **Heat of Formation of NaF and NaH.**

Lattice	ΔH_f (kJmol^{-1})
NaF	-572[58]
NaH	-56.8[59]

In the first study with PTFE an increase in the initial proportion of carbon in the surface layer was observed, in the case of the sodium bombardment of PVDF this was not observed, Figure 7.7 indicates a different behaviour compared to metallized PTFE. A plot of Na(1s) binding energies versus time of reaction shown Figure 7.11 shows that crystalline NaF is formed almost immediately on the polymer surface and we do not observe the low binding energy species shown in Figure 7.6. A possible explanation could be that sticking probabilities of molecular NaF on the PVDF surface may be higher, thus reducing the amount of NaF molecules desorbing from the surface in the initial reaction phase and a more rapid formation of lattice-like NaF. With continued deposition and in common with PTFE the binding energy of the Na(1s) core level electrons shift towards that of metallic Na[35].

Radical crosslinking mechanisms have been shown for PVDF which has been subjected to electron, heavy ion and x-ray bombardment[28-30]. The initial reaction in the literature has been ascribed to excitation and homolytic fission of the C-H bond leading to carbon radical formation which is then able to crosslink with neighbouring polymer chains. We postulate in this study that the defluorination of PVDF leads to the more energetically favourable products namely NaF and consequently the C-F bond is more likely to break in this case. The resulting crosslinking processes are similar to those described in Schemes 1 and 2 above.

Radical crosslinking could also occur via the elimination of HF which has been described in surface modification studies of PVDF[28], following the mechanism indicated in Scheme 4 which can continue until a radical hydrogen species is liberated or radical meets radical and the chain reaction is terminated.

SCHEME 4: Crosslinking and elimination of HF.
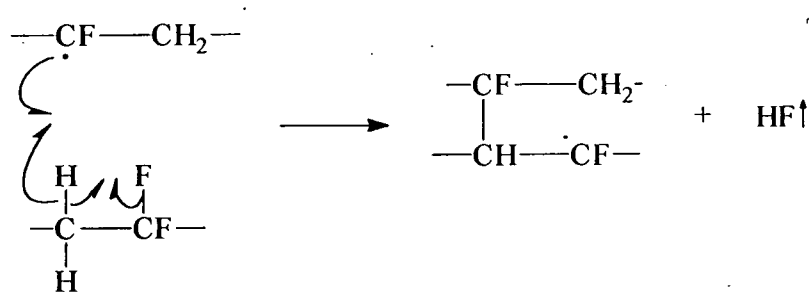
The formation of CF_3 species is observed in Figures 6.9a and 6.10, however they were found in much smaller quantities in the case of PVDF (~7% of carbon environments compared to ~20 % measured for PTFE). If we accept the mechanisms proposed in Schemes 3A and 3B above for the formation of CF_3 groups on PTFE, and apply the same mechanisms to PVDF we can understand why fewer CF_3 species are observed in this case. Scheme 5A shows fluoride ion attack on to the PVDF causing chain scission, the carbanion formed will be less stable than in the case of PTFE and forms an unsaturated bond resulting in a fluoride ion leaving group. Nucleophilic attack at the terminal unsaturated carbon will be less likely because of reduced inductive effects in the more poorly fluorinated system. In addition would necessitate a hydride ion acting as a leaving group and this breaks down the almost catalytic nature of the reaction. Consequently the $\underline{C}H_2$=CF- group formed on the PVDF polymer chain is more stable against nucleophilic attack compared to the $\underline{C}F_2$=CF- group formed from the defluorination reaction of PTFE.

The 1,2 shift mechanism is unable to explain the formation of CF_3 groups in this case due to the absence of fluorine on neighbouring carbon atoms.

SCHEME 5: CF$_3$ formation on PVDF.

(A)

$$Na-F$$

$$-CF_2-CH_2-CF_2-CH_2-$$

$$-CF_3 + {}^-CH_2-CF-CH_2- + Na^+$$
$$\qquad\qquad\qquad |$$
$$\qquad\qquad\qquad F$$

$$-CF_3 + CH_2=CF-CH-$$
$$\qquad\qquad\qquad\qquad |$$
$$\qquad\qquad\qquad\qquad H$$

$$Na-F$$

$$-CF_3 + \quad CFH_2-CF=CH- + Na$$

(B)

$$\overset{\bullet}{C}F_2-\underset{H}{\overset{H}{C}}- \longrightarrow CHF_2-\overset{\bullet}{C}-$$
$$\qquad\qquad\qquad\qquad\qquad\qquad |$$
$$\qquad\qquad\qquad\qquad\qquad\qquad H$$
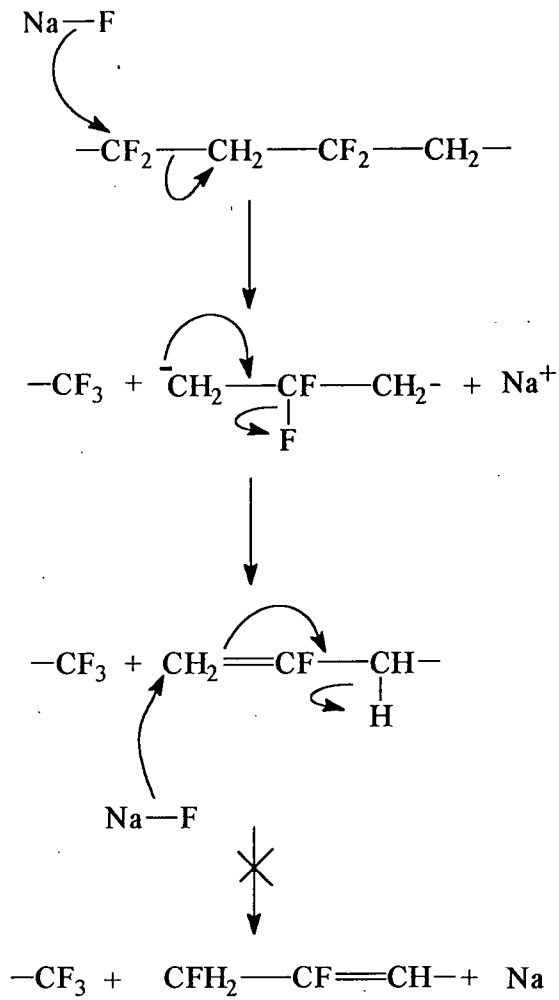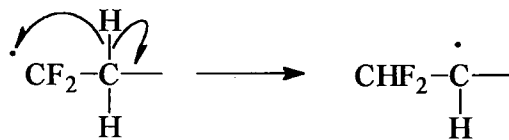
7.5. CONCLUSIONS

The conclusions which we can draw from this work can be divided in to two main areas. Firstly, the general characteristics of the defluorination reaction and the subsequent secondary reactions within the polymer subsurface found to apply to both PTFE and PVDF films must be considered. Secondly, we must elaborate on the specific differences between the two examples which give a more detailed indication of the differing surface chemistries of the respective polymer surface.

Sodium deposition onto PTFE and PVDF polymer surfaces leads to surface defluorination and NaF formation. Longer metal deposition times give rise to sodium atoms diffusing into the polymer subsurface, where trapped NaF moieties can eventually coalesce to form NaF crystallites. Prolonged exposure of sodium atoms causes the build-up of a metallized surface layer. The absence of carbide species is indicative of the single valence electron donation mechanism for defluorination to yield polymer radical species. Secondary reactions of these radical centres causes polymer backbone cleavage, rearrangement, and crosslinking reactions. Whereas the formation of -CF₃ groups is thought to be due to nucleophilic attack of fluoride atoms on to the polymer chain.

Several factors could explain the differences between the reaction of PTFE and PVDF. For example, initial reaction of sodium atoms with PTFE results in an increase in carbon concentration and loss of covalent fluorine at the surface which may be taken as being indicative of desorption of NaF product molecules. However this is not observed to occur for PVDF and this may be due to the increased probability of adhesion of the NaF molecules formed on the PVDF surface leading to more rapid formation of NaF

crystallites for a given amount of Na. We can also see that the rate of defluorination of PVDF is slower than PTFE. This can be linked to the smaller proportion of fluorine in PVDF combined with the fact that the alternative reaction of Na with hydrogen to from NaH is not as energetically favourable as defluorination to form NaF. The secondary reactions of PTFE and PVDF are generally similar, although fewer -CF$_3$ groups as a proportion of the total C(1s) chemical environments resulted from the defluorination of the PVDF. This is primarily due to the greater stability of the partially fluorinated PVDF polymer to nucleophilic attack of the fluoride ion compared to PTFE.

7.6. REFERENCES

1   Shek M.-L., Hrbek J., Sham T. K., Xu G.-Q., *Amer. Phys. Chem. Soc.*, **41**, 3447 (1990).

2   Memmel N., Rangelov G., Bertel E., Dose V., *Phys. Rev. B Cond. Mater.*, **43**, 6938 (1991).

3   Andriotis A. N., *Phys. Rev. B Cond. Mater.*, **42**, 9217, (1990).

4   Hu Z. P., Pan B. C., Fan W. C., Ignatiev A., *Phys. Rev. B Cond. Mater.*, **41**, 9692 (1990).

5   Chandavarkar S., Diehl R. D., Fake A., Jupille J., *Surf. Sci.*, **211**, 432 (1989).

6   Reihl B., Dudde R., Johansson L. S. O., Magnusson K. O., Sorenson S. L., Wilklund S., *App. Surf. Sci.*, **56-58**, 123 (1992).

7   Johansson L. S. O., Reihl B., *Surf. Sci.*, **287/288**, 524 (1993).

8   Batra I. P., *J. Vac. Sci. Technol.*, **8**, 3425 (1990).

9   Starnberg H. I., Soukiassian P., Hurych Z., *Phys. Rev. B Cond. Mater.*, **39**, 12775 (1989).

10   Chang C-A., Baglin J. E. E., Schrott A. G., Lin K-C., *Appl. Phys. Lett.*, **51**, 103 (1987).

11   Cadman P., Gossedge G. M., *Wear,* **51**, 57 (1978).

12   Gong D., Xue Q., Wang H., *Wear,* **148**, 161 (1991).

13   Cadman P., Gossedge G. M., *J. Mater. Sci.,* **14**, 2672 (1979).

14   Chang C-A., Kim Y-K., Schrott A. G., *J. Vac. Sci. Technol. A*, **8**, 3304 (1990).

15   Silvain J.F., Arzur A., Alnot M., Ehrhardt J. J., Lutgen P., *Surf. Sci.*, **251/252**, 787 (1992).

16   Rye R. R., Chin K-M., Hampden-Smith M., Kodas T. T., *J. Electrochem. Soc.*, **139**, L60 (1992).

17   Kim Y-K., Chang C-A., Schrott A. G., *J. App. Phys.*, **67**, 251 (1990).

18   Wheeler D. R., Pepper S. V., *J. Vac. Sci. Technol. A,* **20**, 442 (1982).

19   Rye R. R., Arnold G. W., *Langmiur*, **5**, 1331 (1989).

20   Rye R. R., *J. Polym. Sci.: Part B: Polym. Phys.*, **31**, 357 (1993).

21   Rye R. R. *J. Polym. Sci.: Part B: Polym. Phys.*, **26**, 2133 (1988).

22   Shi M-K., Lamontagne B., Martinu L., Selmani A., *J. App. Phys.*, **74**, 1744 (1993).

23   Ingermarsson P. A., Keane M. P., Gelius U., *J. App. Phys.*, **66**, 3548 (1989).

24   Vogel S. L., Schonhorn H., *J. App. Polym. Sci.*, **11**, 1461 (1967).

25   Minnesota Mining and Mfg. Co., British Patent 265,284 Jan 9, 1957.

26   Yoshiharu T., in Membrane Science and Technology, Osada Y., Nakagawa Y., (Eds.), Marcel Dekker, pp13, 1992.

27   Crowe R., Badyal J. P. S., *J. Chem. Soc. Chem. Comm.*, 958 (1991).

28   LeMöel A., Duraud J. P., Balanzat E., *Nucl. Inst. Meth. Phys. Res.*, **B18**, 59

(1986).

29   Betz N., LeMöel A., Duraud J. P., *Macromolecules*, **25**, 213 (1992).

30   Betz et al, *J. Polym. Sci.:Part A:Polym. Phys.*, **32**, 1493 (1994).

31   Evans J.F., Gibson J.H., Moulder J.F., Hammond J.S., Goretzki H., *Fresenius Z. Anal. Chem.*, **319**, 841 (1984).

32   Clark D. T., Feast W. J., Ritchie I., Musgrave W. K. R., Modena M., Ragazzini M. J., *J. Polym. Sci.: Polym. Chem. Ed.*, **12**, 1049 (1974).

33   Clark D. T., Shuttleworth D., *J. Polym. Sci.: Polym. Chem. Ed.*, **18**, 27 (1980).

34   Kim Y-K., Chang C-A., Schrott A. G., *J. App. Polym. Sci.*, **67**, 251 (1990).

35   Briggs D., Seah M. P., *Practical and Surface Analysis by Auger and X-ray Photoelectron Spectroscopy.*, Wiley, Chichester, 1983.

36   Beamson G., Briggs D., *High Resolution XPS of Organic Polymers-The Scienta ESCA 300 Database*, John Wiley, Chichester, 1992.

37   Birge E. J., Ingram D. J. E., Matthew J. A. D., *Surface Physics*, Prutton Ed. Oxford, 1985.

38   Huheey J. E., *Inorganic Chemistry*, 3rd Ed., Harper and Row: Cambridge, 1983.

39   Rajagopal G., Barnett R. N., Landman U., *Phys. Rev. Lett.*, **67**, 72 (1991).

40   Wheeler D. R., Pepper S. V., *J. Vac. Sci. Technol.*, **20**, 3304 (1981).

41   Chakrabarti N., Jacobus J., *Macromolecules*, **21**, 5487 (1988).

42   Sessler G. M., West J. E., Ryan F. W., Schonhorn H., *J. Polym. Sci.*, **17**, 3199 (1973).

43   Kelber J. A., Rogers J. W. Jr., Ward S. J., *J. Mater. Res.*, **1**, 717 (1986).

44   Michael R., Stulik D., *J. Vac. Sci. Technol. A.*, **4**, 1861 (1986).

45   Rye R. R., Shin N. D., *Langmuir*, **6**, 142 (1990).

46   Schofield C. J., Woods C. J., Wild C., Riviere J. C., Welch L. S., *Mater. Res. Soc. Symp. Proc.,* **25**, 197 (1984).

47   Schonhorn H., Hansen R. H., *J. App. Polym. Sci.,* **11**, 1461 (1967).

48   Da X. X., Griesser H. J., Mau A. W. H., Schmidt R., Liesegang J., *Polymer,* **32**, 1126 (1991).

49   Wells R. K., Ryan M. E., Badyal J. P. S., *J. Phys. Chem.,* **97**, 12879 (1993).

50   Rye R. R., Kelber J. A., *Appl. Surf. Sci.,* **29**, 397 (1987).

51   Iqbal Z., Ivory D. M., Szobota J. S., Elsenbaumer R. L. *Macromolecules,* **19**, 2992 (1986).

52   Kavan L., Bastl Z.,Dousek F. P., Jansta J., *Carbon,* **22**, 77 (1984).

53   Werner B. T., Vreeland T., Mendenhall M. H., Qui Y., Tombrello T.A., *Thin Solid Films,* **104**, 163 (1983).

54   Tan B. J., Fessehaie M., Suib S. L., *Langmuir,* 9, 740 (1993).

55   Hutton D. R., Ph.D. Thesis, University of Durham, 1983.

56   Bayliff A. E., Chambers R. D., *J. Chem. Soc. Perkin. Trans. I,* **2**, 201 (1988).

57   Solomon T. W. G., *Organic Chemistry,* 6th Ed., Wiley, New York, 1996.

58   Dean J. A., *Lange's Handbook of Physical Chemistry,* 14th Ed., McGraw Hill Inc, New York, 1992.

59   Wiberg E., Amberger E., *Hydrides of the Elements of Main Groups I-IV,* Elsevier, Amsterdam, 1971.

8. CONCLUDING REMARKS

Cellulose and poly(tetrafluoroethylene) (PTFE) were chosen for this study because they exhibited certain properties which made them attractive candidates as bioseparation materials. Firstly, they both have good mechanical stability and are able to withstand the fluid pressures experienced in a high performance chromatography system. Although in the case of cellulose some crosslinking was necessary to strengthen the matrix. Secondly they are resistant to chemical degradation, PTFE more so than cellulose by virtue of its extremely stable saturated fluorocarbon structure. The mechanical and chemical stability of PTFE in particular, also allows the chromatographer greater flexibility to fabricate the material in to a range of physical forms, for example an porous membrane or a granulated powdered system.

During the course of this work we have been able to identify several aspects of the surface chemistry of cellulose and poly(tetrafluoroethylene) (PTFE) will prove crucial to their application as bioseparation materials. These include the reactivity and accessibility of the polymer surface. This has primary importance for derivatisation and these considerations become important when designing ligand attachment protocols since on first consideration the likelihood of immobilising a biomolecule can be directly related to the number of binding sites available at the surface.

We have already mentioned that cellulose and PTFE exhibit bulk characteristics of mechanical and chemical stability. However, their surface reactivities differ markedly and cellulose appears to be pre-disposed to functionalisation because of the presence of

surface hydroxyl groups. The rate of reaction of the hydroxyls has been shown to be dependent on the degree of crystallinity of the particular type of cellulose. This may be due to their involvement in the hydrogen bonded structure within the cellulose crystallites and gives rise to a variation in accessibility of the hydroxyl groups. Parallel conclusions can be drawn between the gas phase reaction of the hydroxyl groups with trifluoroacetic anhydride and other solvent based functionalisation studies where a variation in the reactivity of the hydroxyls depending on whether they are in amorphous or crystalline domains was observed.

In contrast to cellulose, PTFE has little surface functionality and we have demonstrated this can be overcome by the introduction of reactive functional groups via surface activation using sodium naphthalenide. Despite the effectiveness and simplicity of this approach we had little control over the quantity and distribution of reactive sites on the surface. The introduction of oxygenated moities was initially thought to be due to reaction of the surface with atmospheric oxygen and water vapour although the defluorination of the surface in a nitrogen atmosphere failed to prevent the introduction of oxygen. The analysis of the defluorination of fluorocarbon polymers via the bombardment with a molecular beam of sodium suggested that the reaction involved valence electron donation to fluorine and that the energetics for the reaction were driven by the formation of NaF. The reaction with sodium naphthalenide also led to a pronounced change in the surface morphology of the PTFE membrane as evidenced by AFM, which was characterised by a roughening of the surface and in the case of the granulated PTFE powder we were able to show the formation of a extensively microporous structure.

The accessibility of potential binding sites for the immobilisation of relatively large biomolecules presents an additional problem. The cellulose study provides the clearest demonstration of this. We have seen that whereas the microporosity of cellulose was relatively stable, the macropores between 400 and 1200 Å in diameter were extremely sensitive to the processing conditions. Crosslinking of the matrix was found to restrict the sizes of the macropores and a relationship was found between the macropore structure and the uptake of bovine serum albumin (BSA). In concept, this highlights the difference between total surface area and the effective surface area of a material available to a large biomolecule and emphasises the importance of the pore structure in providing access to the internal surface of a material.

The dynamic nature of polymer surfaces was demonstrated with respect the pore structure of the cellulose membrane and the activated PTFE particles, and this a consequence of the greater molecular mobility evident in these types of material. As we mentioned above, in the case of cellulose a small amount of crosslinking was shown to have a pronounced effect on the pore structure of the matrix, which was thought to be due to its perturbation of the hydrogen bonding within the matrix. This was similarly the case for the activated PTFE granules, where the microporous defluorinated layer was extremely susceptible to gentle heating. In this case this was attributable to the lower energy configuration achieved in vacuum by the migration of unreacted PTFE polymer chains from the bulk of the polymer to the surface.

APPENDIX A - ABBREVIATIONS

AFM	Atomic Force Microscopy
ATR-FTIR	Attenuated Total Reflection Fourier Transform Infra Red spectroscopy
BET	Brunauer, Emmett and Teller
CAE	Constant Analyser Energy
CHA	Concentric Hemispherical Analyser
EFM	Electrostatic Force Microscopy
FAT	Fixed Analyser Transmission
FTIR	Fourier Transform Infra Red spectroscopy
FRR	Fixed Retarding Ratio
MFM	Magnetic Force Microscopy
PE	Poly(ethylene)
PLA	Poly(lactic acid)
PMMA	Poly(methyl-methacrylate)
PCL	Poly(ε-caprolactone)
PP	Poly(propylene)
PS	Poly(styrene)
PSA	Poly(sebacic anhydride)
PVC	Poly(vinyl-chloride)
PVME	Poly(vinyl-methylether)
PTFE	Poly(tetra-fluoroethylene)
PVA	Poly(vinyl-alcohol)

PVDF	Poly(vinyl-difluoride)
SEM	Scanning Electron Microscopy
SSIMS	Static Secondary Ion Mass Spectrometry
STM	Scanning Tunnelling Microscopy
TFAA	Trifluoroacetic anhydride
UHV	Ultra High Vacuum
XPS	X-ray Photoelectron Spectroscopy
XRD	X-ray Diffraction

APPENDIX B - RESEARCH CONFERENCES

June 1993   SERC/LINK - Biotechnology directorate annual meeting, Warwick

University.

August 1993   11th International Symposium on Plasma Chemistry, Loughborough

University, Loughborough, Leicestershire.

April 1994   3rd North East Medical Sensors Group Meeting, Durham University,

Durham.

APPENDIX C - RESEARCH COLLOQUIA, RESEARCH SEMINARS AND LECTURES.

(* denotes attendance)

1991

Sept. 17   Prof. R. D. Fischer, University of Hamburg, Germany

     Organo-f-element Systems to Organo-Main-Group Polymers

October 17   Dr. J. A. Salthouse, University of Manchester

     Son et Lumiere - a Demonstration Lecture

October 31   Dr. R. Keeley, Metropolitan Police Forensic Science

     Modern Forensic Science

Nov. 6 Prof. B. F. G. Johnson, Edinburgh University

     Cluster-Surface Analogies*

Nov. 7 Dr. A. R. Butler, University of St. Andrews

     Traditional Chinese Herbal Drugs: a Different Way of Treating Disease

Nov. 13   Prof. D. Gani, University of St. Andrews

     The Chemistry of PLP-dependent Enzymes*

Nov. 20   Dr. R. M. O'Ferral, University College, Dublin

     Some Acid-catalyzed Rearrangements in Organic Chemistry*

Nov. 28   Prof. I. M. Ward, IRC in Polymer Science, University of Leeds

     The Science and Technology of Orientated Polymers*

Dec. 4 Prof. R. Grigg, Leeds University

     Palladium-catalyzed Cyclization and Ion Capture Processes

Dec. 5 Dr. W. D. Cooper, Shell Research

     Colloid Science, Theory and Practice*

Dec. 5 Prof. A. L. Smith, ex Unilever

     Soap, Detergents and Black Puddings*

1992

January 22   Dr. K. D. M Harris, University of St. Andrews

Understanding the Properties of Solid Inclusion Compounds*

January 29   Dr. A. Holmes, Cambridge University

Cycloaddition Reactions in the Service of the Synthesis of Piperidine and Indolizidine Natural Products*

January 30   Dr. M. Anderson, Shell Research

Recent Advances in the Safe and Selective Chemical Control of Insect Pests

February 12   Prof. D. E. Fenton, Sheffield University

Polynuclear Complexes of Molecular Clefts as Models for Copper Biosites

February 13   Dr. J. Saunders, Glaxo Group Research

Molecular Modelling in Drug Discovery

February 19   Prof. E. J. Thomas, Manchester University

Applications of Organostannanes to Organic Synthesis

February 20   Prof. E. Vogel, University of Cologne

Porphyrins, Molecules of Interdisciplinary Interest

February 25   Prof. J. F. Nixon, University of Sussex

Phosphalkynes, New Building Blocks in Inorganic and Organometallic Chemistry

March 5   Dr. N. C. Billingham, University of Sussex

Degradable Plastic - Myth or Magic

March 11   Dr. S. E. Thomas, Imperial College

Recent Advances in Organoiron Chemistry

March 12   Dr. R. A. Hann, ICI Imagedata

Electronic Photography - An Image of the Future*

March 18   Dr. H. Maskill, Newcastle University

Concerted or Step-wise Fragmentation in a Deamination-type Reaction

April 7 D. M. Knight, University of Durham

Interpreting Experiments: the Beginning of Electrochemistry*

May 6 Prof. T. Marder, University of Waterloo

Metal-catalyzed Alkene Hydroboration

May 6 Dr. J. C. Gehret, Ciba-Geigy

Some Aspects of Industrial Agrochemical Research

October 15   Dr M. Glazer & Dr. S. Tarling, Oxford University & Birbeck College, London

It Pays to be British! - The Chemist's Role as an Expert Witness in Patent Litigation

247

October 20   Dr. H. E. Bryndza, Du Pont Central Research

Synthesis, Reactions and Thermochemistry of Metal (Alkyl) Cyanide Complexesand Their Impact on Olefin Hydrocyanation Catalysis

October 22   Prof. A. Davies, University College London

The Behaviour of Hydrogen as a Pseudometal*

October 28   Dr. J. K . Cockcroft, University of Durham

Recent Developments in Powder Diffraction*

October 29   Dr. J. Emsley, Imperial College, London

The Shocking History of Phosphorus

Nov. 4 Dr. T. P. Kee, University of Leeds

Synthesis and Co-ordination Chemistry of Silylated Phosphites

Nov. 5 Dr. C. J. Ludman, University of Durham

Explosions, A Demonstration Lecture*

Nov. 11   Prof. D. Robins, Glasgow University

Pyrrolizidine Alkaloids : Biological Activity, Biosynthesis and Benefits

Nov. 12   Prof. M. R. Truter, University College, London

Luck and Logic in Host - Guest Chemistry*

Nov. 18   Dr. R. Nix, Queen Mary College, London

Characterisation of Heterogeneous Catalysts*

Nov. 25   Prof. Y. Vallee. University of Caen

Reactive Thiocarbonyl Compounds

Nov. 25   Prof. L. D. Quin, University of Massachusetts, Amherst

Fragmentation of Phosphorous Heterocycles as a Route to Phosphoryl Species with Uncommon Bonding*

Nov. 26   Dr. D. Humber, Glaxo, Greenford

AIDS - The Development of a Novel Series of Inhibitors of HIV

Dec. 2 Prof. A. F. Hegarty, University College, Dublin

Highly Reactive Enols Stabilised by Steric Protection

Dec. 2 Dr. R. A. Aitken, University of St. Andrews

The Versatile Cycloaddition Chemistry of $Bu_3P.CS_2$

Dec. 3 Prof. P. Edwards, Birmingham University

The SCI Lecture - What is Metal?

Dec. 9 Dr. A. N. Burgess, ICI Runcorn

The Structure of Perfluorinated Ionomer Membranes*

1993

January 20   Dr. D. C. Clary, University of Cambridge

Energy Flow in Chemical Reactions*

January 21   Prof. L. Hall, Cambridge

NMR - Window to the Human Body

January 27   Dr. W. Kerr, University of Strathclyde

Development of the Pauson-Khand Annulation Reaction : Organocobalt Mediated Synthesis of Natural and Unnatural Products

January 28   Prof. J. Mann, University of Reading

Murder, Magic and Medicine

February 3   Prof. S. M. Roberts, University of Exeter

Enzymes in Organic Synthesis

February 10   Dr. D. Gillies, University of Surrey

NMR and Molecular Motion in Solution*

February 11   Prof. S. Knox, Bristol University

The Tilden Lecture Organic Chemistry at Polynuclear Metal Centres

February 17   Dr. R. W. Kemmitt, University of Leicester

Oxatrimethylenemethane Metal Complexes

February 18   Dr. I. Fraser, ICI Wilton

Reactive Processing of Composite Materials*

February 22   Prof. D. M. Grant, University of Utah

Single Crystals, Molecular Structure, and Chemical-Shift Anisotropy

February 24   Prof. C. J. M. Stirling, University of Sheffield

Chemistry on the Flat-Reactivity of Ordered Systems

March 10   Dr. P. K. Baker, University College of North Wales, Bangor

Chemistry of Highly Versatile 7-Coordinate Complexes

March 11   Dr. R. A. Y. Jones, University of East Anglia

The Chemistry of Wine Making

March 17   Dr. R. J. K. Taylor, University of East Anglia

Adventures in Natural Product Synthesis

March 24   Prof. I. O. Sutherland, University of Liverpool

Chromogenic Reagents for Cations*

May 13   Prof. J. A. Pople, Carnegie-Mellon University, Pittsburgh, USA

Applications of Molecular Orbital Theory*

May 21   Prof. L. Weber, University of Bielefeld

Metallo-phospha Alkenes as Synthons in Organometallic Chemistry

June 1 Prof. J. P. Konopelski, University of California, Santa Cruz

Synthetic Adventures with Enantiomerically Pure Acetals

June 2 Prof. F. Ciardelli, University of Pisa

Chiral Discrimination in the Stereospecific Polymerisation of Alpha Olefins

June 7 Prof. R. S. Stein, University of Massachusetts

Scattering Studies of Crystalline and Liquid Crystalline Polymers

June 16   Prof. A. K. Covington, University of Newcastle

Use of Ion Selective Electrodes as Detectors in Ion Chromatography

June 17   Prof. O. F. Nielsen, H. C. Ærsted Institute, University of Copenhagen

Low-Frequency IR - and Raman Studies of Hydrogen Bonded Liquids

Sept. 13   Prof. Dr. A.D. Schlüter, Freie Universität Berlin, Germany

Synthesis and Characterisation of Molecular Rods and Ribbons

Sept. 13   Dr. K.J. Wynne, Office of Naval Research, Washington, USA

Polymer Surface Design for Minimal Adhesion*

Sept. 14   Prof. J.M. DeSimone, University of North Carolina, Chapel Hill, USA

Homogeneous and Heterogeneous Polymerisations in Environmentally Responsible Carbon Dioxide

Sept. 28   Prof. H. Ila, North Eastern Hill University, India

Synthetic Strategies for Cyclopentanoids via Oxoketene Dithioacetals

October 4   Prof. F.J. Feher, University of California, Irvine, USA

Bridging the Gap between Surfaces and Solution with Sessilquioxanes

October 14   Dr. P. Hubberstey, University of Nottingham

Alkali Metals: Alchemist's Nightmare, Biochemist's Puzzle and Technologist's Dream*

October 20   Dr. P. Quayle, University of Manchester

Aspects of Aqueous ROMP Chemistry

October 21   Prof. R. Adams, University of South Carolina, USA

Chemistry of Metal Carbonyl Cluster Complexes : Development of Cluster Based Alkyne Hydrogenation Catalysts*

October 27   Dr. R.A.L. Jones, Cavendish Laboratory, Cambridge

Perambulating Polymers*

Nov. 10   Prof. M.N.R. Ashfold, University of Bristol

High Resolution Photofragment Translational Spectroscopy : A New Way to Watch Photodissociation*

Nov. 17   Dr. A. Parker, Rutherford Appleton Laboratory, Didcot

Applications of Time Resolved Resonance Raman Spectroscopy to Chemical and Biochemical Problems*

Nov. 24   Dr. P.G. Bruce, University of St. Andrews

Structure and Properties of Inorganic Solids and Polymers

Nov. 25   Dr. R.P. Wayne, University of Oxford

The Origin and Evolution of the Atmosphere

Dec. 1 Prof. M.A. McKervey, Queen's University, Belfast

Synthesis and Applications of Chemically Modified Calixarenes

Dec. 8 Prof. O. Meth-Cohn, University of Sunderland

Friedel's Folly Revisited - A Super Way to Fused Pyridines

Dec. 16   Prof. R.F. Hudson, University of Kent

Close Encounters of the Second Kind

1994

January 26   Prof. J. Evans, University of Southampton

Shining Light on Catalysts*

February 2   Dr. A. Masters, University of Manchester

Modelling Water Without Using Pair Potentials

February 9   Prof. D. Young, University of Sussex

Chemical and Biological Studies on the Coenzyme Tetrahydrofolic Acid

February 16   Prof. K.H. Theopold, University of Delaware, USA

Paramagnetic Chromium Alkyls : Synthesis and Reactivity

February 23   Prof. P.M. Maitlis, University of Sheffield

Across the Border : From Homogeneous to Heterogeneous Catalysis*

March 2   Dr. C. Hunter, University of Sheffield

Noncovalent Interactions between Aromatic Molecules

March 9   Prof. F. Wilkinson, Loughborough University of Technology

Nanosecond and Picosecond Laser Flash Photolysis

March 10   Prof. S.V. Ley, University of Cambridge

New Methods for Organic Synthesis

March 25   Dr. J. Dilworth, University of Essex

Technetium and Rhenium Compounds with Applications as Imaging Agents

April 28   Prof. R. J. Gillespie, McMaster University, Canada

The Molecular Structure of some Metal Fluorides and Oxofluorides: Apparent Exceptions to the VSEPR Model.

May 12   Prof. D. A. Humphreys, McMaster University, Canada

Bringing Knowledge to Life